Characterizing Aspects of Groundwater Flow in Discontinuous Permafrost Terrain, Within the Central Mackenzie Valley, NWT

by

Andrew Wicke

A thesis
presented to the University of Waterloo
in fulfillment of the
thesis requirement for the degree of
Master of Sciences
in
Earth Sciences

Waterloo, Ontario, Canada, 2021

Author's Declaration

I hereby declare that I am the sole author of this thesis. This is a true copy of the thesis, including any required final revisions, as accepted by my examiners.

I understand that my thesis may be made electronically available to the public.

Acknowledgements

I would like to acknowledge those that made completion of this thesis possible. First, I would like to thank my advisor Dr. Dave Rudolph for giving me the opportunity to undertake this project. You were always encouraging, motivating and kept me on the right track. Your kindness and understanding also made working with you so enjoyable. Thank you also to my committee members. Dr. Brewster Conant Jr. for all of your guidance, encouragement and for showing me the ropes in the field. Thank you, Dr. Sherry Schiff for all of your understanding, advice and for introducing me to the wonderful world of environmental isotopes.

Second, I would like to thank all the friends I made from the Rudolph Research Group, who provided me with support and were always there for a chat about research or life. Thank you to Andrew Wiebe, our random drop in chats were always appreciated and helped to break up the day. You also had so many great ideas and were always eager to help me out with technical problems. Brittney Glass, I really had a lot of fun working with you on this project, and always appreciated your kindness. Thank you for all the advice and support. Thanks also to Iwona Widuska for helping me prepare for interviews and for being so welcoming all the time. Also, I want to acknowledge all the hard work done by Aaron Vandenhoff both in the field and in the lab. Our pun-offs and "Dad jokes" were also always entertaining.

I would like to also extend a thank you to the people at Husky Energy for sharing their time and data with us. Without their assistance this would have never been possible. Thank you to Jenica Von Kuster and Chris Salewich for their technical and logistical support, and also to Liam Cross and Ken Shepard.

Thank you to everyone who we collaborated and worked with from WLU. Thank you to Anastasia Sniderhan, Jason Paul, and Tom Pretty.

Thank you to the people of the Environmental Isotope Lab who were very accommodating when we needed more fridge space and performed the analysis on all of our amazing isotope data. Thank you to Reem El Mugammar, Rhys Gwynne, Justin Harbin, and Mike Mahkanouk.

I would also like to thank Dr. Shaun Frape, Dr. Thai Phan and Dr. Martin Ross, for allowing me to consult with you on numerous occasions about my research. Thanks also to David Hilger for training me on the core squeezer.

I also want to gratefully acknowledge funding from Global Water Futures through the Northern Water Futures project and the Government of the Northwest Territories Environmental Studies Research Fund. I am highly appreciative of the technical and logistical advice provided to us by Andrew Applejohn and Bruce Hanna (Government of the Northwest Territories). Technical support and field work facilitation were also graciously provided by the Sahtu Renewable Resources Board and we are thankful to Sahtu communities for reviewing and approving our research licenses (ARI Scientific Research License Nos. 16345 and 16581).

Lastly, I want to thank my mom, Janet Wicke, who has been a massive support for me all the way through. Her optimism helped keep me grounded and she was always excited to hear about my research. She never once doubted me and was always encouraging throughout the whole process of completing my Master's. I could never have achieved this without her.

Abstract

With recent developments in oil and gas exploration technologies that have opened regions of Canada's northern territories and the threat of climate change, uncertainties around how these factors may impact the environment in these areas are profuse. To reduce uncertainty and allow for mitigation planning, having effective baseline monitoring of environmental systems, such as groundwater, is critical. However, baseline monitoring studies of groundwater resources in these regions are complex and expensive to undertake as compared to studies in more southern regions. This is due mainly to the remoteness, lack of infrastructure and presence of discontinuous permafrost that complicates the use of traditional groundwater monitoring methods in northern regions.

The work outlined in this thesis set out to improve baseline monitoring studies of groundwater in discontinuous permafrost areas. A suite of geochemical and isotopic tracers combined with physically based hydrologic measurements were tested in two summer field campaigns within the Bogg Creek Watershed, a small subcatchment of the Mackenzie River in the Northwest Territories (NWT). These data were acquired through strategic sampling utilizing portable and lightweight equipment, guided by previous remote sensing work and an aerial infrared survey. This field data was combined with a variety of other data sets acquired through public records and reports, as well as through collaboration with interested third parties.

Physical data provided evidence for groundwater discharge in some areas, while the geochemical and isotopic evidence allowed for fingerprinting of these groundwater sources. In total, 5 groundwater source groups were identified in the study area. These included shallow seepage water and organic active layer porewater (both Ca-SO_4), suprapermafrost groundwater originating from mineral soils (Ca-HCO_3), subpermafrost groundwater from the Little Bear Formation aquifer (Na-HCO_3), and subpermafrost groundwater from the Martin House Formation (Na-Cl/HCO_3).

Evidence of suprapermafrost and subpermafrost groundwater contributions were found in Bogg Creek and its headwater tributaries as well as in several springs. Suprapermafrost groundwater influence occurs throughout the watershed but is most dominant in upland tributaries. Evidence for Little Bear Formation groundwater influence was found in the geochemical and $^{87}Sr/^{86}Sr$ signature of one of the tributaries of Bogg Creek, downstream of several mapped icings. Evidence of Martin House Formation groundwater influence was noted in geochemistry from a spring complex, associated with mapped icings. This spring

water appeared to be mixtures of both subpermafrost and suprapermafrost groundwaters, but this is not certain. There is also evidence for Martin House Formation water in the lower reaches of Bogg Creek. $\delta^{18}O$ and $\delta^{2}H$ data suggest these contributions are quite small within the creek and its tributaries but are more substantial in springs. This highlights the sensitivity inherent in each method, where geochemistry is quite responsive to minor contributions of subpermafrost groundwater due to a much higher degree of contrast between solute concentrations in suprapermafrost and subpermafrost groundwater endmembers. There is less contrast in $\delta^{18}O$ and $\delta^{2}H$. $^{87}Sr/^{86}Sr$ appeared to confirm what was indicated in the geochemical results, while $\delta^{13}C$ in CH_4 and ^{3}H were inconclusive. A conceptual model of the site hydrogeologic system was developed based on this information.

Some uncertainty remains on exact groundwater origins due to the limitations of the geochemical and isotopic species used, but overall results indicate that these techniques could be applied in similar discontinuous permafrost environments. Portable sampling techniques used in the shallow subsurface might be able to effectively characterize suprapermafrost groundwaters in an area quickly and efficiently, limiting the need for extensive monitoring well networks. Large contrasts from this water found in surface water or springs may be indicative of water originating from another source, such as from a subpermafrost aquifer. However, a certain amount of subpermafrost groundwater sampling is needed, as many uncertainties arise with missing endmembers.

Table of Contents

List of Figures

List of Tables

Chapter 1
Introduction

1.1 Environmental Change in Canada's North

Developments in unconventional oil and gas extraction technologies (such as horizontal hydraulic fracturing completions) have opened up new areas in Canada's north for hydrocarbon exploration and extraction (Rudolph et al., 2016a). Moreover, climate change is predicted to disproportionally affect northern areas with increased rates of warming as compared to more temperate regions (Walvoord & Kurylyk, 2016). Oil and gas activities combined with a warming climate have potential to negatively affect sensitive and remote northern region environments (Canadian Water Network, 2015; Lamoureux & Lafrenière, 2018; Walvoord & Kurylyk, 2016). Unconventional petroleum resource exploration and extraction require substantial amounts of water, while the threat of spills, well leakages, or upward migration of mobile hydrocarbons can lead to contamination of groundwater and surface water (Ryan et al., 2015).

In Canada, many northern regions are home to First Nations populations that have always relied on the land to provide a means of life and survival. Firsthand anecdotes from many northern residents recount dramatic impacts of climate warming on animal behavior, permafrost occurrence, and the timings of ice freeze up and spring snowmelt (Golder Associates, 2015). These personal observations are supported by recent scientific evidence that aquatic ecosystems and the surrounding landscape are changing in the north (Walvoord & Kurylyk, 2016; Walvoord & Striegl, 2007). Climate change, clearing of land due to human activities and forest fires are altering permafrost distribution and occurrence (Quinton et al., 2011b; Quinton et al., 2003; Quinton & Pomeroy, 2006). This in turn is leading to impacts on both regional surface (Connon et al., 2015) and subsurface hydrology (Jacques & Sauchyn, 2009; Walvoord & Striegl, 2007) as well as the surficial landscapes (Quinton et al., 2011b).

Uncertainty about anthropogenic and climatic stress to the environment requires an understanding of the natural baseline conditions in order to better predict how a system may respond (AMEC, 2013; Rudolph et al., 2016a). Unfortunately, these areas also remain some of the most data scarce and remote, making *baseline monitoring* studies logistically challenging and prohibitively expensive to undertake. Baseline monitoring is monitoring done to establish the natural hydrologic (or another environmental system) conditions, including variability within the system caused by natural fluctuations. More

traditional methods utilized in temperate regions remain impractical within this environment, however. In particular, the study of groundwater flow systems is much more challenging in these environments than in more southern latitudes.

The Northwest Territories (NWT) of Canada had recently seen an uptick in interest for extraction of unconventional oil and gas (Rudolph et al., 2016b). The Sahtu Settlement Area (SSA) located in the Central Mackenzie Valley (CMV) of NWT has undergone exploration of the Canol Formation shale within the last decade. Since 2014 however, most exploration activities in the area have ceased (Rudolph et al., 2016b). However, several baseline hydrologic monitoring programs related to petroleum exploration have been established and are still ongoing within this region, providing a crucial data source. These data represent an important first step in characterizing aspects of the hydrologic environment, but there remains a need to expand the baseline monitoring activities in the area, specifically related to groundwater.

Within the CMV, references exist of natural hydrocarbon seeps that are known to occur along the Mackenzie River and several of its tributaries. These seeps were first recorded in 1789 by the explorer and namesake to the river, Alexander Mackenzie (Babiy, 2013; Hayes & Dunn, 2012). Several hydrocarbon compounds have been identified as being present naturally in some surface waters during ongoing monitoring activities (Northern EnviroSearch Ltd [NESTL]., 2015; Rudolph et al., 2016b). This makes it more challenging to conclusively determine if activities related to petroleum exploration and development have led to further release of these substances without first quantifying background levels, but also provides an opportunity to use them as tracers.

Within this remote northern terrain, characterized by discontinuous permafrost conditions (Rudolph et al., 2016b), several key challenges exist that prevent the utilization of traditional groundwater monitoring and characterization methods. Access within the region is limited, with transportation by road occurring mostly on winter ice-roads, and boat transport limited to summer months only (Babiy, 2013). Expanses of thick black spruce forest and an abundance of wetlands and waterlogged ground limit ground transportation inside exploration leases to only within cleared land or constructed roads. Movement of heavy equipment for activities such as drilling of wells must be conducted on built-up roads or on frozen ground in winter (Babiy, 2013). To further complicate monitoring, the presence of discontinuous permafrost limits the usefulness of drilled monitoring wells and presents a further challenge to maintaining infrastructure. Site access and the tendency for monitoring wells to freeze and remain frozen

even in summer make installation expensive and difficult to implement, and limit groundwater sampling opportunities (Sutphin et al., 2006). Despite these limitations, traditional methods are still undertaken in pursuit of baseline monitoring by consulting and oil and gas companies. The need for additional monitoring tools is therefore crucial to expanding and improving upon baseline monitoring of groundwater.

One region within the CMV that has recently been the focus of fairly intensive site investigation is the unconventional petroleum exploration lease area on the southwest side of the Mackenzie River between Norman Wells and Tulita, NWT (Rudolph et al., 2016b). In 2010, Husky Energy established a baseline investigation program in advance of their exploratory drilling operations in 2012 within their leases. Previous studies in this region of the CMV had been primarily undertaken by the petroleum industry and environmental consultants, with older studies conducted by academia (Michel, 1986; Utting et al., 2013; van Everdingen, 1982). As part of this baseline work, Husky and their consulting teams initiated annual monitoring of surface waters, groundwater and ecological features within the leased lands in 2012 (Golder Associates, 2015; Husky Oil Operations Ltd., 2018; NESTL, 2015; Rudolph et al., 2016a; Rudolph et al., 2016b). Since the start of the monitoring program, an extensive data set has been established including surface water quality and flows, ecological features and some hydrogeologic information. These data represent some of the most comprehensive hydrologic characterization information within the entire CMV (Rudolph et al., 2016b). Although the baseline monitoring program provides invaluable information on the existing natural hydrologic conditions, there remains a paucity of information regarding the nature of groundwater flow within this environment, a component of the hydrologic cycle influenced by the presence of discontinuous permafrost. As groundwater flow is anticipated to be a major pathway for deeper petroleum compounds to reach ground surface, and also considering the potential role of groundwater in the evolution of permafrost in this rapidly warming region, additional investigation into the nature of groundwater occurrence and mobility in this complex environment is warranted.

In collaboration with Husky Energy, the Government of Northwest Territories and local indigenous collaborators in Norman Wells, the current study was initiated to expand the hydrogeological understanding within this region of the CMV. Building on the existing information available for this area, including the invaluable baseline data bases established by Husky Energy, a multi-year field investigation program was designed and implemented within petroleum lease areas to explore methodologies for hydrogeologic site characterization and for enhancing the understanding of the hydrogeologic conditions

in the region. This work will focus on a small subcatchment within the Husky lease areas referred to locally as the Bogg Creek Watershed (Figure 1). A combination of isotopic and geochemical data supplemented by physically based hydrologic measurements were collected by portable and lightweight instruments. Site selection was aided by previous work utilizing remote sensing to look for indicators of groundwater discharge (Glass, 2019) and through the use of infrared sensing technologies (Conant Jr, 2009; Conant Jr, 2019). This work was designed to be a *proof-of-concept study,* so show that collection of indirect GW/SW data can provide insight into baseline groundwater flow conditions on an intermediate-regional scale within a discontinuous permafrost landscape in transition.

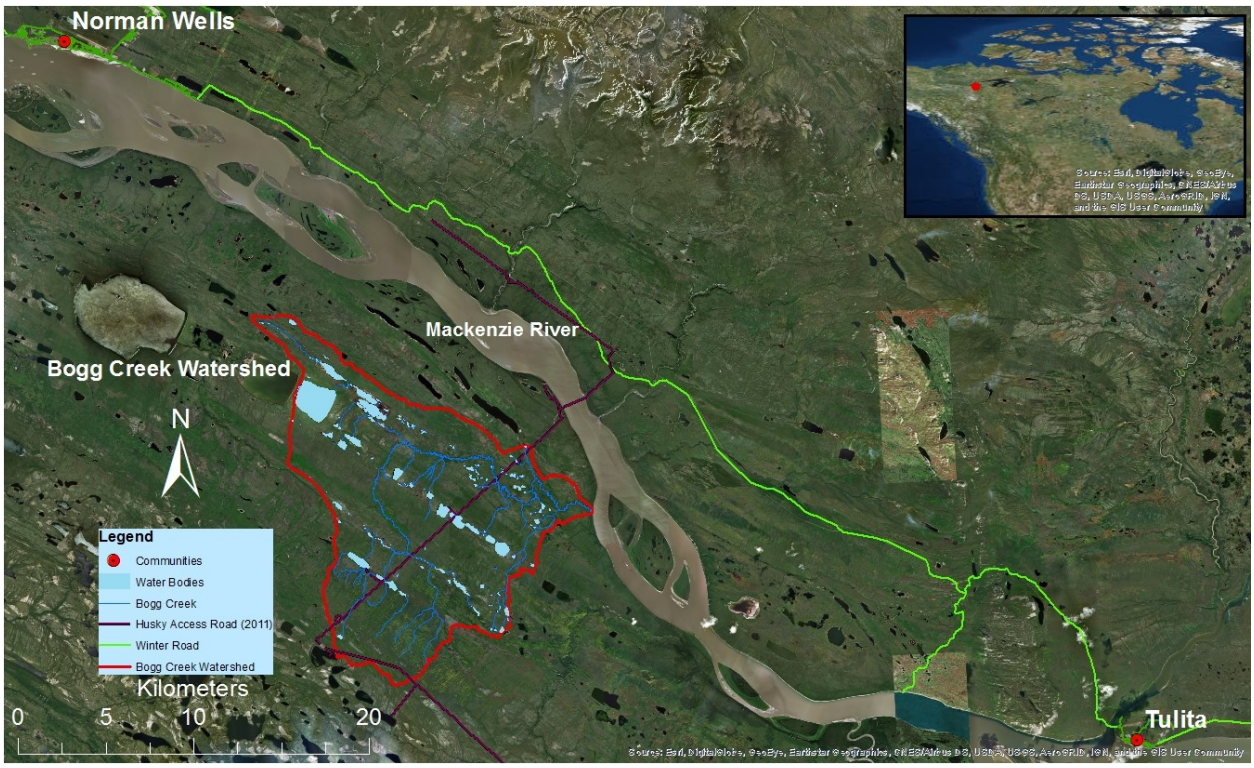

Figure 1: Satellite photo of study area and surrounding communities of Norman Wells and Tulita. Inset map showing study area relative to the rest of Canada. Satellite photo provided as part of ArcGIS basemap feature.

1.2 Objectives

The objectives of this research were to:

1. Compile and aggregate current baseline knowledge for the CMV into a central database, notably within the Bogg Creek Watershed and several areas within the surrounding Husky Energy leased lands;
2. Explore and implement various field methods to expand upon the current baseline understanding of study area hydrogeology and groundwater-surface water interactions;
3. Develop a site-specific conceptual model of the hydrogeologic system of Bogg Creek, utilizing the data gathered through the current fieldwork campaigns and in conjunction with previously available information from the site;
4. Provide recommendations for conducting hydrogeologic baseline studies in discontinuous permafrost environments based upon the methods explored.

Chapter 2
Background Information

2.1 Permafrost Hydrogeology

Permafrost is rock or soil that remains below 0°C for at least 2 consecutive years (French, 1996). Based on this definition, permafrost can include, for example, unfrozen, high salinity groundwater with a depressed freezing point. Permafrost ground may therefore be partially frozen, frozen or unfrozen depending on moisture and solute content (French, 1996). Permafrost water is typically found as ice frozen within pore spaces but can also include ice wedges or massive ground ice. Overlying the top surface of the permafrost, or *permafrost table*, lies the *suprapermafrost zone* and the *active layer* (French, 1996; Kokelj & Burn, 2005; Lemieux et al., 2016). The active layer consists of a region of the suprapermafrost zone that actively freezes and thaws seasonally (Lemieux et al., 2016). Permafrost initially forms from a negative energy balance, with heat loss occurring in winter exceeding heat gain in summer. Permafrost therefore forms from the top down and maximum depth is reached when the heat loss at depth is balanced by the geothermal gradient (French, 1996). Below the base of the permafrost lies the *subpermafrost zone* (Lemieux et al., 2016).

Due to the presence of permafrost, the groundwater hydrology in cold regions varies greatly from more temperate regions as groundwater flow dynamics will be influenced by frozen ground. Typically, frozen soil and rock will act as an impermeable barrier to flowing groundwater or infiltrating soil water, depending on saturation levels (Burt & Williams, 1976; French, 1996; Lemieux et al., 2016; Utting et al., 2013). Hydraulic conductivity in soils may decrease by as much as 4-5 orders of magnitude as water temperatures decrease from 0°C to -0.5°C, depending on the soil water content and soil texture (Burt & Williams, 1976).

In aquifer units located within a permafrost terrain, much or all of the available flow system may be frozen or separated by frozen zones, thereby making groundwater movement very slow or stagnant. Areas that remain unfrozen in and around permafrost are referred to as *taliks,* which may lie within, above or below permafrost (French, 1996), and may be considered aquifers if they consist of permeable material that transmits water (Lemieux et al., 2016). Groundwater flow may work to maintain these taliks either through the movements of freezing point depressed water or by circulation of thermal waters (Utting, 2012). Taliks may form and remain below a large body of water (French, 1996) due to the residual heat

stored in the water body through winter. If the surface water bodies are deep enough the freezing front cannot penetrate to the streambed or lake bottom, and a talik will be maintained (French, 1996).

A talik may form a simple unfrozen, saturated bulb below a water body surrounded by permafrost. Such taliks are referred to as *closed* (French, 1996; Lemieux et al., 2016). A*n open* talik penetrates the permafrost completely, creating a connection from subpermafrost to suprapermafrost layers or to surface water bodies (Lemieux et al., 2016; Utting et al., 2013; Walvoord et al., 2012). Closed taliks are common under minor surface water bodies, while major surface waters that do not freeze to the bottom in winter are often underlain by open taliks (French, 1996; Walvoord et al., 2012).

Both closed and open taliks may act as potential conduits for groundwater to flow all year round. This means groundwater flow is effectively partitioned into distinct components, above, below or within the permafrost (Lemieux et al., 2016). Shallow, *suprapermafrost* groundwater flow consists of young, often relatively quickly circulating groundwater that flows mostly during summer months while the active layer is unfrozen (Lemieux et al., 2016; Quinton et al., 2009, 2003). This shallow water often experiences short flow paths through thin aquifers of organic and mineral soils. Although highly dependent on seasonal precipitation and recharge, water tables are often high, promoting growth of fens and peat soils (Jessen et al., 2014; Quinton et al., 2009; Zoltai et al., 1988). Deeper *subpermafrost* groundwater is characterized by older, often mineral-rich water that takes regional or intermediate flowpaths (Bense et al., 2009; Lemieux et al., 2016; Walvoord et al., 2012). This water may have been recharged hundreds to thousands of years ago, and may ultimately discharge into major surface water bodies or as springs (Walvoord et al., 2012). This water may be brackish or subjected to geothermal heating, thereby keeping taliks open (Utting et al., 2013). Flow and mixing between each zone may occur where open taliks exist through the *intrapermafrost zone*. Recharge of deep groundwater flow may occur as depression focused recharge, beneath surface water features or as distributed recharge through fractures or small taliks (Ireson et al., 2013; Lemieux et al., 2016). Intrapermafrost groundwater flows through closed or open taliks, or in suprapermafrost taliks found between the frozen active layer and the permafrost table (Lemieux et al., 2016).

Groundwater discharge to the surface may continue to occur even in winter under appropriate conditions. When this happens large sheets of ice can form on the ground surface as freezing fronts cause subsurface pressures to build and force water to the surface (van Everdingen, 1982; Yoshikawa et al., 2007). These features are called *icings* or *aufeis* and can extend for meters to even kilometers from their

source (Yoshikawa et al., 2007). Recent research suggests icings can be identified from remote sensing techniques, allowing potential groundwater discharge locations to be mapped on a large scale (Glass, 2019; Glass et al., 2020).

2.2 Permafrost Degradation Effects on Groundwater Flow

Recent research has shown that Northern Canada is experiencing dramatic changes due to human disturbances and a warming climate (Connon et al., 2014; Lamoureux & Lafrenière, 2018; Walvoord & Kurylyk, 2016). Permafrost distribution is maintained through delicate energy balances between the heat lost in winter and that gained in summer. Removal of vegetation (Connon et al., 2014; Wright et al., 2001), increasing summer temperatures (Environment Canada, 2019), longer summers (Lamoureux & Lafrenière, 2018), and shifts in precipitation (Spence et al., 2011) have begun to upset that energy balance. This has initiated thawing of permafrost in some areas, which can alter hydrologic regimes (Walvoord & Kurylyk, 2016). Once thawed, a positive feedback loop may begin whereby pooling of water in thawed bulbs prevents complete refreezing and promotes further permafrost thaw (Quinton et al., 2003). For example, thawing of permafrost within the Scotty Creek Basin, NWT has led to dramatic changes to surface hydrology such as draining of once isolated bogs and lakes (Connon et al., 2014).

Vegetation disturbances such as removal of forest for transportation or infrastructure construction can also initiate thaw (Quinton et al., 2011a). Seismic lines cut for oil and mineral exploration have been shown to cause degradation of permafrost by increasing the transmission of sunlight normally intercepted by vegetation and the tree canopy (Quinton et al., 2009). As seismic lines are common in the northern landscape, these areas have the potential to have degraded permafrost acting as conduits for groundwater and surface water to flow.

Decreases in permafrost coverage have been demonstrated to lead to increased stream baseflow, increased groundwater storage capacity and increased overall groundwater discharge (Walvoord & Kurylyk, 2016). These changes have also been demonstrated in modelling activities (McKenzie & Voss, 2013) and at several field sites (Jacques & Sauchyn, 2009). Walvoord & Striegl, (2007) examined streamflow records for the Yukon River Basin, noting that during winter months surface and near-surface runoff decreases to negligible levels. Winter streamflow would therefore be comprised almost entirely of baseflow originating from groundwater. The authors noted that baseflow contributions increased since records had begun; attributing this phenomenon to increased suprapermafrost groundwater flow from newly thawed areas. In a similar study, Jacques & Sauchyn, (2009) examined Mackenzie River basin

streamflow records. Their work concluded that of 23 gauging stations used in their analysis, 9 had statistically significant increases in annual streamflow and 20 showed increases in baseflow contributions. Smaller basins appeared to show larger increases in total baseflow inputs compared to larger basins. In these smaller basins, permafrost is generally more continuous and so this baseflow component was dominated more by suprapermafrost groundwater (Walvoord et al., 2012). Even a minor reduction of permafrost coverage and increased baseflow could lead to decreased seasonal variability in stream discharge and temperatures, a decrease in river ice thickness, earlier timing of ice breakup and altered aquatic chemistry (Walvoord & Kurylyk, 2016; Walvoord et al., 2012). These may have major implications for altering river and lake dynamics, fish habitat, transportation routes and flood risks (McKenzie & Voss, 2013; Walvoord & Striegl, 2007; Walvoord et al., 2012).

2.3 Geologic Controls on Groundwater Movement and Discharge

Folded and faulted sedimentary rock sequences can create complex, regionally confined aquifer systems (Cook, 2003; Fetter, 2001; Yager & Ratcliffe, 2010). Gently folded coarse-grained sedimentary rocks may receive recharge water either through overlying leaky confining layers or in places where the confining layer has been removed by erosion and the aquifer is exposed near the surface (Cook, 2003). Confining layers in the CMV include shales and mudstones as well as perennially frozen ground. For regional groundwater flow to occur in this environment, sufficient recharge would be needed in higher topographic areas to maintain a regional gradient and to drive groundwater flow (Cook, 2003; Fetter, 2001; Kresic & Stevanovic, 2010). In the CMV, this recharge may occur in unfrozen portions of exposed coarse-grained rocks and sediments, and through fractured fine-grained confining layers. As taliks are often found below major water bodies, higher elevation lakes or rivers may act as losing water bodies, recharging underlying aquifers (Walvoord et al., 2012). Flow through coarse-grained taliks or along open fractures in bedrock can provide hydraulic connectivity from the surface to subsurface. Regional folding can create joint patterns that are oriented parallel and perpendicularly to the fold axis. These can also affect the anisotropy of aquifer permeability and create a secondary porosity that affects groundwater flow and solute transport (Cook, 2003).

Faults may create either conduits or barriers for groundwater flow (Cook, 2003; Fetter, 2001; Kresic & Stevanovic, 2010). Fault gouges and breccias formed due to the movement of faulting create low-permeability obstacles to groundwater. Fault breccias with larger particle sizes and porosity may allow for increased permeability, thereby creating high conductivity windows or conduits for groundwater to be

transmitted instead (Cook, 2003). Faults can create linear patterns of springs in discharge zones and allow for mixing of groundwater of various ages (Cook, 2003; Fetter, 2001; Kresic & Stevanovic, 2010). Faults allow for short-circuiting of flow across several formations that may otherwise behave as aquitards, and are often associated with warmer thermal springs (Grasby et al., 2016). Geologic structure greatly controls the expression of surface hydrology and contributions from groundwater (Cook, 2003; Fetter, 2001; Kresic & Stevanovic, 2010; Twidale, 2004; Yager & Ratcliffe, 2010).

Regional flow in the current study area is hypothesized to be dominated by recharge in the Mackenzie Mountains and foothills in the west and Franklin Mountains in the east, with flow towards the Mackenzie River and its tributaries. Direct evidence for recharge occurring in the Franklin mountains does exist (Michel, 1986). Karst and geothermal springs have been noted to occur in the area along the base of the Franklin Mountains, however these discharge zones lie outside the study area on the northeast side of the Mackenzie River (Michel, 1986; van Everdingen, 1982). Limestone and dolostone are not major rock types within the Bogg Creek study area and so are unlikely to be major conduits for water (Fallas & MacNaughton, 2013, 2014). Thicker glacial deposits and peat also obscure much of the underlying bedrock lithology and structure, so direct observations of springs originating from bedrock aquifers remains difficult in this area.

2.4 Groundwater/Surface Water Interactions

Groundwater and its influence on surface water bodies is well understood, and baseflow is often a large component of streamflow (Rosenberry & LaBaugh, 2008). Streams, lakes, seeps and springs are often an approximate surface expression of the water-table, but are more complex due to multiple water contributors (Deitchman et al., 2009; Kresic & Stevanovic, 2010). These contributions may be from groundwater originating from different aquifers, recirculating hyporheic zone water, overland flow, soil interflow and precipitation or icings (Fetter, 2001). Melting of river icings in spring can contribute a substantial portion of water to total streamflow. Icings can store up to 40% of total winter streamflow, and contribute to 4% of total annual streamflow (Woo, 2012). Icing meltwaters can continue to provide a source of water well past the spring freshet and into the summer months.

In permafrost regions, frozen ground restricts groundwater flow and promotes more efficient runoff, (French, 1996). Below and adjacent to water bodies the frozen ground may be thinner or absent entirely, providing a pathway for discharging subpermafrost groundwater, or allowing for recharge of underlying aquifers (Walvoord & Striegl, 2007). Besides springs, which are a direct point discharge of groundwater

on the surface but often harder to locate, lakes and streams may provide another avenue for characterizing deep and shallow groundwater flow because taliks associated with them act as hydraulic windows through the permafrost for flow to occur. Groundwater modelling in permafrost terrain has demonstrated that large upward gradients form across regions of permafrost that coincide with areas of concentrated lakes (Walvoord et al., 2012).

Several techniques exist to characterize and quantify the interactions occurring in streams or lakes. These include the use of drive-point and mini-piezometers, push-point samplers, seepage meters, stream gauging, hydrograph separation and groundwater tracers (Dingman, 1994; Rosenberry & LaBaugh, 2008). Piezometers and samplers allow for in-situ measurement of hydraulic head, vertical hydraulic gradients and for obtaining water samples. In the case of piezometers, depending on annulus width, they may allow continuous temperature and head monitoring (Fetter, 2001; Rosenberry & LaBaugh, 2008). Seepage meters and stream gauging methods both provide estimates of flux into or out the stream reach in question, while piezometers and seepage meters also allow for point estimations of streambed hydraulic conductivity (Dingman, 1994; Rosenberry & LaBaugh, 2008). Stream gauging permits a bulk estimate of water gained or lost between two gauging points, but is often prone to estimation and rounding errors (Dingman, 1994). Stream gauging of differing high, low and moderate flows however can lead to the creation of stage-discharge curves which allow total stream discharge to be quantified more easily using only a stream water-level. This allows for use of hydrograph separation techniques to quantify groundwater fluxes into or out of a stream reach (Dingman, 1994). These techniques are useful for characterizing aspects of water quantity and flow directions, but water quality can also be utilized to explore groundwater/surface water interactions (Conant Jr et al., 2019). Stream geochemistry reflects the various water sources that contribute to streamflow. These sources can be conceptualized as a general mixture between direct precipitation, groundwater, soil water or interflow, and surface runoff. Just like water level fluctuations, water quality is transient and subject to changes due to chemical and biological reactions within the hyporheic zone, varying inputs of precipitation or groundwater and interactions with bed or suspended materials (Conant Jr. et al., 2019). This spatial and temporal variability is important to consider and monitor over time, especially within an ever-changing environment.

2.5 Groundwater Tracers

The use of environmental tracers in hydrogeology is common practice (Clark & Fritz, 1997; Coplen et al., 2000; Leibundgut et al., 2009). Tracers can be any natural or anthropogenic components, substances,

properties or isotopes of water that record or infer groundwater sources, flowpaths or residence times (Clark & Fritz, 1997; Leibundgut et al., 2009). Tracers may be used to complement direct measurements, while also providing insight into the water's history (Leibundgut et al., 2009). For this research, environmental tracers are an attractive solution for discerning groundwater flowpaths and quantifying inputs to Bogg Creek and surrounding area. Several studies have been conducted in similar permafrost environments in the past utilizing a variety of environmental tracers (Clark et al., 2001; Coplen et al., 2000; Michel, 1986; Quinton et al., 2003; Utting et al., 2013). For this work, tracers explored include temperature, hydrogeochemistry and several environmental isotopes.

2.5.1 Heat as a Groundwater Tracer

Temperature is a simple and effective tracer of groundwater and surface water interactions (Anderson, 2005). Flowing groundwater transfers heat by convection either by temperature-dependent density differences or by gradient driven groundwater flow (Anderson, 2005, Constantz, 2008). Similarly, conduction of heat may occur through water-saturated pores or through the geologic medium itself. These processes of convection and conduction are analogous to solute transport mechanisms of advection and diffusion (Anderson, 2005). Groundwater temperature fluctuations are less variable than surface water and air temperature (Conant Jr, 2004). Because of this stability, temperature acts as a useful tracer for locating and characterizing groundwater and surface water interactions through temperature contrasts. Direct temperature measuring data loggers or infrared (IR) cameras may be used to measure these temperature differences (Constantz, 2008).

Stream and lakebed temperatures are a function of a heat transport balance from surface and groundwater temperature differences. In a discharge condition this is through conductive heat transport from overlying surface water, and upwelling groundwater convection. During recharge both convection and conduction will be downwards from infiltrating surface water (Conant Jr, 2004; Schmidt et al., 2007). Simple temperature measurements of stream water and streambed temperatures down to around 0.2-0.3 m below bed surface may allow for reasonable qualitative and quantitative estimation of groundwater fluxes, provided deeper groundwater temperatures are known or accurately estimated (Conant Jr, 2004).

Recent developments with infrared sensing technology and the advent of portable thermal imaging cameras have led to application of these technologies in locating groundwater discharge locations (Conant Jr, 2009, 2019; Deitchman et al., 2009; Pandey et al., 2013). Temperature contrasts between ground and surface water or between springs and nearby vegetation allow for visual detection of groundwater

discharge (Conant Jr, 2009, 2019). The greater the temperature differences, the easier this type of detection is. In summertime at midday when surface water temperatures are much warmer than groundwater, discharge can be highly visible by use of an IR camera. The opposite occurs in mid-winter when surface waters are much colder compared to groundwater (Conant Jr, 2009, 2019; Schmidt et al., 2007). This technology has proven useful when paired with a helicopter and a visual camera, allowing rapid characterization and identification of groundwater discharge locations for a large area (Conant Jr, 2009, 2019; Utting, 2012). In an area with little information about groundwater movements to surface water, this technology pairing is very promising to aid in selecting monitoring locations.

2.5.2 Geochemistry and Environmental Isotopes

2.5.2.1 Geochemistry

Inorganic ions in water can often be used as groundwater tracers. Solute concentrations in groundwater evolve as water flows and encounters differing lithologies (Hem, 1985). In most natural waters, the majority of salinity is composed of 7 species, Ca, Mg, Na, K, HCO_3, Cl and SO_4. Concentrations and proportions of these ions are largely controlled by lithology, water-rock interactions, flowpaths and residence time.

Initially, solute evolution begins with rain or snowfall, which contains atmospherically derived solutes (Herczeg & Edmunds, 2000). Near marine coasts, rainwater chemistry is often dominated by salts such as Na-Cl, but further inland tend to be dominated more by Ca-SO_4 (Herczeg & Edmunds, 2000). Interacting with geologic materials, waters then begin to reflect the dominant rock and soil types of an area as a result of weathering reactions and mineral dissolution. Addition of CO_2 from the atmosphere or degradation of organic matter or hydrocarbons forms carbonic acid that aids in dissolution of minerals and adds to dissolved inorganic carbon (DIC) concentration (Hem, 1985). High HCO_3 concentration in water samples is therefore not always associated with carbonate rocks but can indicate organic breakdown or redox reactions such as reduction of SO_4 (Hem, 1985; Herczeg & Edmunds, 2000). Shallow groundwater and surface runoff typically have had limited time to participate in weathering reactions. Surface runoff and flow through high hydraulic conductivity organic soils will limit the contact time with minerals and so the water will retain a similar chemical composition (of mostly inorganic ions) as the initial rainwater. Chemistry of shallow groundwaters in mineral soil are therefore often dominated by more soluble minerals such as calcite, dolomite and plagioclase, producing Ca-HCO_3 type waters (Herczeg & Edmunds, 2000; Jessen et al., 2014; Keller et al., 2010; Walter et al., 2017). Longer residence times or

flow through silicate rocks allow for less soluble silicate minerals to be dissolved, providing a source of additional ions and further geochemical evolution towards a Na-HCO_3 type (Hem, 1985; Walter et al., 2017). Ion exchanges, dissolution of evaporites or diffusion of connate seawater in clay soil or rock confining layers may lead to depletion of Ca and an increase in Na and Cl in groundwater. At greater depths, these processes dominate, pushing waters toward a Na-Cl composition (Herczeg & Edmunds, 2000; Walter et al., 2017).

Hydraulic connection between shallow and deep aquifers allows for mixing of groundwaters to occur. Ion compositions are often plotted on Piper diagrams, which allow basic geochemical endmembers to be established and provide visual indication of potential mixing. Of the major ions, Cl is the most conservative, participating in few reactions and being a constituent of many highly soluble minerals (Coplen et al., 2000; Hem, 1985). This makes it a good tracer in discerning mixing processes in groundwater, which typically ignores potential adsorption or reactions that may occur to change concentrations of other ions (Dyke et al., 2002; Herczeg & Edmunds, 2000).

Although not truly conservative, SO_4 ions may be assumed to behave conservatively if the water is saturated in its primary source mineral such as gypsum, and is under aerobic conditions which prevents SO_4 reduction (Hem, 1985; Herczeg & Edmunds, 2000). Hydrocarbon compounds may also act as tracers as they are mostly associated with deep reservoir fluids but are subject to biodegradation. Natural seeps of petroleum exist within the vicinity of the current study area, along the Mackenzie River (Babiy, 2013) and may act as tracers for deeper subpermafrost flow (Rudolph et al., 2016b).

2.5.2.2 Stable Isotopes of Oxygen and Hydrogen

Oxygen is known to have three stable isotopes and numerous unnaturally occurring radioactive isotopes, while hydrogen has two stable isotopes and one radioactive isotope. In isotope hydrology, the oxygen isotopes ^{18}O and ^{16}O and hydrogen isotopes ^{2}H and ^{1}H are commonly used to study the sources and flow dynamics of groundwater or surface waters (Clark & Fritz, 1997). These isotopes are typically expressed in delta (δ) notation, in units of permille (‰). This notation expresses the ratio of heavier (^{18}O and ^{2}H) isotopes to lighter isotopes (^{16}O and ^{1}H) that there are in a sample, over the same ratio in a standard (typically the Vienna Standard Mean Ocean Water or VSMOW). Globally, $\delta^{18}O$ and $\delta^{2}H$ in precipitation is controlled by moisture sources, topography, and latitude and longitude; typically, their values are higher in warmer regions and lower in colder regions. Measuring $\delta^{18}O$ and $\delta^{2}H$ in precipitation throughout a given year in a particular area forms a straight line when graphed, called the Local Meteoric Water Line

(LMWL) which is unique to a region. Precipitation $\delta^{18}O$ and $\delta^{2}H$ will vary seasonally and as such the precipitation source of groundwater within shallow groundwater flow systems may be recognizable by its $\delta^{18}O$ and $\delta^{2}H$ compared to a LMWL. Typically, snow will be more isotopically "light" (lower values, containing fewer heavy isotopes) and summer rains will be more isotopically "heavy" (higher values, containing more heavy isotopes). In many regions, LMWLs have been established through prior studies and data may be included in the Global Network of Isotopes in Precipitation (GNIP) database for a region near a study area.

A water sample that falls higher up the slope of the LMWL or is more isotopically heavy is generally composed mostly of summer precipitation that is also heavier. In contrast, water that is lower on the LMWL is more isotopically light and is often comprised of lighter sources such as snow (Clark & Fritz, 1997). Other conditions can produce isotopically light water can be contributors, however, which can make interpretations difficult without other lines of evidence. Old groundwater recharged during the past in a colder climate such as during the last glaciation or water recharged at a higher elevation can both be light isotopically (Clark & Fritz, 1997; Lacelle et al., 2014; Michel, 1986; Michel & Fritz, 1982). Some of this old water can be flowing through subpermafrost aquifers or potentially locked up as permafrost ice. Modern groundwater in shallow aquifers is often comprised of a mixture of light and heavy isotopic waters corresponding to the amounts of snow and rainwater that recharges the aquifer. Reflecting this mixture, the $\delta^{18}O$ and $\delta^{2}H$ of modern groundwater is often around the same value as that of the weighted mean precipitation for a region (isotope values normalized to amount of precipitation) (Clark & Fritz, 1997).

In surface water, evaporation of water from an open body of water causes selective enrichment of $\delta^{18}O$ and $\delta^{2}H$ values, and a deviation off the LMWL onto a Local Evaporative Line (LEL). The distance from the LMWL a that a sample falls along the LEL indicates the relative amount of evaporation that has occurred (Clark & Fritz, 1997). Groundwater with an evaporated signature suggests that the water has undergone evaporation from a shallow aquifer or was recharged by an evaporating water body (Clark & Fritz, 1997; Coplen et al., 2000). Weighted averages of $\delta^{18}O$ and $\delta^{2}H$ can be determined through direct measurements or by tracing the LEL back to where it intercepts the LMWL. However, weighted averages (and mean groundwater value) determined this way can be biased when selective recharge occurs primarily from one precipitation source (Clark & Fritz, 1997).

Water frozen as permafrost will contain the isotopic signature reflecting the climate it was formed in and also fractionation that occurs during freeze-up (Lacelle et al., 2014; Michel & Fritz, 1982). Michel & Fritz, (1982) noted that permafrost cores in their study area allowed a glimpse into climate and freezing history. Within the active zone, groundwaters maintained a signature similar to modern precipitation. Deeper within their core the authors observed very isotopically negative ice, formed during the last glaciation with a maximum shift from top to bottom of -11‰ $\delta^{18}O$ due to changes in climate.

2.5.2.3 Tritium

The radioactive isotope of hydrogen, ^{3}H, commonly referred to as tritium, is another routinely used tracer of the water molecule. With a half-life of 12.43 years, ^{3}H allows a relative or even absolute age constraint for young groundwater to be determined (Solomon & Cook, 2000). Tritium is often reported in Tritium Units (TU), in which 1 TU is equal to 1 tritium atom per 10^{18} Hydrogen (^{1}H) atoms. It is produced naturally in Earth's atmosphere, but nuclear power generation and atomic bomb testing also produces appreciable amounts of tritium. Cold War atomic bomb testing from the 1950's to 1960's led to considerable quantities of tritium production in the atmosphere, peaking in the 1960's. Levels of tritium have since decreased steadily since the bomb peak, but due to the prevalence of nuclear power generation and natural generation, atmospheric TU values can fluctuate wildly. Due to its short half-life, presence of a measurable amount of tritium in water provides an excellent indication of groundwater that has been recharged within the last 50-60 years (Clark & Fritz, 1997; Solomon & Cook, 2000). A more detailed, vertical profile of groundwater can be collected to better understand the chronological stratification in the groundwater, while also providing insight into infiltration and recharge rates (Clark & Fritz, 1997). TU values in groundwater >15 usually indicates water that still retains some of the bomb peak and so is likely close to 50 years old, while undetectable TU generally indicates water that is older than 50-60 years. Values in between may indicate modern water of a specific age or mixtures of paleogroundwater and modern groundwater (Clark & Fritz, 1997).

2.5.2.4 Strontium

Strontium is a metal with two useful stable isotopes for groundwater tracing from a specific aquifer unit or rock type, these being ^{87}Sr and ^{86}Sr. The atomic structure of strontium is similar to calcium, and strontium may bind itself in a mineral structure that typically accepts a calcium atom. The levels of ^{86}Sr have remained relatively constant throughout Earth's history while ^{87}Sr has increased from radioactive decay of

^{87}Rb. The ratio of these two isotopes, $^{87}Sr/^{86}Sr$, is often unique to a mineral at the time of formation and will increase over time with ^{87}Rb decay. The ratio of a mineral is therefore determined by its affinity to host rubidium in its crystal structure, which often substitutes for potassium. The most important ^{87}Sr bearing minerals are feldspars, micas and clay minerals; the latter two of which typically have high ratios due to their higher rubidium contents. Generally $^{87}Sr/^{86}Sr$ are low in carbonate minerals. (McNutt, 2000). In water samples, the ratio of $^{87}Sr/^{86}Sr$ is often determined in the dissolved strontium. Geologic materials will often contain a unique $^{87}Sr/^{86}Sr$ made of a weighted average of the $^{87}Sr/^{86}Sr$ of all the minerals in that material (Clark & Fritz 1997). Groundwater flowing through an aquifer will dissolve strontium from minerals within the rock, resulting in a specific $^{87}Sr/^{86}Sr$ of the dissolved strontium similar to the aquifer host material. Residence time is important, however, as minerals have varying solubilities and $^{87}Sr/^{86}Sr$ values. Eventually the water will come to equilibrium and share a similar $^{87}Sr/^{86}Sr$ as that of the whole rock, while continued dissolution will increase the concentration of strontium. Typically, carbonates will have low $^{87}Sr/^{86}Sr$ (less radiogenic signature) but high strontium concentrations while clastics will have intermediate to high (more radiogenic signature) $^{87}Sr/^{86}Sr$ and variable strontium concentrations (McNutt, 2000).

In unconsolidated sediments and soil, the use of $^{87}Sr/^{86}Sr$ ratios is more complex due to the higher variability in water flow paths and soil mineralogy; but typically, it will contain higher, more radiogenic $^{87}Sr/^{86}Sr$ and lower strontium concentrations compared to many rocks. This is due mainly to the short flowpaths and residence times that support dissolution of more soluble silicates with a higher $^{87}Sr/^{86}Sr$ which dominate over that derived from carbonates (Keller et al., 2010; McNutt, 2000; Shand et al., 2009). In surface waters, $^{87}Sr/^{86}Sr$ will depend on water sources as well as inputs from atmospheric and dust deposition and sediment weathering (Keller et al., 2010; McNutt, 2000). Runoff and very shallow groundwater signatures are typically higher in $^{87}Sr/^{86}Sr$ but with low strontium concentrations, and groundwaters have lower ratios but higher strontium concentration in general (McNutt, 2000). For these reasons, $^{87}Sr/^{86}Sr$ makes a unique tracer of groundwater sourced from a particular formation, if the ratio for the aquifer can be determined (McNutt, 2000). This makes it difficult to interpret strontium data without appropriate endmembers. Whole rock $^{87}Sr/^{86}Sr$ values can be determined for different aquifers and used to constrain endmembers. However, there is some evidence that rock ratios do not always match ratios of their groundwater exactly, but these can be used to assess potential upper and lower bounds of dissolved $^{87}Sr/^{86}Sr$ endmembers when water endmembers are unavailable (Frost & Toner, 2004). Rock age also is important to consider, as rates of continental weathering and crustal spreading rates have

caused $^{87}Sr/^{86}Sr$ levels to fluctuate. $^{87}Sr/^{86}Sr$ ratios in the Devonian were slightly higher than Cretaceous ratios for instance (Clark & Fritz, 1997; McNutt, 2000; Veizer, 1989). Strontium isotopes have been demonstrated to provide information about groundwater flow paths and mixing (Frost et al., 2002; Frost & Toner, 2004), groundwater/surface water interactions (Neumann & Dreiss, 1995) and more recently, as a tracer for tracking permafrost thaw (Keller et al., 2010). Compared to some other tracers, $^{87}Sr/^{86}Sr$ values do not evolve along a flowpath once equilibrium has been established with the aquifer material unless a different lithology is encountered, preserving that signature.

2.5.2.5 Carbon

Carbon isotopes are frequently used as tracers of groundwater flow paths and to infer sources of inorganic or organic carbon and can even be used to date residence time for groundwater (Clark & Fritz, 1997). Those used are primarily the stable ^{13}C and ^{12}C and radioactive ^{14}C isotopes. Stable carbon isotopes are expressed in similar notation as the stable isotopes of water, calculated as a measure of the ratio of the heavy to light isotopes in a sample over the same ratio in a standard.

$\delta^{13}C$ in dissolved inorganic carbon (DIC) is useful in determining whether the source of carbon was primarily from plant and microbial respiration or from carbonate mineral dissolution (Clark & Fritz, 1997; Utting et al., 2013). $\delta^{13}C$ in soil CO_2 is often quite negative (-24-30‰), while atmospheric $\delta^{13}C$ only slightly (-7‰) (Utting, 2012). Marine carbonates typically fall around 0‰ with evaporate minerals being slightly positive (10‰) (Clark & Fritz, 1997; Kresic & Stevanovic, 2010; Utting, 2012). CO_2 in recharge water will quickly take upon the values of soil CO_2, and remain relatively stable in an open system (Utting, 2012). As carbonic acid is consumed in carbonate weathering the $\delta^{13}C$ increases towards that of carbonate minerals (0‰). In an open system such as an unconfined aquifer where the water remains in relative equilibrium with soil CO_2 this approaches -15‰ to -18‰ (Clark & Fritz, 1997; Utting et al., 2013). Within closed systems such as confined aquifers further weathering may occur along the flowpath, pushing the values to around -12‰ (Utting, 2012; Utting et al., 2013). A closed system may be an aquifer confined by an aquitard or by permafrost (Utting, 2012).

Methane can also be utilized as a tracer by analyzing the $\delta^{13}C_{CH4}$, which will depend on the processes involved in its formation. Thermogenic methane is produced through thermal breakdown of hydrocarbons. This methane may migrate upwards as a gas or dissolved in groundwater (Grasby et al., 2016; Philp & Monaco, 2012). Biogenic methane is produced through the microbial breakdown of organic matter in water-logged soils or wetlands. These different processes fractionate $\delta^{13}C_{CH4}$ differently (Clark

et al., 2001; Philp & Monaco, 2012). Biologic degradation of organic matter preferentially breaks the weaker ^{12}C-^{12}C bonds, promoting isotopic depletion in biogenic gases. Thermogenic degradation also follows a similar preference for the weaker bonds, however with increasing maturity and longer timescales a higher proportion of ^{12}C-^{13}C bonds will be broken, increasing the $\delta^{13}C$ (Philp & Monaco, 2012). Biogenic $\delta^{13}C$ is often very isotopically light, between -80 to -42‰, while thermogenic methane is often higher at between -30 to -50‰ (Philp & Monaco, 2012). One caveat with interpreting thermogenic samples is the occurrence of methane oxidation, which leads to an increase in $\delta^{13}C_{CH4}$ values within the residual methane, as weaker bonds are broken in this reaction first. Care must be taken when interpreting samples from aerobic environments (Barker & Fritz, 1981).

Chapter 3
Study Area

The study area lies approximately 30 km south-southeast of the town of Norman Wells and 40 km northwest of Tulita, NWT within the CMV (Figure 1). Much of the CMV lies within the Sahtu Settlement Area, a land claim agreement which allocated the traditional 41,000 km^2 region to the Sahtu Dene First Nations and Metis People. Oil exploration and production has occurred in and around Norman Wells since the 1920s and has greatly expanded into the surrounding valley in recent decades (Babiy, 2013). Land and oil rights leases known as Exploration Licenses (EL) allow companies to explore for, develop and produce hydrocarbons under certain conditions and consultations. The study area encompasses the EL494 leased by Husky Oil Operations Ltd. (hereafter referred to as Husky), which until 2015 was conducting exploration activities. The Bogg Creek Watershed, a small tributary of the Mackenzie River sits within the Husky lease area and was chosen as the regional focus. This watershed drains around 190 km^2 of land, and many of the Husky exploration activities were situated within the watershed. This included construction and maintenance of infrastructure such as a large, gravel all-season road and several bridges that cross Bogg Creek and provide easy access to several lakes. This road divides the study area and provides unique access to the subwatershed. In partnership with Husky, this infrastructure was made available. Exploration activities also included completion of detailed hydrogeological and hydrological baseline monitoring by Husky. The baseline monitoring activities utilized a network of overburden and bedrock groundwater monitoring wells and permafrost monitoring thermistors, and surface water sampling locations. Baseline monitoring by Husky was performed as part of their annual permitting duties to determine baseline conditions and to detect potential changes caused by exploration activities. Monitoring wells were sampled in 2013 and again in 2019, prior to their removal, while thermistor data was downloaded every year until removal in 2019. Husky continues to conduct surface water sampling on an annual basis, providing historical data for stream geochemistry. Much of the data collected as part of the baseline monitoring program was made available for the current study by Husky, either directly or through public records. In addition, fieldwork for this study was formulated around the existing Husky monitoring strategy. This study will focus primarily on the area of the Bogg Creek Watershed (Figure 1) and other areas within EL494.

3.1 Physical Setting

3.1.1 Climate

The Sahtu region experiences a subarctic climate consisting of mild, short summers and long, cold winters, with an average yearly temperature of -5.7°C and annual precipitation of around 310 mm (Golder Associates, 2015). The spring freshet is reportedly the dominant driver of streamflow and groundwater recharge within the CMV (AMEC, 2013; Michel, 1986). Air temperatures (see Figure 2Figure 2) in Norman Wells have been increasing steadily since measurement began in the 1940s (Environment Canada, 2019). Additionally, 30-year monthly averages in precipitation (for years 1953-1982 and 1982-2011**,** Figure 3) show a small shift towards a lower summer precipitation and a greater proportion of average monthly precipitation falling as rain as opposed to snow (Environment Canada, 2018).

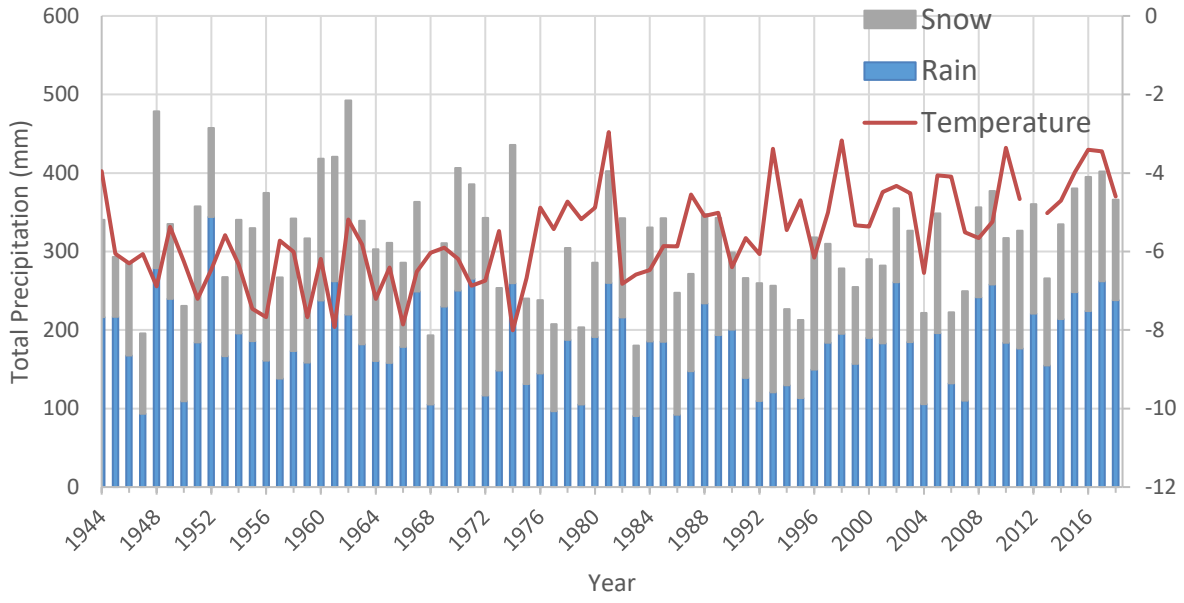

Figure 2: Average annual temperatures and precipitation for Norman Wells. Complete records began in 1944 and continue to the present day. Proportion of precipitation that falls as snow is shown in white and the proportion of rain is shown in blue. Data obtained from Environment Canada (2018).

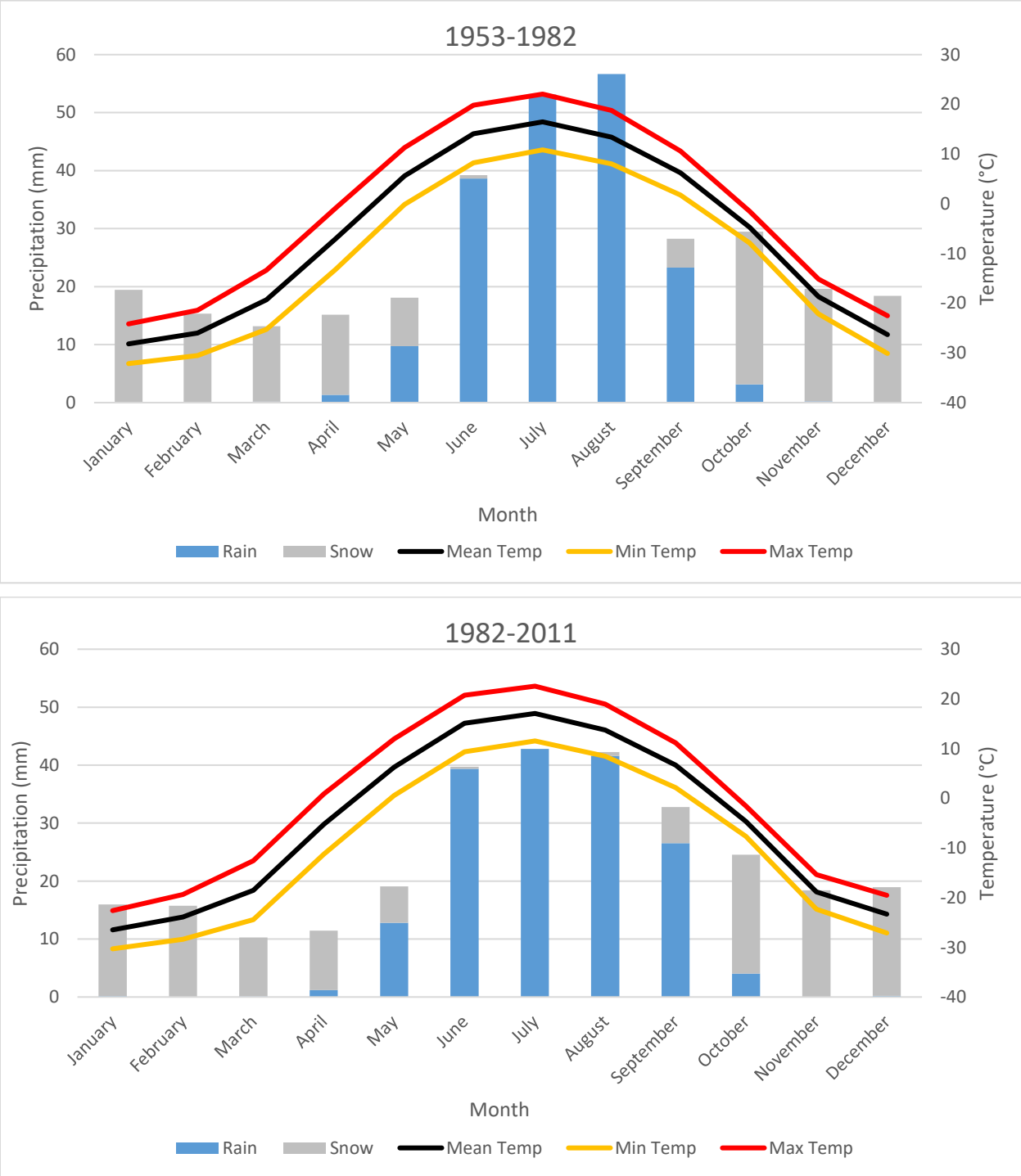

Figure 3: 30-year climate normals for Norman Wells, years 1953-1982 (top) and 1982-2011 (bottom) including minimum, maximum and average monthly temperatures and average monthly precipitation as a proportion of snow and rain. Data obtained from Environment Canada (2018).

3.1.2 Geology and Regional Hydrogeology

The study area mostly resides within the geological province of the Northern Foreland Belt. The Northern Foreland Belt is made up of three sedimentary basins, the Mackenzie Mountains in the west, the Franklin Mountains to the east and the Mackenzie Plains between the two (Golder Associates, 2015). Bedrock in the region consists of folded and faulted sedimentary rocks of Devonian to Cretaceous ages (Fallas & MacNaughton, 2014; Fallas et al., 2013; Maclean, 2012). Sequences of westward prograding sediments were deposited during several orogenic events, while warmer climates also promoted formation of limestone and evaporites. Through the Cretaceous to Tertiary, compressional deformation mainly caused flexure and folding as opposed to faulting, although many major faults do exist within the region. Many rock formations in the area are known to be petroleum bearing. Oil production in Norman Wells began in 1920 and continues to present day (Golder Associates, 2015; Hayes & Dunn, 2012).

The major structural feature in the area is a folded syncline in the south end of the study area (Figure 4). The southwestern limb of this syncline forms the foothills and northeastern margins of the Mackenzie Mountains, while the northeastern limb outcrops as the Franklin Mountains (Hayes & Dunn, 2012). The oldest formation in the study area is the Late Devonian aged shale and limestones of the Horn River Group. The Canol Formation member of this group is the primary target for unconventional oil and gas exploration in the area and lies approximately 1650 m below the ground surface in the study area (AMEC, 2013; Raska, 2017). Moving west lies the Late Devonian aged Imperial Formation (IF), a shale and mudstone unit with minor sandstones. An erosional unconformity marks the transition to the Early Cretaceous Martin House Formation (MHF), which consists of a beige, quartz sandstone and conglomerate unit (Hayes & Dunn, 2012; Maclean et al., 2015). This formation, also referred to as the Basal Cretaceous, has a potential to be an important, although thin, aquifer unit within the study area (Hayes & Dunn, 2012). Overlying this is the Arctic Red Formation (ARF), which consists of dark grey shale with minor siltstone and gypsum beds. The Late Cretaceous aged Slater River formation (SRF) is the thickest unit in the area, which consists of dark grey shale and siltstone with minor beds of muddy sandstone. The transition to this formation is marked by a substantial increase in radioactivity (Hayes & Dunn, 2012). The youngest formation in the study area is the Little Bear Formation (LBF), described primarily as a grey quartz or greenish-grey lithic wacke sandstone interbedded with siltstone (Fallas & MacNaughton, 2014; Fallas et al., 2013) This unit is the primary bedrock aquifer for many oil companies in the region, and forms the erosional resistant cap of the syncline in the southwest end of the study area (AMEC, 2013). Most of these units outcrop or subcrop near the Mackenzie Mountains along the western

limb of the syncline fold, as well as along the eastern limb within the study area. Potential for confined groundwater flow may also occur through fractures and coarser grained sections of major aquitard units such as the IF. Golder Associates, (2015) have proposed that recharged groundwater from the Franklin Mountains may flow westward to discharge in the Mackenzie Plains on the southwest side of the Mackenzie River.

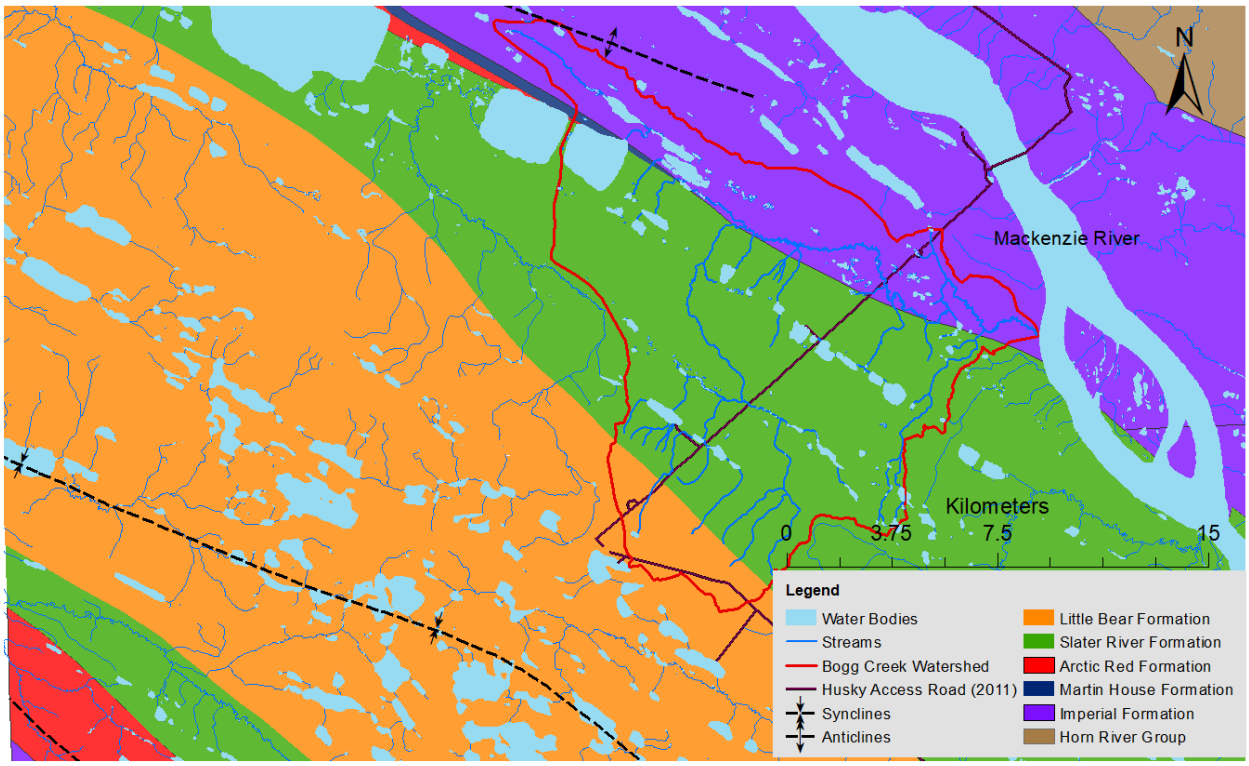

Figure 4: Bedrock geology of Bogg Creek and surrounding region. The major Twentyfive Mile Syncline lies to the west of the watershed. Geologic map obtained from Fallas & MacNaughton (2014).

Surficial geology of the area is primarily glacial in origin, mostly deposited during the Last Glacial Maximum. At least 2 glacial retreats and re-advances are recorded within 2 fine-grained till sheets in the region (Michel, 1986). During this time the Mackenzie Lobe of the Laurentide Ice Sheet converged towards the separate Cordilleran Ice Sheet along the Mackenzie Valley (Dyke, 2004). Much of the CMV was ice covered between 18 kya to 14 kya, with a slow convergence of the two ice sheets to the west near the Mackenzie Mountains. Within the CMV primary ice flow direction was towards the northwest, following the valley slope (Dyke, 2004). Ice began receding around 13 kya from the Cordilleran Ice Sheet margin and from high topographic areas, and by 12 kya ice was receding within the Mackenzie Valley

(Dyke, 2004). Isostatic depression caused by the weight of the ice formed glacial lake Mackenzie, which stretched 800 km from near Fort Simpson to Fort Good Hope (D. G. Smith, 1992). Pro-glacial silty lake deposits as well as ice-marginal sand and gravel were deposited within the lake. Braided rivers and channels draining the once glaciated Mackenzie Plain formed glacio-fluvial deposits, while deltas formed at the lake margins (Couch & Eyles, 2008). Along the lakeshore sand dunes developed from aeolian transport. A dune field resides to the northwest of the watershed, parallel to the Mackenzie River (Michaud & Bégin, 2001). While major sand dune deposits are not mapped in the Bogg Creek Watershed, some areas are covered by a thin veneer of sandy beach sediment, such as the north of the watershed (Côté et al., 2013). Exposures of glacial deposits can be found along sections of the creek. In Bogg Creek and surrounding area, surficial geology is primarily mapped as fine-grained till. Silts, fine sands and clays of glaciolacustrine origin and sands and gravels from modern alluvium can be found situated closer to the Mackenzie River (Figure **Error! Reference source not found.**5) (Côté et al., 2013). Glacial overburden thicknesses vary considerably in the area, generally thickening towards the Mackenzie River (Waterline Resources Inc., 2013a, 2013b). High water tables due to the fine grained sediment and permafrost have produced a continuous layer of peat and organic soil over much of the CMV (Golder Associates, 2015). A summary of regional aquifers and aquitards is presented in Table 1.

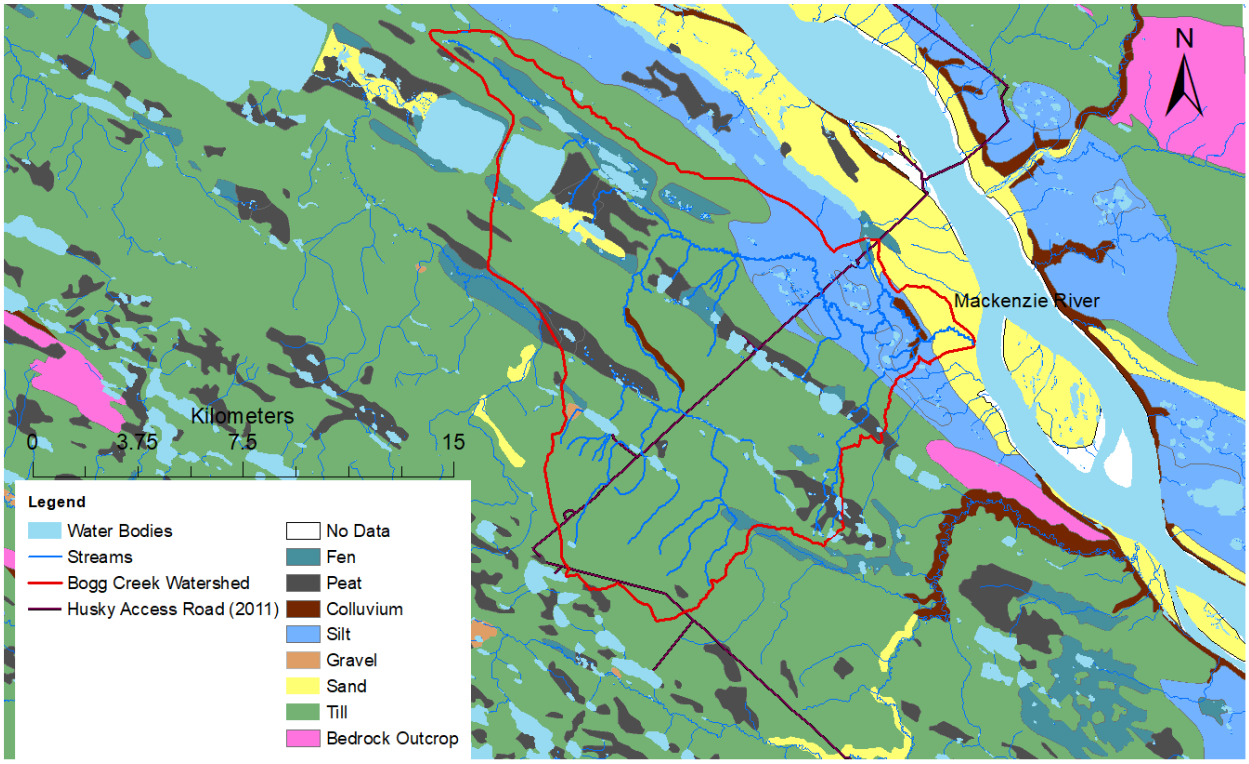

Figure 5: Surficial geology (primary material) of Bogg Creek and surrounding region. Geologic map obtained from Côté et al. (2013).

Table 1: Surficial and bedrock hydrostratigraphy summarized from Côté et al., 2013; Fallas & MacNaughton, 2014; Fallas et al., 2013; Raska, 2017; Waterline Resources Inc., 2013a.

Period		*Formation*	*Lithology*	*Local Thickness*	*Potential Hydrostratigraphic Unit*
Quaternary	Late	Bog, fen	Organics, peat	1-2.5 m	Variable
		Fluvial	Sand, silt, gravel	1-2m	Aquifer
		Colluvium	Boulders, gravel	N/A	Variable
		Glaciofluvial	Sand, gravel	N/A	Aquifer
		Glaciolacustrine	Silt, clay, sand	5-15 m	Variable
		Till	Various (clay to cobbles)	1-20 m	Variable
Unconformity					
Cretaceous	Late	Little Bear	Sandstone, mudstone, shale, coal	230	Aquifer, aquitard interlayers
		Slater River	Shale, mudstone, sandstone	616	Aquitard, aquifer interlayers
	Early	Arctic Red	Shale, mudstone	0-79	Aquitard
		Martin House/Basal Cretaceous	Sandstone, shale, mudstone	25.5	Aquifer, aquitard interlayers
Unconformity					
Devonian	Late	Imperial	Shale, siltstone, sandstone, limestone	193	Aquitard, aquifer interlayers
		Canol (Horn River Group)	Shale	230	Aquitard

Notes: Variable in regard to the Hydrostratigraphic Unit refers to the uncertainty of the local deposit composition, with coarser grained sediments or more porous organic soils units likely acting as aquifers and finer grained or less porous organics acting as aquitards. Units such as glaciolacustrine sediments or till may be comprised of a range of particle sizes and so may act as aquifers or aquitards in different local environments.

3.1.3 Hydrology

Bogg Creek and its lakes appear to be strongly controlled by bedrock structure. Many lakes are rectangular in shape and aligned roughly parallel to the strike direction of bedrock (northwest-southeast) as can be seen in Figure 4. Several strings of oriented lakes are found in the watershed and are often connected via channels, fens and creeks that form an orthogonal pattern. This drainage pattern is common in regions with folded and faulted sedimentary rocks, with major joint sets and bedding planes allowing for preferential erosional pathways that form a trellis-like drainage pattern (Twidale, 2004). This pattern is more pronounced in the headwaters and tributaries of Bogg Creek, with relatively straight, orthogonal reaches. This effect is also evident in the north of the watershed but becomes diminished in the east. Meandering of Bogg Creek increases with distance downstream considerably, and the stream begins to deviate from its orthogonal pattern (Figures 4 and 5). This is possibly due to increasing thickness of glacial overburden and a flattening of the land surface, diminishing the bedrock control on stream patterns. Permafrost limits drainage so peatlands and wetlands are a major feature on the landscape. Wetlands such as fens and bogs are common, and channel fens and tributaries act as major purveyors of surface water in addition to streams (Aylsworth & Kettles, 2001; Zoltai et al., 1988).

Previous hydrogeological work commissioned by Husky identified an upwards gradient between two of their bedrock wells, located on the northeastern limb of the syncline. Screened in two separate sandstone units of the Little Bear Formation and separated by a thick unit of shale, a pumping test also demonstrated that these two units were hydraulically connected. Hydraulic heads in these wells were also within 12 m of the ground surface, despite being screened 90-110 mbgs and below the permafrost base (Waterline Resources Inc., 2013b). Groundwater flow within the overburden has not been documented by Husky, although one shallow well was situated in a permafrost free zone and contained water (Waterline Resources, 2013a). References to springs in the Sahtu are also common. Although not reported within the Bogg Creek Watershed, there are springs that are documented as occurring to the southeast along the Little Bear River (Golder Associates, 2015).

3.1.4 Permafrost

In the Sahtu, the area is underlain by discontinuous permafrost (by definition, a zone is designated as discontinuous permafrost when permafrost underlies 30-90% of the land surface) (Golder Associates, 2015). Permafrost can typically be found 0.5 to 2 m below the ground surface and may be even deeper or absent around surface water bodies. Thicknesses of permafrost are typically about 5 to 45 m, while near

the town of Norman Wells permafrost as thick as 100 m was observed (S. L. Smith et al., 2017). Taliks are known to exist beneath water bodies in the region, with closed taliks residing below smaller lakes and streams and open taliks below large water bodies such as the Mackenzie River (Burgess & Smith, 2001, Taylor et al., 2001). One groundwater monitoring well, MW19B, was installed by Husky within a talik, with no permafrost encountered along the length of the borehole, about 9.9 m (Waterline Resources Inc, 2013a). This well was not situated near any major surface water bodies.

Chapter 4
Methods

4.1 Database and Map Creation

The creation of a Geographic Information System (GIS) and spreadsheet database was the first step in characterizing the surficial, topographical, and geologic conditions in the area to guide future field work. The database was compiled using several publicly available datasets of geographic and geologic features as well as geochemical data digitized into spreadsheets or GIS. All datasets were input into ArcMap v10.6 (ESRI) and projected into the NAD83 coordinate system, UTM Zone 9N. The watershed of Bogg Creek was delineated using a DEM and formed the basis of the area of focus. Husky monitoring site coordinates were imported into GIS. High-resolution satellite imagery was utilized from the ArcMap basemap feature at a resolution of 1 m. These maps provided geographical and geological context to develop a conceptual understanding of the study area. This in turn aided in fieldwork design, allowing for survey routes and ground sites to be established prior to visiting the study area.

Databases were also constructed using Microsoft Excel. Data provided by Husky included ground temperatures for 8 thermistor boreholes (years 2013-2019), groundwater levels and geochemistry for 3 monitoring wells (2013), as well as surface water geochemical data for 23 surface water monitoring sites (years 2012 to 2019). These points were spread across the Husky lease area and many fell within the watershed. These data also helped construct the conceptual understanding of the area by identifying areas that were potentially impacted by groundwater flow. These sites were explored further in this study and formed the basis for fieldwork. Additional data included long-term weather data from Norman Wells (1944-2011). For a full list of data descriptions and sources see Table A-1 (Appendix A).

4.2 Site Monitoring Strategy

As taliks act as hydraulic windows for subpermafrost groundwater to interact with the suprapermafrost system, the main goal of fieldwork was to find locations that could be accessed, sampled, and investigated for subpermafrost groundwater discharge. These sites could then become part of the baseline monitoring network and could potentially be monitored over several site visits in future work. A site monitoring strategy was implemented utilizing other datasets to narrow down the number of potential sampling sites to those that had evidence of groundwater discharge, or to expand on the current baseline monitoring network established by Husky. A screening process was also implemented in order to prioritize those sites

that had thermal anomalies tracked by IR and were accessible by helicopter. The majority of initial baseline monitoring sites were those previously established by Husky and therefore had several years of historical data associated with them. Of the 23 historical Husky sites, 7 were inside the Bogg Creek Watershed. These were considered priority over those that fell outside the watershed, and therefore would be sampled in more detail during fieldwork.

Monitoring wells, thermistor strings (installed with temperature sensors at various intervals below the ground surface) and test boreholes (locations that were drilled and logged but had no well installed) can be seen in Figure 6. These monitoring locations provided a glimpse into the groundwater flow system below the permafrost as well as provided information on local geology and permafrost conditions. The upwards hydraulic gradient measured in monitoring wells MW09A and MW09B suggested that groundwater may be flowing upward from subpermafrost aquifers in areas where the land surface was lower than the hydraulic head. This evidence of potential subpermafrost groundwater flow prompted the following monitoring strategy of examining bedrock geology and topography, noting general areas where springs might occur. These areas included breaks in slope, creek headwaters, or along bedrock contacts. Previous work by Glass, (2019) and Glass et al., (2020) identified areas where potential icings had formed, either recurring year after year or only sporadically. These icings represent possible groundwater discharge zones and so several individual and clustered icings were chosen as sites to explore further. These were incorporated into the list of potential sites to visit. In 2019, additional sites along Bogg Creek were chosen to improve the spatial resolution of longitudinal sampling along the main channel of the creek. Important aspects to consider were whether a site was accessible or not. To verify this, high-resolution satellite photos were used to identify places that were clear of large trees and potentially permit landing of a helicopter. Screening of these sites as well as identification of several new sites was accomplished through a low altitude aerial IR survey during the 2018 field season.

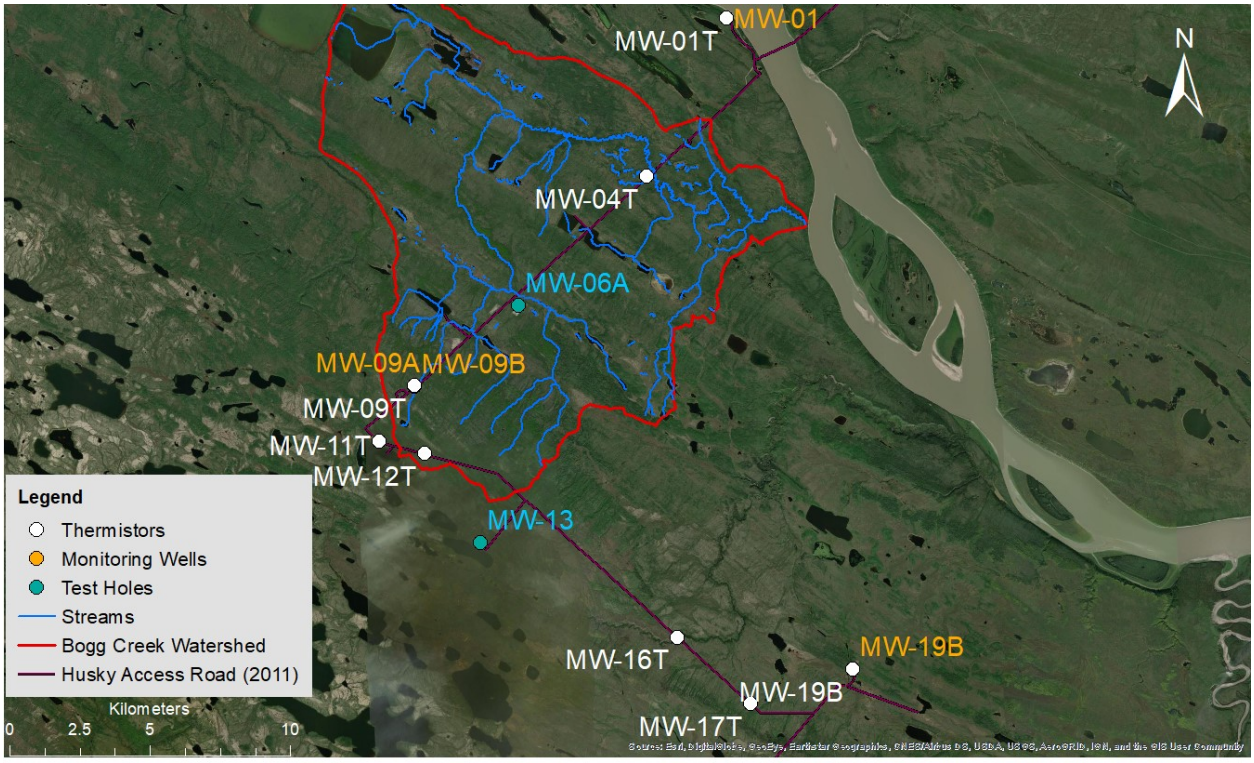

Figure 6: Monitoring wells, thermistors, and test holes within the study area. Air photo supplied by ESRI ArcGIS Basemap feature, 1 m resolution.

To investigate stream reaches, lakeshores and general areas where icings were noted to occur and those with a potential for spring activity, an aerial infrared/optical survey was conducted utilizing a helicopter-based system. This campaign was designed and undertaken by B. Conant Jr., a brief progress report of these activities can be found in Conant Jr. (2019). A FLIR Model T650sc thermal infrared camera (FLIR Systems Inc.) was used in conjunction with a Sony HDR-PJ430V camera to obtain imagery of ground temperatures over several traverses. To facilitate this, one side door of the helicopter was removed. Thermal anomalies would appear cold against the warmer surface water or surrounding vegetation. Individual times were recorded in a notebook every time a piece of equipment was turned on or off as well as anytime interesting anomalies were sighted. Continuous footage combined with a GPS logging system taking positions every second allowed for interesting sites to be located geographically by comparing video time stamps to the GPS logger or by the comparison of landmarks in footage and satellite photos. Several flight paths were prepared in advance and included a pass over the lower, middle, upper and headwater reaches of Bogg Creek, as well as over several lakes and sections of creek where

icings had been observed. Additional sampling locations selected in this way were identified as potential field sites to collect terrestrial data.

4.3 Collection of In-Situ Field Data and Water Samples

4.3.1 Field Sampling Strategy

The field sampling approach aimed at capturing evidence of groundwater discharge at each field site. This included direct observations, through hydraulic head or temperature measurements, or indirect evidence inferred through the presence of specific ions or isotopes in the surface water that may be linked to one or more known groundwater sources. To obtain a representative sample of potential groundwater discharge, shallow groundwater was collected either directly below or adjacent to the surface water at select sites using portable sampling tools. At each of the established Husky sites, surface water samples for water quality were collected by Husky personnel while isotope samples were collected by UW researchers. Groundwater samples were obtained at several of the Husky sites using the methods described below. At the sites additionally identified by UW as being locations of interest, groundwater would be sampled primarily but surface water, if present, was also sampled. Other data that would be collected at a site included hydraulic heads, ground temperatures, the depth to the permafrost table and in field water quality parameters such as temperature, electrical conductivity (EC), total dissolved solids (TDS), pH and dissolved oxygen (DO).

4.3.1.1 Water Sampling Protocols

Surface water sampling was conducted primarily by Husky personnel, and analyses were consistent between each location. These included metals, major ions and several organic compounds such as polycyclic aromatic hydrocarbons (PAHS), volatile organic compounds (VOCs), benzene, toluene, ethylbenzene and xylene (BTEX) and other hydrocarbons. Details about the sampling procedures are outlined in Husky Oil Operations (2017). In summary, a YSI Multiparameter Probe was used to measure EC, TDS, temperature, pH and DO, and grab samples of all analytes were taken from the shore. All water samples were kept in coolers and then submitted for analysis to ALS Ltd. in Edmonton, AB at the end of the day. These raw data (and data for subsequent years) were made available directly to UW by Husky in spreadsheet form. Water samples were collected from the Husky monitoring wells when they were first installed in 2013 and analyzed for the same analytes detailed above. These were collected by a submersible pump installed in the wells prior to their freezing. These data were retrieved from the

consultant's reports, Waterline Resources (2013a, 2013b). During the winter of 2019 these wells, now partially frozen, were thawed out and resampled by Waterline Resources prior to their decommissioning. These data were provided directly to UW by Husky and their consultants.

Analyses performed by UW personnel included isotopes, ($\delta^{18}O$ and $\delta^{2}H$, ^{3}H, $^{87}Sr/^{86}Sr$ and $\delta^{13}C$ in CH_4) major ions, BTEX and methane. Samples were taken from both surface water and groundwater, although major ion and BTEX concentrations in some surface water bodies were provided by Husky to reduce redundancy of duplicate sampling at Husky monitoring locations. Duplicates of major ions and BTEX were taken randomly from surface water. Isotope samples were collected from surface water by UW, following procedures outlined in Clark & Fritz, (1997) and by the UW Environmental Isotope Lab (EIL). All sample bottles were provided by ALS Ltd. in Yellowknife, NWT. Metals and Strontium isotopes were filtered within 12 hours of collection by 0.45 µm membrane syringe filters and preserved with 1 mL 1:4 nitric acid. All samples of volatile compounds or evaporation sensitive isotopes were collected with zero-headspace. Samples were stored in coolers kept to about 4°C in the field and refrigerated upon returning from the field. Samples for ion concentrations were sent either by Husky or Waterloo, depending on who collected them, to ALS Ltd in Edmonton. Isotope samples were collected by Waterloo and were analyzed at the EIL at the University of Waterloo. For a summary of samples taken see Appendix A Table A-2 and for protocols and sample bottles see Table A-3.

4.3.1.2 Groundwater Sampling Methods

Shallow groundwater sampling was conducted through the use of simple and portable tools, namely the PushPoint "Henry" Sampler (MHE Products Ltd.) or pre-constructed mini-piezometers. These devices could be used to not only take subsurface water samples but could also be used to obtain hydraulic head measurements. Shallow groundwater was taken opportunistically at the Husky sites and was almost always attempted at sites identified by UW.

The PushPoint Sampler is a small drivepoint piezometer designed for taking groundwater samples from the shallow subsurface or below surface water bodies with only occasional need for additional equipment such as handheld hammers (Figure 7). It consists of stainless-steel tubing with a narrow drive-point tip and slotted screen at one end, and a small, welded handle and sampling port on the other. An inner rod remains inside the sampler during insertion to minimize the amount of formation material entering the screen and to provide stability to the sampler walls. This rod is then removed prior to sample collection. Three lengths of sampler were ordered directly from MHE Products (62 cm, 124 cm and 184 cm). In soft

sediments the 62 cm and 124 cm probes could be inserted into the ground by hand easily, while the longer 184 cm probe might require the use of a mallet due to its larger diameter construction. Once the inner rod is removed, groundwater level measurements could be taken using a narrow diameter water level tape. For collection of a groundwater sample, ¼" inner diameter (ID) plastic tubing was attached to the sampling port at the top of the device and a syringe or vacuum pump were used to extract water. The vacuum pump was attached to two 250 mL Erlenmeyer flasks to collect the sample and prevent water from entering the pump. Rubber stoppers in the top of the flasks were drilled with two holes and rigid ¼" outer diameter (OD) tubing was used to connect each flask. The secondary hole would then allow for extra tubing to extend from the flasks and be connected to the vacuum pump and the sampler with flexible tubing. After obtaining water samples the sampler was removed by hand, leaving only a small hole behind. Each sampler would be cleaned of sediment after each use. The PushPoint samplers are limited in their utility somewhat by their small diameter and small slotted screen, and so obtaining large volumes of water for all the sampling requirements can be time consuming. As well, the screens have a tendency to clog in fine grained sediments, so the use of an outside mesh screen was pertinent to reduce clogging.

Figure 7: Photos of the PushPoint sampler unit showing positive hydraulic head at a discharge location (left) and using a syringe to obtain samples below surface water (right). Photo on the left was taken by Brewster Conant Jr.

Mini-piezometers were used in locations where the PushPoint sampler would easily clog or where a higher volume of sample was needed. The pre-constructed mini-piezometers consisted of small mesh screens wrapped around polyethylene tubing (3/8" OD) that had been notched to allow for water entry. The tips averaged 10 cm in length and were connected to a smaller ¼" OD tubing cut to the desired depth of installation (Lee & Cherry, 1979). The mini-piezometer would be installed in sediments by manually driving a ½" steel pipe with an expendable tip to the desired depth. The pipe functions as a temporary access tube to permit the installation of the mini-piezometer and is subsequently removed from the ground, exposing the mini-piezometer tip. Groundwater samples were collected from the mini-piezometer by connecting a syringe or vacuum pump, to the ¼" diameter plastic tube and groundwater levels were measured using a small diameter Solinst P4 Model 102 water level tape.

Under artesian conditions, hydraulic heads in both the PushPoint sampler and the mini-piezometer could be measured simply by allowing for the water to climb the clear tubing and then measuring this height. Water quality parameters were measured on the groundwater samples in the field with an Oakton CON 150 Portable Conductivity Meter, or a YSI Professional Plus Multiparameter Probe by partially filling a sample bottle and submerging the probe. The main parameters of concern were EC, TDS and temperature.

4.3.1.3 Shallow Permafrost Depths and Ground/Bed Temperatures

Permafrost depths (depth to the permafrost table) were measured using either a graduated steel probe or a PushPoint Sampler manually pushed into the subsurface in conjunction with a tape measure. The steel probe was custom built by research colleagues at Wilfrid Laurier University (WLU) and consisted of a square steel rod 1.5 m in length with welded handle and engravings demarcating every 10 cm. Because of the length limitation on the permafrost probe, permafrost depths of greater than 1.5 m could not be determined. Where feasible, the depth to the permafrost table was also measured below surface water features like streams and lakes, and several meters away from the water's edge. The larger PushPoint Sampler (184 cm, obtained in 2019) could also be used for this purpose.

Ground and streambed temperatures were measured using an Oakton Temp-14 Thermistor Thermometer. The thermistor cable was housed within an aluminum rod assembly constructed by UW personnel for insertion into streambeds, and markings were placed every 10 cm along the rod. The rod would be driven into the bed to a maximum depth of 1 m by a steel mallet, or if the ground was soft enough, by hand. Temperature measurements were taken every 20 cm to the maximum depth of 1 m.

4.3.2 Field Data Collection Campaigns

4.3.2.1 2018 Summer Field Campaign

Initial field data were collected over 5 days in late August 2018. During the first 3 days the 23 Husky sites within and around the Bogg Creek Watershed were sampled with Husky personnel as part of their annual monitoring activities. Water samples were collected by Husky and UW personnel and submitted for chemical and isotope analysis. Analysis performed by Husky included metals, major ions and several organic compounds such as PAHS, VOCs, BTEX and other hydrocarbons. Analysis by UW also included major ions and metals and BTEX as well as isotopes ($\delta^{18}O$ and $\delta^{2}H$, ^{3}H, $^{87}Sr/^{86}Sr$ and $\delta^{13}C$ in CH_4), and methane at selected sites from surface water or shallow groundwater. Sample locations within the study area can be seen in Figure 8**.**

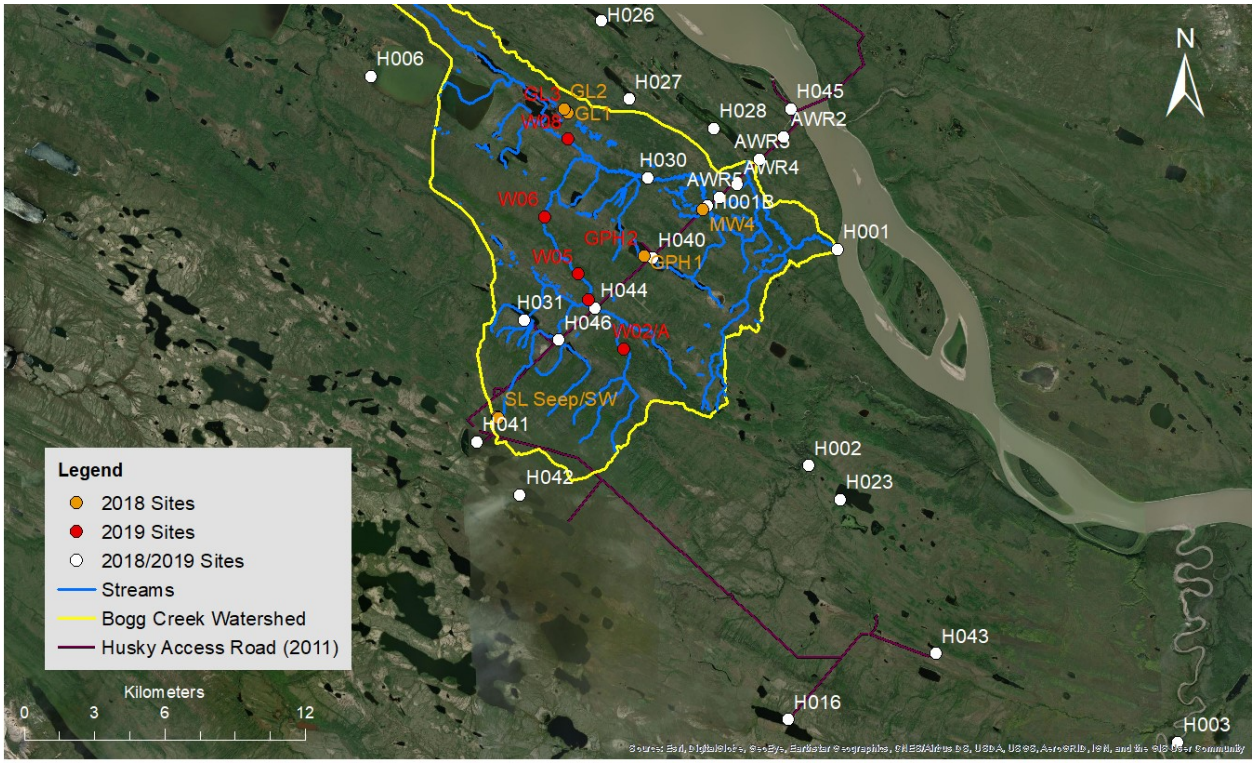

Figure 8: Regional map of sampling sites taken in the study area for each year. Satellite photos provided as part of the ArcGIS basemap feature, 1 m resolution.

The last 2 days consisted of visiting identified icings and temperature anomalies as well as revisiting creek sites for additional data collection. Data collected included that outlined above from surface and groundwater at the other field sites. These additional sample locations were guided based on icing

coordinate data provided by Glass et al., (2020) and from the infrared camera survey performed on August 28, 2018 (Conant Jr., 2019). A subset of the thermal anomalies that were identified were visited by helicopter to confirm groundwater discharge conditions and to collect samples. Discharge was established through the measurement of hydraulic gradient between the groundwater level measured at approximately 1 m below the ground surface and the surface water level.

At the icing and seep locations a sample was taken from ponded water in the vicinity and from 1 m below the ground surface using the PushPoint Sampler. Collection volume was limited however, especially in silty or clayey materials, with a tendency for the screen to clog up.

Two drive-point piezometers (DPP), one PVC 1" ID schedule 40 with 10 slot screen installed in a stream bed and one steel one at a cleared monitoring pad within the study area. The PVC DPP and a stilling well placed in the stream for surface water level monitoring were installed into the streambed of Bogg Creek near H001B (Figure 9). Both the DPP and stilling well were outfitted with an electronic level logging device and the instruments were left for 48 hours to record data. Hydraulic head did not completely stabilize in the DPP over this time period. The steel DPP was manually driven into fine grained sediment within the monitoring pad site (MW04 GW, Figure 9) to a depth of approximately 2 m. The piezometer did not yield any water after the installation, presumably because the screen was clogged with clay and silt. An alternative approach was attempted at the monitoring pad site that did yield water. A mini-piezometer was installed to a depth of around 1 m and a groundwater sample was collected from this device.

4.3.2.2 2019 Winter Data Collection

During February 2019, Husky and their consultants, Waterline Resources Inc. decommissioned the existing monitoring and groundwater production wells. Monitoring wells MW09A and MW09B were thawed out during this time and resampled. Analyses included the standard inorganic and organic analytes collected by Husky outlined in previous sections as well as the isotope suite and methane. Husky and their consultants also revisited some of the surface water sampling locations to collect samples for the current study. These surface water samples underwent the same analyses as in summer 2018 campaign. As each of the surface water sampling locations was iced over at this time an ice-auger was used to access water below and samples were collected. For the summary of the samples collected in winter see Table A-2.

4.3.2.3 2019 Summer Data Collection

The final fieldwork program took place late in August, 2019. This campaign aimed at obtaining permafrost cores, expanding the number of surface water monitoring locations along Bogg Creek and its tributaries and revisiting potential spring locations for additional monitoring.

Travelling with Husky personnel, 27 surface water locations were visited, with stable water isotope samples being obtained from 14 of them. Samples for ^{87}Sr were obtained from locations within the Bogg Creek Watershed during this time as well. Along Bogg Creek, 6 new samples were taken to investigate the surface water evolution along the length of the water course. Springs identified during the previous year's field work at GL1 and GPH (Figure 9) were also revisited to obtain duplicate samples and to attempt to take a geochemical profile from several depths with the PushPoint Sampler. GL1 and GL2 could not be sampled and so a new location, GL3 was chosen. At this spring site, an electromagnetic induction survey was also carried out across the area. This was performed using a Geonics EM-38 unit, which measures the electrical conductivity of the ground with a coil spacing of 1 m and penetration depths of 0.4 to 1.5 m (horizontal dipole and vertical dipole, respectively). Measurements in horizontal and vertical dipole were obtained over a horizontal distance of 135 m.

4.3.2.4 Permafrost Coring and Porewater Extraction

Permafrost coring was performed using a modified Stihl gas powered auger and 2" coring system borrowed from the Northwest Territories Geological Survey. Coring was performed and overseen by J. Paul from Wilfrid Laurier University. The auger was progressively advanced into the ground by 10-20 cm increments resulting in a small, free standing core sample being exposed in the bore hole. A separate core barrel on the end of a long metal rod was then placed into the hole over the core and maneuvered around until the core detached from the frozen ground. The core sample was subsequently removed from the bore hole before progressing to the next sampling increment. Approximately 2 m long cores were taken from two locations near the MW04T and H040 field sites (Figure 8). A duplicate core was also collected at the H040 site about 1 m from the original core. The cores were visually logged for geologic and permafrost characteristics and subsequently bagged with zip-top plastic bags and placed in a cooler with ice packs. The core samples were then kept frozen and transported to the University of Waterloo.

Sample preparation in the laboratory after shipping and placement into a freezer, consisted of resealing the permafrost cores into new plastic zip-top bags, which were wrapped tightly around the core to minimize evaporation. As much excess air was removed as possible by squeezing the bag, which was then

placed inside another closed plastic bag to prevent leaks. Several core sections would then be left to sit out at room temperature for 18-24 hours or until completely thawed. Water from the core sections was sampled the same day as they were thawed.

Porewater was extracted from the thawed core samples of the permafrost soils using methods similarly outlined in Moncur et al., (2013). This method utilizes a hydraulic jack and custom-built squeezing tubes to contain the core and allow for sampling with a syringe. Thawed cores were placed into thin walled (0.127 cm) 5.1 cm diameter aluminum tubes that were custom fit to house the thawed core, as well as a piston, a filter disc and a collection base. The piston, filter and base were all constructed of nylon rod that were machined to house a rubber O-ring for a tighter seal in the tube. As cores were not necessarily uniform in length, each tube had to be pre-cut to the correct length to accommodate the core. This differs from the method outlined in the paper, where cores are already contained within aluminum tubing due to the coring method. After cutting each tube, the edges of each tube opening were flared out slightly and any burrs filed away in order to allow for easier insertion of the pieces and prevent scraping of the O-ring. The tubes were then scrubbed in soapy water with a bottle brush, then rinsed with DI water and allowed to dry.

Assembly of the squeezing tubes started with insertion of the filter disc, after which a small 5 cm diameter membrane filters (0.45μm) was placed on the bottom of the filter disc. Next, the collection base would be placed into the tube so that the filter paper was tightly sandwiched between the disc and base. Electrical and Teflon tape was wrapped around the inside of the base to provide a better internal seal, while Teflon tape worked to seal the space between the outside of the tube and the base. Insertion into the tube often required a hammer for assembly and disassembly and also ensured that there was a tight seal between the tube and O-ring. A small rubber septum was inserted into the collection port that was machined into the base. A second membrane filter was added to the top of the filter disc and the unfrozen core was placed directly in after. The membrane filter not only acted to provide a cleaner, pre-filtered water sample but also prevented core material from plugging the holes in the filter disc. Lastly, the piston was inserted into the top and placed into the jack assembly.

The hydraulic jack was placed within a housing that contained a sliding aluminum plate on the bottom and plate that was secured with nuts at the top. Plastic rods of about 15-40 cm were then used to drive the piston into the core barrel. The jack would push the lower plate up and force the plastic rod and piston to move further into the tube, causing compression of the sample. A 30 mL syringe was used with 18-gauge

needles to pierce the septum and apply vacuum, allowing the sample water to enter. The syringe was removed approximately every 5 minutes in order to add the water to a sample bottle and reapply the vacuum. Three to four pumps of the jack were applied every 5-15 minutes depending on the material: organics such as peat could be pumped more quickly than clays could. This procedure continued until the core became hard to squeeze any further or enough water had been collected. Squeezed water was filtered again through 0.45 μm syringe filters to remove any organics or material that had made it through the pre-filters and placed into sample bottles. Similar protocols for field sampling were used in the collection of these porewaters, including adding of preservatives. Cores were analyzed for major and minor ions as well as stable water isotopes. One peat sample from the H040 site was analyzed for $^{87}Sr/^{86}Sr$.

4.4 Data Visualization

Geochemical data were plotted in various ways to examine relationships and assist in interpretations. Major ions in water samples were used to construct Piper plots in a specialized Excel file created by the Nevada United States Geological Survey (USGS) and provided online in the Excel for Hydrology Package. This program converts raw mass concentrations of the 8 major ions plus fluoride (F) to a molar ratio and from there into a coordinate corresponding to a position on a Piper diagram. This allows comparisons between the major cations and anions to be drawn easily and waters to be characterized by type. Piper diagrams were constructed for all data collected inside the watershed. Other plots were constructed in Excel to demonstrate relationships of various geochemical constituents or isotopes in site waters. $\delta^{18}O$ and $\delta^{2}H$ plots included a LMWL taken from van Everdingen (1982). $^{87}Sr/^{86}Sr$ was plotted against the reciprocal of Sr concentration (1/Sr), which flattens mixing lines and allows for easier visualization.

A geologic cross-section was built along the all-weather road (AWR) (Figure 9) using the British Geological Survey's (BGS) Groundhog© Desktop software and CorelDraw (Corel). In constructing the cross section both the geological map and a pre-constructed regional cross-section (Kalo Stantec Ltd., 2014) that covered a larger area were used to guide placement of major subcrops and inform the general shape of folds. Several Husky wells were also used. One conflicting difference between the map and the cross-section was the complete absence of the MHF and ARF in the geologic map, which was present in the cross-section. Since the regional cross-section was more recently constructed using Husky seismic data, the decision was made to include these formations in the AWR cross-section. Size and thicknesses of the formations were guided by monitoring and exploration well data from Husky as well as the Kalo-

Stantec regional cross-section. Surficial geology was interpreted in a similar way, first using formation contacts directly from the surficial geology map and refined with monitoring well and seismic shothole data (I. R. Smith, 2015). Seismic shotholes provided a rough estimation of overburden thicknesses in areas with little monitoring well coverage but were not used to make decisions about lithology. The reason for this is that lithology descriptions in shotholes were inconsistent and lacked important details such as a lack of depth information about where materials began and ended. Many descriptions were often lumped together within a large interval of 5-15 m including bedrock and overburden. Future conceptual models or cross-sections may wish to use these data in a more rigorous fashion, such as ranking hole logs based on their description accuracy and eliminating poorer quality logs.

Chapter 5

Results and Interpretation

5.1 Locating Groundwater Monitoring Sites

Maps of the study area and important sites are shown in Figures 9 and 10 below.

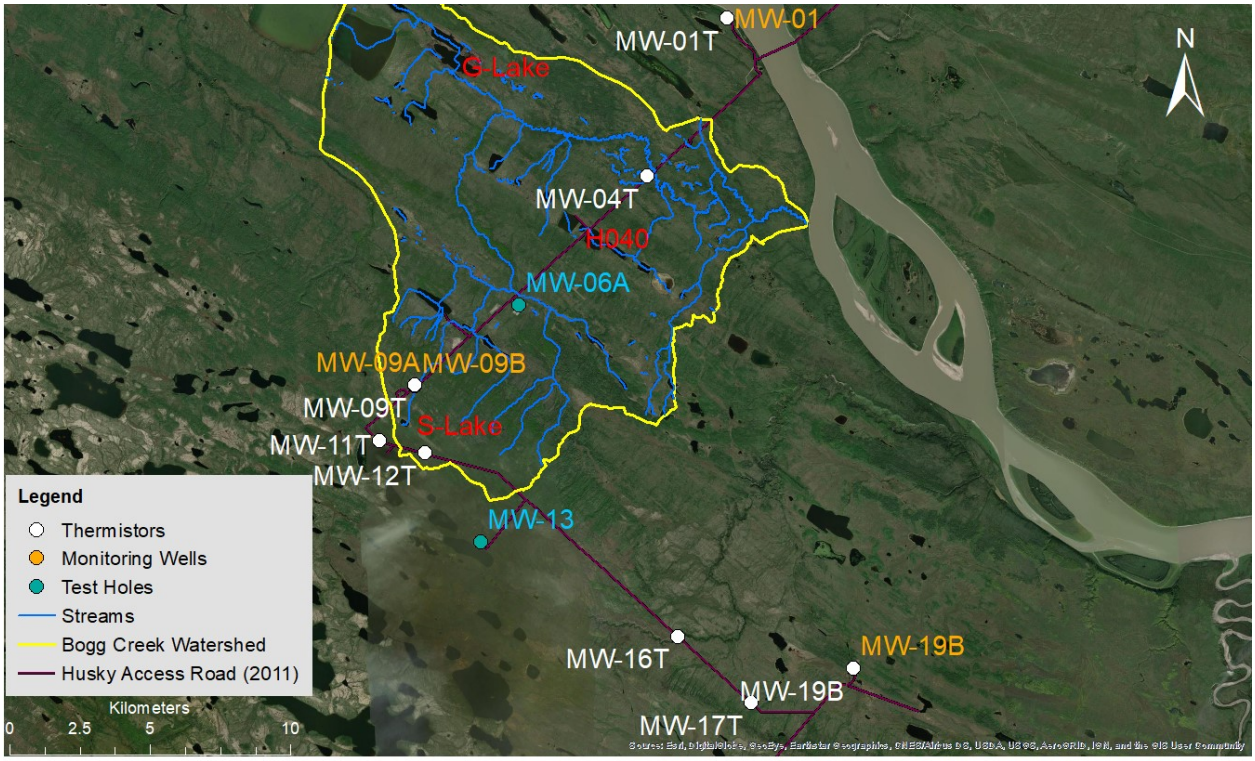

Figure 9: Map of groundwater and temperature monitoring wells as well as test holes within the study area. Key sites are labelled in red (G-Lake/GL, S-Lake/SL, and H040). Sample locations for deep subpermafrost groundwater from the MHF are not in this area and so are not shown.

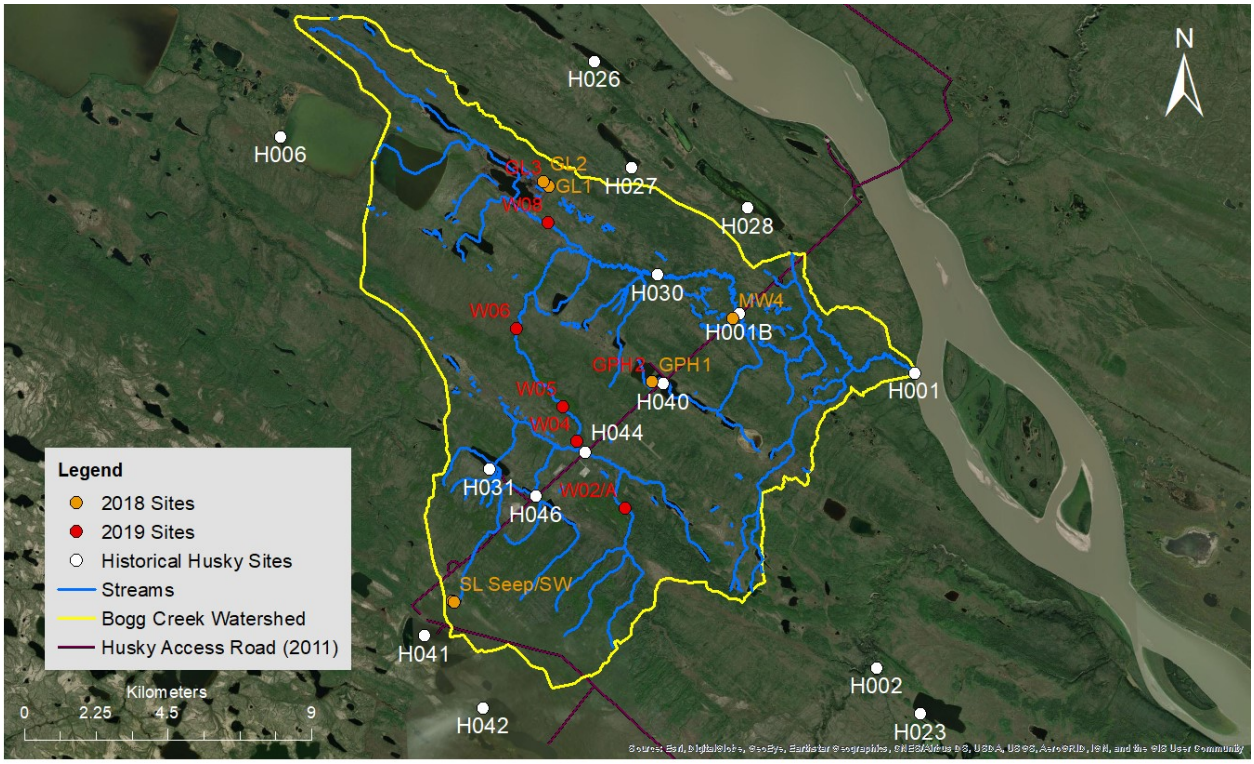

Figure 10: Surface water and spring sampling locations for 2018 and 2019 are shown in orange and red, respectively, while historical Husky sites are shown in white. Some Husky sites (namely those located at small culverts that were not analyzed for this study) are omitted on this map. Also note that some locations overlap with one another at this scale, such as GPH1/2, GL1/2/3 and W02/A.

5.1.1 Preliminary Site Selection

Initial site selection utilized the geologic maps and DEM of the study area to find areas where springs could be likely to occur. The geologic contact between the sandstone rich Little Bear Formation (LBF) and shale rich Slater River Formation (SRF) occurs near the bottom slope of a subtle ridge formed at the center of the regional syncline. This ridge is formed almost entirely by the LBF (see Figure 4 between contact of LBF and SRF near MW09A and MW09B). Hydraulic head measurements of the MW09A and MW09B monitoring wells in 2013 revealed that the water was under a small upwards gradient of about 4.0×10^{-3}, rising to about 10-12 mbgs. Where the hydraulic head is greater than the land surface elevation, such as might occur downslope from the terrace, it is possible this deeper groundwater may discharge through taliks. The slope of the terrace is also where many of Bogg Creek's headwaters originate, either at the top or bottom of this slope. The possibility of these headwaters to be spring-fed by discharging groundwater lead these headwaters areas to be selected for additional surveying using the IR camera

system (see Section 5.1.2). One lake that appeared as a source for one of these headwater streams was identified on the south end of the watershed and was selected for further surveying. This lake was referred to as S-Lake for the purposes of this study (Figure 9). Other sections of Bogg Creek were chosen for surveying, such as the lower reaches and upper tributaries, particularly reaches where icings were observed to occur.

Icings were also identified occurring in clusters in some regions (Glass et al., 2020). Several clusters of recurring icings appeared near a group of lakes connected by channels and wetlands (Figure 12). This lake complex is referred to as G-Lake for the purposes of this study. The position of G-Lake in the northern portion of the watershed places it between two geologic features of interest, these being the contacts between the Martin House Formation (MHF) aquifer and Imperial Formation (IF) aquitard to the south, and an anticlinal ridge formed to the north of the lake. This lake and its surrounding wetlands were chosen for IR surveys to look for any evidence of discharging water that could be the source of the icings.

The linear string of lakes located roughly in the center of the watershed was also identified as possibly following a natural lineation of the underlying geology as they were oriented along a similar strike direction as the geologic contacts. It was therefore reasoned that these lakes could be receiving groundwater through a fault or other lineation. Icings also appeared along the edges of some of the lakes. One site chosen for surveying was already being monitored by Husky (H040) (Figure 10), and another, referred to as GPH (Figure 10), was identified during the IR survey. S-Lake was chosen in the southwest portion of the watershed as there was the possibility for groundwater exchange to occur there from the LBF.

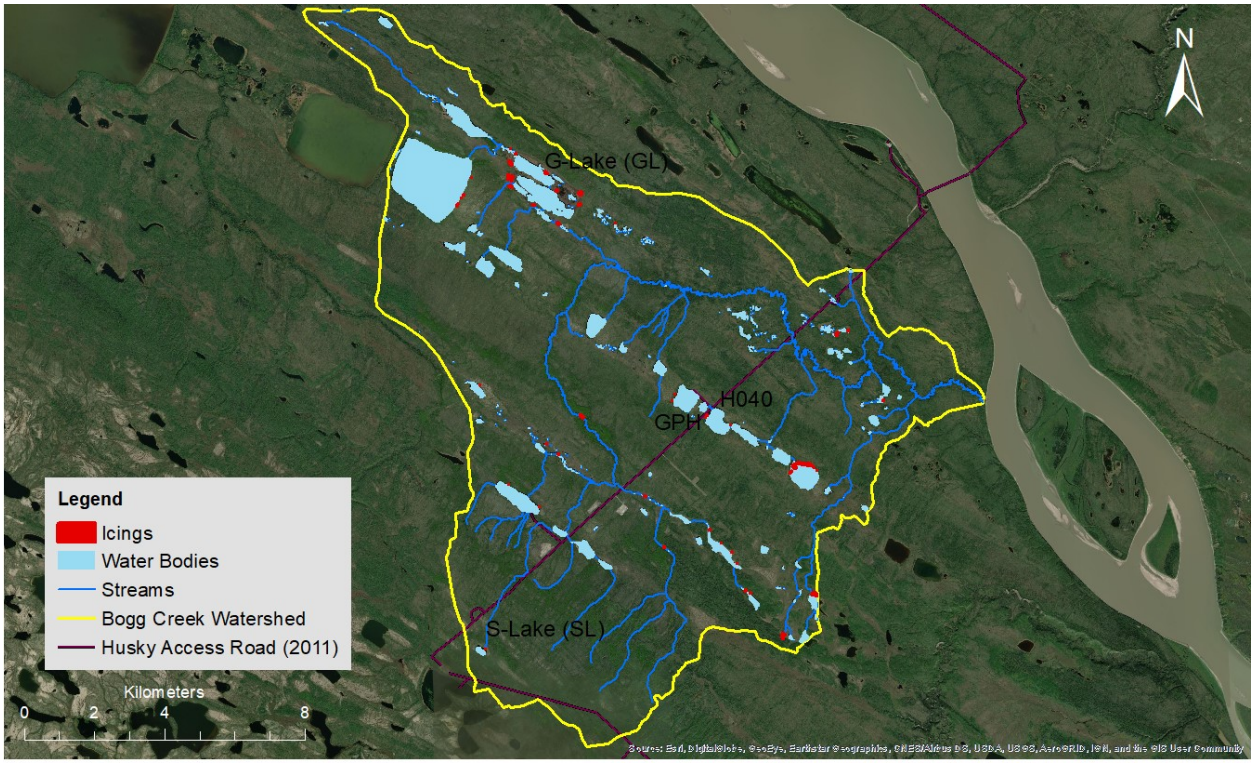

Figure 11: Map of study area and icings from 2016-2017. Note that icings are enlarged to show locations and are not representative of the actual area covered by these icings as determined by Glass et al., (2020).

5.1.2 IR Camera Survey

The airborne IR and visual camera surveys were performed along the headwaters, middle and lower reaches of Bogg Creek as well as along the edges of several lakes (Conant Jr., 2019). The IR camera picked out areas of colder surface conditions or thermal anomalies among the warmer land surface vegetation, which were anticipated to represent the discharge of cold groundwater. As noted above, these temperature anomalies assisted in the successful location of groundwater discharge points within the study area (e.g., the G-Lake or GL sites). Often anomalies appeared individually, as a cluster of well-formed points, and as large formless bodies and channels (Figure 12).

A.

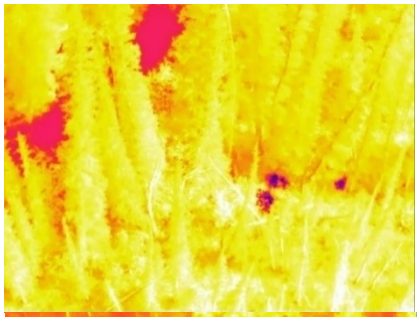

B.

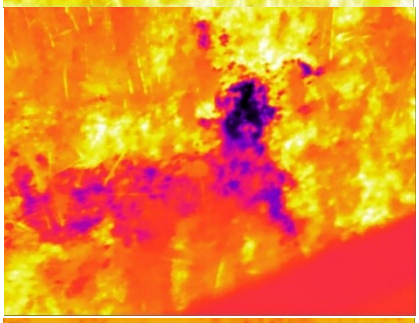

C.

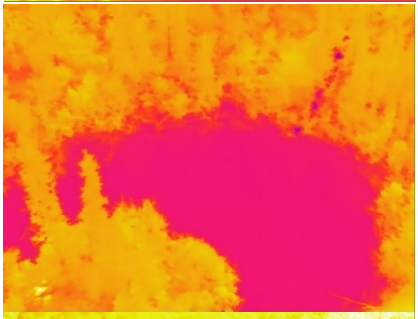

D.

E.

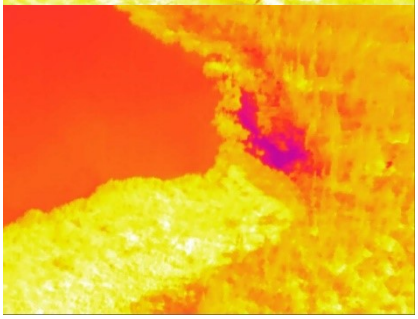

Figure 12: IR and visual imagery from the aerial IR survey for: A): Lower reach of Bogg Creek. B): Near H044 along a seismic line. C): Small channel draining to Bogg Creek. D): Thermal anomalies at GL, two springs appear red, with various animal tracks throughout. E): Pool next to a lake where GPH was draining to. Colour ramp proceeds from white (hot) to yellow (warm) to red (cool) to blue (cold). (From, Conant Jr., 2019).

Although it was possible to confirm groundwater discharge conditions at some of the locations on the thermal anomalies, the anomalies may not always be associated with locations of deeper groundwater discharge associated with a regional flow system but can represent cooler discharges of shallow groundwater related to recent interflow or shallow seepage. Shallow water temperature can be influenced by the cooling presence of the permafrost table as well. For example, one thermal anomaly (site SL) appeared geochemically as mostly dilute runoff or possibly active layer interflow rather than more mineralized water as would be anticipated for deeper groundwater discharge as discussed in more detail below. As such, ground-truthing is required in order to confirm the origin of the anomaly as illustrated through the hydraulic head and gradient data. Additional insight related to groundwater discharging conditions can also be obtained from the subsurface temperature data, discussed below.

5.2 Physical Hydrogeology, Hydrology and Permafrost Conditions

The following subsections detail the data compiled or collected during the course of this study that assist in building the initial conceptual model of the Bogg Creek Watershed groundwater flow system. This includes examination of areas of groundwater discharge and the current permafrost conditions in the area.

5.2.1 Vertical Groundwater Flow Directions Determined by Hydraulic Head and Temperature Measurements

5.2.1.1 Hydraulic Heads

As mentioned in the previous section, subpermafrost groundwater in at least one aquifer (LBF) was measured as being under a slight upwards gradient, with water levels rising to about 10-12 mbgs in monitoring wells MW09A and MW09B. A head difference of 0.11 m was measured between MW09A (233.01 mASL) and MW09B (232.90 mASL). Both wells are completed within the LBF. MW09A is completed in a lower sandstone unit (109-120 mbgs) and MW09B in an upper sandstone unit (81-89 mbgs), separated by approximately 20 m of shale. A pumping test demonstrated a hydraulic connection through the shale exists between the two aquifers (Waterline Resources Inc., 2013b). Transmissivity values of 150 m^2/day and 270 m^2/day were calculated by Waterline Resources for MW09A and MW09B

respectively. Based on aquifer thicknesses of 11 and 9 m, this provides hydraulic conductivity values of 13.6 m/day (1.6×10^{-4} m/s) in MW09A and 30.0 m/day (3.5×10^{-4} m/s) in MW09B. Other local aquifers within the bedrock geology may also contain groundwater under artesian pressure and be connected to the surface via open taliks. This hypothesis forms the initial basis of the conceptual model: that subpermafrost groundwater may contribute to Bogg Creek streamflow in some areas where the hydraulic head intersects the land surface.

Several of the potential groundwater discharge locations that had been tentatively identified with remote sensing and infrared surveys were visited during the field campaigns. Because these locations could provide information relative to deep, regional groundwater flow systems, additional data collection focused specifically on these sites was of interest. Of particular interest were the anomalies spotted around G-Lake (Figure 10), specifically those within the northeastern corner of the wetland surrounding the lake. These coincided with a recurring icing complex identified in Glass et al., (2020). During the 2018 field campaign, vertical hydraulic gradient measurements were made at the GL1 and GL2 sites (Figure 10) by installing the PushPoint Sampler to a depth of approximately 100 cm below the groundwater surface and monitoring the hydraulic head in the sampler relative to the ground surface elevation. The ground surface at the sites was dominated by shallow surface water with wetland vegetation. At both sites, groundwater flowed out of the top of the sampler indicating an active upward groundwater flow gradient, verifying groundwater discharge conditions. At the GL1 site, there was about 5 cm of head difference between the ground surface/surface water elevation and groundwater, indicating an upward gradient of 0.04 at the time of the measurement. In 2019, similar measurements were collected from the GL3 site (Figure 10) and again, upward groundwater flow conditions prevailed at this location as well. The combined hydraulic gradient measurements confirmed the presence of groundwater discharge conditions at this set of sites that had been previously identified through the remote sensing techniques. The assessment of additional data collected at these locations is discussed in a later subsection.

Other hydraulic gradients were measured opportunistically at creek and lake sites but their measurements were not always possible due to screen clogging with the PushPoint Sampler. At H001 (Figure 10) a hydraulic head difference of approximately 5 cm was noticed between a mini-piezometer (depth 60 cm) and the surface water in the creek, indicating local discharge conditions. A vertical, upwards gradient was estimated of about 0.9 in this location. At several lake sites outside of the watershed a gradient determination was attempted but not successful. Sites H026 and H027 (Figure 10) however, showed signs of groundwater discharge in the form of heavy iron staining on the edge of the lake.

These initial data highlight the complexity of this regional flow system, consisting of shallow unconsolidated aquifers, such as the glaciolacustrine deposits near the lower reaches of Bogg Creek and potential bedrock aquifers such as the LBF. While it is not always possible to obtain a direct hydraulic head measurement in this environment, additional data may be used to supplement the understanding of the groundwater flow system characteristics.

5.2.1.2 Vertical Hydraulic Gradients Determined via Temperature Profiles

Groundwater temperature profiles were collected in 2018 at the spring site of GL1 and in 2019 at spring site GL3. In 2019 profiles were also taken along several reaches of Bogg Creek where a hydraulic gradient could not be reliably measured with conventional methods (W05, W06, H046, H044 and H046, see Figure 10). These profiles were collected at these sites to provide evidence for vertical groundwater flow directions based on temperature differences. They complement direct gradient measurements based on hydraulic head data but were anticipated to act as an alternative measurement method when a gradient could not be otherwise determined. Vertical temperature profiles from locations near surface streams (Figure 13, creek) and springs (Figure 14) are presented below.

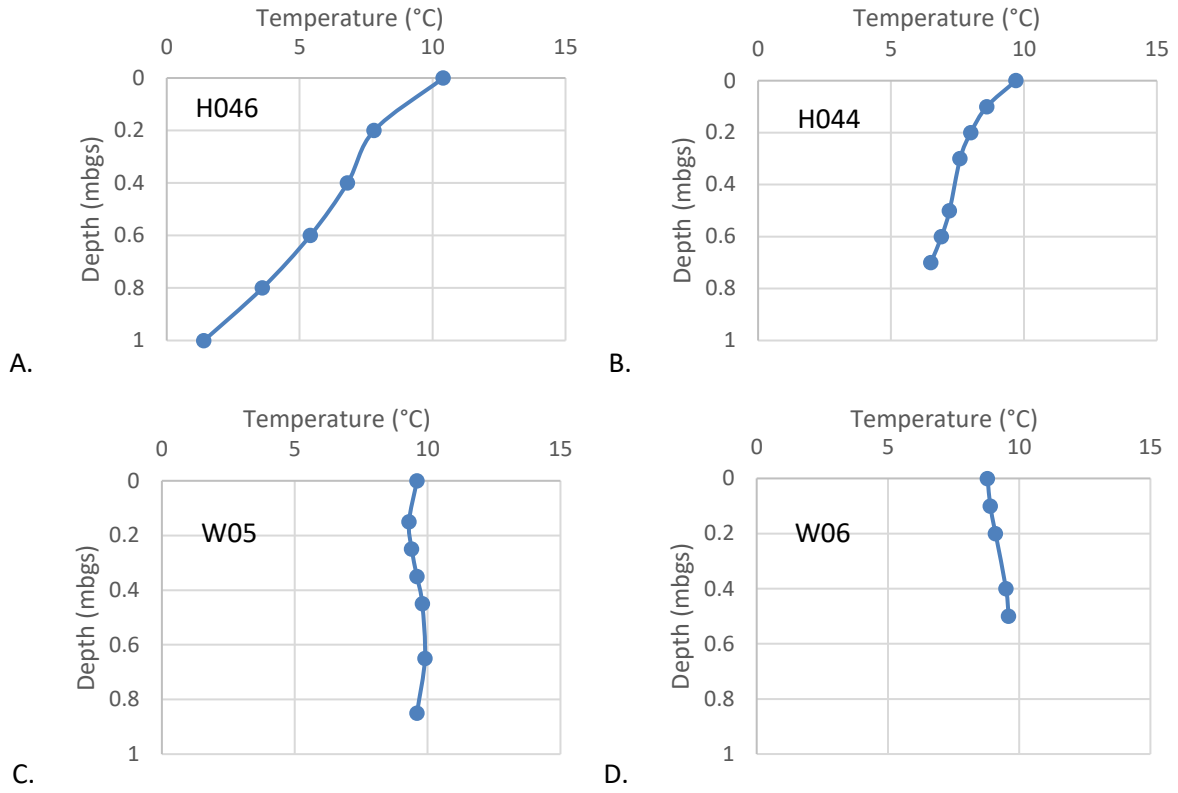

Figure 13: Temperature profiles taken at several creek reaches in summer 2019. Profiles are for A. H046 B. H044 C. W05 and D. W06.

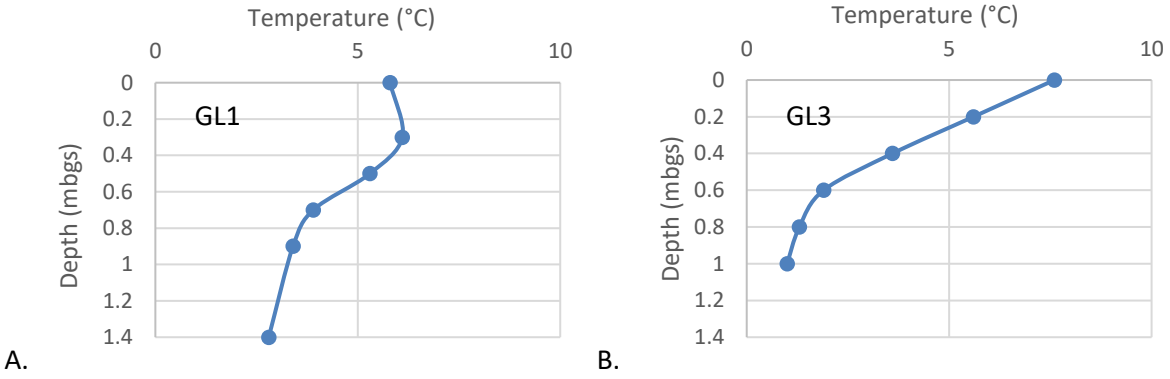

Figure 14: Spring temperature profiles for A. GL1 (2018) and B. GL3 (2019).

Temperature profiles were taken at four locations along Bogg Creek, revealing losing and gaining reaches in 2019. H046 had a temperature profile that indicates decreasing temperatures with depth which is consistent with a reach that is gaining colder groundwater. A steady decrease can be observed with a

shallow slope after a depth of 0.20 mbgs which may indicate a low flux of groundwater into the stream. At H044 (Figures 10 and 13B) temperature profiles appeared to decrease with depth with a relatively shallow slope as might be expected in a reach that is gaining cold groundwater at a relatively moderate rate. Temperatures decrease steadily with an inflection point at 0.50 m flattening out the temperature profile slightly. W05 displayed very little contrast in temperature with depth. This may be indicative of infiltrating surface water or a reach that is neither gaining nor losing or undergoing hyporheic exchange. Forming a slight "S-like" pattern, temperatures in the stream were slightly warmer (9.6°C) than the first 0.35 m, warming until 0.75 mbgs after which temperatures again begin to decrease slightly. At W06 temperatures in the stream were colder than in the subsurface, with temperatures increasing with depth. This is possibly a result of infiltrating surface water or hyporheic exchange in a losing reach of stream. Temperatures of >8.5°C indicate that a small talik likely underlies the stream at this reach, similar to W05. Temperatures appear to begin stabilizing around 0.50 mbgs, the maximum depth of the temperature profile. In summary, streambed temperature profiles of these four locations along Bogg Creek show that the creek is gaining and losing water along its path. At the two upland tributary sites of H046 and H044 discharge conditions were occurring, while in the middle reaches there may be recharge or very little exchange with groundwater happening. This does suggest that discharge conditions are not consistent everywhere along the streams and may reflect local or larger scale patterns.

The last two temperature profiles were collected at the GL1 and GL3 spring sites (Figure 10). GL1 has a profile that is generally decreasing in temperature with depth. A small temperature difference between the pooled surface water and the shallow subsurface (0.30 m) is likely due to diurnal temperature fluctuations. A sharp inflection point at a depth of 0.50 to 0.70 mbgs marks the transition to a steeper temperature gradient that persists past the maximum measurement depth of 1.40 mbgs. This steep slope is possibly due to a higher flux of discharging groundwater. GL3 shows a moderate decrease in temperature to a depth of 0.60 mbgs after which the temperature gradient steepens substantially. This is further confirmation that these locations are areas of groundwater discharge as was observed in the hydraulic head data. The actual source of this groundwater will be explored in later sections, but this does imply that a talik exists next to G-Lake and has actively flowing groundwater. The depth and extent of this talik is unknown.

5.2.2 Hydrologic Regime

Some data on surface water streamflow has been collected in the Bogg Creek Watershed. In 2012, 2013 and 2014 hydrometric measurements (stage, discharge) were taken during the open water season (from June to October) at H001 (2012-2013) and H001B (2013-2014) (Figure 10). The raw data could not be obtained, however it is reported on in NESTL (2015), as seen in Figure 15. Exact timing of the spring freshet is unknown; however, it seems to precede the stream gauging activities in all years. These data provide insight into the timing of important hydrological events and when the creek is likely to be comprised mostly of groundwater baseflow, such as late summer. During this period, stored meltwaters in shallow flowpaths begin to drain and the remaining water in the shallow system is slightly older and more solute rich. Stream chemistry will become more dominated by the various sources of groundwater, suprapermafrost and subpermafrost, that make up the baseflow during the low water periods.

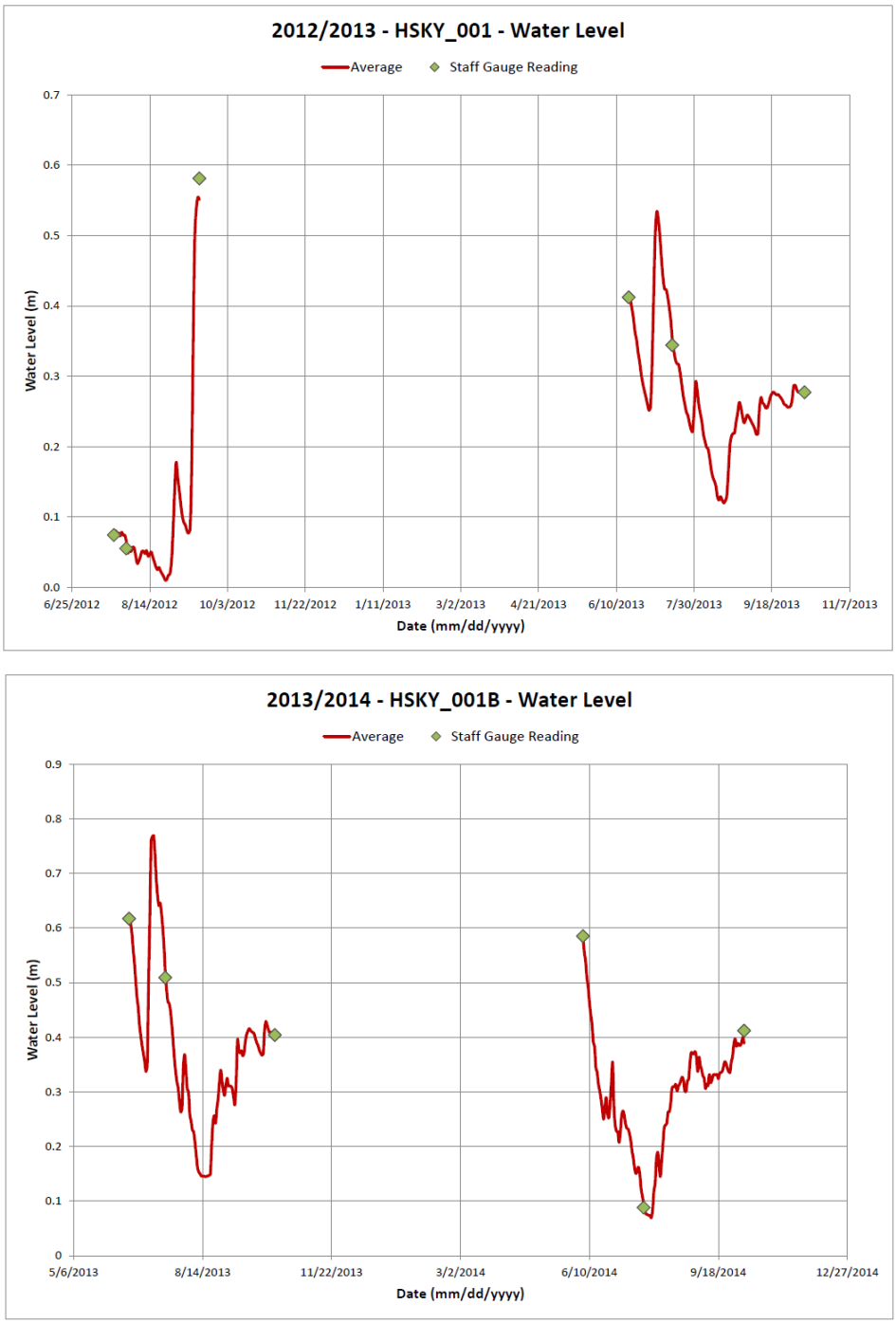

Figure 15: Bogg Creek Hydrographs for the open water periods between 2012 to 2014. Stream stage measurements were done at H001 (top) and H001B with measurement overlap in 2013. Figures were taken directly from NESTL, (2015) with permission.

At H001, 2012 measurements begin around July 18 and continue until about September 14 (NESTL, 2015). During the early monitoring period from July to Late August, water levels were receding mostly, before bottoming out at fairly low water levels around August 30. After this a substantial increase in water level is observed likely after a significant period of rainfall in early autumn. A single dip occurs once over several days and then water levels continue increasing until the monitoring period ends. 2013 measurements of water level in H001 were the last for this reach of stream. Following early measurements sometime in late June, water levels were dropping significantly over a span of about 2 weeks, however another large event (possibly another melt event) likely occurred that brought water levels back up over a span of 3 weeks. After this the recession continued, reaching the lowest values around Mid-August. Water levels remained around this level for about 2 weeks until fall precipitation events brought water levels higher. These remained fairly stable until pressure transducers were removed in October.

H001B water levels were monitored during the same open water period in 2013 and showed a very similar trend and magnitude of change to H001. Initially water levels dropped over a span of about 2 weeks, with a melt or precipitation event causing water levels to rise over the subsequent 3 weeks. Lowest water levels again occurred for about 2 weeks in Mid-August, similarly to what occurred in H001. Additional precipitation events appeared to increase water levels after this time until October. Final water level measurements were conducted in H001B from early June to early October, 2014. Water levels are recorded falling during the early monitoring period starting in June. This period of low water levels began sooner than in 2013, starting after July 20 and lasted roughly 10 days. After this water levels increased then leveled out around mid-August, remaining stable towards the end of the monitoring period.

In summary, Bogg Creek streamflow appears to follow similar patterns as other watersheds in Sub-Arctic environments, with peak high streamflow occurring just after the spring snowmelt. This tapers off throughout the summer, hitting a peak low in late July to early/mid-August. Large events likely cause a large spike in water levels and discharge, especially near the end of the summer, which then dissipate within a few days. Spring freshet appears to continue to influence water levels even after the peak discharge has ended, likely due to some of this water remaining stored within wetlands and lakes or as icings and groundwater. Small peaks appear to be responses to individual events (although without rainfall data this can only be speculated), but an overall decreasing trend beginning in June continues until late in the summer, as this stored melt water is depleted. Despite peak streamflow being controlled largely by spring melting, a significant amount of streamflow continues in the fall prior to freeze up. Small

variabilities between lows and highs occur during this time, as fall precipitation events lead to increased storage. Thawed active layers during this period may also contribute to increased storage and a decrease in “flashiness”. This data can help in predicting when the creek is likely to consist mostly of baseflow and can direct proper sampling times to capture this baseflow undiluted by precipitation. With limited streamflow data it is not possible to get an accurate picture of when exactly the stream consists mostly of baseflow as it may change year to year, but a general sense can be gained.

5.2.3 Permafrost

5.2.3.1 Physical Measurements of Permafrost

Permafrost distribution throughout the area of study was highly variable. Measurements made beneath or in the immediate vicinity of surface water bodies (lakes and streams) indicated that the permafrost table was generally deeper than 1.5 m, which was the measurement limit of the field probe equipment. The average permafrost depth based on measurements made throughout the watershed, away from the water bodies was around 0.7 mbgs for both years. As these measurements were taken near the end of the summer, they are likely representative of the maximum depth the active layer.

Near stream and spring sites, the actual permafrost table could not be discerned with the 1.5 m probe directly under the water body but the depth to permafrost usually decreased rapidly with distance from the water, at many sites. Near the creek sites of H044, H001B and H030 (Figure 10) the permafrost depths exceeded 1.5 m beneath the surface water as did the depth to permafrost at the spring sites of GL1, GL2 and GPH1 (Figure 10). In 2019 GL3 thaw depth was measured as exceeding 1.8 m by use of a longer PushPoint Sampler.

At the H046 site (Figure 10) a longitudinal profile of permafrost depth was taken starting in the ditch next to the AWR and ending just within the creek (Figure 16). The ditch next to the road was mostly devoid of vegetation with standing water, but the area near the edge of the creek was forested. As illustrated in Figure 16, the permafrost was measured as being >1.2 mbgs next to the creek and quickly rose to within 1 mbgs up about 1 m away from the stream bank. The forested section appeared to be a permafrost plateau, as the land surface was slightly higher, and the permafrost table was at around 0.5 mbgs. The depth to the permafrost again increased approaching the road bank and ditch.

Sites where cores of shallow permafrost were taken near MW04T and H040 (Figure 10) had different active layer thicknesses. MW04T core was unfrozen to a depth of 95 cm and H040 core to 35 cm. One

core near H040 also had a small 7 cm thick unfrozen zone within the frozen profile at a depth of 43 cm. This was not observed in a replicate core collected about 1.5 m away. Data from these cores are explained in more detail in Sections 5.3.1.1.3 and 5.4.1.2.3.

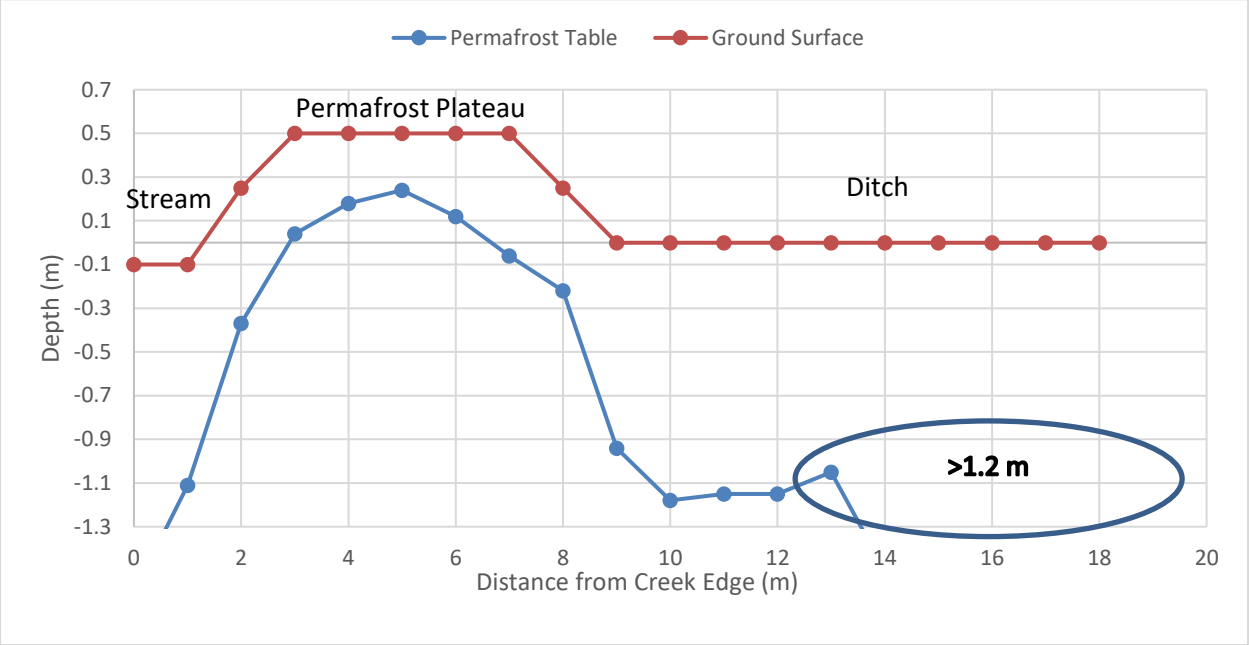

Figure 16: Permafrost and ground surface profile across a transect at H046.

5.2.3.2 Ground Temperatures Monitored within the Husky Thermistor Strings

As part of the original baseline monitoring work conducted by Husky Energy beginning in 2013, a series of vertically installed clusters or strings of thermistors (6 thermistors in each string) were installed at varying depths throughout the lease area as explained within the Methods Section. Out of the eight total thermistor strings, two were selected for analysis of the evolution of ground temperature over time as part of the current project. This included MW01T and MW09T (Figure 9). These thermistor strings were chosen for analysis (despite MW01T lying outside the watershed) as both included a shallow monitoring interval installed within the first 1.0m of the ground surface. Other thermistors did not contain as shallow of an interval as these two, usually beginning below the permafrost table. This was anticipated to provide a clearer picture of temperature fluctuations in the active zone. Lithologies encountered during borehole drilling were different between the two locations. MW01T was installed into silt and silty sand on the floodplain of the Mackenzie River (approximately 200 m from the water's edge), while MW09T is installed in the upland area in clayey silt and shale bedrock. Elevation difference between MW01T and

MW09T is about 191 m. MW01T includes 6 thermistors installed between the depths 0.75 m to 10.75 m below ground surface, and MW09T contained 6 thermistors situated at depths of 0.85 m to 4.6 m below ground surface. At both areas, the surrounding area was cleared of vegetation, which was then mulched and laid down over the area to provide insulation. Temperature vs time plots for both thermistor strings from the time of installation can be seen in Figure 17.

MW01T shows a reduction in magnitude between maximum and minimum temperatures at each depth, but this is most obvious at 0.75 m. Lowest temperatures occur around early to mid-March. At this shallow depth, temperatures drop below -5°C in 2013 and 2014, but these minimum temperatures increase to around 0°C during 2015 and 2016. The next two years see a decrease to around -5°C during 2017 and 2018. The highest temperatures occur around mid to late July, and a definite cooling trend can be seen throughout all years. Maximum temperatures are around 8°C in 2013 and drop to about 2°C by 2018. Some time lag between peak temperatures can be observed in 0.75 m and 2.75 m data sets of about 22 weeks illustrating the slow depth of penetration of the warming front during the summer season. In general, this thermistor string appears to be recording a general cooling trend in some intervals within the first few meters of overburden at this location, and a possible warming trend below 4 m.

In contrast, temperature data from the MW09T thermistor string shows no flattening of maximum and minimum temperatures but instead a warming trend is observed in all thermistor intervals until 2016 (Figure 17). After this, annual temperature variations appear to stabilize. Peak temperatures at 0.85 m rise from about 7°C to 13°C between 2013 and 2016, after which they level off and do not increase anymore. This trend of an increase followed by stabilization is also apparent in deeper intervals. A similar trend is observed for the lowest temperatures, which increase from -14°C in 2013 to -3°C in 2016, after which temperatures stabilize and reach similar values in later years. Interestingly, all thermistor intervals rise to around 0°C by 2016 and even rise above it. A definite and progressively expanding lag-time between peak temperatures at adjacent depth intervals occurs on the order of about 3-4 weeks, with around 10-12 weeks passing between peak temperatures in 0.85 m and 4.6 m. This time lag is significantly shorter than that in MW01T, likely reflecting the different overburden materials or other site conditions. As well, this data from MW09T appears to be recording a warming trend, which is in contrast to MW01T.

Figure 17: Average daily ground temperature vs date for two thermistor strings, MW01T (top) and MW09T (bottom). Thermistor intervals differ between each string, as MW01T penetrates deeper into the ground, which shows diminishing temperature fluctuations at these lower intervals. It is also observable that permafrost thaw and active layer thickening is occurring with time in MW09T, while this does not appear to be the case in MW01T.

Temperature profiles with depth are shown in Figure 18 including the minimum temperatures averaged over all years, and the maximum temperatures for each year starting in early March 2013 (when measurements began). Profile MW01T shows a relatively wide range between minimum and maximum temperatures. Most of the variance in the temperature differences occurs in the top intervals, narrowing

with depth due to dampened temperature effects. Like the temperature vs time profiles shown above, a small increase in temperature at depths 2.75-10.75 m can be observed each year, although temperatures do not exceed 0°C. In fact, thaw depth in this profile seems to remain stable.

Comparatively, MW09T showed a dramatic increase in thaw depth every year, changing from 1.5 m to >4.5 m between 2013 to 2018. MW09T was not installed quite as deep and so the depth at which the ground temperature remains stable is not visible. This thermistor string appears to record a very dramatic warming of ground temperatures and a thawing of permafrost. The most change in thaw depth was between 2015-2017, with a 1.5 m increase in active layer thickness. The permafrost table resides below the maximum measurement interval in 2018.

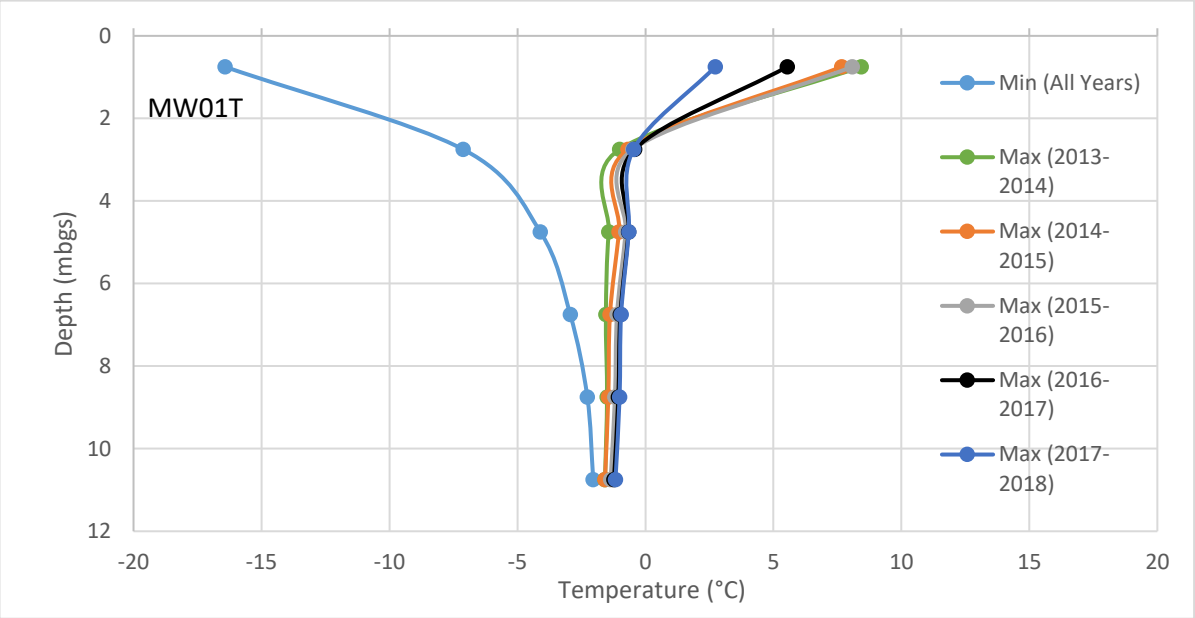

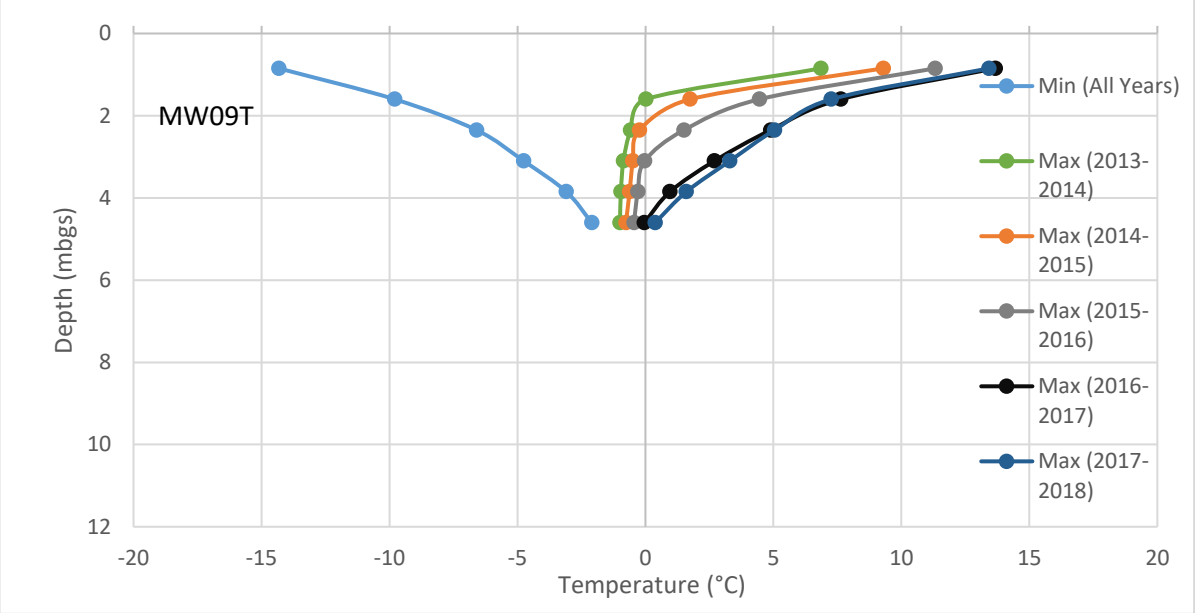

Figure 18: Temperature vs Depth profiles for MW01T (top) and MW09T (bottom). Both profiles show a warming trend in their lower intervals but only MW09T shows a change in the thaw depth (active layer) base.

MW09T seems to represent an extreme example of increased summer energy flux and decreased winter energy flux, thawing the ground considerably. Contrastingly, MW01T shows much more modest warming below the permafrost table and slight cooling within the active zone. Installation of these thermistors

involved clearing land of vegetation to form an open pad, with a layer of mulched vegetation laid down over top of soil to act as insulation. This insulation appears to be working well in MW01T but not in MW09T. This may be due to the thermal properties of the different thermistor well lithologies, moisture contents, elevation and micro-climatic effects that have created a positive feedback loop within MW09T that is not occurring in MW01T to the same degree. Modifications to the insulating mulch may have also occurred, but this information could not be obtained. Cooler, active zone waters may be flowing more frequently in this zone, potentially modulating the temperature response. In conclusion, these data suggest that thawing is occurring across the region at least where there are cleared areas, but it is not consistent. Some areas that have been cleared may be experiencing greater levels of thaw than others, deepening taliks and a thickening of active layers. These may also be releasing stored solutes into the groundwater flow system. Meanwhile in some areas, the permafrost system appears more resistant to changes.

5.2.4 EM38 Transect

An EM38 survey was conducted at GL3 along a transect of approximately 135 m long. Ground EC was collected in both the vertical and horizontal dipoles. The results of this survey are shown below in Figure 19.

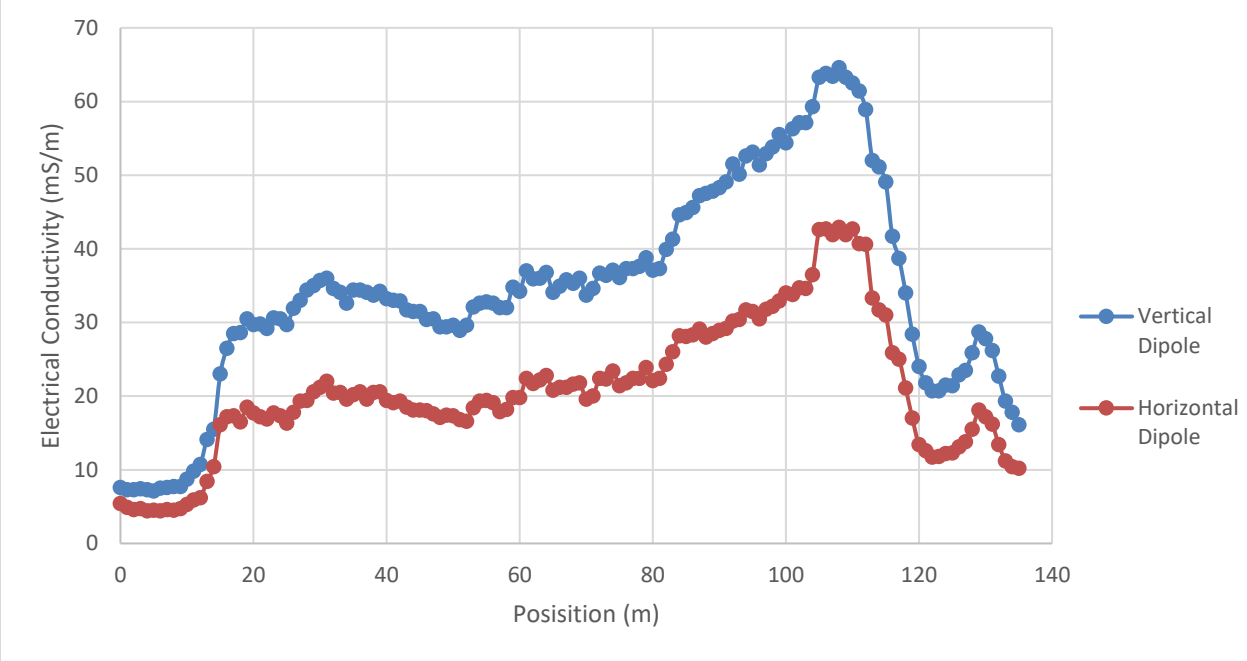

Figure 19: EM38 survey transect conducted over GL3 and surrounding wetlands.

This transect began on the top of a small permafrost plateau, about 10 m in from the edge. An increase in EC can be seen in this figure corresponding to the location of GL3 at around 30 m. EC remains relatively stable, ranging from 29 to 39 mS (vertical dipole) until about 80 m into the transect. At this point EC increases substantially to a peak of 65 mS (vertical dipole) at 108 m, where it begins to taper off again as permafrost is once again encountered. This high conductivity area was not investigated further through water sampling. The high EC is hypothesized to coincide with areas of spring activity, where the discharging water contains a high number of dissolved solutes. The vertical and horizontal dipole data mirror each other quite well, but the vertical dipole data is generally higher in EC than the horizontal.

5.3 Geochemistry

5.3.1 Major Ion Chemistry

5.3.1.1 Water Source and Aquifer Endmembers

The hydrogeologic system of Bogg Creek Watershed was conceptualized as consisting of the suprapermafrost and subpermafrost groundwater flow systems of a typical discontinuous permafrost environment. The surface water is hypothesized to be fed primarily by shallow or surficial sources of water such as shallow seeps/interflow and active layer/suprapermafrost groundwater during mid to late summer. Open taliks are hypothesized to potentially occur either regionally or locally below specific bodies of surface water, providing a hydraulic connection between the surface water features and the underlying sediments and bedrock that may facilitate subpermafrost groundwater inputs to the surface water. With this model in mind, the compilation of the various datasets led to identification of 5 potential distinct water sources within the Bogg Creek Watershed. These five sources were determined based on their location and unique geochemistry. These include: 1. shallow seepage, 2. organic soil or shallow active layer porewaters and 3. suprapermafrost groundwaters (mineral soils), and deeper subpermafrost groundwater from the 4. Little Bear and 5. Martin House Formations (Figure 20). Direct runoff water such as overland flow samples could not be obtained, and due to the nature of the porous organic soils is not hypothesized to be a major contributor, except during early spring melts. Thawed permafrost porewater is also explored in this section but was not considered a major source for surface water. For site location reference, Figures 20 and 21 are shown again below. These include the groundwater monitoring wells and thermistors and the surface water monitoring sites.

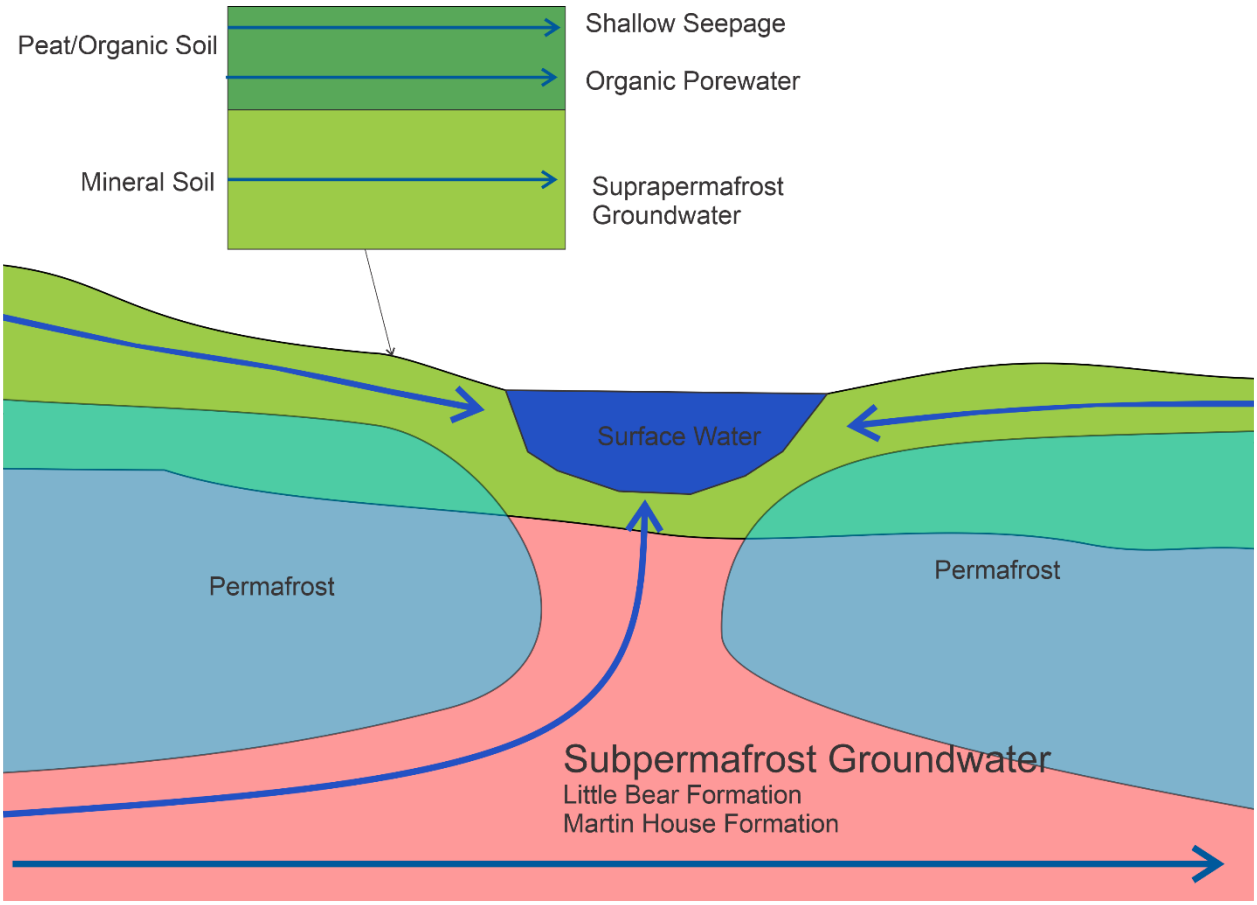

Figure 20: Generalized conceptual model of the different water sources that were obtained.

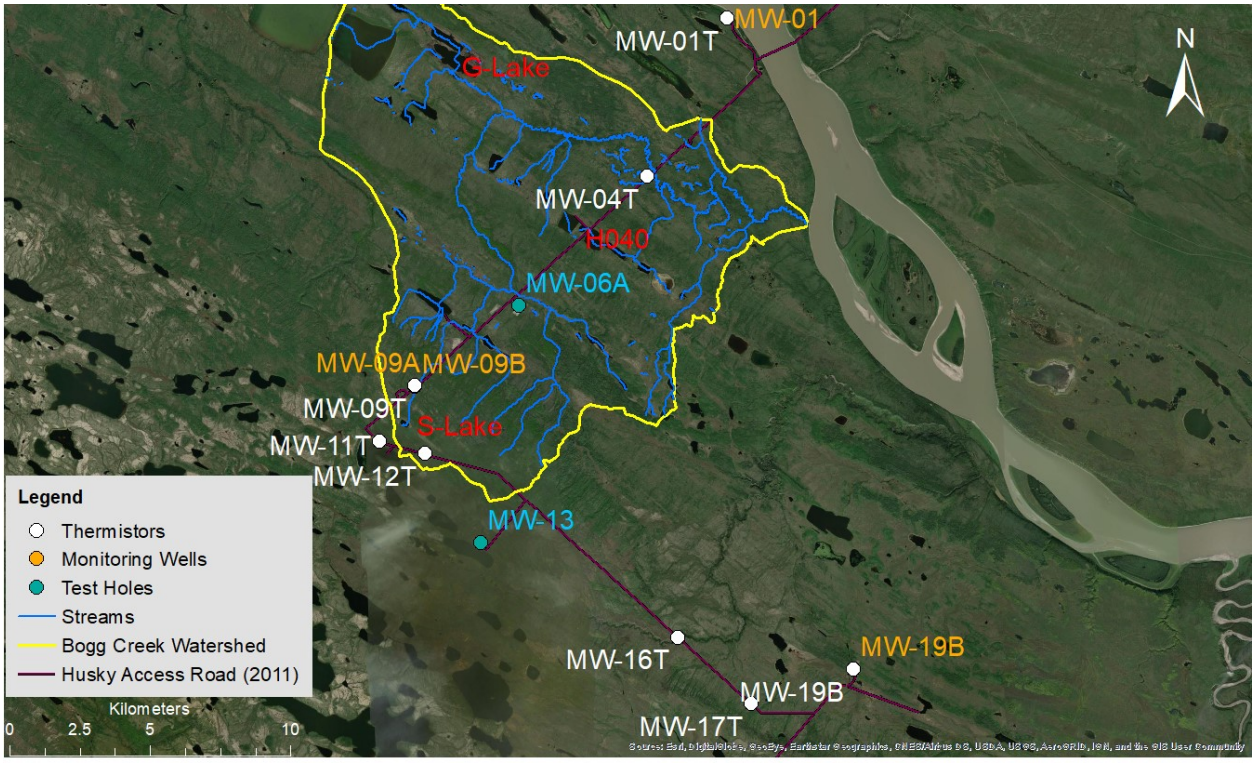

Figure 21: Map of groundwater and temperature monitoring wells as well as test holes within the study area. Key sites are labelled in red (G-Lake/GL, S-Lake/SL, and H040). Sample locations for deep subpermafrost groundwater from the MHF are not in this area and so are not shown.

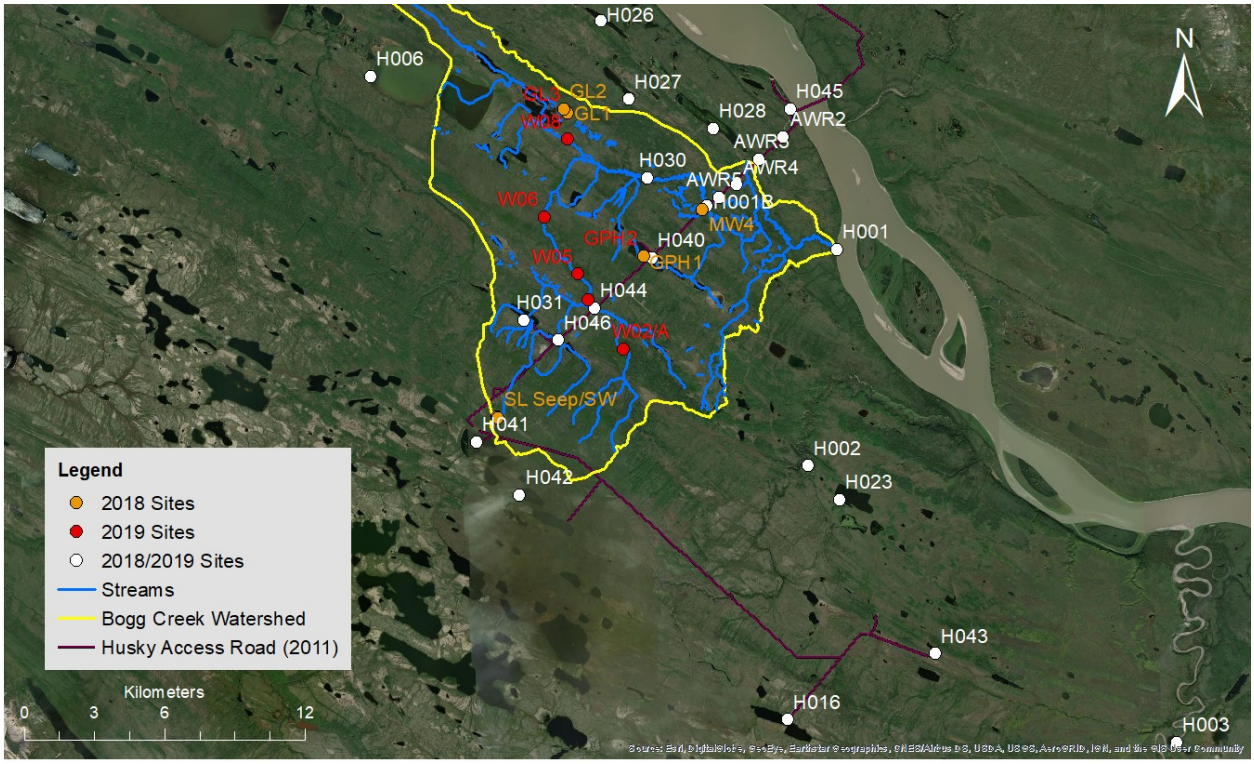

Figure 22: Surface water and spring sampling locations for 2018 and 2019 are shown in orange and red, respectively, while historical Husky sites are shown in white. Some Husky sites (namely those located at small culverts that were not analyzed for this study) are omitted on this map. Also note that some locations overlap with one another at this scale, such as GPH1/2, GL1/2/3 and W02/A.

5.3.1.1.1 Subpermafrost Groundwater

The subpermafrost groundwater data were compiled from Husky for the LBF (Figure 4), (Waterline Resources Inc., 2013b), and ConoccoPhilips (Golder Associates, 2015) and MGM Energy for the MHF (Figure 4) (Hayes & Dunn, 2012). Both ConoccoPhilips and MGM operations are outside of the Bogg Creek Watershed. Samples from the LBF were taken in 2013 and again in 2019 by Waterline Resources from MW09A and MW09B (Figure 23) and are dominated by Na-SO_4 with some HCO_3. All samples demonstrate very little variability between themselves despite each well being screened across a different interval of the formation (approx. 90 and 110 mbgs) and even with resampling 6 years later. MHF samples were taken from monitoring well WW04-A, northwest of the study area by ConoccoPhilips. This water was dominated by Na-Cl and HCO_3 with very low levels of SO_4. Similarly, in another part of the aquifer, MHF water was dominated by Na-Cl with less HCO_3, but higher overall TDS compared to the

WW04-A water. This water was obtained during drill stem tests of petroleum well I-78 by MGM (Hayes & Dunn, 2012).

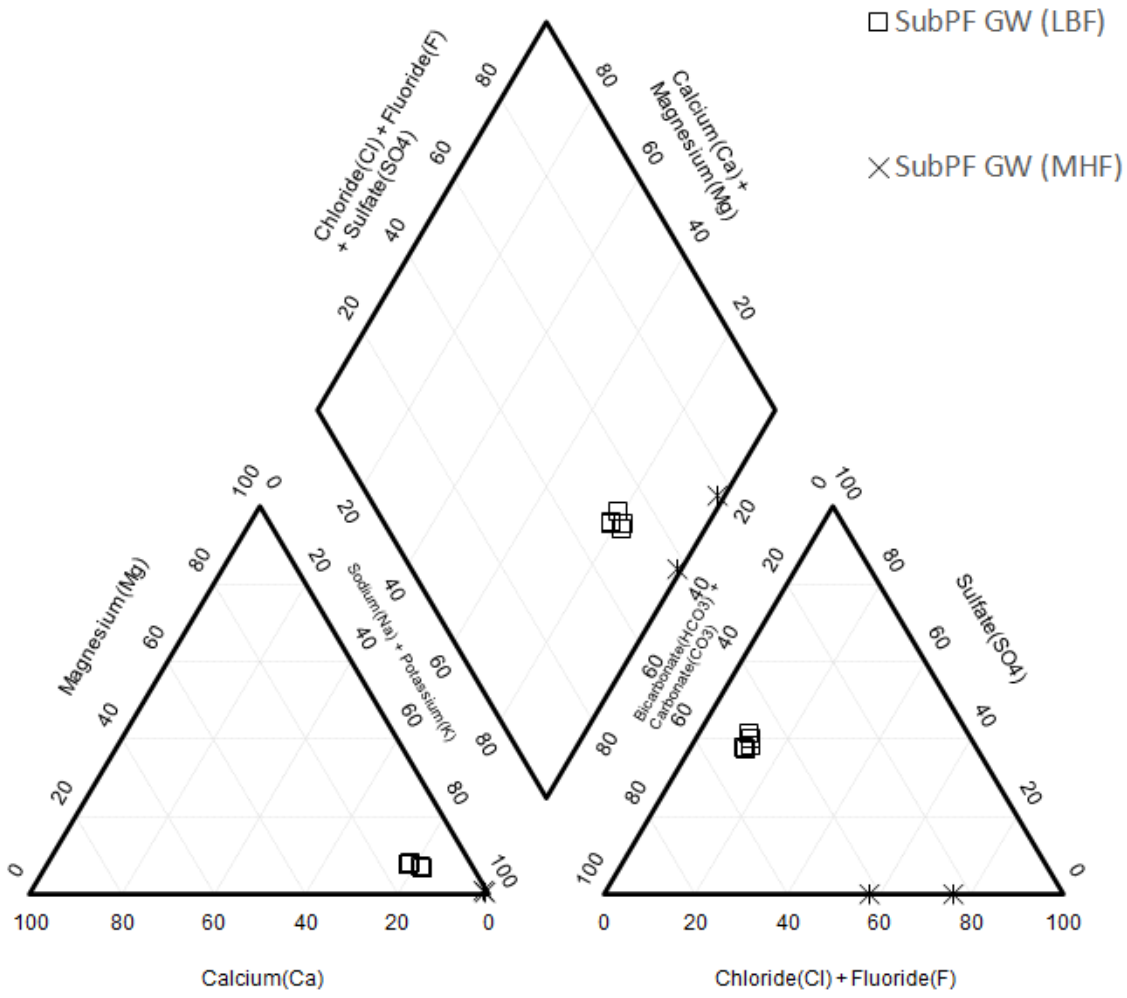

Figure 23: Piper diagram of subpermafrost groundwater from the Little Bear and Martin House Formations. Data obtained from Waterline Resources, (2013a) and Hayes & Dunn, (2012).

Cl appears as an attractive tracer of subpermafrost groundwater flow in Bogg Creek, but some data show this may not always be the case. For example, frozen soil samples were collected by Husky Energy during their shallow drilling campaign and analyzed for salinity. This included all major ions and the data are shown in Appendix A, Figure A-2. At MW04T (Figure 21), soil samples taken from 10.7-21.5 m showed elevated amounts of Cl compared to other soil samples in the watershed. These Cl levels ranged from 123-609 mg/kg_{soil}. It should be noted that at these depths the soil was frozen, meaning active flowing

of groundwater is unlikely. These samples were taken from a till layer and from weathered shale. The source for this elevated Cl is unknown but could be related to glacial transport of a small amount of halite or the shale itself. This till layer appears to extend throughout the watershed and may act as an additional source of Cl to flowing groundwater if these saltier units are continuous. In general, suprapermafrost samples typically did not exceed 9 mg/L Cl.

Levels of SO_4 were inversely related to Cl in these soil samples, generally higher when Cl was low and vice-versa. Therefore, at least in the Bogg Creek Watershed, a high Cl and low SO_4 content may not necessarily be indicative of subpermafrost groundwater influence. Due to the depth of these saltier layers (13-21 mbgs at MW04T), it is possible that what appears to be subpermafrost groundwater discharge may in fact be influenced by a supra or intrapermafrost talik. If this saline unit is more continuous and not localized around the vicinity of MW04T, then it may be unfrozen or thawing in some areas and influencing the geochemistry of other waters. This will be discussed further in subsequent sections.

5.3.1.1.2 Suprapermafrost Groundwater and Shallow Seeps

Previous studies on soils in the area across the Mackenzie River to the northwest and northeast indicated that much of the glacial till and modern alluvium is calcareous in nature (Day & Rice, 1964). This is consistent with shallow groundwater and permafrost porewater data, which show that Ca, Mg and HCO_3 are common solutes contributing to the dissolved load. Shallow groundwater was collected from two locations, one by Waterloo researchers at the MW04T (sample MW04) well site at a depth of 1 mbgs (via mini-piezometer), and the other by Waterline Resources from the MW19B monitoring well (Waterline Resources Inc., 2013a). These locations are shown in Figure 21. The shallowest sample from MW04 was collected from a silty fine sand mapped as being glaciolacustrine in origin. Well MW19B was screened across three different lithologies, unconsolidated silty clay till, siltstone and weathered shale. Temperature data from the nearby MW19T thermistor suggests that a talik exists at least to a depth of 9.9 mbgs at this location. Water levels at the time of sampling were around 6.8 mbgs. Despite this well lying outside of the Bogg Creek Watershed it showed some similarities to the suprapermafrost groundwater from site MW04. Both samples are dominated by Ca-Mg-HCO_3 with some SO_4 and very little Cl (Figure 23). MW19B had twice the TDS value of MW04 (1137 mg/L vs 580 mg/L) and contains an appreciable amount of Na and K compared to MW04, likely as a result of interactions with the weathered bedrock. These samples are understood to represent the suprapermafrost groundwater within mineral soil, although MW19B may be located within a suprapermafrost or intrapermafrost talik.

Water was collected from a small seep at S-Lake (SL Seep, see Figure 21 and 22) which appeared as a thermal anomaly during the IR survey. Geochemically, this water was very dilute and was distinct from other spring waters, with small amounts of Ca and SO_4 (Figure 24). Because of this it was assumed to represent the conceptualized component of interflow or very shallow groundwater seepage.

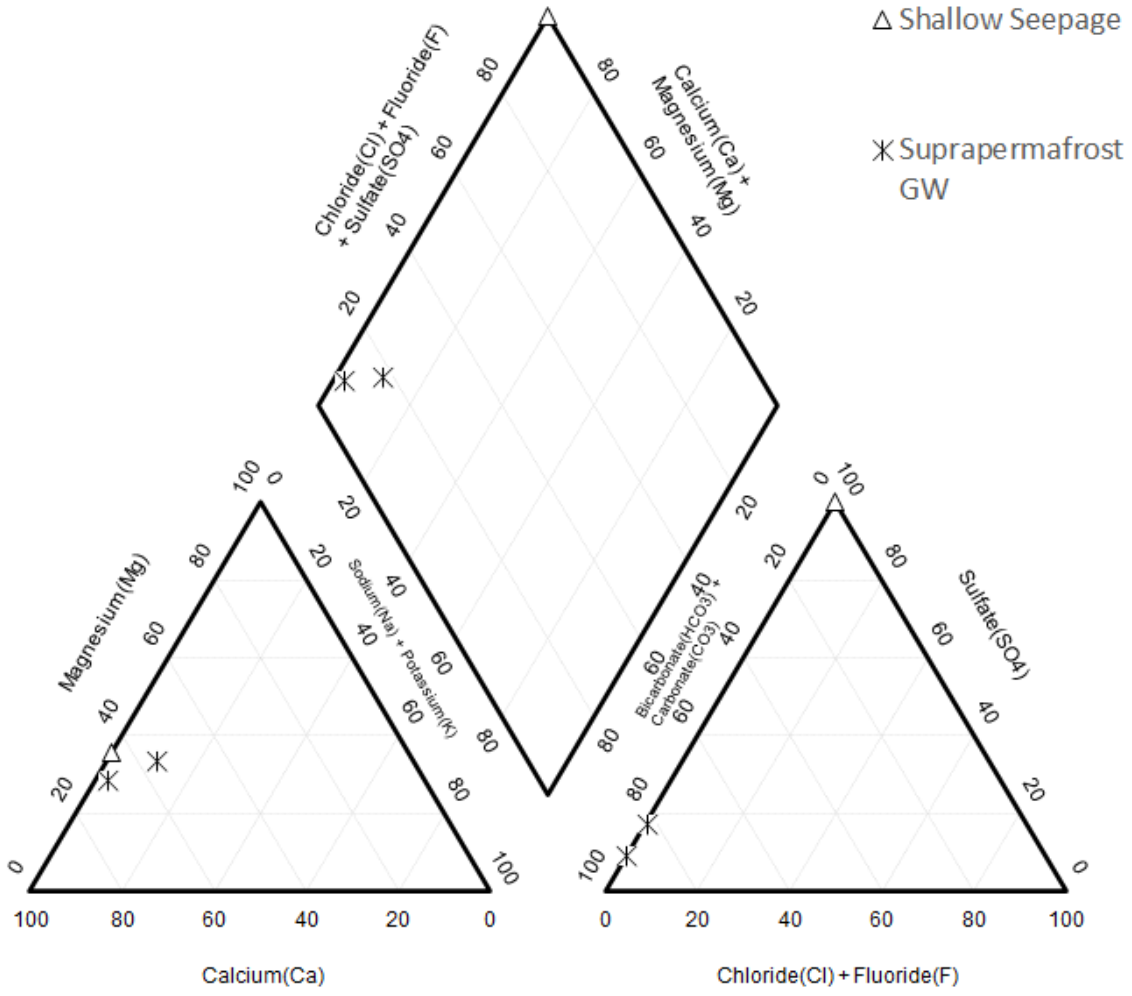

Figure 24: Piper diagram of suprapermafrost groundwater and shallow seepage from SL Seep (S-Lake).

While there are only a few samples that were collected and the degree of variability in geochemistry across the watershed is largely unknown, these samples form the basis for the analysis of groundwater and surface water interactions in the following sections.

5.3.1.1.3 Active Zone and Permafrost Porewaters

Core logs for the two cores extracted from H040 and MW04 can be seen in Appendix A, Figure A-3, and Figure A-4. The 1.55 m long core taken from H040 was dominated by fine-grained sediment, consisting mostly of silt with clay and some organic matter. A peculiar, “burnt” or charcoal-like smell was noted in much of the core. Three main layers were identified. The top 50 cm consisted of peat with some silt and clay with about 20 cm being frozen. The second 30 cm thick layer was a silty clay with high organic content that was frozen throughout. The third layer was a clayey silt with some organics at about 70 cm thick. This layer was also completely frozen. A 7 cm section in the peat layer was observed as being unfrozen and saturated with water, below about 20 cm of frozen soil. This is likely the base of the active layer, which had likely not completely thawed out by this time (Mid-August).

Core taken from near MW04, with a total length of 210 cm appeared to consist of about 70 cm of silty fine sand and trace clay, 20 cm of clayey silt with some sand, 30 cm of silty clay with minor sand and then about 100 cm of clay with some sand. No odour was detected. The core was unfrozen to a depth of about 100 cm and partly saturated to saturated, after which it was frozen and variably saturated.

Geochemical profiles of concentration vs depth in H040 porewater are shown in Figure 25. Most ions show a spike in concentration coinciding with the unfrozen layer discussed earlier. This lends more evidence to this zone being the base of the still partially frozen active layer. An increase in ion concentration would result from cryo-concentration caused by a slowly advancing freezing front, leading to increased solute concentrations at the ice-water interface.

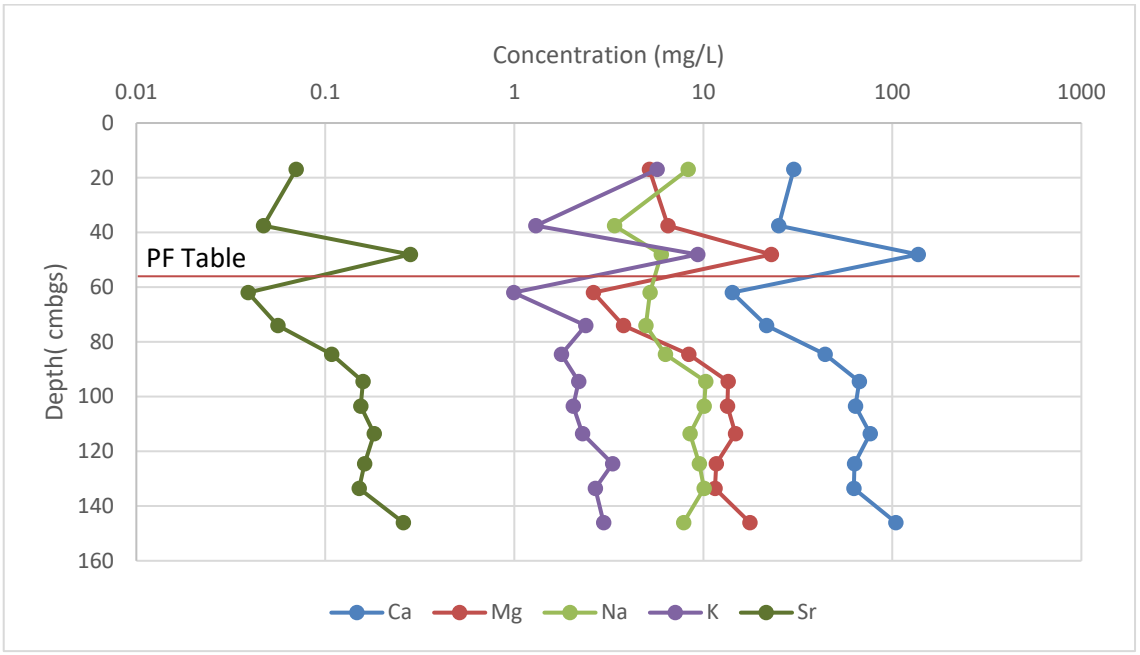

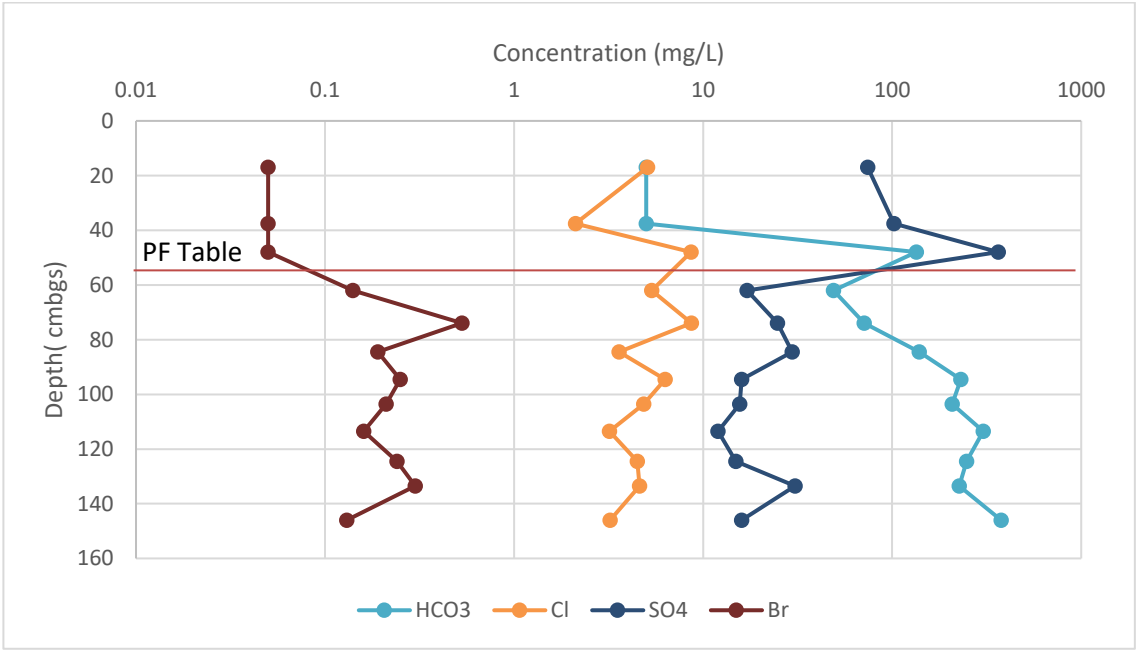

Figure 25: Geochemical profiles for some metals (top) and anions (bottom) in H040 core porewaters. Concentration is logarithmic in order to show trend in lower concentration ions.

Most metals and some anions appear to increase with depth, especially Ca, Mg and Sr. Cl and SO_4 seem to show a decrease with depth while HCO_3 matches Ca and Mg trends by increasing. As discussed in previous studies (Keller et al., 2010) the active layer becomes progressively leached of many minerals

such as carbonate over time, while the frozen permafrost soil is not exposed to this leaching process and remains less weathered. This appears to be the case in this core as well. A Piper diagram of these samples is shown in Figure 26. The unfrozen porewaters located in the peat soil in the top 55 cm appears to be primarily a Ca/Mg-SO_4 type water, while the water taken from frozen mineral soil is mostly Ca/Mg-HCO_3 type. Two samples appear to be somewhat transitional, showing a slight predominance in SO_4 compared to lower permafrost samples. These two samples were located within the top 30 cm of the frozen permafrost core.

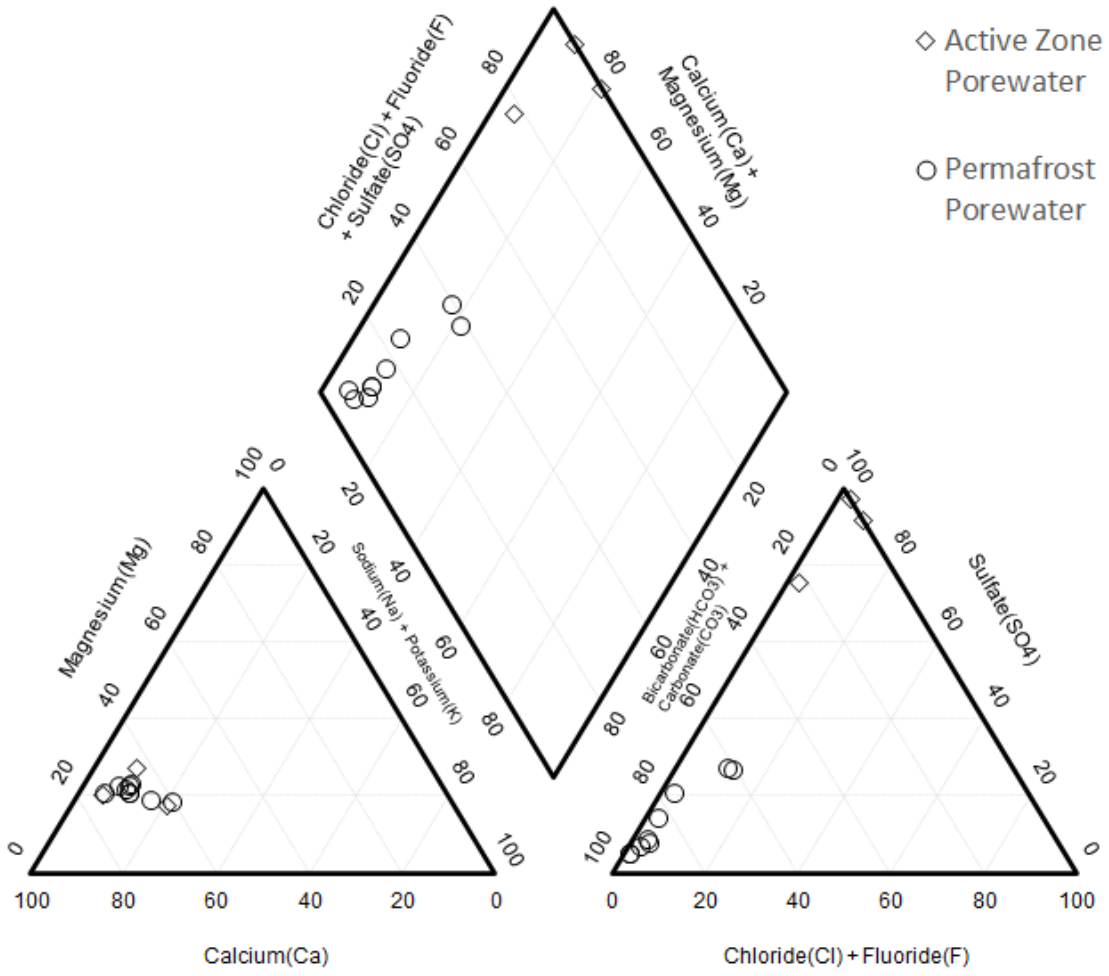

Figure 26: Piper diagram of active zone and permafrost porewaters from core taken at H040.

Porewaters from core at MW04 showed a comparable geochemical pattern as that seen within the H040 core, however not as much water could be extracted so data resolution is coarser (Figure 27). Water

extracted from adjacent core sections were amalgamated to get adequate water for analysis. HCO_3 concentrations were not determined for these samples, so for this reason, a Piper diagram was not constructed for water extracted from this core. Generally, most cations increase with depth although K, Na and Ca show a moderate decrease until about 70-115 before increasing. Cl initially decreases until 115 cm then increases, while SO_4 decreased until 70 cm then increases. The highest concentrations of all solutes are found in the bottom interval at 170 cm.

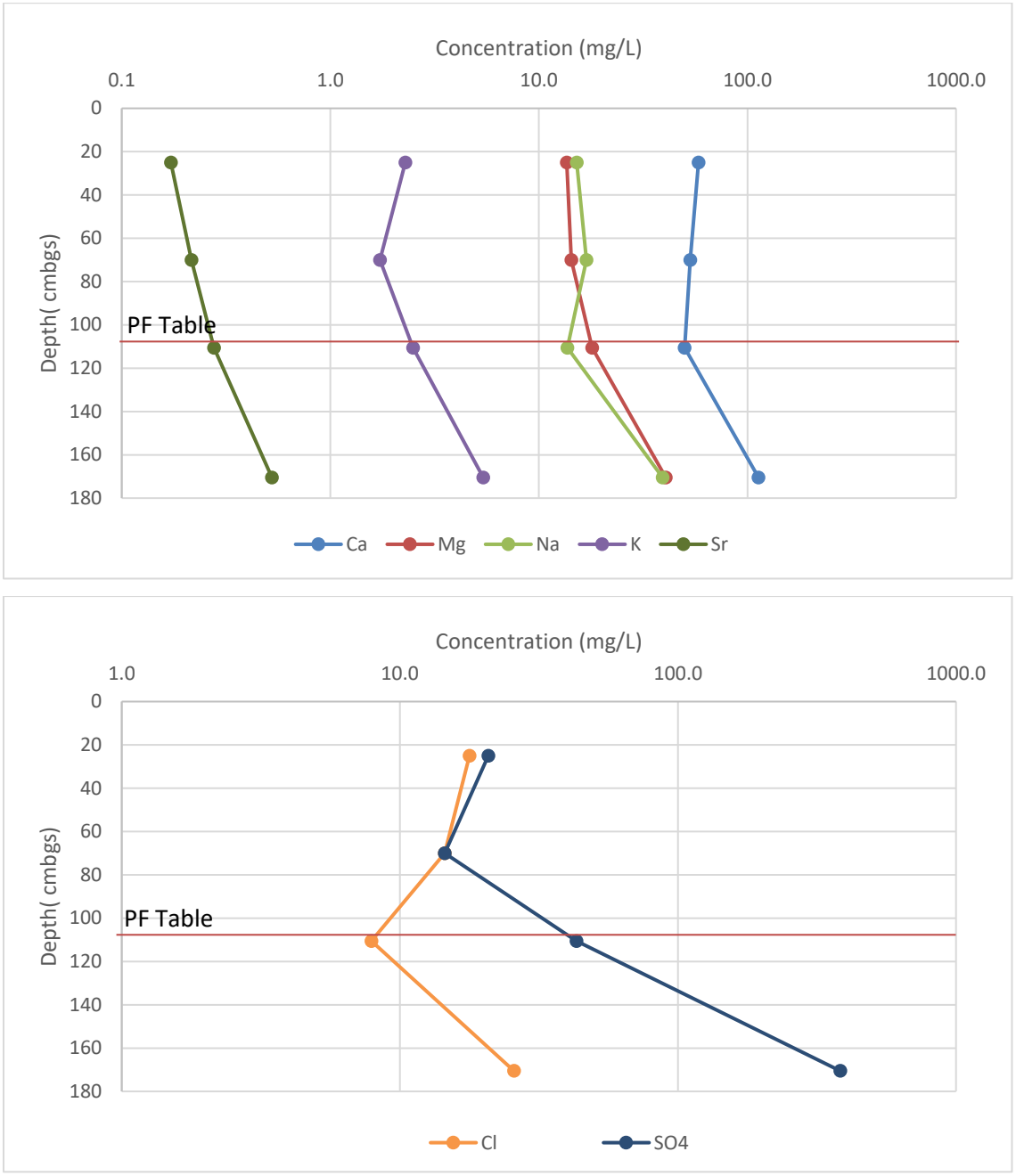

Figure 27: Geochemical profiles for some metals (top) and anions (bottom) in MW04 core porewater. Concentration is logarithmic in order to show trend in lower concentration ions.

In summary, these cores show that some solutes increase with depth into the frozen mineral soil. Over time, as climate warms and permafrost thaws these solutes may be released into the suprapermafrost groundwater system, resulting in temporarily elevated solute levels in streams and lakes that are fed by shallow groundwater. These may act as future tracers of permafrost thaw.

5.3.1.2 Springs

Springs were identified at numerous points within the Bogg Creek Watershed. IR survey results show that cold anomalies are frequent along banks of creeks, near lakes, and along seismic lines. Two thermal anomalies were found at the G-Lake site (Figure 22), which coincided with observations of recurring icings (Glass et al., 2020). These locations were visited in 2018 (GL1 and GL2) and were attempted again in 2019 (GL3). Observations of flowing artesian conditions from a PushPoint Sampler in this area confirmed these were springs. GL springs, groundwater and surface water, were all characterized by a similar geochemical signature (Figure 28). The dominant ions were Ca/Na-HCO_3 with a high concentration of Cl and very low levels of SO_4. GL1 had almost double the Cl concentration of the other two samples while having similar amounts of Ca and Na. On the Piper diagram (Figure 28) these samples plot left of center, within the Ca/Mg-HCO_3 diamond. GL3 groundwater contained more Ca-HCO_3 and less Na-Cl than the other GL samples. On the cation triangle, the samples all cluster along a line between the suprapermafrost and MHF subpermafrost samples, which is similar in the anion plot. Here, samples fall along the bottom line, indicating very little SO_4 and varying amounts of Cl and HCO_3. This suggests that one possible origin of this water could be mixing of brackish, Na-Cl rich subpermafrost and Ca-HCO_3 suprapermafrost groundwater. The second origin for this water could be from water interacting with the saltier till layer that was observed in MW04T, which had been under SO_4 reducing conditions. A recently thawed talik through this zone could explain why Na and Cl are high, as over time it would be anticipated that any salt present in this overburden would be leached out by flowing groundwater. If this were the case Na and Cl levels may decrease in these springs over time. Ponded surface water from GL1 and GL2 was collected in 2018 and had slightly different geochemistry to the groundwater emerging from the spring and were also distinct from one another. The ponded water was characterized primarily by similar cation ratios but GL1 surface water had very little Cl compared to GL2 surface water. The GL surface water may have been diluted by direct precipitation and runoff, which could explain the lower TDS values, but similar ion ratios, compared to the spring water. Based on the geochemical characteristic alone, it is difficult to identify the source of the spring water.

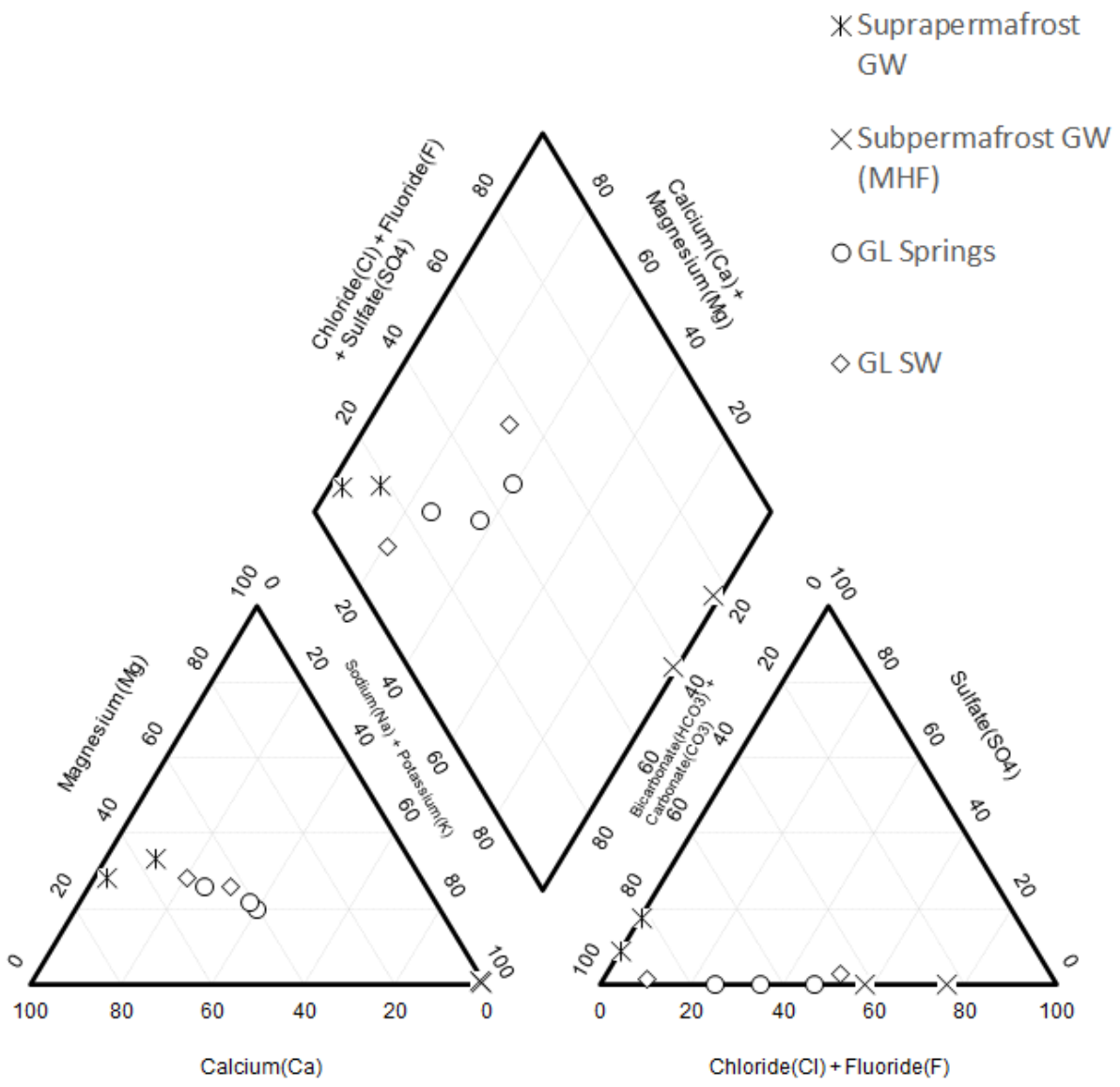

Figure 28: Piper diagram of GL springs surface water and groundwater, with groundwater samples for comparison. Some data obtained from Waterline Resources, (2013a, 2013b).

GPH1 was a spring located by following a small rivulet draining to a thermal anomaly back to its source using the IR camera (Figure 22) This spring occurred near a small pond with surrounding emergent grasses. Surface water in the spring area was sampled for geochemistry while groundwater was sampled for isotopes. GPH1 surface water is characterized by a predominance of Ca-SO_4, similar to the active

layer porewater (Figure 29). An attempt to revisit the spring and collect missing geochemistry data was endeavored in 2019 but due to equipment problems and time constraints the exact site was not found. The new location, GPH2 groundwater was sampled for geochemistry and isotopes. Surface water was not collected at this location. GPH2 groundwater was mostly dominated by Ca-HCO_3, while containing small amounts of Cl and SO_4. It is likely that GPH1 was isolated from GPH2, the latter comprising mostly of suprapermafrost groundwater discharge. Geochemistry at these sites did not reveal any strong evidence of deeper groundwater discharge, meaning these could be more localized, shallow springs that were detected by IR. However, due to the lack of GPH1 groundwater geochemistry a definite conclusion about the water origin cannot be made.

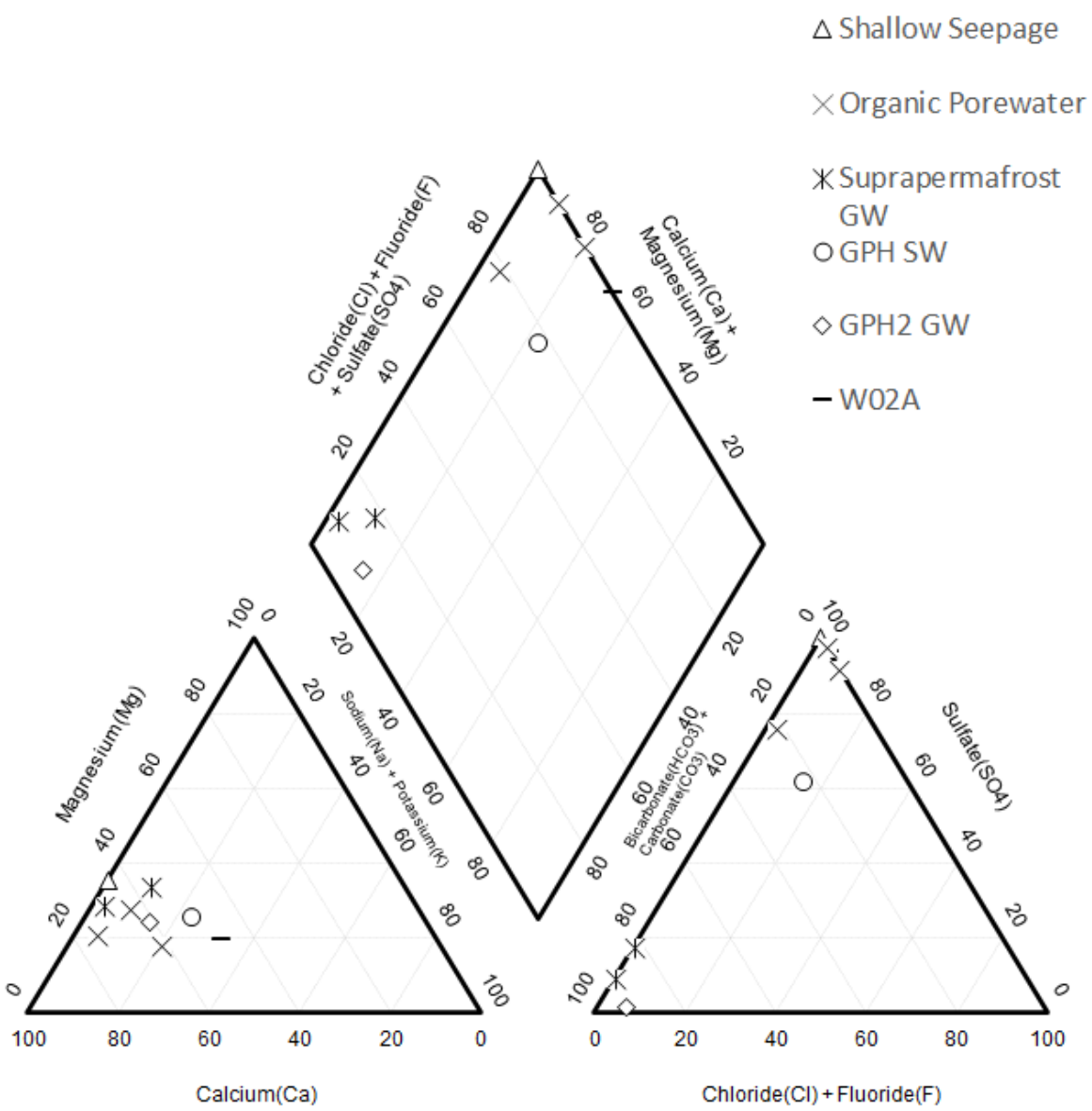

Figure 29: Piper diagram of GPH and W02A as well as the various water sources.

Located about 15 m from W02 (Figure 22), a small pool was discovered that had evidence of Fe and Mn oxidation, which was believed to be a spring. A hydraulic gradient and groundwater sample below this feature was attempted but these could not be obtained. The geochemistry of this pool was dominated by Ca/Na-SO_4 with no HCO_3 (Figure 29). This appeared to be dominated by very recent shallow seepage and active layer porewater like GPH1 rather than a spring. This pool was isolated from the stream at W02.

In conclusion, the geochemistry of these sites indicates that subpermafrost groundwater may be a contributor to some springs around the Bogg Creek Watershed, while others appear to be more localized springs that maybe discharging very shallow groundwater from the active zone. Thermal imagery is very useful in locating these features but is not able to distinguish between them. The true origin of these springs remains unclear as geochemical tracers may be sourced from multiple aquifers.

5.3.1.3 Surface Water Geochemistry

Water quality in Bogg Creek evolves significantly with increased distance downstream, over a distance of about 40 km. This section will explore the spatial and temporal variability in Bogg Creek surface water (Figure 22) starting upstream at the headwaters (W02, H046 and H044) and moving downstream towards the middle reaches (W04, W05, W06) and lower reaches (H030 and H001B) to the outflow at the Mackenzie River (H001). Historical Husky data and data collected during the 2019 field season will be explored in terms of geochemical evolution moving downstream. The historical Husky samples will be put into a seasonal context to explore baseline variability in geochemistry of the headwaters and lower reaches. Water samples collected by Husky along the AWR crossing points were taken in duplicates (H001B, H044 and H046, upstream and downstream), several meters upstream or downstream of the bridge crossings. Data for each site will be presented moving downstream.

5.3.1.3.1 Upland Tributaries

The furthest upstream point that was sampled during 2019 was W02, which was located upstream of H044 (Figure 22). TDS at this site was relatively low, at 233 mg/L. Geochemically this sample was distinct from most others, plotting on the margin between the Ca-HCO_3 and Na-HCO_3 zones (Figure 30). This unique geochemical signature could possibly be the result of mixing between these water types, such as suprapermafrost and subpermafrost groundwaters. As this site was added by UW during this study in 2019, historical data for this location does not exist.

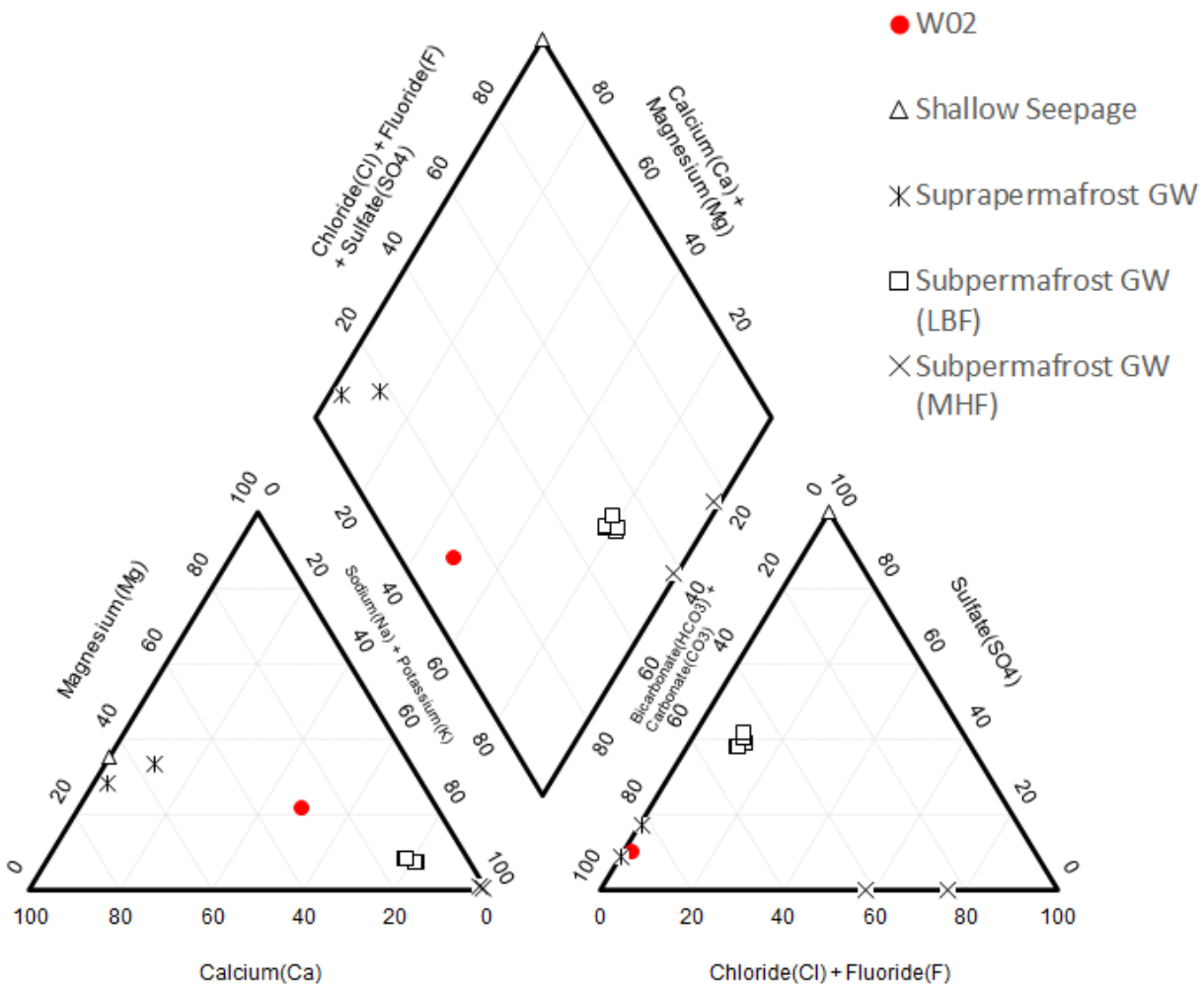

Figure 30: Piper diagram of W02 compared to groundwater and shallow seepage.

Historical data since 2014 does exist for the other tributary locations, H044 and H046 (Figure 22) which have very distinct geochemical characteristics. Because of the differences in sample timing, it is difficult to detect long term changes that may be occurring that are not due to natural seasonal variability over the 6-year monitoring period. However, some seasonal trends do appear in these data. On a Piper diagram (Figure 31) H044 generally plots between a Ca-Na-HCO_3 and Ca-Na-Cl type with highly variable TDS (Table 2). This water type is similar to water from the LBF but with higher TDS in general. H044 shows variability between years, with 2017 showing a drastically different geochemistry than the other years. There were also stark differences between upstream and downstream locations during this

period. In general, cations plot along a uniform line from Ca/Mg dominated to Na/K dominated, while anions plot between HCO_3 to SO_4 spaces with slightly more scatter due to differences in Cl content.

Table 2: TDS values and sample dates for each sampling period for H044.

Year	Sampling Days	TDS (mg/L)
2014	June 15	932
2015	August 29/30	680
2016	August 21	1404
2017	August 29	474
2018	August 30	320
2019	August 20	1305

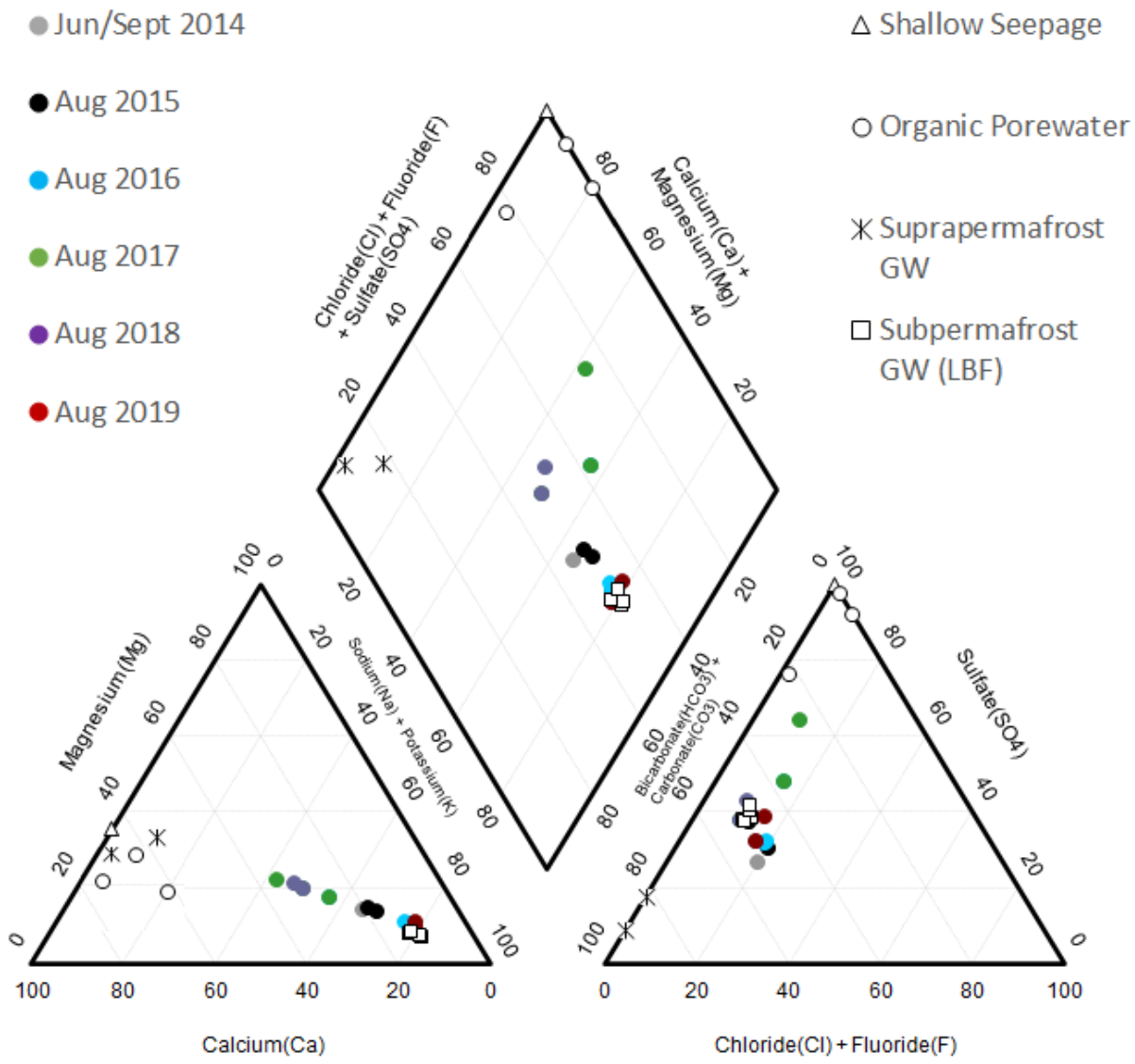

Figure 31: Piper diagram of H044 with, shallow seepage, organic porewater, suprapermafrost and subpermafrost groundwater for comparison.

In June 2014 H044 shows slight dominance of Na-HCO_3 with moderate TDS. In mid-August 2016 and 2019 samples are similarly Na-HCO_3 dominated with a high TDS. These also show slightly higher concentrations of Cl compared to other years. Greater variance can be seen in Late August samples from 2015, 2017 and 2018. Generally, TDS is lower during this time. In 2015 H044 was most like the previous year, being dominated by Na-HCO_3 with some more influence of Cl. 2017 saw great differences even

between sampling points upstream and downstream. Upstream was more Ca-SO_4 dominated while downstream saw a greater influence of Na-Cl and HCO_3. TDS was similar between sampling points and was very low. In 2018 the geochemistry became relatively even in proportions of Ca/Mg and Na/K as well as HCO_3 and SO_4, plotting roughly in the center of the Piper diagram. TDS was lowest during this period. Overall, stream water at this location appears to be highly similar to subpermafrost groundwater from the LBF during 2016 and 2019. Temperature data suggested that this part of the stream was gaining groundwater. Other inputs of Ca-SO_4 rich waters appear to be occurring during 2017/2018, possibly from increased surface runoff, shallow seepage, or active layer porewaters contributions. The nearby AWR which consists of shale and limestone aggregate could also be releasing ions locally in this location A groundwater sample was taken via PushPoint Sampler along the right bank of H044. This site showed heavy iron staining and the water sampled had a very high TDS (5390 mg/L). This sample was characterized by very high levels of Ca/Na and SO_4 and could be influenced by weathering shale in the AWR.

Contrastingly, H046, a separate tributary from H044, plots as primarily a Ca/Mg-HCO_3 type, with some variability from year to year (Figure 32 and Table 3). No samples were collected in June or July. Mid-August samples were collected in 2016 and 2019 and show similar TDS and Ca/Mg-HCO_3 dominated water types, with 2016 showing slightly higher SO_4 than 2019. Late August samples were taken in 2015, 2017 and 2018. All years have very similar ion ratios, being Ca-HCO_3 dominated while 2018 has less SO_4 compared to the other years. In the early fall, September 2014 had the most distinct chemistry, with an equal dominance of HCO_3 to SO_4. Finally, the samples taken from below ice in February 2019 had the highest TDS and were strongly dominated by Ca-HCO_3. This tributary appears to be mainly influenced by suprapermafrost and active layer water and diluted by runoff and shallow seepage, which vary seasonally. It also appears to be fed by lake outflow (H031). The geochemistry does not provide any evidence of subpermafrost groundwater discharge in this tributary. Compared to H044, TDS values do not seem to follow the same pattern, with the highest levels recorded in 2018, when H044 was lower compared to other years. Samples taken during wetter times of the year typically plot closer to the Ca-SO_4 type waters of shallow seepage water and active layer porewater which was a similar case in H044, while those taken during drier times of the year such as 2016 and 2019 plot closer to the Ca-HCO_3 type suprapermafrost waters. The AWR may be having some impact locally on shallow groundwater in this area, as a sample taken nearby H046 showed. While TDS (614 mg/L) was not as high as groundwater near H044, the sample contained high SO_4 (Data not shown). This does not appear to be impacting the stream itself.

Table 3: Table of TDS values and sampling times for each sampling period at H046.

Year	Sampling Days	TDS (mg/L)
2014	September 20	ND
2015	August 29/30	ND
2016	August 21	69
2017	August 29	78
2018	August 30	61
2019	February 10 & August 20	260/68

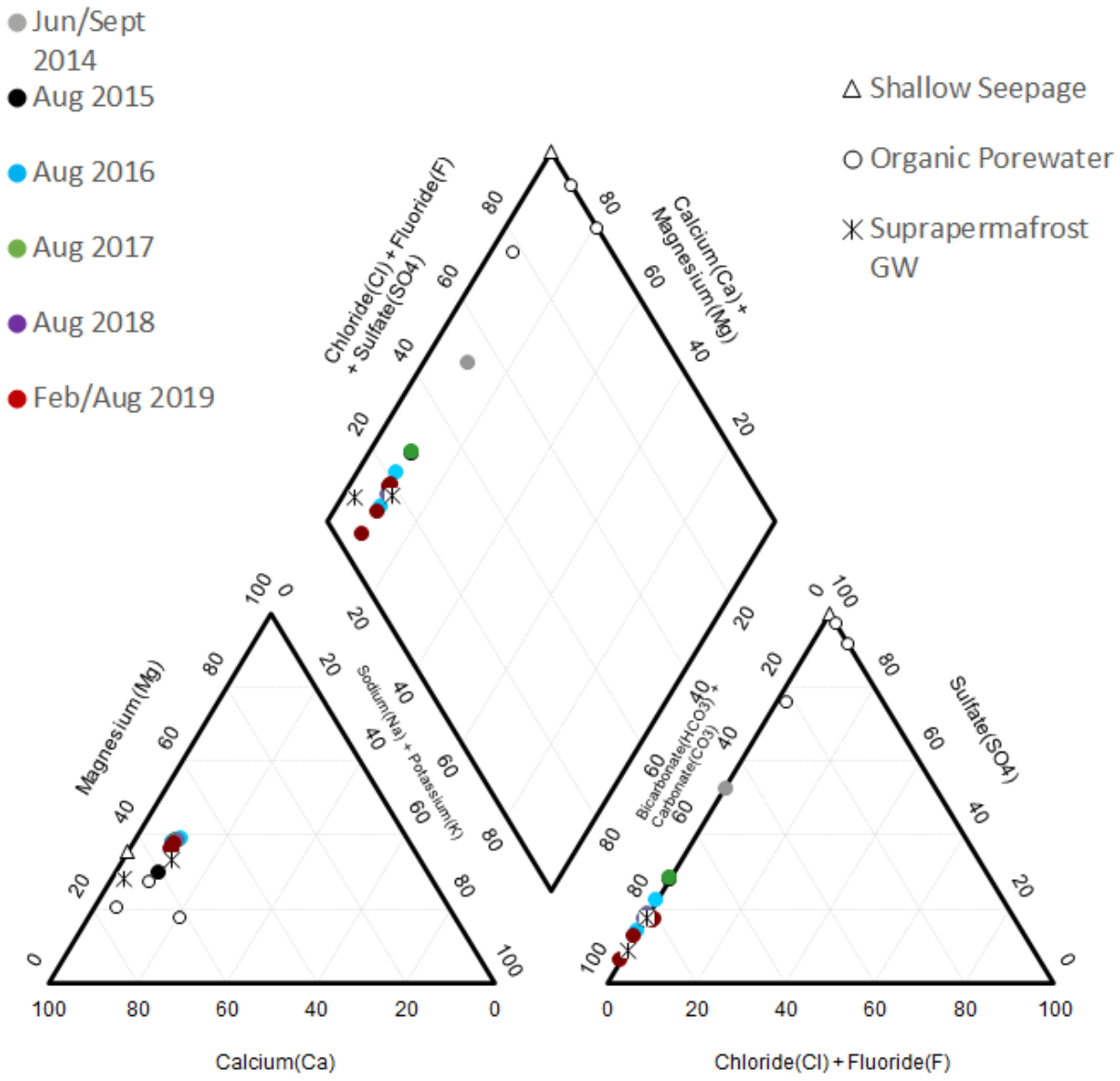

Figure 32: Piper diagram of H046, with shallow seepage, organic porewater and suprapermafrost groundwater for comparison. Data obtained directly from Husky and from Waterline Resources (2013a, 2013b).

5.3.1.3.2 Middle and Lower Reaches

The middle reaches of Bogg Creek (located downstream of H044 and upstream of H030) were added to the sampling list in summer 2019. These locations consisted of W04, W05 and W06 (Figure 22). Geochemically, these locations were similar to each other and plotted closest to H044 on a Piper diagram (Figure 33). Upon examining ion compositions, these reaches appear to primarily represent mixing of

H044 and H046 tributaries, although this is difficult to observe in the Piper diagram. Geographically, W04 is just downstream of the H044 and H046 tributaries. Geochemistry between each site was quite consistent, suggesting the possibility of these being losing reaches or areas with little groundwater discharge or infiltration occurring, and no tributaries adding to flow.

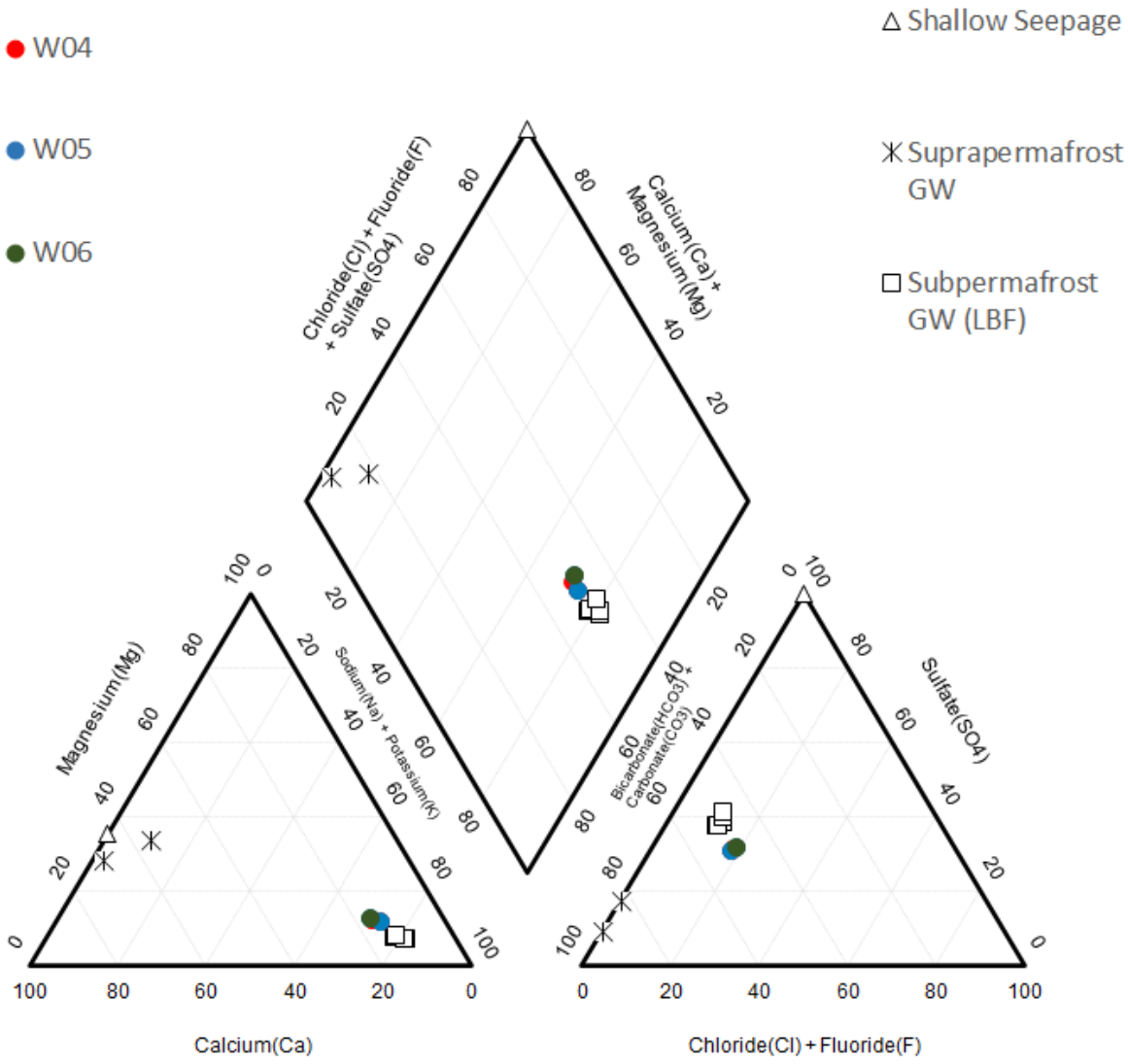

Figure 33: Piper diagram for middle reaches, with shallow seepage, subpermafrost and suprapermafrost groundwater for comparison. Data obtained directly from Husky and from Waterline Resources (2013a, 2013b).

Data in the lower reaches of Bogg Creek were collected at three sites, in order of downstream appearance, H030, H001B and H001 (Figure 22), which have been grouped together for each sampling

period as they are very similar in geochemical composition. Typically, samples plot around the center of the Piper diagram, with some variability between sampling periods (Figure 34 and Table 4).

Table 4: TDS values for the lower reaches of Bogg Creek for each sampling year.

Year	Sampling Days	TDS (mg/L)
2012	July 27	362
2013	June 18 & September 14	173/300
2014	June 15 & September 20	175/466
2015	August 29/30	363
2016	August 21	469
2017	August 29	318
2018	August 30	202
2019	February 10 & August 20	634/394

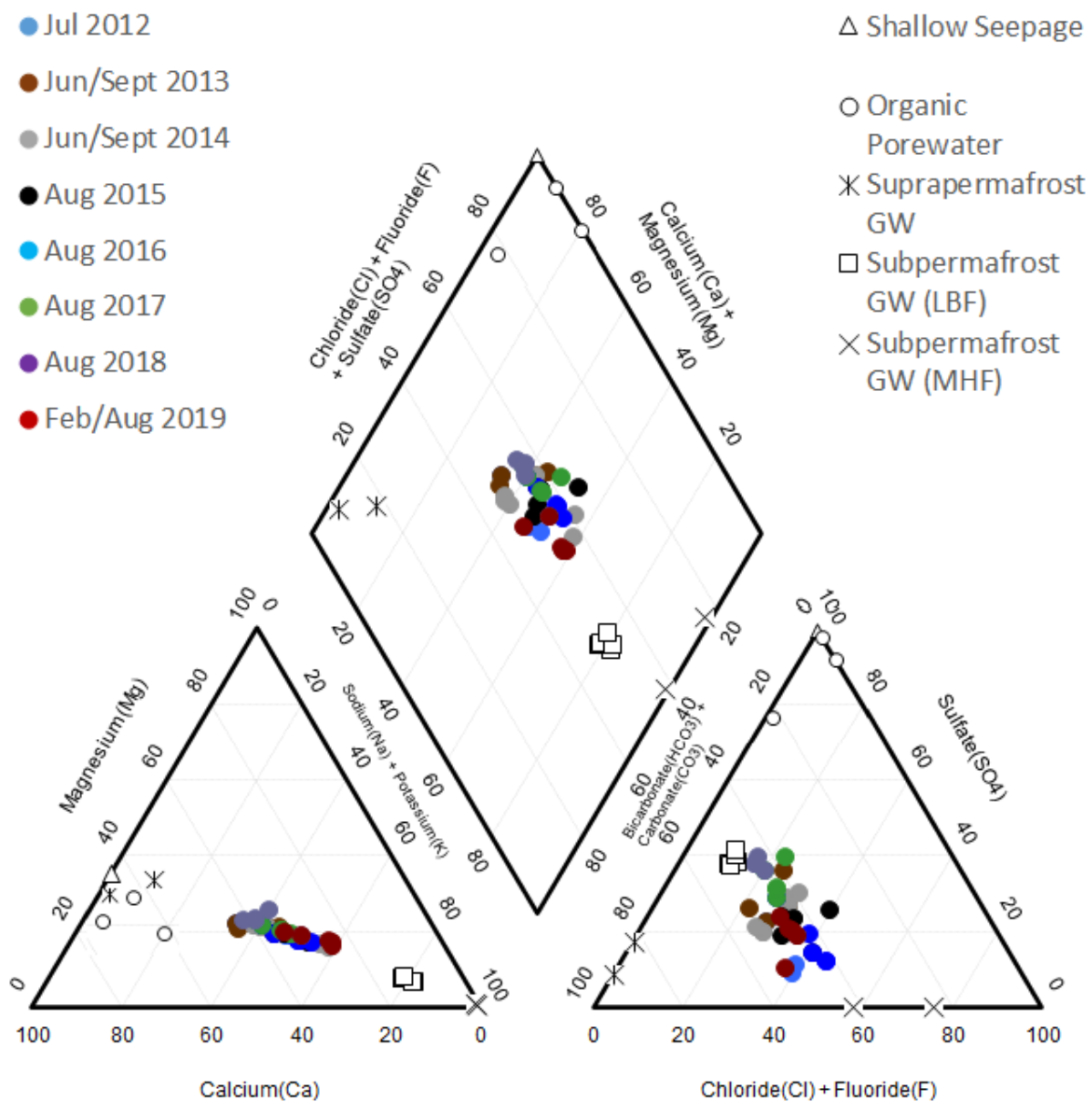

Figure 34: Piper diagram of H001, H001B and H030 for all sampling years with all groundwater and shallow seepage sources for comparison. Data obtained directly from Husky and from Waterline Resources (2013a, 2013b).

On the cation plot, samples fall along a line from Ca/Mg dominated towards being Na/K dominated. On the anion plot a line with some spread is formed from the HCO_3/SO_4 dominated zone towards the HCO_3/Cl zone. Within this clustering samples plot closer together if they are taken at the same time of the

year on a Piper plot. Very little difference was noted between duplicate samples taken upstream and downstream from the bridge.

June 2013 and 2014 samples fall slightly within the Ca-HCO_3 zone with a lower to moderate TDS, while July and Mid-August samples from 2012, 2016 and 2019 generally plot between the Ca-SO_4 and Na-Cl diamonds and with higher TDS. Comparatively, year 2016 and 2019 see some differences with regards to TDS and ion ratios, 2016 has a slight dominance of HCO_3/Cl over 2019. Late August of 2015, 2017 and 2018 are slightly more Ca-SO_4 rich with some falling slightly within the Na-Cl zone. Year 2015 and 2016 show similar proportions of cations, but anions are slightly more dominated by Cl than SO_4. Year 2019 shows higher proportions of Ca-Mg and SO_4 while HCO_3 remains relatively constant throughout each year. An outlier, sample H030 in 2015 showed higher amounts of Na, Cl and SO_4 compared to the other samples. Similarly, in September 2013 samples plot slightly within the Ca-SO_4 zone but also on the margins of Na-Cl, while in 2014 these fall slightly within the Na-Cl diamond. Most differences between years are in the form of higher incidences of Na/K in 2014 with similar proportions of anions. Finally, a sample obtained from H001B in February plotted slightly within the Ca-HCO_3 zone and with a moderate TDS. This sample also had low proportions of SO_4 much like samples from July.

These ion ratios may be indicative of mixing occurring in the stream with different proportions of the various water sources. Similar to the tributaries, early summer and late summer/early autumn appear more strongly influenced by organic porewaters/shallow seepage than in mid-summer, while early summer appears less influenced by suprapermafrost groundwater than late summer/early autumn. Samples range between the shallow (suprapermafrost, organic porewaters and shallow seepage) and subpermafrost (LBF and MHF) waters.

Figure 35 demonstrates the changes that occur moving downstream from W02 to H001 from August 20-22, 2019. No precipitation fell during this period and so this likely provides a suitable snapshot of stream geochemistry spatially.

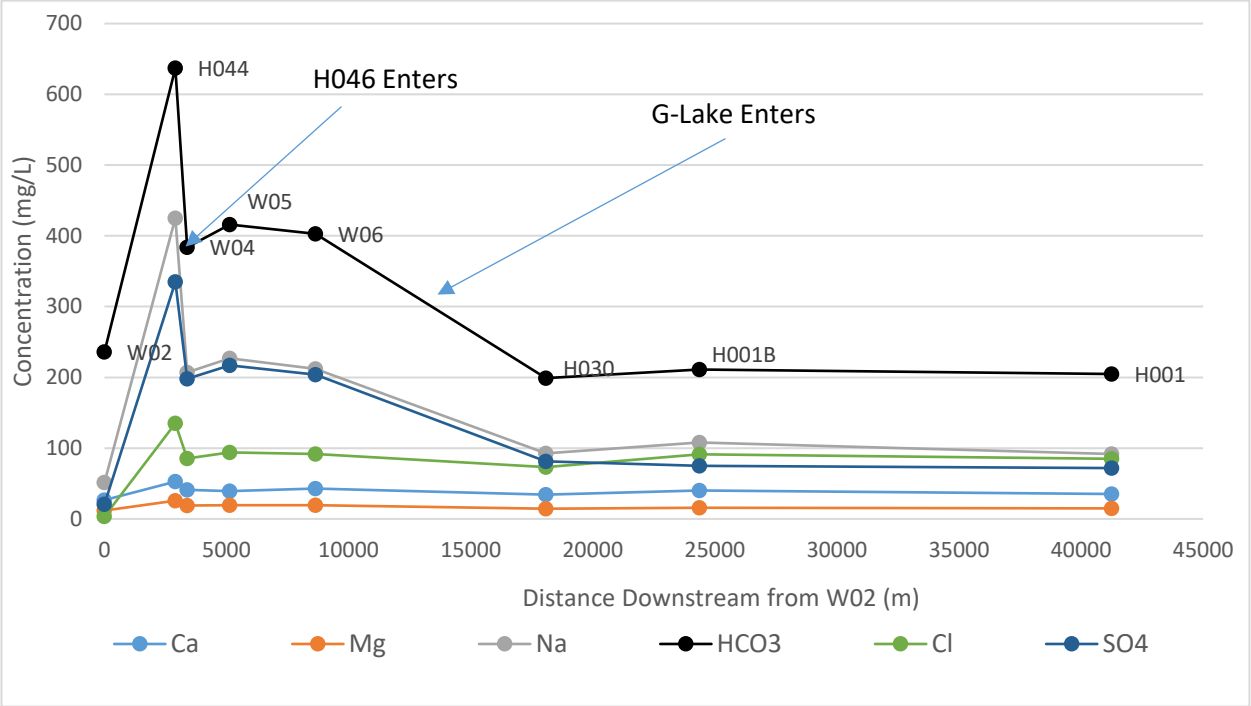

Figure 35: Concentration of major ions over distance along Bogg Creek in 2019, starting in the headwaters at W02.

W02 was generally more dilute in most solutes than other samples except for HCO_3. In general, HCO_3 is the most dominant ion for all reaches. Moving downstream to H044 all solutes spiked considerably. Downstream at W04 solutes drop but remain elevated in comparison to W02, due to the influx of H046 stream water. Solutes again see a small increase at W05, possibly due to influx of another tributary or groundwater input. Some dilution occurs downstream towards W06, and even further dilution occurs towards H030 which is downstream of G-Lake and W08. Very little change occurs except for a slight elevation in solutes around H001B, and Cl becomes slightly more dominant than SO_4. This trend continues at H001.

In summary, large changes in geochemistry appear to be associated with locations downstream of major tributaries or lakes such as G-Lake (see Figure 21), and small changes may be due to minor tributaries or lakes, although spatial resolution is likely not fine enough to be completely certain. Groundwater inflow may also play a part here, either directly (springs or bank seepage) or indirectly (groundwater inflows to lake tributaries). Groundwater flow to Bogg Creek is evident based on these findings, with subpermafrost groundwater being a significant component to at least one tributary and possibly a minor component to the furthest downstream reaches. The middle reaches of the creek do not appear to be gaining much

groundwater and instead may be losing reaches, as was suggested by temperature profile data in Section 5.2.12, Figure 14.

5.3.1.3.3 Lakes

Two lakes within the Bogg Creek Watershed were sampled by Husky and consultants, these being H031 and H040 (Figure 22). Data was provided for these lakes from 2016-2019. These lakes were sampled each year while H040 was also sampled in February 2019. Plotted on a Piper plot these lakes show distinctly different chemistries (Figure 36).

H031 plots as primarily a Ca-HCO_3 type water with minimal variability between years (Figure 36 and Table 5). TDS was low and ranged from 69-79 mg/L. This signature seems to indicate some influence of suprapermafrost groundwater that is diluted by very young water either through runoff, shallow seepage or active layer organic porewaters. Geochemistry and TDS were very similar to that of H046, which also appeared to consist of shallow seepage and suprapermafrost groundwater.

Table 5: TDS values and sampling dates for H031 during years 2016-2019

Year	Sampling Days	TDS (mg/L)
2016	August 20	70
2017	August 28	79
2018	August 29	69
2019	August 20	73

In H040 samples are dominated by Ca/Mg-SO_4 with high incidences of Na and Cl (Figure 36). TDS ranged from 315-939 with the highest TDS sample occurring in February 2019 (Table 6). These samples do not fit neatly between established water sources on a Piper diagram and are likely the result of natural geochemical variability between sources as well as geochemical reactions. The high concentration of SO_4 implies large inputs of Ca-SO_4 rich water such as GPH1 spring water or active layer organic porewater. Cl also appears to be quite high in this lake, suggesting a possible component of subpermafrost or other groundwater source. On a Piper plot, samples from 2016 and 2019 plot slightly lower than 2017 and 2018. This is likely due to decreased inputs of Ca-SO_4 water. Winter 2019 plots the lowest on a Piper diagram, and slightly towards suprapermafrost groundwater, suggesting some of the Ca-SO_4 inputs are shallow and not subpermafrost water. The February sample represents a time when the active layer is likely frozen,

minimizing flow from this area. There is likely more flow coming from deeper mineral soils during this time.

Table 6: TDS values and sample times for H040 during years 2016-2019.

Year	Sampling Days	TDS (mg/L)
2016	August 20	346
2017	August 28	370
2018	August 30	315
2019	February 10 & August 20	939/326

Each lake appears to have the highest summer TDS in 2017, and the lowest summer TDS in 2018. This contrasts with creek waters which generally had lower TDS during 2017 and highest during 2016. In H031 2016 had the second lowest TDS. These differences may be due to heterogeneous evapo-concentration occurring at each lake. The highest TDS overall in H040 occurred in winter 2019, which may have been as a result of cryo-concentration combined with increased groundwater inputs.

In 2019, W08 (Figure 22) was added to the sampling list, aimed at collecting a representative sample draining G-Lake. While the actual tributary could not be reached, a wetland that was connected to the water course was sampled instead. A sample was taken from the surface water and groundwater immediately adjacent to the wetland in organic soils. W08 surface water was characterized as a Ca-Cl type water, while W08 groundwater was more like GL spring water (Section 5.3.1.2) as a Ca-HCO_3/Cl type. Both samples had elevated Cl concentrations comparable to surface water from Bogg Creek, but it was the lack of any SO_4 that implies either subpermafrost groundwater discharge influences or flow through a closed overburden system with high salt content and reduction of SO_4. Anions in W08 surface water were similar to MHF groundwater. This geochemical signature appears to be consistent in at least 2 parts of the Bogg Creek Watershed in the vicinity of G-Lake. G-Lake appears to be fed extensively by this unique type of groundwater, the effect of which can be seen in the downstream geochemistry.

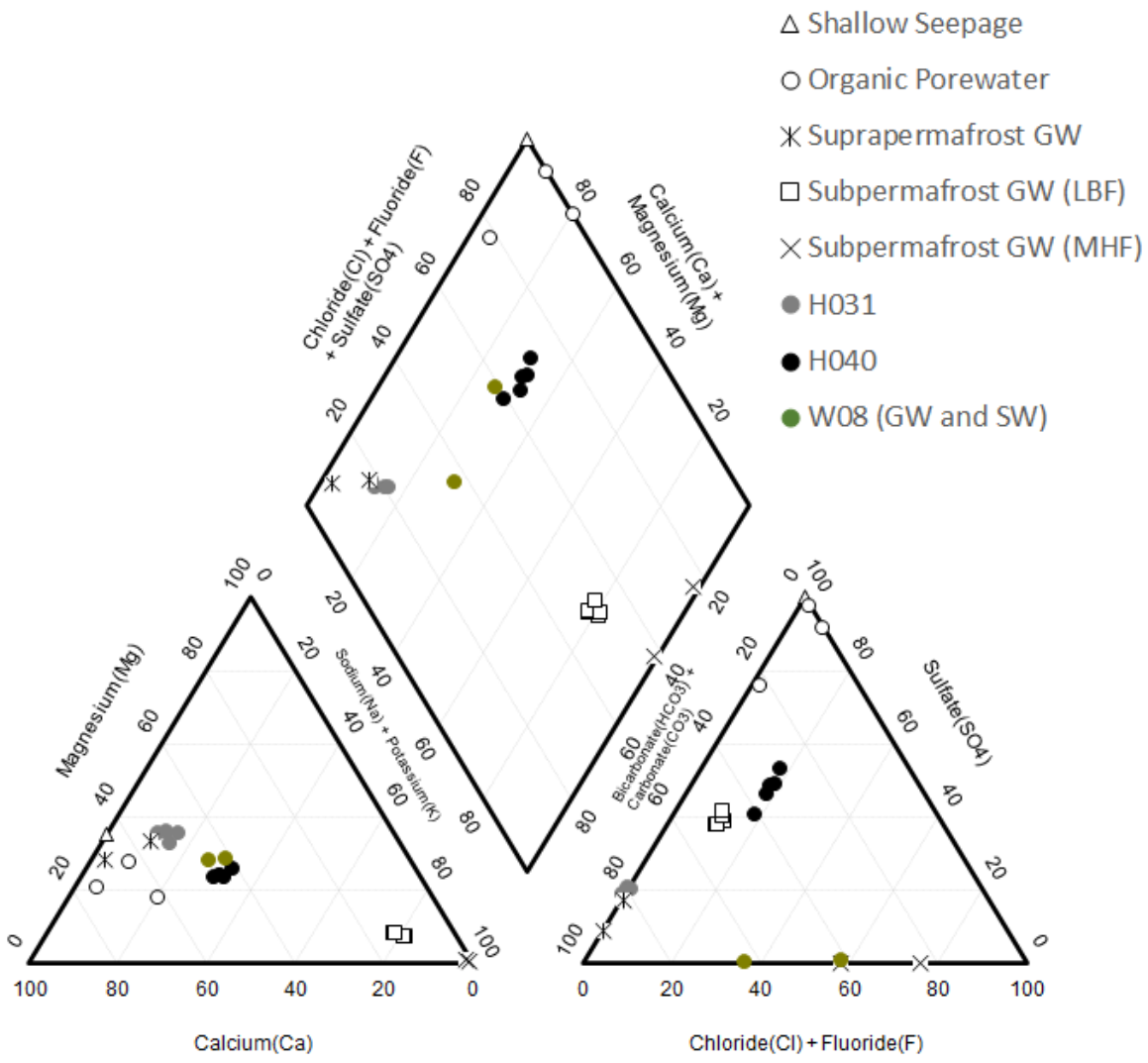

Figure 36: Piper diagram of the two lakes, H031 and H040 and the tributary draining from G-Lake, W08.

A number of lakes outside of the Bogg Creek Watershed also have been sampled historically. These lakes can be seen outside the catchment boundaries in Figure 22 and a Piper plot of these lakes is shown in Figure 37. A general analysis of these data was performed to see any trends of these lakes in relation to site geology and to compare with lakes within Bogg Creek Watershed.

Most lakes (H006, H016, H023, H027, H041, H042, H043) plot as a Ca/Mg-HCO_3 type water. These lakes are also located primarily northwest or south of the Bogg Creek Watershed, with H027 being the exception. H027 is located in proximity to H026 and H028, north of G-Lake. These lakes also share similar geochemical signatures of a higher Cl, lower SO_4 content than the other Ca-HCO_3 dominated lakes. This could suggest that these lakes have a similar source of saltier water as G-Lake does, with this major source aquifer residing in this region of the study area. These lakes are situated upon bedrock mapped as IF shale, similar to G-Lake.

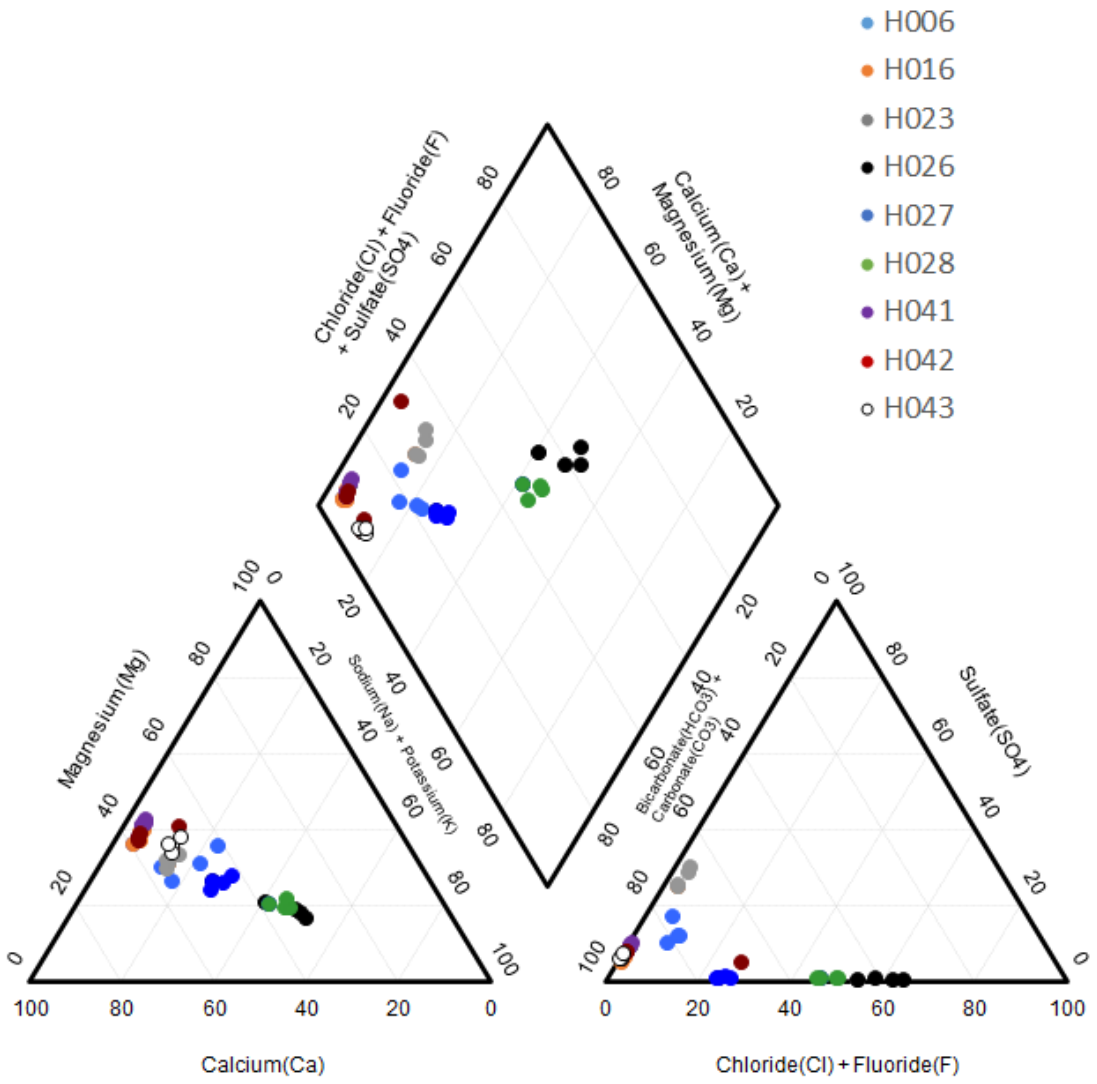

Figure 37: Lake geochemistry Piper diagram for lakes outside of the Bogg Creek Watershed, 2016-2019 samples. Data obtained directly from Husky Energy.

In summary, lakes in the Bogg Creek Watershed show great variability between each other in their geochemical signatures, suggesting variability between sources. While shallow groundwater inputs are evident in most lakes, some lakes such as G-Lake, H040, H026, H027 and H028 may be receiving subpermafrost groundwater as well. Lake H031 is connected to tributary H046 and shares a similar geochemistry consisting of shallow groundwater inputs, while H040 is connected to a larger series of rectangular lakes that are aligned along a northwest/southeast axis. Localized springs can be found along the margins of these lakes (such as GPH). As water was obtained from H040 in February, it is possible that a talik exists below these lakes that allow for groundwater flow into or out of them year-round. These lakes drain towards the northeast, connecting to Bogg Creek downstream of H001B. This does not appear to have a significant impact on the geochemistry of the creek as very little change is noted between H001B and H001. This is in contrast to G-Lake, which does appear to impart a significant change on the geochemistry between W06 and H030. G-Lake and the springs that feed it are very similar to the lakes outside of the watershed (H026, H027 and H028) and are likely fed by a similar source of groundwater.

5.3.2 Organic Chemistry

5.3.2.1 Regional Summary

Toluene and Benzene were detected in WW04A (ConoccoPhilips well, not shown in figure) in appreciable levels. This raised the possibility of BTEX as a potential tracer which was analyzed at select sites (Table 7). In 2018 sites analyzed for BTEX included GL1, GPH, and SL. In 2019 BTEX was sampled in H001B, H040, H046 and MW09A/B. Appreciable quantities of BTEX were found in MW09A and MW09B; only ethylbenzene was not detected in MW09A. MW09B also had higher quantities of all BTEX compounds and toluene concentration was the highest in these samples. BTEX was not detected in these wells in 2013. Toluene was also detected in H046 and in August 2016 and February (was not detected in a duplicate) and August of 2019, ranging from 0.00064 to 0.00321 mg/L. GL1, GL2 were sampled in August 2018 and GL3 in 2019. Sample GL1 had contained toluene at 0.0142 mg/L. BTEX was not detected in any other GL samples. Lastly, lake H031 in 2012 also had detectable toluene levels at 0.00064 mg/L. Between these surface and near-surface samples no other species of BTEX were detected. The lack of other species in conjunction with toluene suggests a potential biogenic origin of toluene in these environments as opposed to thermogenic (Richards & Sandau, 2018).

Table 7: Organic analyte (methane and BTEX) concentrations for various samples. Includes surface water, spring water and groundwater. Some data provided by Waterline Resources (2013a), AMEC 2013.

Sample	Sample Date	Sample Type	Methane (mg/L)	Benzene (mg/L)	Ethyl-Benzene (mg/L)	Toluene (mg/L)	o-Xylene (mg/L)	m+p-Xylene (mg/L)	Xylenes (mg/L)
H001B	2/10/2019	**Creek**	0.003	<0.00040	<0.00040	**0.00059**	<0.00040	<0.00080	<0.00089
H046	8/21/2016	**Creek**	-	<0.00050	<0.00050	**0.00064**	<0.00050	<0.00050	<0.00071
H046	2/10/2019	**Creek**	2.100	<0.00040	<0.00040	**0.0013**	<0.00040	<0.00080	<0.00089
H046	8/21/2019	**Creek**	-	<0.00050	<0.00050	**0.00321**	<0.00050	<0.00050	<0.00071
GL1 GW	9/1/2018	**Spring**	**1.470**	<0.00050	<0.00050	**0.0142**	<0.00050	<0.00050	<0.00071
GL2 GW	9/1/2018	**Spring**	**1.930**	-	-	-	-	-	-
GPH GW	9/1/2018	**Spring**	**0.802**	-	-	-	-	-	-
MW-09A	2/3/2013	**Well**	-	<0.00050	<0.00050	<0.00050	<0.00050	<0.00050	<0.00071
MW-09A	2/6/2019	**Well**	<0.003	**0.00046**	<0.00040	**0.0017**	**0.00062**	**0.0014**	**0.0021**
MW-09B	2/21/2013	**Well**	-	<0.00050	<0.00050	<0.00050	<0.00050	<0.00050	<0.00071
MW-09B	2/8/2019	**Well**	**0.006**	**0.00077**	**0.0005**	**0.0025**	**0.0012**	**0.0026**	**0.0038**
MW-09BD	2/8/2019	**Well**	<0.003	**0.00078**	**0.0005**	**0.0025**	**0.0012**	**0.0026**	**0.0038**
MW-19B	2/10/2013	**Well**	-	<0.00050	<0.00050	**0.00057**	-	-	<0.00071
WW04A	2/8/2013	**Well**	-	**0.0023**	<0.0005	**0.0074**	-	-	<0.0005

5.4 Isotopes

The isotope analyses are discussed in the following subsections. the locations of the isotope sampling locations are shown on the site maps which are displayed again as Figures 38 and 39.

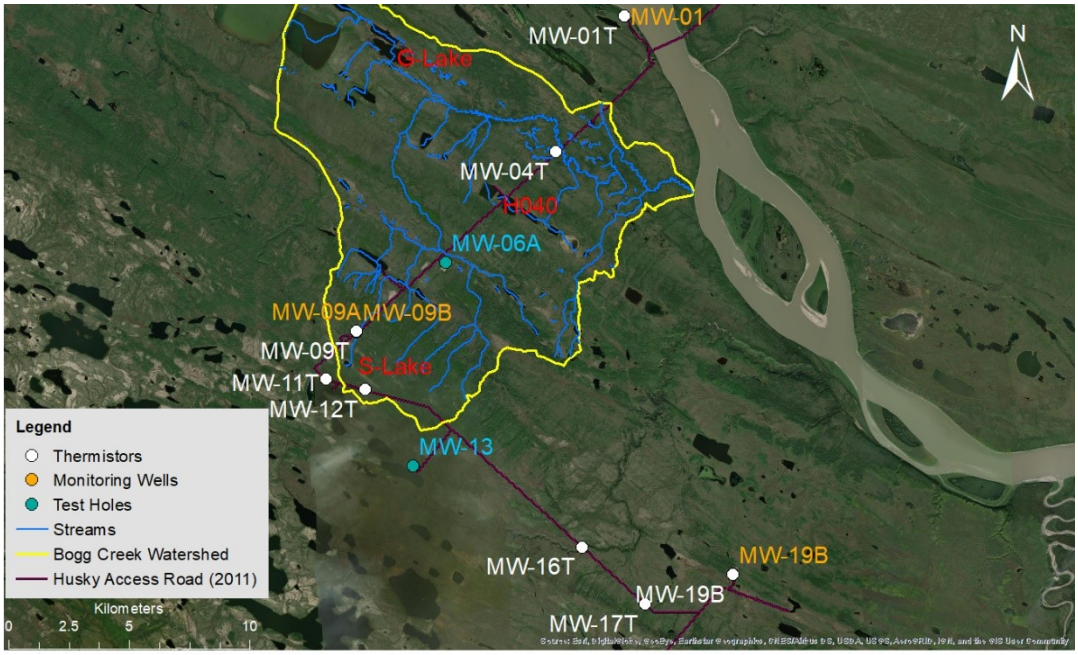

Figure 38: Map of groundwater and temperature monitoring wells as well as test holes within the study area. Key sites are labelled in red (G-Lake/GL, S-Lake/SL, and H040). Isotopes were obtained by Husky in MW19B and MW09A and MW09B in 2013, and again from MW09A and MW09B in 2019.

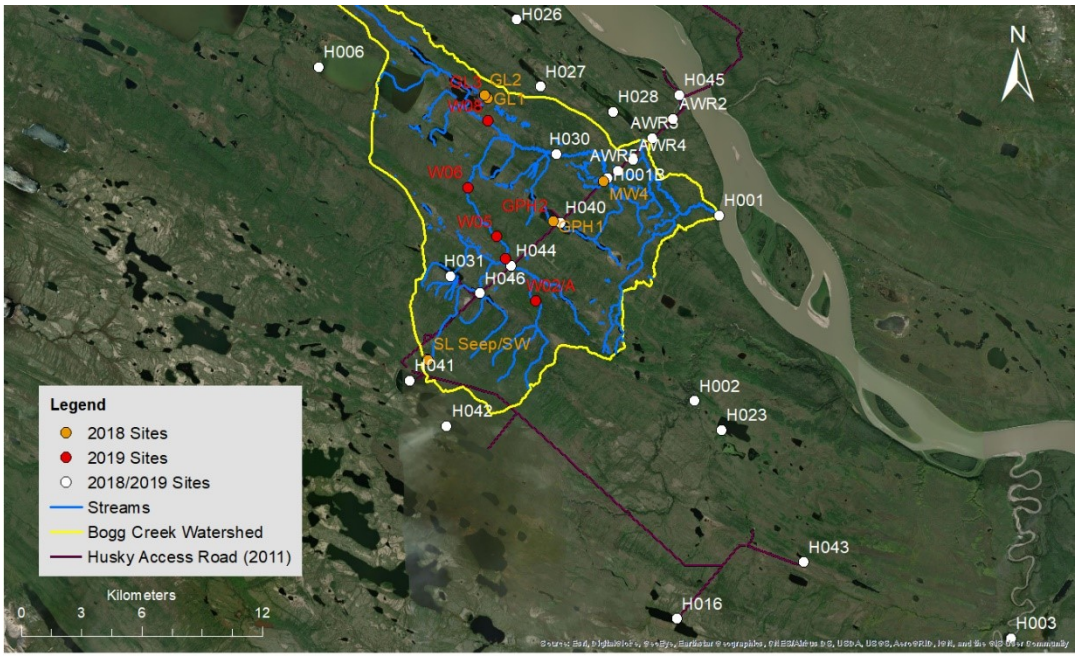

Figure 39: Surface water and spring sampling locations for 2018 and 2019 are shown in orange and red, respectively, while historical Husky sites are shown in white. Isotopes were taken from select

locations, for complete record see Appendix A, Table A-2. Also note that some locations overlap with one another at this scale, such as GPH1/2, GL1/2/3 and W02/A.

5.4.1 Stable Water Isotopes ($\delta^{18}O$ and $\delta^{2}H$)

5.4.1.1 Regional Summary

Regional surface water $\delta^{18}O$ and $\delta^{2}H$ values were determined throughout the watershed and the surrounding area by Husky once in 2012 and by Waterloo in 2018 and 2019. Many sampled surface water bodies fall outside the Bogg Creek Watershed but provide a glimpse into surface water dynamics in the region. Surface water samples either fall on the Local Meteoric Water Line (LMWL) ($\delta^{2}H=7.86*\delta^{18}O+1.82$) for Norman Wells (van Everdingen, 1982) or along a Local Evaporative Line (LEL) (Figure 40). It is unknown how much data were used to estimate the LMWL, but this seems to fit the non-evaporated data points quite well. The next closest stations to Norman Wells that have established a LMWL would be Snare Rapids, NWT or Yellowknife, NWT. It should be noted that not all locations were resampled after 2012, and some new locations were added in subsequent years. In 2012 $\delta^{18}O$ and $\delta^{2}H$ values ranged from -22.7‰ to -12.8‰ and -175.0‰ to -128.0‰ respectively. In 2018 the data ranged from -21.6‰ to -14.4‰ and 159.1‰ to -134.3‰ and in 2019, -20.5‰ to -13.3‰ and-162.0‰ to -127.2‰. While the greatest range was during the earlier sampling period in 2012, it should be noted that the data sets are slightly different as not all points sampled in 2012 were resampled in subsequent years.

These data produce three LELs when plotted. Linear regression of the LEL in each year returns slightly different LEL equations (Table 8).

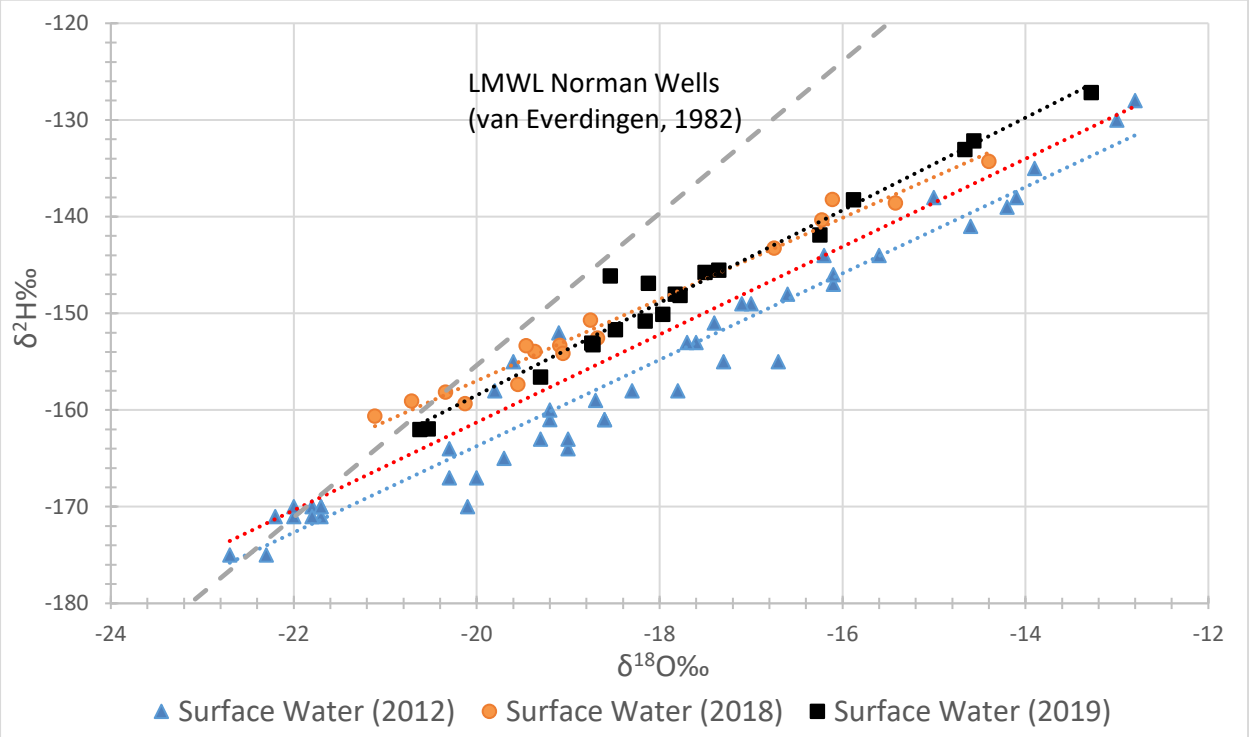

Figure 40: Surface water $\delta^{18}O$ and $\delta^{2}H$ from Bogg Creek and surrounding watersheds and the different LELs formed. LEL for all years is shown as red line. Includes data from MWH, (2012).

Table 8: LEL slope comparison between each sampling period for waters in the study area.

Date	LEL Regression Equation	LMWL Intersection $\delta^{18}O$ Values (‰)	LMWL Intersection $\delta^{2}H$ Values (‰)
July 2012	y = 4.467x - 74.405	-22.4	-175.0
August 2018	y=4.785x - 62.780	-21.1	-165.9
August 2019	y = 5.098x - 57.751	-21.5	-168.8
All years	**y = 4.5434x - 70.415**	**-21.8**	**-169.8**

Slopes differ between each year, as do the LMWL intercepts. Following each line back to where it intercepts the LMWL allows for estimation of the weighted average for regional precipitation. In 2012 the intersection is around $\delta^{18}O$ -22.4‰, -21.1‰ in 2018, and -21.5‰ in 2019. 2012 was sampled in late July during a wetter than average year that had more snow than 2018, while 2018 had more rain than 2012. The increased amount of snow plus the collection earlier in the year may have meant that surface water was under more influence from snowmelt/early spring rain during this time. Combining all data and performing linear regression provides another estimate for precipitation average ($\delta^{18}O$ -21.8‰ and $\delta^{2}H$ -169.8‰). This average is also oftentimes indicative of the isotopic composition of shallow groundwater, which when composed of a mixture of seasonal precipitation will have similar $\delta^{18}O$ and $\delta^{2}H$ values. This provides a good point of comparison, as we would expect samples sourced from snowmelt or Pleistocene groundwater or groundwater derived from thawing of permafrost to be more isotopically depleted than this value (Michel, 1986; Michel & Fritz, 1982). Through dating of LBF water it was estimated that recharge of this formation occurred during the Last Glacial Maximum, and this water had a characteristically depleted isotope signature (Waterline Resources Inc., 2013b). Conversely, waters recharged more by warm summer rains would be anticipated to be more isotopically enriched than the average value.

Examining a plot of the combined isotopic data from all springs, groundwater (collected from wells) and surface water bodies collected during the three sampling campaigns uncovers some general patterns (Figure 41). Surface water largely plots on or around the LEL, with some falling onto the LMWL. This reveals the variability in surface water balances in the region, with some surface water experiencing heavy evaporation with little replenishment of more isotopically light water (such as groundwater or less evaporated surface inflow) and other surface water bodies showing minimal evaporation and more potential groundwater replenishment. Some surface water bodies (such as creeks) also appear to be less affected by evaporation and so plot closer to the LMWL. Groundwater is not affected by evaporation and so falls on the LMWL. A more detailed analysis of the stable isotope results is included below.

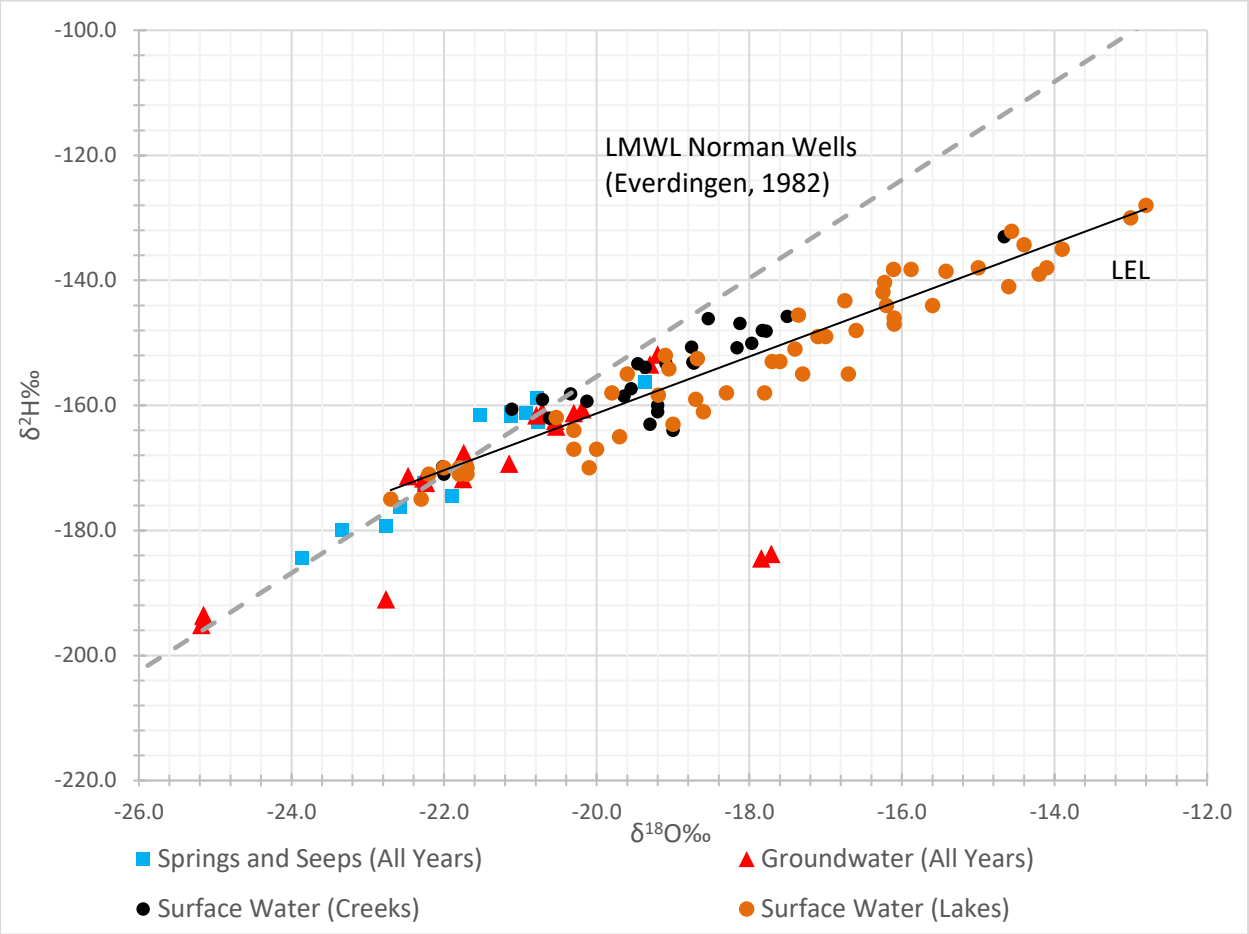

Figure 41: $\delta^{18}O$ and $\delta^{2}H$ for site-wide waters, including groundwater, springs and surface water. The average LEL is indicated in black and the LMWL in gray. Includes data from MWH, (2012) and Waterline Resources, (2013a, 2013b).

5.4.1.2 Water Source and Aquifer Endmembers

Groundwater and porewater from cores of shallow active layer and permafrost were collected from several locations throughout the watershed by both Husky and UW personnel (Figure 38). Groundwater was sampled from Husky monitoring wells, MW09A, MW09B, MW19B (Figure 38) in 2013, following their initial installation. Then MW09A and MW09B were resampled in 2019 by Husky and their consultants when they were decommissioned. Shallow samples of groundwater were collected from the active zone with mini piezometers and PushPoint Samplers at a series of sites within the Bogg Creek Watershed (Figure 39). Some samples were collected beneath or in close proximity to surface water

bodies. Porewaters from the active layer and permafrost core samples were obtained by thawing the samples in the laboratory and extracting the porewater.

5.4.1.2.1 Subpermafrost Groundwater

Groundwater from the subpermafrost bedrock unit LBF obtained from Husky monitoring wells MW09A and MW09B (Figure 38) in 2013 were the most isotopically depleted samples in the watershed (Figure 42).

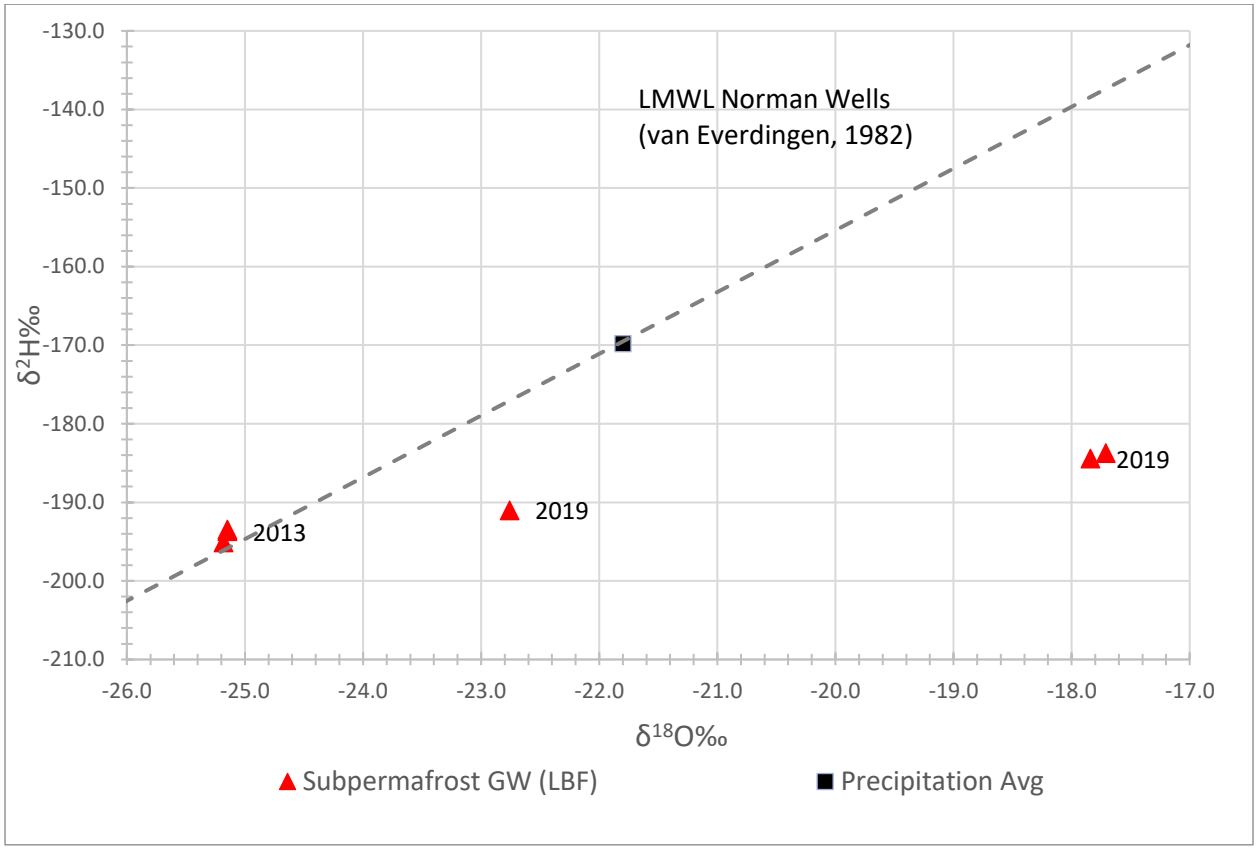

Figure 42: $\delta^{18}O$ and $\delta^{2}H$ for subpermafrost groundwater from the Little Bear Formation in 2013 and 2019, as well as the estimated precipitation average for comparison. Waterline Resources, (2013a, 2013b).

With an average $\delta^{18}O$ of -25.2‰ and $\delta^{2}H$ of -194.1‰ these samples were interpreted as being Pleistocene-aged groundwater (Waterline Resources Inc., 2013b). Carbon dating of this water seemed to confirm this interpretation by placing the age of the water between 17,000-22,000 years old (Waterline Resources Inc., 2013b). In 2019 these wells were sampled again and a significant change in $\delta^{18}O$ and $\delta^{2}H$ was noted, with the average now being -19.4‰ and -186.4‰ respectively. These samples fell off the

LMWL substantially. The reason for this is not clear but could be due to water-rock interaction within the aquifer, or fractionation brought about by the thawing process. No other water isotope samples were available for subpermafrost groundwater formations within the Bogg Creek Watershed. It is speculated that water residing below the LBF would increase in age, and that this water would share characteristically low $\delta^{18}O$ and $\delta^{2}H$, allowing it to be a tracer for subpermafrost groundwater discharge.

5.4.1.2.2 Suprapermafrost Groundwater and Shallow Seepage

Suprapermafrost groundwater from MW19B (obtained from a well, depth of 9.9 m) (Figure 38) is comparatively enriched in both $\delta^{18}O$ and $\delta^{2}H$ relative to shallow groundwater collected from MW04 (obtained via mini-piezometer, depth of 1.0 m) (Figure 43, $\delta^{18}O$ -20.8‰, -22.3‰ and $\delta^{2}H$ -162.0‰, -171.7‰, respectively).

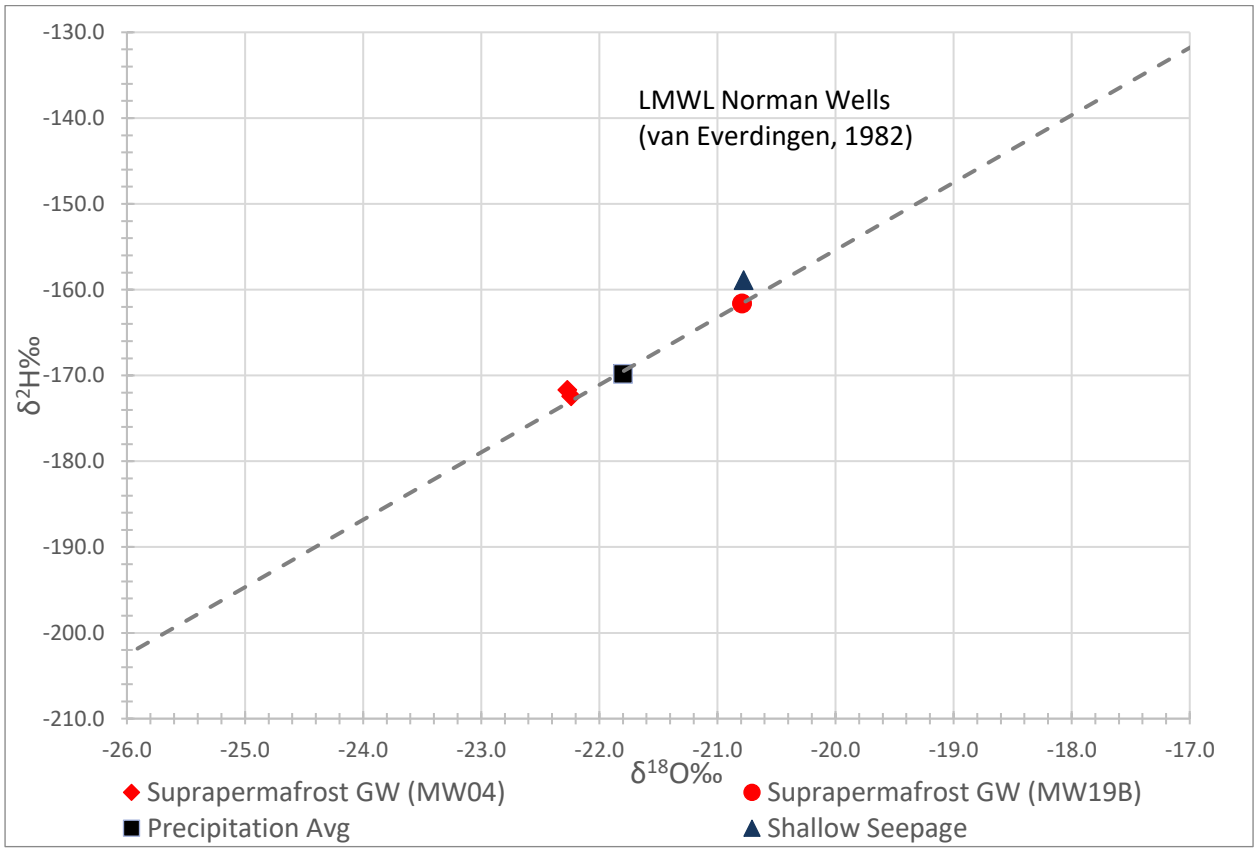

Figure 43: $\delta^{18}O$ and $\delta^{2}H$ in suprapermafrost groundwater from MW04 well pad mini-piezometer in 2019 and the MW19B monitoring well in 2013. Waterline Resources, (2013a, 2013b).

MW19B is slightly enriched compared to the estimated weighted yearly average for precipitation but does not fall off the LMWL, while MW04 appears to be slightly below this average. MW04 was taken by PushPoint Sampler from about 1 mbgs, which is roughly where the permafrost table was located during coring of MW04. It is possible that water taken from this location had a higher proportion of snowmelt or possibly some thawed permafrost water, making it more depleted than the deeper MW19B water. Other suprapermafrost groundwater in the watershed was taken from nearby lakes and streams, which is discussed further in the relevant sections. The average of all suprapermafrost groundwater samples between all years is $\delta^{18}O$ is -21.5‰ and $\delta^{2}H$ -167.5‰. This is just slightly heavier than the estimated precipitation average of $\delta^{18}O$ -21.7‰ and $\delta^{2}H$ -169.9‰.

$\delta^{18}O$ and $\delta^{2}H$ from water obtained from SL Seep, (Figure 38) which was assumed to be representative of shallow seepage or other, young recent water due to its diluted nature, is also shown in Figure 43 and appears to be more isotopically enriched compared to average precipitation and suprapermafrost groundwater from MW04. This higher value is expected during the summer months for water with a meteoric origin.

5.4.1.2.3 Active Layer and Permafrost Porewater

Shallow porewater extracted from active layer cores (thawed) generally showed slightly heavier isotopic values comparable to suprapermafrost groundwater and precipitation average, while falling along the LMWL (Figure 44). Permafrost porewaters from H040 and MW04 however, were more depleted in $\delta^{18}O$ and $\delta^{2}H$ and were more comparable to some spring waters (Section 5.4.1.3).

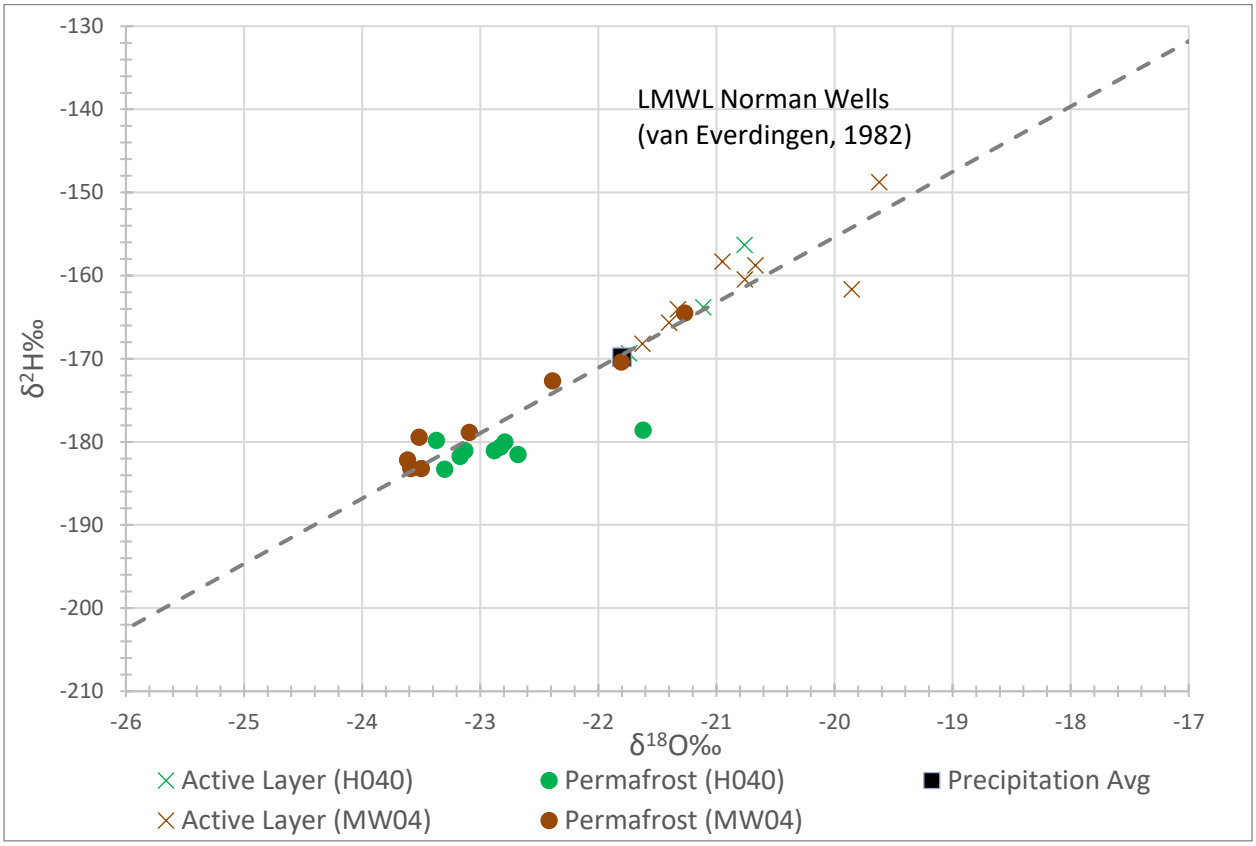

Figure 44: $\delta^{18}O$ and $\delta^{2}H$ of porewaters squeezed from H040 and MW04 cores. Includes active layer and permafrost waters as well as estimated average annual precipitation for comparison.

Values of active layer and permafrost porewater in H040 (Figure 38) $\delta^{18}O$ ranged from -20.8‰ to -23.3‰ and $\delta^{2}H$ from -156.3‰ to -183.3‰ (Figure 44). MW04 permafrost core (Figure 37) had much more variability through the active layer (Figure 44), which was partially frozen during sampling. $\delta^{18}O$ ranged from -19.6‰ to -23.6‰ and $\delta^{2}H$ ranged from -148.7‰ to -183.2‰ throughout the whole core. These values are likely reflective of the transient nature of active layer water, with quick flushing of depleted snowmelt waters by late summer and a signature dominated by summer rain. Meanwhile the permafrost values suggest possible recharge originating during a colder climate, such as shortly after retreat of glacial ice. Profiles of $\delta^{18}O$ and $\delta^{2}H$ with depth are shown below in Figure 45.

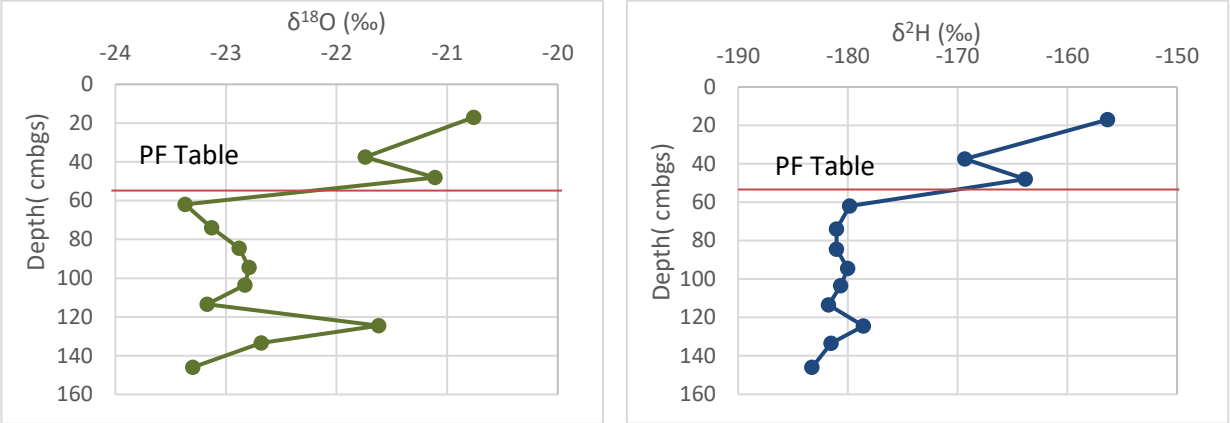

Figure 45: $\delta^{18}O$ (left) and $\delta^{2}H$ (right) vs depth profiles for H040 permafrost core porewater.

$\delta^{18}O$ and $\delta^{2}H$ profiles of H040 show general isotopic depletion with increased depth. The more enriched intervals are at 18 cm and 44 cm. These intervals represent the unfrozen top and bottom of the active layer, respectively. In between these intervals the sample was more depleted, likely due to fractionation in the residual water during freeze up. This phenomenon has been noted in other permafrost cores such as those analyzed by Michel & Fritz (1982). These samples are all similar to the estimated weighted average for precipitation ($\delta^{18}O$ -21.8‰ and $\delta^{2}H$ -169.8‰), indicating a modern, meteoric origin. The shallower portion of the active layer is the most enriched. Below the active layer a sharp isotopic depletion can be seen in both plots. Enrichment, then depletion, can be seen between 62 cm and 114 cm, before another sharp increase in heavy isotopes at 125 cm. There is less enrichment in $\delta^{2}H$ compared to in $\delta^{18}O$, and this sample falls off the LMWL (Figure 44 and 45).

$\delta^{18}O$ and $\delta^{2}H$ data with depth in shallow core samples collected at the MW04 site is shown below in Figure 46. Overall, a decrease is observed with depth, with variation in between. Water in the thawed active layer (depth of about 115 cm) varies slightly but is isotopically heavier than the precipitation average ($\delta^{18}O$ -21.8‰ and $\delta^{2}H$ -169.8‰). A sawtooth pattern is observed along the length of the profile, with spikes occurring at 50 and 65 cm in the active layer then again at 125 cm within the permafrost. This spike at 125 cm is quite considerable, with a change of about $\delta^{18}O$ 1.8‰ over 10 cm. It is possible that these spikes that occur in both H040 and MW04 were caused contemporaneously during some climatic event in the permafrost's history. Below this the isotopes remain quite light, staying fairly consistent at around $\delta^{18}O$ -23.5‰.

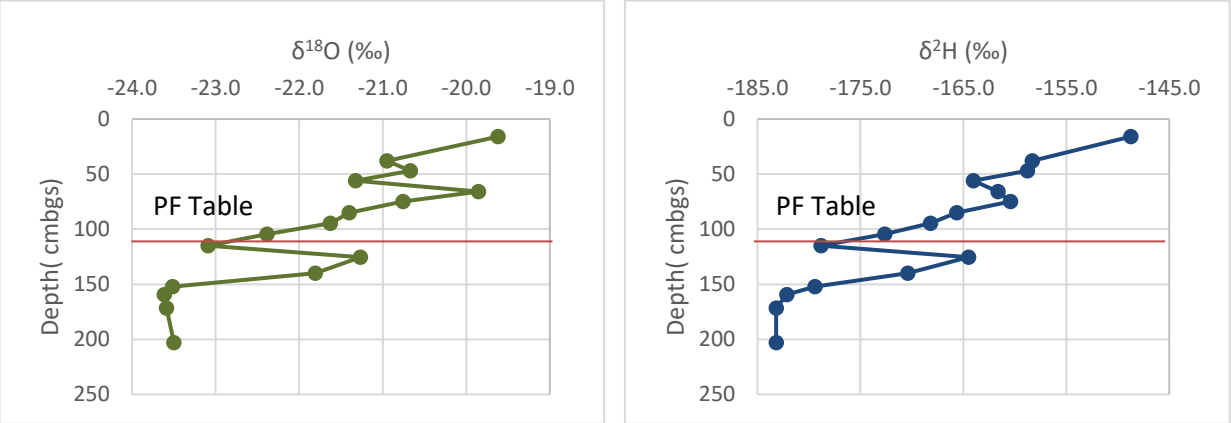

Figure 46: $\delta^{18}O$ (left) and $\delta^{2}H$ (right) vs depth profiles for MW04 permafrost core porewater.

In general, stable water isotopes were useful in investigating the general trend inherent in an active layer and permafrost profile. Freezing history of the permafrost could be gleaned from this information, but this is outside the scope of this investigation. As was hypothesized, permafrost contains isotopically lighter water that suggests it was recharged during a period of colder climate, such as after the last glaciation. It may be possible to utilize this to detect permafrost thaw in the future.

5.4.1.3 Springs

The isotope composition of spring water collected at the GL1 and GL2 spring sites (Figure 38 and 39) in 2018 were more depleted (average $\delta^{18}O$ -22.7‰) than the suprapermafrost groundwater samples (average $\delta^{18}O$ -21.5‰) and average for precipitation ($\delta^{18}O$ -21.8‰) (Figure 47 and Table 9). In 2019, a spring sample collected at the GL3 site (Figure 38) was around the same $\delta^{18}O$ value as the precipitation average at -21.9‰. All samples fell on or close to the LMWL. Water that is a mixture of both shallow active layer groundwater and upwelling deep groundwater could be expected to have these slightly depleted values, which would be consistent with results outlined in the geochemistry (Section 5.3.1.2). GL3 may have experienced greater increase of its lighter isotopic signature by mixing with more enriched water in 2019. GPH1 spring groundwater was the most isotopically negative (average $\delta^{18}O$ -23.6‰) of the spring water samples. The origin for this isotopically negative water is unclear as the geochemistry data is missing. GPH2 in 2019 was more enriched than GPH1, but still lighter than suprapermafrost groundwater. Preferential snowmelt recharge or contributions of old permafrost meltwaters could explain these values. GL and GPH surface water were more isotopically heavy compared to their groundwater, at an average $\delta^{18}O$ of -21.3‰ and -20.9‰, respectively. This likely reflects additional inputs to these ponds of shallow

seepage and direct precipitation. In general, the spring water $\delta^{18}O$ and $\delta^{2}H$ is more isotopically depleted than suprapermafrost groundwater and the precipitation average, suggesting influence of a more depleted source. As well, water ponded on the surface of the spring tended to be more isotopically enriched than the water below. $\delta^{18}O$ and $\delta^{2}H$ in spring samples appears to be useful in detecting potential mixing or preferential recharge, although this is not entirely clear which is occurring.

Table 9: $\delta^{18}O$ and $\delta^{2}H$ for GL and GPH springs over the 2018 and 2019 sampling periods.

	Sample	Date	$\delta^{18}O$ (‰)	$\delta^{2}H$ (‰)
2018 (Summer)	GL1 SW	9/1/2018	-21.5	-161.6
	GL1 GW	9/1/2018	-22.8	-179.5
	GL2 SW	9/1/2018	-21.2	-161.5
	GL2 GW	9/1/2018	-22.6	-176.2
	GPH1 SW	9/1/2018	-20.9	-161.2
	GPH1 GW#1	9/1/2018	-23.3	-180.0
	GPH1 GW#2	9/1/2018	-23.9	-184.5
2019 (Summer)	GL3 GW	8/23/2019	-21.9	-174.5
	GPH2 GW	8/23/2019	-22.3	-172.5

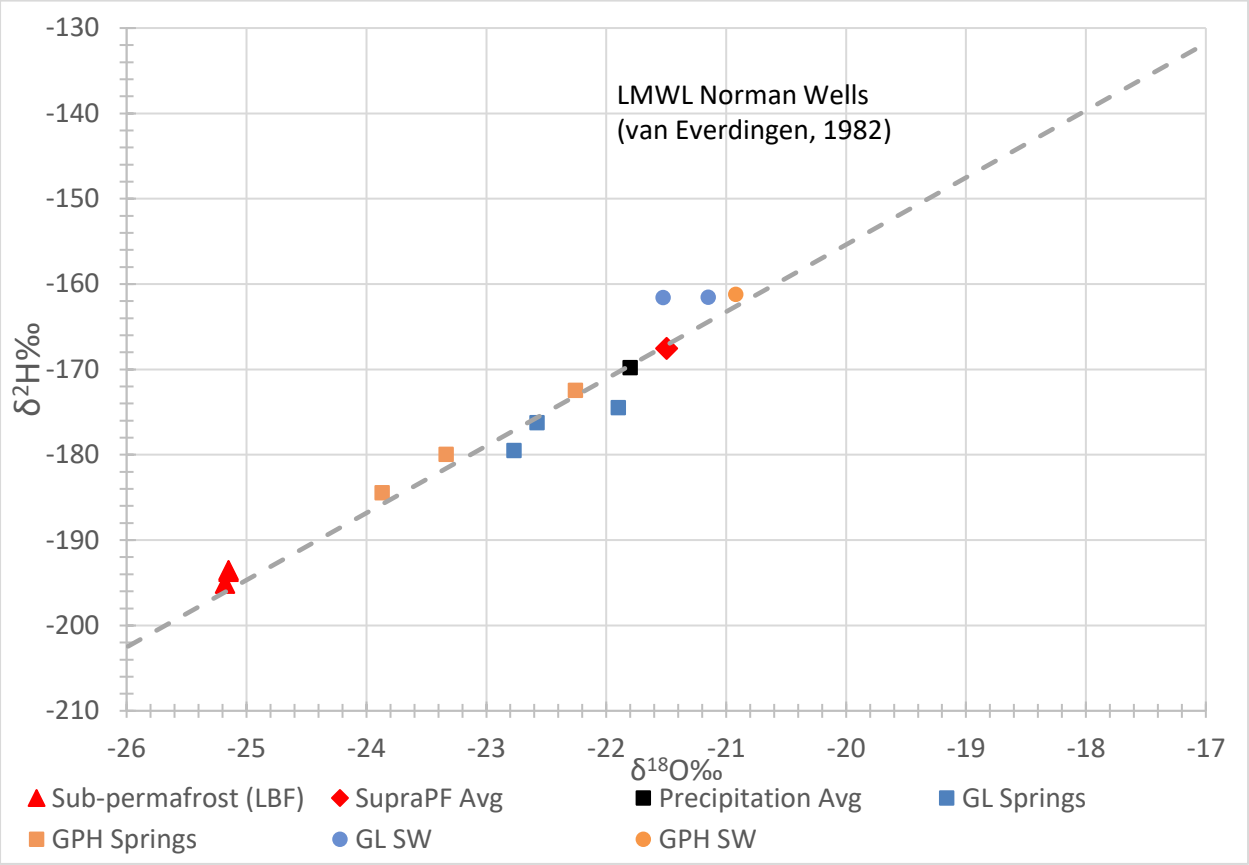

Figure 47: $\delta^{18}O$ and $\delta^{2}H$ for upwelling spring water and for the ponded surface water, as well as the groundwater and precipitation averages for comparison. Outlier data from MW09A and MW09B is not shown.

5.4.1.4 Surface Water

5.4.1.4.1 Upland Tributaries

Tributary $\delta^{18}O$ and $\delta^{2}H$ values can be seen below in Table 10. Generally, tributaries showed some degree of evaporative enrichment relative to the average precipitation value, which was more pronounced during 2019 than 2018. Data are shown in Table 10 and Figure 48.

Table 10: Table of tributary $\delta^{18}O$ and $\delta^{2}H$ values for each sampling year, 2018 and 2019.

	Sample	Date	$\delta^{18}O$	$\delta^{2}H$
2018 (Summer)	H044	8/30/2018	-21.1	-160.6
	H044b	8/30/2018	-21.1	-161.1
	H044b GW	8/30/2018	-21.7	-168.1
2019 (Winter)	H046	2/10/2019	-22.0	-169.8
2019 (Summer)	H044 GW	8/21/2019	-21.2	-169.3
	H046	8/21/2019	-17.8	-148.0
	H046 GW	8/21/2019	-20.5	-162.5
	W02	8/22/2019	-20.6	-162.0

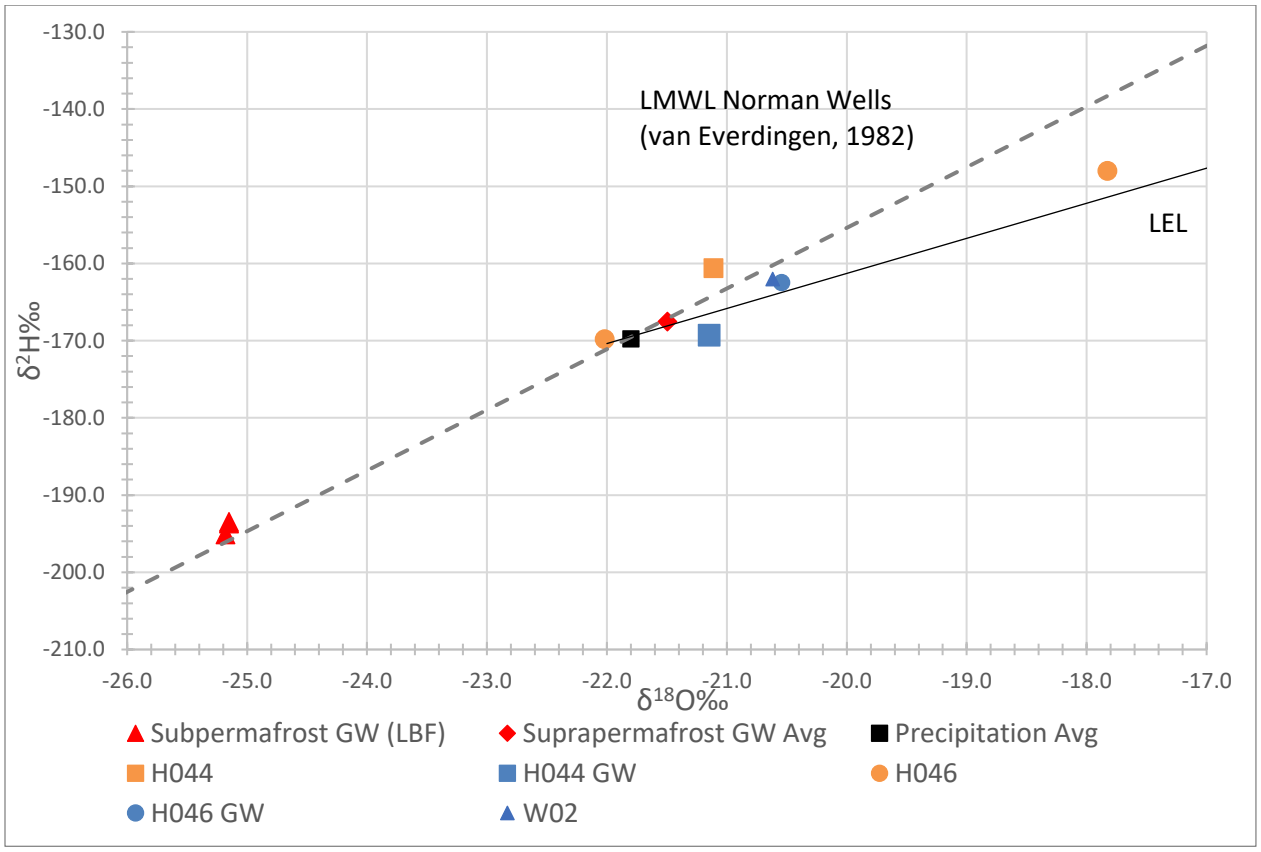

Figure 48: $\delta^{18}O$ and $\delta^{2}H$ for the tributaries, H044, H046 and W02 as well as groundwater and precipitation average. Outlier data from MW09A and MW09B is not shown.

At furthest upstream sampling point W02 (Figure 39), water isotopes were relatively depleted compared to other creek waters, ($\delta^{18}O$ -20.6‰ and $\delta^{2}H$ -162.0‰) and falls on the LMWL, near the precipitation average. This suggests very minimal evaporation and a water input dominated by recent shallow seepage or suprapermafrost groundwater flow.

$\delta^{18}O$ and $\delta^{2}H$ at H044 were taken in the summer of 2018. 2018 values for $\delta^{18}O$ were -21.1‰ and $\delta^{2}H$ -160.6‰., falling mostly on the LMWL. A drainage channel along the AWR was spotted as a thermal anomaly during the IR survey. This drainage channel (H044b) had similar $\delta^{18}O$ and $\delta^{2}H$ values to H044, being -21.1‰ and -161.1‰ respectively. Shallow groundwater taken below this channel was slightly more depleted in $\delta^{18}O$ and $\delta^{2}H$, these values being -21.7‰ and -168.1‰ respectively. These relatively depleted isotope samples suggest minimal evaporation or some influence of lighter waters at this location.

At H046 Samples for $\delta^{18}O$ and $\delta^{2}H$ were taken in winter and summer 2019. Values for H046 taken in February were the most depleted compared to other creek waters at $\delta^{18}O$ -22.0‰ and $\delta^{2}H$ -169.9‰, falling along the LMWL. In August 2019 these values were much more enriched, at $\delta^{18}O$ -17.8‰ and $\delta^{2}H$ -148.0‰, falling upon the LEL. H046 was more isotopically light and fell further along the LEL suggesting evaporation is higher along the reach upstream of H046. In summary, the headwater tributaries of Bogg Creek do not appear to be gaining a substantial amount of isotopically depleted water as they do not generally plot below the estimated precipitation average. It is possible that this water has been influenced somewhat by old sources but has been subjected to evaporative enrichment or influenced by younger, meteoric water. This limits the use of these isotopes in the surface water, as it is inherently less sensitive (due to lower contrasts) to potential mixing.

5.4.1.4.2 Middle and Lower Reaches

The middle and lower reach $\delta^{18}O$ and $\delta^{2}H$ values show variability between each sampling point and between different years as can be seen in Figure 49 and Table 11. The middle reaches of W04, W05 and W06 (Figure 39) were sampled in summer 2019 and all fall on the 2019 LEL. At sampling points W04 and W05 $\delta^{18}O$ and $\delta^{2}H$ values remained fairly static, with no change in $\delta^{18}O$ (-18.7‰) and a very slight change in $\delta^{2}H$ (-153.2‰ to -153.1‰). Evaporative enrichment seems to occur between W05 and W06, as $\delta^{18}O$ and $\delta^{2}H$ values increase slightly ($\delta^{18}O$ of -18.2‰ and $\delta^{2}H$ of -150.8‰). This may be indicative of slightly higher inputs of isotopically lighter water between W04 and W05.

Lower reaches of the main channel at sites H001 and H030 (Figure 39) were sampled for $\delta^{18}O$ and $\delta^{2}H$ first in 2012 then again in 2018 (including H001B) and 2019. Generally, these samples fall on the LEL,

but in 2012 the lower reaches plotted on a different LEL like other surface water in the region at this time (Section 5.4.1.1). Between H030 and H001 $\delta^{18}O$ decreased from $\delta^{18}O$ -18.6‰ to -19.2‰ and $\delta^{2}H$ -161.0‰ to -164.0‰, although these were taken a day apart. However, little change was anticipated to occur between these sampling days.

In 2018 H001, H001B and H030 have very similar $\delta^{18}O$ and $\delta^{2}H$ values, although H030 is slightly lighter than H001 and H001B. A similar phenomenon is observed in 2019 between H030 and H001. Although slight, H030 appears to be impacted more by evaporation than H001 and H001B, suggesting that some amount of isotopically light water is replenishing the creek downstream of H030. In winter of 2019, H001B was sampled and had $\delta^{18}O$ and $\delta^{2}H$ that were only slightly lighter than in the previous summer. These values also shifted down closer to the LEL, which may reflect the lack of surface runoff and shallow seepage during this time. The lack of a significant negative shift suggests that if isotopically light groundwater is discharging to the creek in the winter its effect is minimal on the isotopes.

In 2018, H001 $\delta^{18}O$ and $\delta^{2}H$ for surface and streambed water were very similar. An upwards gradient was measured at this location. The similarity of the isotopic signature between these surface and groundwater samples indicates this is likely hyporheic recirculating exchange rather than direct groundwater discharge occurring in this reach. H001B had contrasting values for surface and groundwaters, with the more depleted signature found in the groundwaters. The direction of the vertical hydraulic gradient was not measured at this site.

Table 11: $\delta^{18}O$ and $\delta^{2}H$ for middle and lower reaches of Bogg Creek in 2018 and 2019.

	Sample	Date	$\delta^{18}O$ (‰)	$\delta^{2}H$ (‰)
2012 (Summer)	H001	7/27/2012	-19.2	-164.0
	H030	7/29/2012	-18.6	-161.0
2018 (Summer)	H001	8/29/2018	-19.4	-153.9
	H001B	8/30/2018	-19.5	-153.3
	H030	8/28/2018	-19.1	-153.3
	H001 GW	8/29/2018	-19.3	-153.7
	H001B GW	8/30/2018	-21.8	-171.8
2019 (Winter)	H001B	2/10/2019	-19.6	-158.5

	Sample	Date	$\delta^{18}O$ (‰)	$\delta^{2}H$ (‰)
2019 (Summer)	H001	8/20/2019	-17.8	-148.1
	H030	8/20/2019	-17.5	-145.8
	W06	8/22/2019	-18.2	-150.8
	W05	8/22/2019	-18.7	-153.1
	W04	8/22/2019	-18.7	-153.2

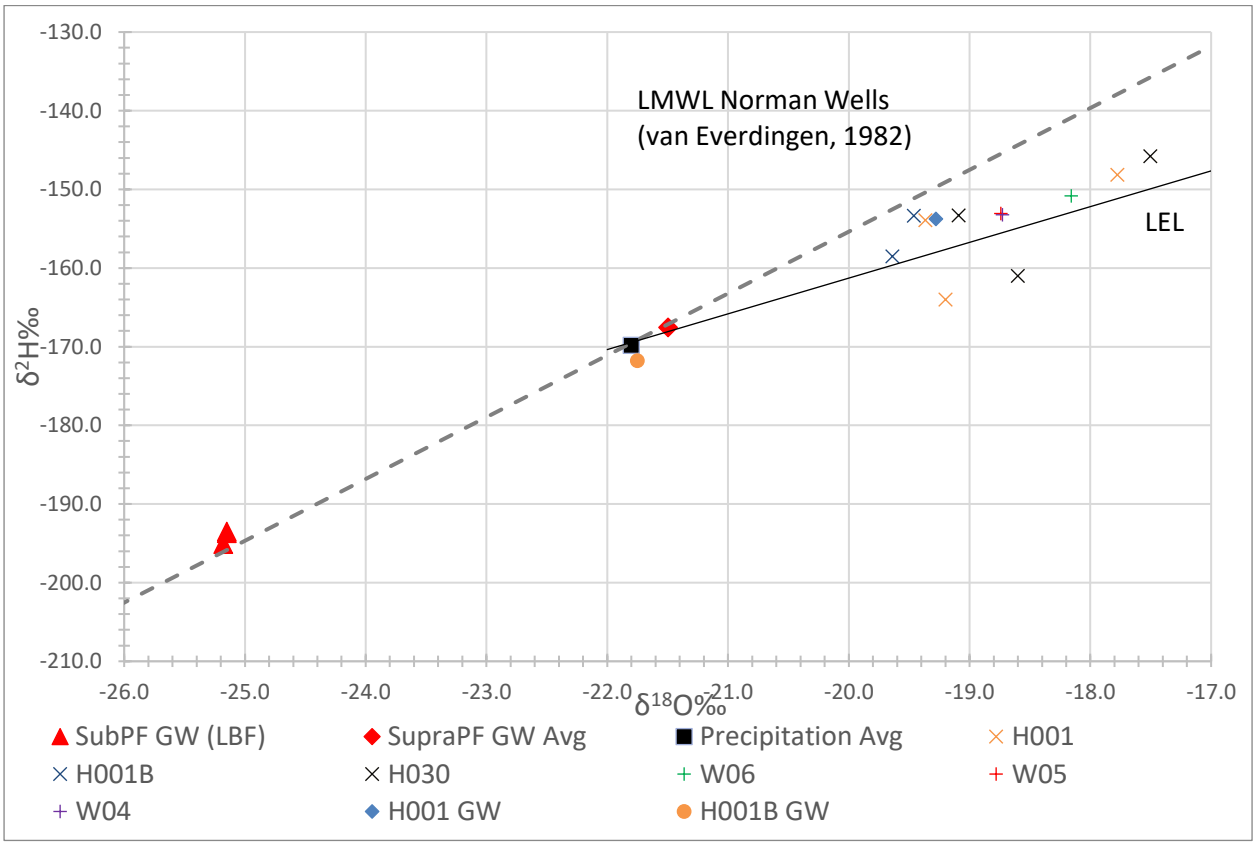

Figure 49: $\delta^{18}O$ and $\delta^{2}H$ in the lower and middle reaches of Bogg Creek for all years as well as groundwater and the precipitation average. Outlier data from MW09A and MW09B is not shown.

A plot of $\delta^{18}O$ over distance starting in the headwater region at W02 and ending at the Bogg Creek outlet to the Mackenzie River (Figure 39) is shown below in Figure 50. $\delta^{18}O$ starts out more depleted and increases with distance towards W04. Between W04 and W05 little change occurs, but then increases are seen again until H030. After this we see a slight decrease at H001. Although this represents only a few

data points along a long stretch of stream, the data illustrate how variable the water source is in the main channel of the Bogg Creek Watershed along the drainage course and suggests that there are inputs of isotopically light water between H030 and H001 that counteracts additional evaporative enrichment that may be occurring along here. This can be observed in each year, with H030 typically being slightly enriched when compared to downstream monitoring points H001B and H001. This isotopically lighter water could be sourced from groundwater entering the stream either directly or indirectly through tributaries. The isotope data again is less sensitive to mixing relationships, however, when applied to longitudinal sampling, can show general changes in isotopic composition moving downstream.

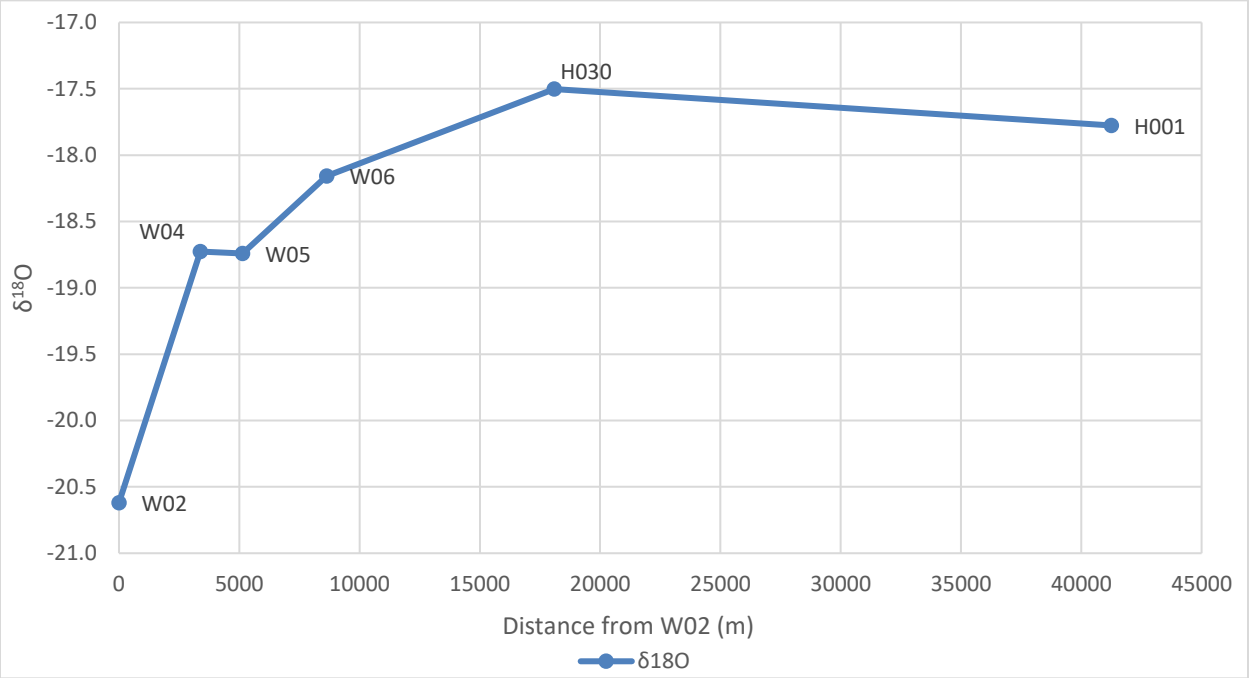

Figure 50: $\delta^{18}O$ over distance starting from W02 in summer 2019.

5.4.1.4.3 Lakes

Surface water samples were taken directly from two lakes in the watershed, and indirectly from lake drainage near G-Lake (GL springs) (Figure 39). Groundwater was also sampled adjacent to these water bodies. The combined data are presented in Figure 51 and Table 12.

Table 12: $\delta^{18}O$ and $\delta^{2}H$ for lakes H031 and H040, as well as from near the stream draining G-Lake (where GL samples are located) at W02. Groundwater values are also shown.

	Sample	Date	$\delta^{18}O$ (‰)	$\delta^{2}H$ (‰)
2018 (Summer)	H031	2018-08-29	-19.1	-154.1
	H031 GW	2018-08-29	-22.5	-171.3
	H040	2018-08-30	-16.2	-140.1
	H040 GW	2018-08-30	-21.7	-167.9
2019 (Winter)	H040	2019-02-10	-19.2	-158.4
2019 (Summer)	H031	2019-08-20	-17.4	-145.5
	H040	2019-08-21	-14.6	-132.1
	W08	2019-08-22	-18.54	-146.13
	W08 GW	2019-08-22	-20.19	-160.59

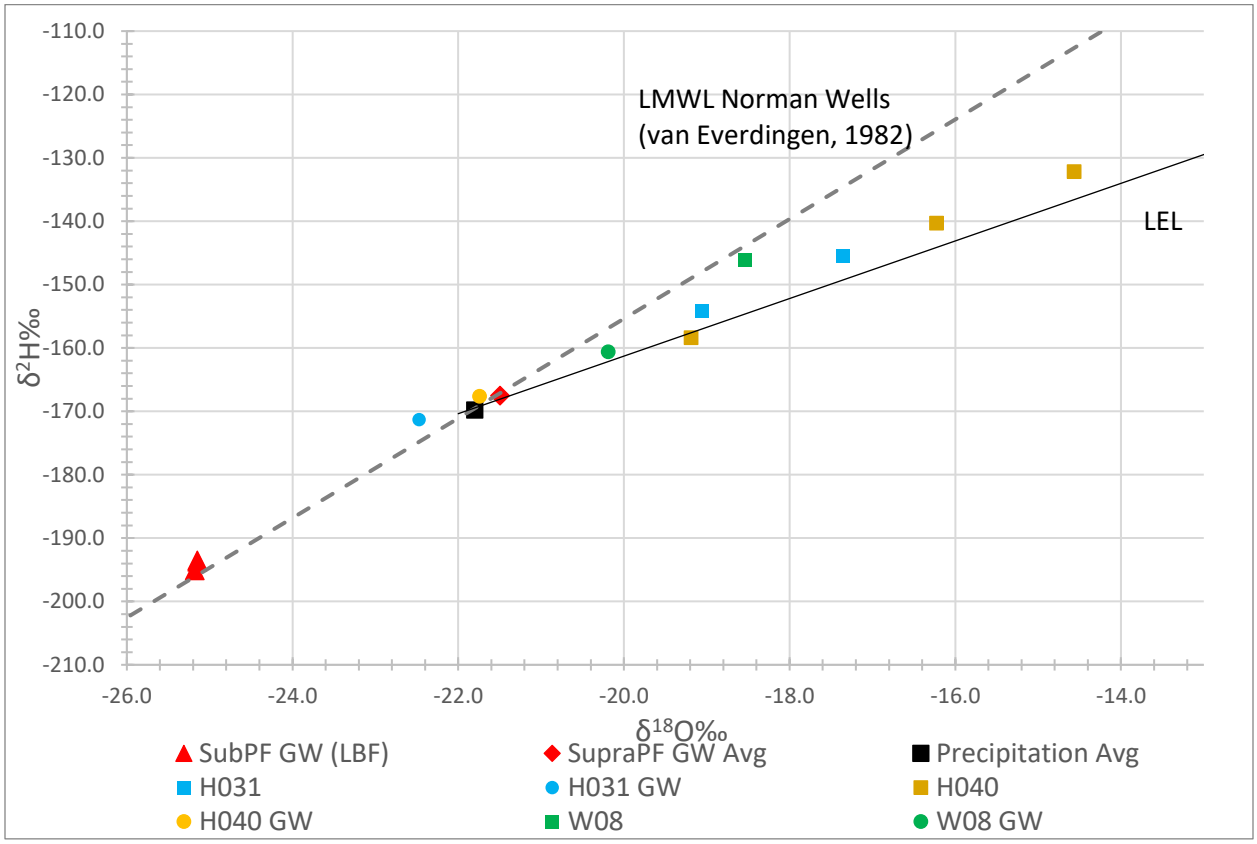

Figure 51: $\delta^{18}O$ and $\delta^{2}H$ of lakes in Bogg Creek and groundwater taken adjacent to them. Groundwater and the precipitation average are also shown for comparison. Outlier data from MW09A and MW09B is not shown.

In 2018 values for H031 were $\delta^{18}O$ -19.1‰ and $\delta^{2}H$ -154.1‰, while H040 was $\delta^{18}O$ -16.2‰, $\delta^{2}H$ -140.3‰. Groundwater samples were much more depleted isotopically, at $\delta^{18}O$ -22.5‰, $\delta^{2}H$ -171.3‰ and $\delta^{18}O$ -21.7‰ and $\delta^{2}H$ -167.6‰, respectively. H040 lake water was also sampled in February 2019, having the most isotopically light signature for H040, at $\delta^{18}O$ -19.2‰ and $\delta^{2}H$ -158.4‰. This may be a result of movement of more isotopically light water into the lake after freeze-up and increased lighter isotope groundwater flow. However, the plot does not show any preferential recharge from any one source. When these surface water bodies were resampled in 2019, they were more isotopically enriched, likely a result of enhanced evaporative enrichment during the drier 2019 year.

Water draining from near G-Lake collected from the surface water of W08 was more enriched than suprapermafrost water but appeared to fall closer to the LMWL than LEL, indicating less evaporative enrichment compared to other surface water bodies. This may suggest minimal connection to G-Lake or

that there is high replenishment of lighter water and precipitation to counterbalance evaporation. W08 groundwater was slightly lighter than the surface water at W08 but was still more enriched than other suprapermafrost water from other locations.

5.4.2 Tritium (^{3}H)

The tritium (^{3}H) concentrations in various sources of water within the Bogg Creek Watershed are shown in Table 13. Tritium was collected from groundwater wells MW19B, MW09A and MW09B in 2013 by Husky, and again from the MW09 wells in 2019 by Waterline Resources (Figure 38). ^{3}H was also collected from select sites in 2018 and 2019. These include surface, spring and groundwater samples.

Table 13: Tritium values for waters throughout the watershed, includes groundwater, surface water and springs.

Type	Sample	Date	^{3}H (TU)
Suprapermafrost Groundwater	MW19B	10/02/2013	5.2
	MW04 GW	9/2/2018	10.1
Subpermafrost Groundwater	MW09A	2/3/2013	<0.8
	MW09B	2/21/2013	<0.8
	MW09A	2/6/2019	<0.8
	MW09B	2/8/2019	<0.8
	MW09BD	2/8/2019	<0.8
Springs	GL1 GW	9/1/2018	7.9
	GL2 GW	9/1/2018	5.3
	GL3	8/23/2019	4.9
	GPH1 GW	9/1/2018	8.1
Surface Water	H044GW	8/22/2019	3.9
	H001B	2/10/2019	9.3
	H040	2/10/2019	10.3
	H046	2/10/2019	9.4
	H046	2/10/2019	9.3
	W02A	8/22/2019	10.6

Subpermafrost groundwater samples from the MW09 wells were below the detection limit which is consistent with the estimated age of LBF groundwater. Tritium values did not change during resampling in 2019. MW19B was at 5.2 TU which may suggest mixing; however, this was not apparent in the geochemistry. More likely this is modern water that has been circulating for a number of years. Suprapermafrost groundwater from MW04 GW had a value of 10.1 TU and is likely modern.

Tritium was taken from GL1 and GL2 in 2018 and from GL3 in 2019. Tritium values were as follows, GL1 7.9 TU, GL2 5.3 TU and GL3 4.9 TU. These values seem to support both hypotheses for GL spring origins, as mixtures of waters of different ages could produce these relatively lower TU values, as could modern water that had undergone decay along a flowpath. GPH1 had a tritium value of 8.1 TU, which was similar to GL1. Spring origins for GPH are also unclear but these tritium values could suggest either mixing or tritium decay. A groundwater seep located near H044 had the second lowest tritium values in the watershed of 3.9 TU. Based on geochemistry this is likely a sample of mixed ages.

Tritium was also collected from below ice in February 2019 in H001B, H040 and H046. All TU values in creek samples (H001B and H046) were less than modern groundwater from MW04 GW, while the lake sample (H040) was similar to MW04 GW. While mixing of subpermafrost and suprapermafrost water may produce these values, there is little evidence for subpermafrost groundwater inputs to these stream segments. Inputs also may vary considerably seasonally, and the extent is uncertain. In summary, tritium appears to be less useful as mixtures of old and modern water could produce the observed values, as could water that has undergone decay over several years. The technique may be more useful if $^{3}H/^{3}He$ dating could be applied as well.

5.4.3 Strontium ($^{87}Sr/^{86}Sr$)

$^{87}Sr/^{86}Sr$ and the Sr concentration provide a glimpse into the rock-water interactions that may have occurred in the water's history, and therefore offer insight into a potential aquifer source. This section outlines the results of the Sr analysis, first by establishing the "endmembers" for the different conceptualized water sources of groundwater and shallow seepage water, then by visual comparison of these endmembers with the surface water and spring samples taken during the course of this study.

5.4.3.1 Groundwater and Shallow Seepage

Groundwater (suprapermafrost and subpermafrost from the LBF), active layer (AL) porewater from H040 core and S-Lake (Figure 38) shallow seepage $^{87}Sr/^{86}Sr$ vs the (log) 1/Sr concentration are shown below in Figure 52.

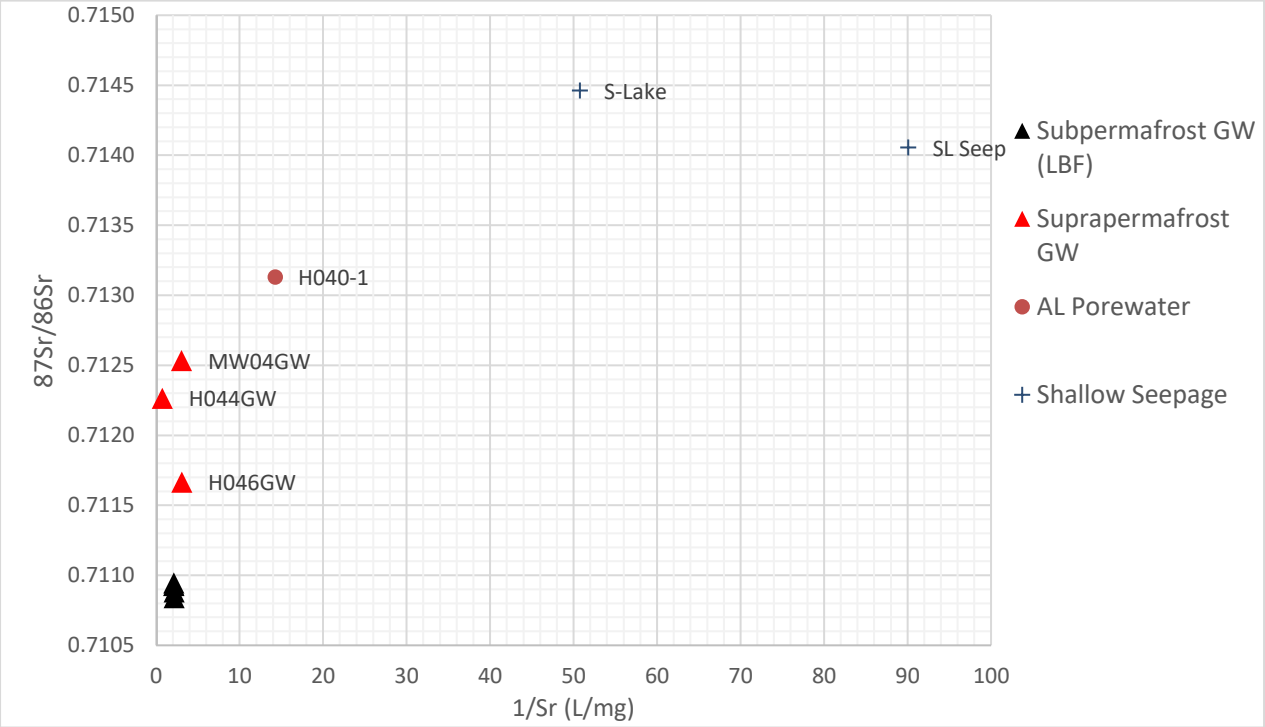

Figure 52: $^{87}Sr/^{86}Sr$ and the inverse of Sr concentration for groundwater, organic porewaters and shallow seepage water.

LBF water was originally sampled for $^{87}Sr/^{86}Sr$ from the MW09 wells and MW19B in 2013 (Figure 38). $^{87}Sr/^{86}Sr$ values were 0.71084 in MW09A, 0.71093 in MW09B, and 0.70144 in MW19B. MW19B has a value just slightly less radiogenic (lower $^{87}Sr/^{86}Sr$ values) than the MW09 wells. Sr concentrations were not determined for these samples. When the MW09 wells were sampled again in February 2019, Sr isotopes and concentrations were determined. Sr isotope ratios did not change, and concentrations were quite high compared other samples in the watershed.

MW04 suprapermafrost groundwater Sr ratio was determined to be more radiogenic (higher $^{87}Sr/^{86}Sr$ values) than subpermafrost water from MW09A and MW09B and the suprapermafrost water from MW19B at 0.71254. Sr concentration was moderately high. These values likely reflect the shorter residence time of groundwater in the shallow subsurface at MW04. Suprapermafrost groundwater from nearby H044 and H046 are also included. H044 was moderately radiogenic and had a very high concentration. H046 was less radiogenic than MW04 but had a very similar concentration. The overall geochemical analysis of H044 and H046 groundwater samples suggest that they may have been impacted by the nearby AWR, which would also impact the Sr signature.

SL Seep and S-Lake sites (Figure 38 and 39) were the most radiogenic of any other samples (Figure 53). Because of the low concentrations of all solutes in these samples and high $^{87}Sr/^{86}Sr$, S-Lake and SL Seep were chosen as representative samples of shallow seepage or other young water that had not interacted significantly with surficial materials. Enough extra water was extracted from the top of the organic active layer in H040 (H040-1) to be analyzed for $^{87}Sr/^{86}Sr$. This porewater had a lower concentration and slightly higher Sr ratio than MW04 groundwater. In summary, shallow seepage water, and shallow waters that have not had much time to interact with surficial materials seem to have both a higher $^{87}Sr/^{86}Sr$ and a lower concentration than samples that have had ample time in contact with surficial materials. Bedrock $^{87}Sr/^{86}Sr$ from the LBF appears to be lower in comparison with other samples and also has a relatively high concentration. Generally, the $^{87}Sr/^{86}Sr$ appears consistent within the bedrock aquifer, and so makes an excellent tracer of this type. The variability within the shallower samples complicates the use, however, but with proper characterization of this variability, this may be possible to address.

5.4.3.2 Springs

Spring $^{87}Sr/^{86}Sr$ and 1/Sr are shown below in Figure 53, with groundwater and organic porewater shown for comparison. Strontium samples from GL1, GL2 and GPH1 (Figure 38) were all taken in 2018 while GL3 and GPH2 were sampled in 2019.

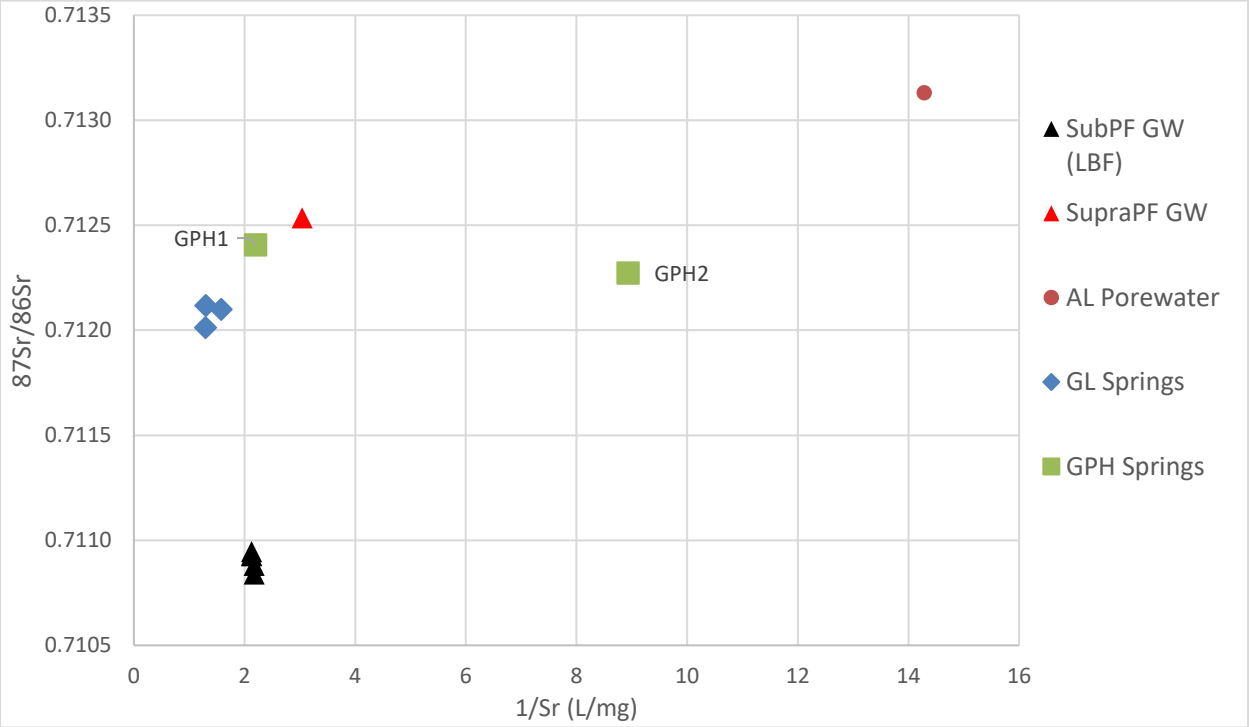

Figure 53: $^{87}Sr/^{86}Sr$ and 1/Sr for spring sites and groundwater.

$^{87}Sr/^{86}Sr$ and Sr concentrations between GL sites were quite consistent with a $^{87}Sr/^{86}Sr$ average of 0.724667, and high concentrations when compared to most other groundwaters. GL1 was slightly less radiogenic than GL2 or GL3. GPH1 and GPH2 had similar $^{87}Sr/^{86}Sr$ (average 0.712340) but differed in concentration, with GPH1 being higher. GPH1 was also slightly more radiogenic than GPH2. GPH1 and GPH2 were geochemically distinct from one another, however they seem to derive their Sr from a similar source, with GPH1 having a longer residence time. Coincidentally, GPH1 and the GL sites plot along a trend line with the suprapermafrost MW04 groundwater. Whether this indicates a relationship is uncertain but may imply geochemical evolution of shallow groundwater taking a deeper flowpath and then discharging as a spring. Another possibility is mixing between a shallow and deeper, unknown endmember. Either way, these hypotheses (spring waters taking a longer flow path and experiencing geochemical evolution or mixtures of water) imply that the flow system supplying these springs is inherently deeper and more complex than the typical suprapermafrost zone. The $^{87}Sr/^{86}Sr$ does not seem to confirm or reject either hypothesis, as critical endmembers are missing for comparison.

5.4.3.3 Upland Tributaries

$^{87}Sr/^{86}Sr$ values vary significantly between the two headwaters of Bogg Creek. Samples from H046 were taken in summer 2018 and 2019 as well as winter 2019, while samples from H044 and W02 were taken in summer 2019. A plot of $^{87}Sr/^{86}Sr$ is shown below in Figure 54. Three basic groups are formed, suprapermafrost, (which includes MW04 groundwater, active layer porewater from the top of H040 core, and H046 winter baseflow), very recent shallow seepage, and subpermafrost (MW09A and MW09B LBF groundwater). A triangle to demonstrate potential mixing between these groups is drawn, with each tributary sample falling somewhere within this triangle.

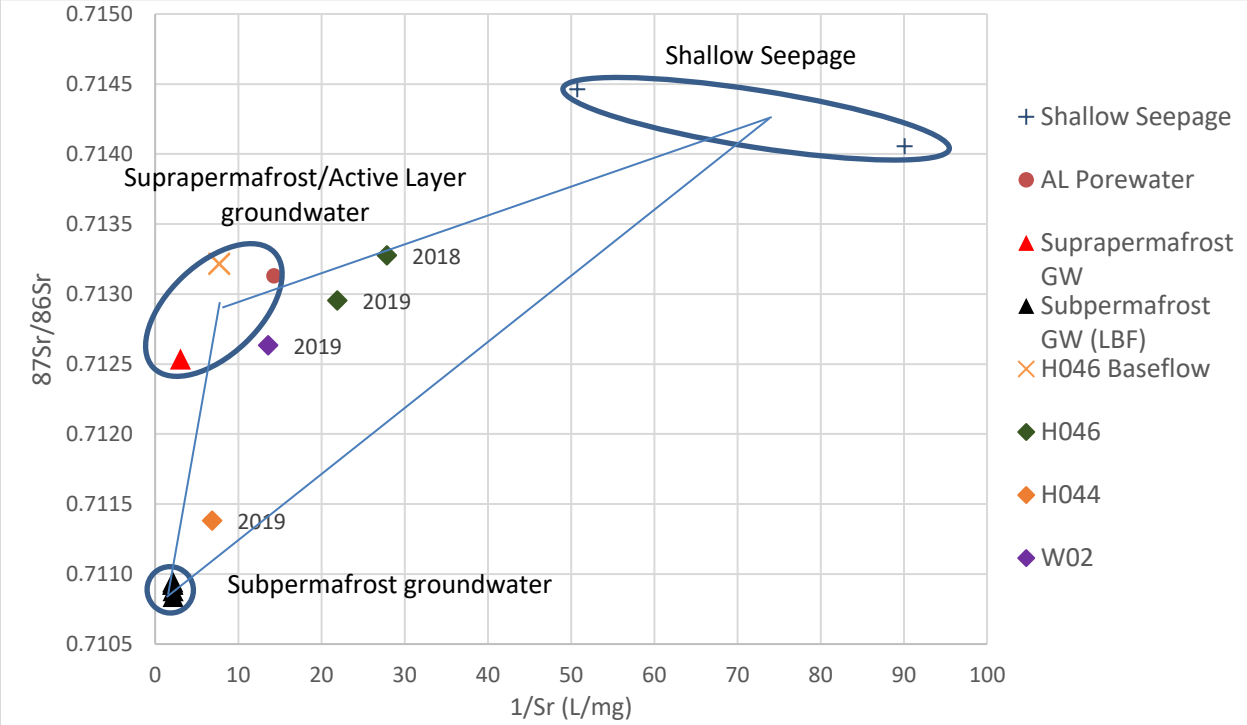

Figure 54: $^{87}Sr/^{86}Sr$ vs 1/Sr for Bogg Creek tributaries and groundwater/porewater and shallow seepage endmembers.

Upstream of H044, W02 had a more radiogenic $^{87}Sr/^{86}Sr$ (0.712634) and lower concentration Sr signature. Falling closer to H046 baseflow and the lower reaches, there is possibly some small influence of subpermafrost groundwater at W02 and a strong influence of recent meteoric waters such as shallow seepage and suprapermafrost water.

H046 ratios are fairly radiogenic (average 0.71323) and concentrations low. Ratios stayed around the same values in summer 2018 and winter 2019 but concentrations increased in winter. Winter baseflow

was geochemically similar to suprapermafrost groundwater and its $^{87}Sr/^{86}Sr$ plots in the vicinity of AL porewater and MW04 suprapermafrost water. In summer 2019 H046 was less radiogenic (0.712955) with a moderate concentration and does not line up with the other samples from the previous summer and winter. In the mixing triangle, H046 plots mostly between suprapermafrost and shallow seepage. The $^{87}Sr/^{86}Sr$ values provide further evidence of more shallow seepage influence during 2018, as these samples plot closer to this group. These results are consistent with geochemistry, which suggested minimal, if any influence of deeper groundwater on this stream reach. Instead, the stream appears to be fed mostly by suprapermafrost groundwater discharge.

H044 was the least radiogenic (0.711381) and had the highest concentration compared to other creek samples. Only one sample was taken, in 2019. Of all creek samples this also plots the closest to the LBF subpermafrost groundwater group. This may be more evidence of the subpermafrost groundwater influence on H044 as suggested by the geochemistry. However, interestingly the concentration of Sr in H044 was not as high as the LBF while all other ions such as Ca were much higher compared to the LBF. The reason for this is unclear. The $^{87}Sr/^{86}Sr$ data appears to confirm what the geochemical evidence was suggesting for both tributaries. This highlights the usefulness of $^{87}Sr/^{86}Sr$ when endmembers are known.

5.4.3.4 Middle and Lower Reaches

$^{87}Sr/^{86}Sr$ for the middle and lower reaches of Bogg Creek is shown below in Figure 55.

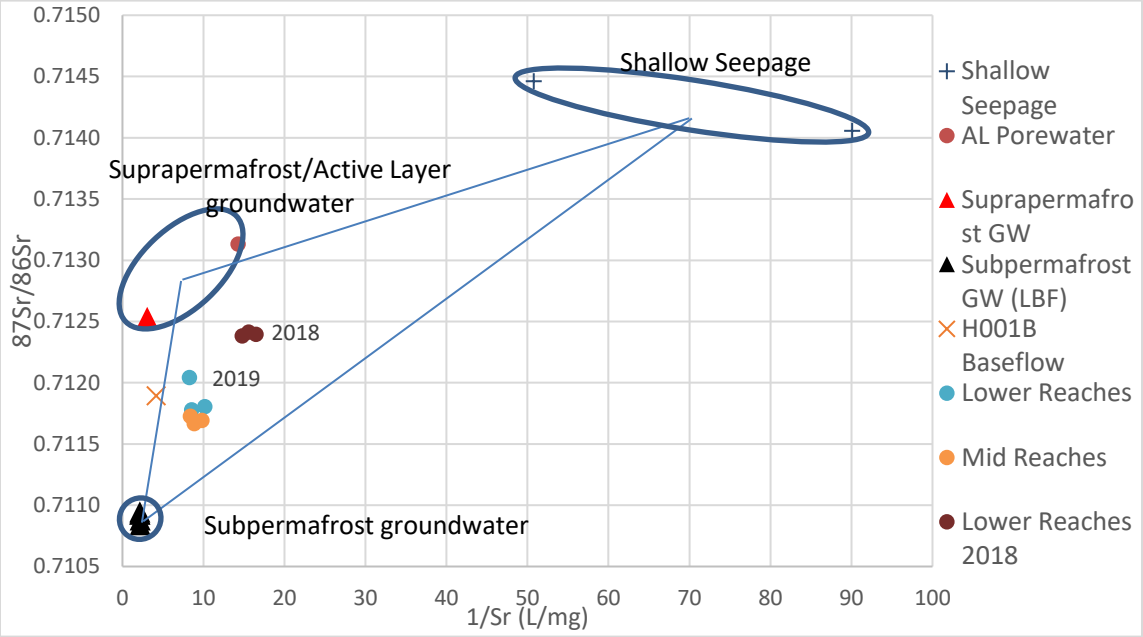

Figure 55: $^{87}Sr/^{86}Sr$ vs 1/Sr for middle and lower reaches of Bogg Creek as well as groundwater and shallow seepage endmembers.

The middle reaches of Bogg Creek had very similar $^{87}Sr/^{86}Sr$ values and concentrations (average 0.711695), with a slight increase in ratio moving downstream. W04 and W06 had the most comparable concentrations, with W05 being slightly less concentrated in dissolved Sr.

In 2018 the lower reaches of Bogg Creek (H001, H001B, H030) had a similar $^{87}Sr/^{86}Sr$ (average 0.712397) and slightly variable Sr concentration. They were also more radiogenic compared to winter (0.711893) and summer 2019 (average 0.711875) and had a lower concentration. All samples plot within or near the mixing triangle. The highest concentration occurred in winter in H001B which plots in between the subpermafrost and suprapermafrost endmembers, indicating no runoff or shallow seepage influence compared to the samples taken during the summer. 2019 samples also seemed to be less influenced by shallow seeps, which is consistent with geochemistry. While H001B and H030 plot very close to one another, H001 is slightly more radiogenic than the other samples. This may imply further inputs of another more radiogenic source, such as suprapermafrost groundwater or spring water (Section 5.4.3.2) downstream of H001B. Again, this would be consistent with geochemistry and the other isotope results.

While winter baseflow from H001B plots on the line between the suprapermafrost and subpermafrost endmembers, it is very unlikely that the LBF is a major contributor due to its distance away from this

reach. In Figure 55 H001B baseflow plots somewhat closely to the GL samples, albeit with a less radiogenic, lower concentration Sr signal. This may be hinting at an unknown endmember (or multiple endmembers) influencing both creek and springs. This underscores the complexity of the Bogg Creek water sources in such a varied geologic environment. This data also confirms what the geochemistry was initially suggesting, despite lacking one of the potential endmembers (MHF groundwater).

5.4.3.5 Lakes

H040 was analyzed for $^{87}Sr/^{86}Sr$ in winter 2019 and W08 in summer 2019. This data can be seen below in Figure 56.

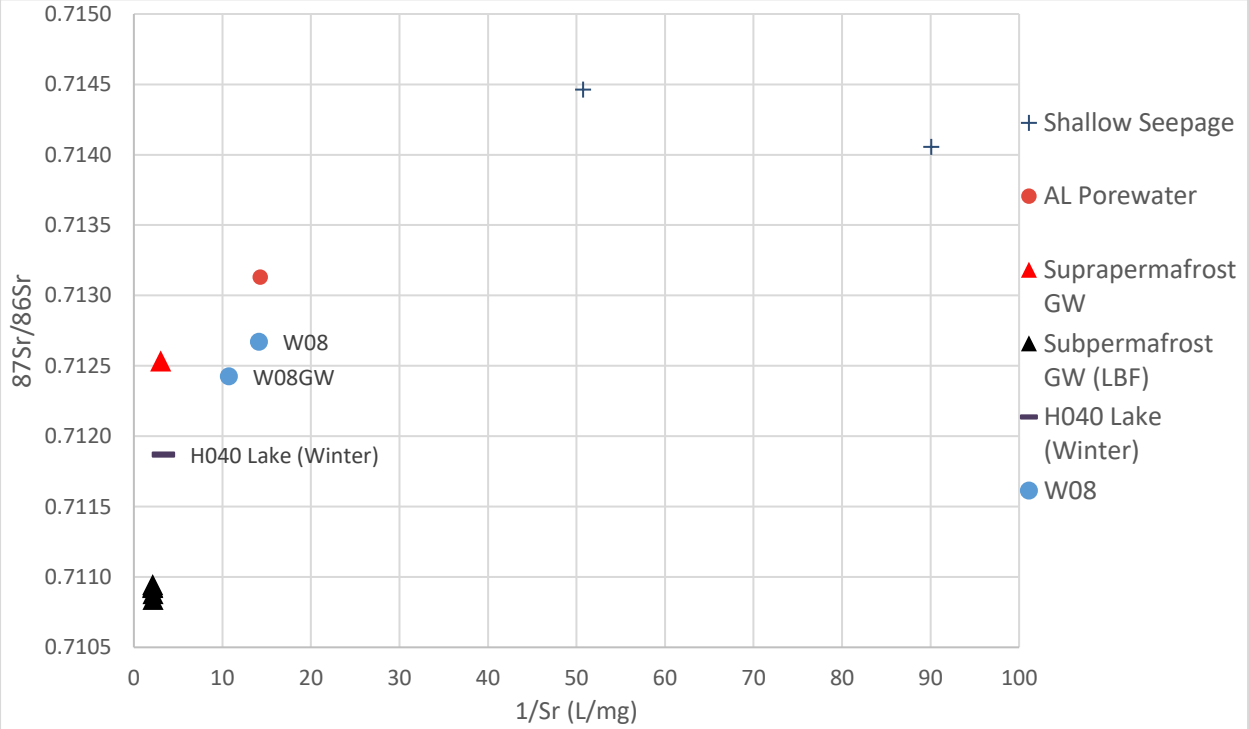

Figure 56: $^{87}Sr/^{86}Sr$ vs 1/Sr for H040 and W08, along with groundwater, porewater and shallow seepage.

The $^{87}Sr/^{86}Sr$ value was quite radiogenic with a high concentration of dissolved Sr in H040. This sample is comparable to baseflow taken from H001B in winter 2019 suggesting similar sources of dissolved Sr. It also plots between the suprapermafrost and subpermafrost groups. W08 and W08 groundwater had $^{87}Sr/^{86}Sr$ values comparable to MW04 suprapermafrost water with lower concentrations. There does not appear to be any significant evidence for deep groundwater influence in the Sr data at this location, which may be due to lack of some endmember values.

5.4.4 Methane (^{13}C)

Data obtained from OROGO (See Appendix A, Table A-1) included $\delta^{13}C_{CH4}$ values for methane and other gases taken from the Canol Formation in well N-09. Isotope values ranged from -43.2‰ to -35.2‰ with an average of -38.6‰, well within the range of a thermogenic (implying a gas that has undergone thermal maturation within a reservoir) gas endmember (Clark & Fritz, 1997). Concentrations are unknown. Thermogenic gases could imply that there is a connection between deeper, petroleum bearing strata, and the surface and near-surface environment. In winter 2019, dissolved methane was detected in MW09B at 0.006 mg/L, with a $\delta^{13}C_{CH4}$ value of -38.8‰, quite similar to that from the Canol Formation. This may be methane sourced from a deeper reservoir or could be sourced from local coal deposits, (as reported in Golder Associates, 2015) as the isotopic value implies a thermogenic origin. This methane from the LBF provided the thermogenic endmember in the watershed, as concentration data from the Canol Formation was not available. Available data from the watershed are shown below in Figure 57.

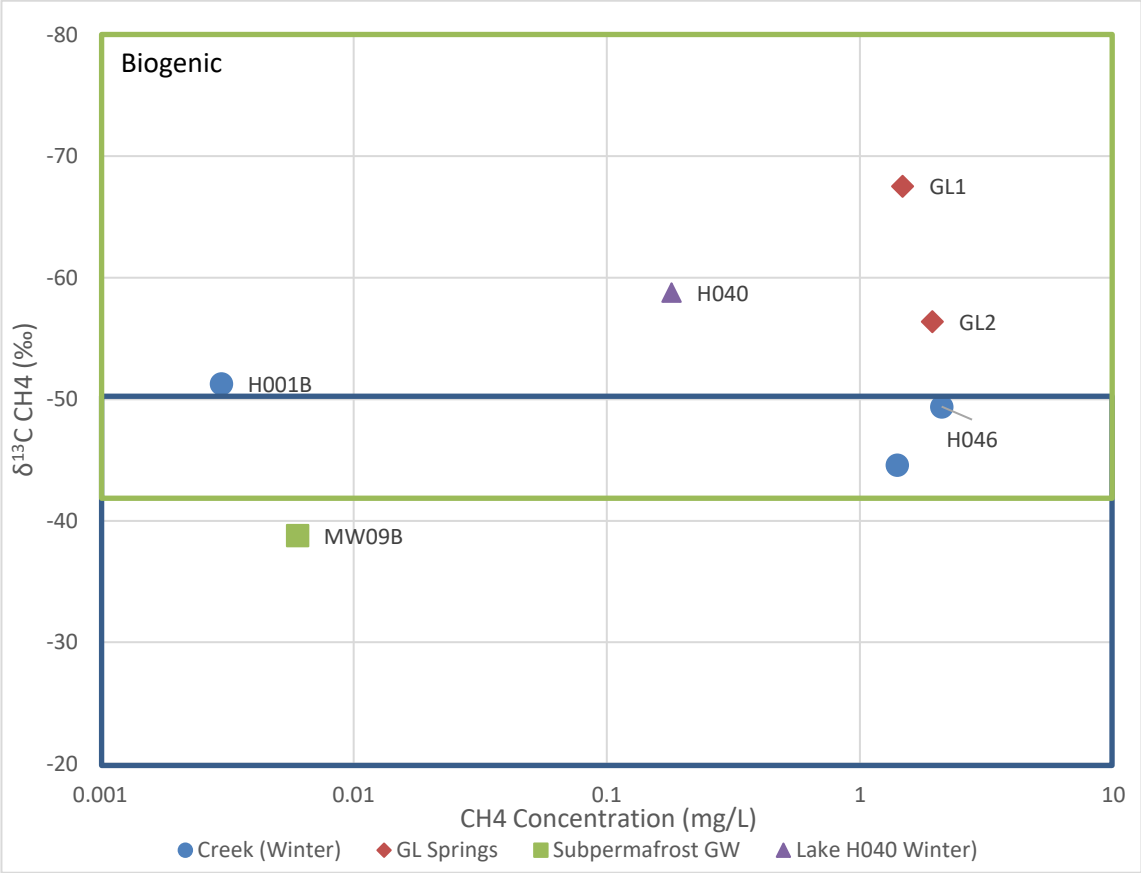

Figure 57: $\delta^{13}C_{CH4}$ vs (log) CH_4 Concentration for several samples in the watershed. Boundaries for thermogenic methane are shown in the blue, and for biogenic in the green (Clark and Fritz, 1997).

$\delta^{13}C_{CH4}$ and concentrations were collected from several locations in 2018 and 2019. In 2018 these were taken from GL1 and GL2, methane concentrations were 1.47 mg/L and 1.93 mg/L, respectively. $\delta^{13}C_{CH4}$ values were -67.5‰ and -56.4‰, which appear to be mostly biogenic (produced through biological processes, often at or just below the surface), although GL2 approaches the lower bounds of biogenic.

$\delta^{13}C_{CH4}$ was also collected from H046 during the February 2019 sampling event. Methane concentrations were relatively high in this section of the creek, approximately 1.4 to 2.1 mg/L. Isotope values were quite heavy, and $\delta^{13}C_{CH4}$ ranged from -44.6‰ to -49.4‰. These samples plot within the overlap zone between thermogenic and biogenic gases. Similarly, H001B was quite isotopically heavy, although lighter than H046, plotting just outside the overlap boundary into the biogenic territory, with a low concentration. Lake H040 $\delta^{13}C_{CH4}$ was light and biogenic, and concentrations moderately high.

Oxidation of methane from groundwater is noted to occur when groundwater discharges into aerobic conditions. This process shifts the $\delta^{13}C_{CH4}$ to be more ^{13}C rich in the residual methane. This may therefore produce isotopically heavier samples that mimic that of thermogenic methane. This is likely the case in the surface water samples taken in the winter (H001B, H046 and H040). The ratios here likely reflect this oxidation process and are not representative of mixed thermogenic and biogenic gases.

Chapter 6
Discussion

6.1 Groundwater Flow and Baseline Conditions in Bogg Creek

The previous sections outline the evidence for groundwater flow and interactions with surface water within the Bogg Creek Watershed. Groundwater origin was interpreted from the data but there remains some uncertainty. Headwaters and upland lakes of Bogg Creek see influence of mostly shallow, suprapermafrost groundwater, while in the midlands and lowlands there is evidence of specific groundwater inputs that may have a deeper origin. Overall, shallow groundwater in the active layer and in suprapermafrost taliks is quite active in the summer and may still seep into partially unfrozen water bodies at least until February. There is some evidence for subpermafrost groundwater discharge, the strongest being from the LBF or an aquifer with a similar mineralogy as the LBF. MHF groundwater could also be contributing to streams and springs, but this remains unclear as isotope endmembers could not be obtained for this water and so inferences were made using only geochemistry.

Suprapermafrost groundwater and porewater from mineral soils show geochemical and isotopic variability across the watershed, but generally have a low to moderate TDS and a Ca-HCO_3 type composition due to carbonate and dolomite weathering with minor silicates in shallow soils (MW04, MW19B). Other weathering reactants may include organic compounds in more shallower soils and peat layers which may shift the composition to more of a Ca-SO_4 type (such as in the organic active layer). Carbonate rocks are largely absent in the study area except for being a component of the AWR construction, and so it is safe to assume that the Ca-HCO_3 water type is primarily suprapermafrost in origin within Bogg Creek. Isotopes reflect modern, meteoric origins of the water with variations caused by the amount of rain or snowmelt. Suprapermafrost groundwater appears to activate in early summer, beginning with the shallow organic rich active layer, then progressing to the deeper mineral soils at the base by late summer/early autumn. In some areas this water may continue to flow until at least mid-winter, especially within deeper flowpaths within the suprapermafrost zone that do not freeze. This may be shifting with land clearing and climate change, with a potential for flow to continue until later in the winter. Frozen permafrost porewaters extracted from two sites had similar geochemical signatures, being dominated by Ca-HCO_3 ions.

Subpermafrost groundwater does not appear to be wholly stagnant, as there is indirect evidence for subpermafrost groundwater discharge at ground surface in the watershed. An upwards gradient measured in the LBF groundwater suggests possible discharge conditions may be possible where heads are higher than the land surface elevation, such as just downslope of the monitoring wells MW09A and MW09B. This could occur along the contacts of LBF and SRF, along the base of a ridge. Recharge that occurred during the last glacial period could have entered the formation in the southwest and be flowing laterally northeast, towards the Mackenzie River. Open taliks may exist that connect surface waters to these deeper aquifers, but their extent and distribution are uncertain.

In the LBF, groundwater had a moderate TDS, and a distinct Na-HCO_3 composition. Very little variability was noticed in geochemistry or most isotopes besides $\delta^{18}O$ and $\delta^{2}H$ between 2013 and 2019 sampling events. Without further information it is suspected that the anomalous $\delta^{18}O$ and $\delta^{2}H$ composition is due to the well thawing process or from water-rock interaction. The SRF may contain groundwater with a similar geochemical composition to the LBF, but information on this and other deeper bedrock aquifers are limited. MHF groundwater is primarily Na-Cl/HCO_3 in nature and shows substantial variability between the two samples featured in this work but retains this signature. Evidence for inputs of higher Cl, lower SO_4 (similar to the MHF water) was demonstrated in spring samples and in the lower reaches of Bogg Creek. Isotopes in these formations were not collected and so remain largely unknown variables. This limits tracers of these groundwaters to chemistry only, specifically Cl which may not be unique to them. Evidence for saltier overburden layers at MW04T was discovered during salinity analysis by Husky, but the origin of these salts is unknown. Where there is evidence of Na-Cl inputs with low SO_4 to surface water it could be water interacting with this overburden and then undergoing reducing conditions, causing reduction of any SO_4 present.

There is also the issue that geochemistry samples for the MHF were collected outside the watershed and may have experienced different geochemical evolution than water residing below the watershed. Secondly, evolution along the flowpath that occurs between where these waters were collected within the formation and where they may be discharging could alter the geochemistry substantially if these flowpaths are long. Despite limited deep monitoring well installations, the existing wells allow for a snapshot of subpermafrost groundwater and provides a basis for some qualitative analysis of creek and spring water components, especially since the deeper subpermafrost groundwaters tend to have very high Cl and low SO_4 contents, in general. This type of geochemistry may be expected in other watersheds of

similar clastic geology, deep subpermafrost groundwater will have high TDS and possibly be dominated by Na/K and Cl/HCO_3 from silicate weathering. This contrasts with shallow groundwater which is dominated by Ca/Mg and HCO_3 from calcite and dolomite dissolution within soils. A contrast between the two could be expected in similar regions underlain by sedimentary rock.

6.1.1 Springs

Thermal anomalies and icings in the Bogg Creek Watershed are common along the edges of the stream, lakes and associated wetland areas. At least two were confirmed as being springs, these being the sites of GL (G-Lake) and GPH1. The springs along G-Lake have an uncertain origin, but an upwards hydraulic gradient that was observed during 2 consecutive summers combined with temperature profiles, confirmed these as discharge features. These springs appear to be spread over a large area, without visible flow under normal conditions. The EM38 survey ran across GL3 confirmed that high-conductivity water is likely emerging below much of the area of wetland but could be taking preferential pathways leading to less mixing/dilution by suprapermafrost water.

Geochemically the springs have very similar anion proportions as deep subpermafrost groundwater such as that from the MHF and cation ratios like that of suprapermafrost groundwaters. This suggests that one possible origin explanation of this water is mixing of subpermafrost groundwater discharge with suprapermafrost or intrapermafrost groundwaters. Saltier till layers as identified at MW04T may also be a source of the Na-Cl in these springs, suggesting a shorter flowpath but potentially through a relatively shallow talik. Given enough time it would be anticipated that any salts in the glacial sediments would eventually be leached out, suggesting that a talik through this zone may have to have recently formed if this is the case. Data for these sites seems to suggest both hypotheses could be correct. $\delta^{18}O$ and $\delta^{2}H$ and ^{3}H values would agree with the first hypothesis, assuming that subpermafrost groundwater would be older and recharged during a time when climate was colder, however this could be explained by snowmelt recharge. The isotopically more enriched sample in 2019 suggests slightly altered sources during this time, or evaporation occurred during or after sampling. ^{3}H supports either hypothesis, as mixing of ancient water containing 0 TU with modern water could produce the values of the GL springs, as could a longer flowpath with ^{3}H decay over time. Presence of toluene in GL1 also appears to support this first hypothesis initially as the MHF is known to contain hydrocarbons. However, other species of BTEX were below detection limits which can be indicative of biogenic toluene production or biodegradation of the other organic compounds. Isotopes of $^{87}Sr/^{86}Sr$ and $^{13}C_{CH4}$ also do not directly support this mixing hypothesis,

but do not reject it either. $^{87}Sr/^{86}Sr$ were only slightly less radiogenic than shallow groundwater, while $^{13}C_{CH4}$ appears strongly biogenic. The $^{87}Sr/^{86}Sr$ similarity to suprapermafrost groundwater could be due to geochemical evolution of shallow water or mixing of two endmembers. Low SO_4 suggests a lack of interaction with underlying sulphide-bearing shales or intense SO_4 reduction. This could possibly be due to the groundwater flowpath being primarily below or through the permafrost allowing for reducing conditions.

In terms of physical evidence for these hypotheses, there is very little. Geologically, the nearby lake is relatively close to the contacts between the SRF, MHF and IF. The MHF is the only potential aquifer but is still located about 1.1 km to the southwest of the springs according to mapping as the IF underlies the entire lake and spring complex. Significant lateral flow would need to occur for this aquifer to act as a supply to the lake, or the IF could have similar geochemical signatures and be acting to supply the lake instead. A ridge to the north of the lake is mapped as being covered by glaciolacustrine shore deposits (sand and silt) and till. This could potentially be the recharge area for a shallower, intrapermafrost groundwater flow system that is discharging to the springs, as it rises about 40 m above the lake. Future work could investigate this ridge on the ground to probe for permafrost, take hydraulic gradients and monitor the springs for hydraulic heads. Icing samples would also prove useful as they may reveal the source of the winter water.

GPH1 appears to be a spring that is interacting with highly organic soils or potentially sulphide rich bedrock. Upwards flow was observed through temperature profiles. Without detailed geochemistry the origins of this spring are highly uncertain, although there is the possibility of there being a component of subpermafrost discharge here, as was suggested by the $\delta^{18}O$ and $\delta^{2}H$. Results from the $^{87}Sr/^{86}Sr$ were inconclusive. GPH2 appears to be dominated by inorganic soils and may also be derived mostly of snowmelt or even some thawed permafrost waters.

In summary, the springs investigated in this work demonstrate unique geochemical and isotopic characteristics that suggest possible upward migration and mixing of subpermafrost groundwaters or thawing and remobilization of permafrost waters. The physical, geochemical, and isotopic evidence work best when used together and are promising additions to the baseline groundwater data in the watershed.

6.1.2 Tributaries and Headwaters

The two tributaries analyzed in this work show evidence of groundwater discharge as conceptualized in the initial flow system model. The branch connected to H046, which includes several small lakes, show

evidence for Ca-HCO_3 inputs that may be originating from suprapermafrost groundwater, while H044 shows evidence for subpermafrost groundwater inputs from water with a geochemical composition similar to LBF water.

H046 shows a definite influence of mostly Ca-HCO_3 dominated waters, likely as a result of minor suprapermafrost groundwater discharge which is diluted by runoff and shallow, low concentration, seeps. Discharge conditions at the bridge crossing were observed in temperature data. While the surficial geology around the reach and its headwaters is primarily mapped as till, there may be localized aquifers contributing groundwater to the stream as the active layer thaws throughout the summer. As much of the area is also overlain by peat, organic solutes also contribute to the bulk chemistry of the reach. Winter sampling revealed that some suprapermafrost groundwater continues to seep into the creek even in February, suggesting that a shallow talik may exist here. Methane isotopes also seemed to suggest that there may be leakage of thermogenic gases that accumulate under ice in the winter, however, due to the likelihood of oxidation this is likely not the case.

H044 geochemistry suggests that it is primarily sourced from a high TDS, Na-HCO_3 water. Temperature measurements also suggested that local discharge conditions were occurring near the bridge crossing. Other inputs such as shallow seepage and suprapermafrost waters likely make up the bulk of the stream water, as suggested by the $\delta^{18}O$ and $\delta^{2}H$, but geochemistry and $^{87}Sr/^{86}Sr$ strongly resemble that of the LBF. Very minor inputs of subpermafrost groundwater could be occurring upstream at W02 as well. Both sampling points overlie the SRF, with the LBF subcropping 4.2 km away to the southwest. This would make it unlikely that the LBF is directly influencing both sampling points without significant lateral flow, although discontinuous permafrost distribution does not mean it is impossible. It could be possible for W02 to be fed by springs draining the LBF as the headwaters upstream do originate near the subcrop of the LBF. TDS in H044 is 2 to 3 times higher than LBF groundwater. It is possible that this water is primarily sourced from LBF water with higher TDS than selected endmembers, possibly as a result of continued geochemical evolution along the groundwater flowpath. Drill cutting samples from N-09 noted sandstone intervals through the LBF (102-230 mbgs) and through the SRF (328.5-473.5 mbgs). No artesian flow was noted in this sandstone, but actual water level measurements were not obtained. Core logs from borehole MW06, which is the closest to H044, also indicate the presence of trace sandstone intervals from 58-91 mbgs, which may subcrop below the stream in some areas. Water with similar geochemistry as the LBF but with higher TDS may be flowing freely beneath the creek in this unit, discharging as springs and into lakes that feed H044. Another observation is that since W02 does not

appear to contain such a strong subpermafrost signal as H044, it is possible that much of this signal is coming from the other branch upstream of H044 that was not accessible for sampling. A number of icings were identified in this upstream area (Glass et al., 2020), meaning that subpermafrost fed springs may be a major contributor to the streamflow of H044.

The combined evidence in these headwater regions is very promising and agrees with the initial conceptual model. Icings discovered through remote sensing and seeps found during the IR survey provide additional evidence for potential groundwater flow, especially along the headwaters upstream of H044.

6.1.3 Middle and Lower Reaches

Geochemical and isotopic evidence for groundwater inputs along the lower and middle reaches are more subtle than the two tributary branches, but physical evidence in the form of thermal anomalies along banks and stream temperature profiles suggest it is occurring. Major geochemical changes occur when moving downstream that coincide with mixing of waters from lakes and other stream branches. Inputs seem relatively minor between W04 (underlain by silt and sand) to W05 (underlain by till), and from H030 to H001B (underlain by silt), with slightly more changes occurring between H001B and H001. Streambed temperature profiles suggested that the middle reaches may be losing between W05 and W06, which is consistent with the relatively minor change in isotopes and geochemistry.

Another, unnamed lake is connected downstream of H030 that has evidence for substantial icing occurrence which may be the source of geochemical changes along the lower reaches. This may be the case for most of Bogg Creek, its water depth in the winter might not be great enough to support an open talik to the subpermafrost zone, but localized taliks may exist below lakes and perennial springs, feeding subpermafrost groundwater more indirectly. However, flowing water was found below ice at H001B in February 2019, so the stream may continue to flow and gain groundwater well into the winter months. Geology at two monitoring points (H001B and H030) is mapped as glaciolacustrine, underlain by IF, shale while H001 is located in Mackenzie River alluvium and is also underlain by the IF, but localized aquifers are hypothesized to occur. Changes in geochemistry and $\delta^{18}O$ and $\delta^{2}H$ along the length of the stream suggest minor inputs of higher Cl, lower SO_4 and isotopically lighter water may be occurring moving downstream past H030.

Historical geochemical evidence suggests that seasonal changes may be related to active layer thaw depth, with slightly deeper flowpaths feeding the stream in late summer. The main caveat with this

evidence is that it is spread across multiple years, and so may be reflecting longer-term changes that could be mistaken for seasonal, or vice versa. It appears that in general however, samples taken during June are likely at the end of the spring freshet influence and are likely still dominated by surface runoff and interflow through highly porous organic soils with very little suprapermafrost groundwater inputs as this zone remains mostly frozen. In July there is a shift in cation proportions towards slightly more Na-K and an increase in TDS, while anions shift with a greater proportion of Cl. This may occur due to reductions in runoff and peat porewaters and with baseflow making up a greater amount of creek water, this primarily being sourced from more Cl-rich subpermafrost groundwater. Influence of suprapermafrost groundwater continues to increase, but this zone remains mostly frozen still, limiting inputs. Mid-August sees some variability between years 2016 and 2019 in TDS and ion ratios which could be due to differences in rainfall between the different years. In 2016 Norman Wells measured approximately 16.6 mm of rain for the month of August prior to sample collection while 2019 received 75.3 mm in the same time period (Environment Canada, 2019). This is also reflected in the higher TDS for 2016 compared to 2019. Late-August precipitation in 2015 was much lower than in 2017/2018, having received 36.8 mm compared to 106.7mm and 102.4 mm respectively. However, timing of this precipitation showed that at least one rain event seemed to occur during sample collection in 2015, while several days had passed between rain events and sampling in 2017/2018. This could explain the lower proportions of SO_4 since water tables and lake levels may have been lower in 2015, limiting input of SO_4 richer waters and promoting more influence from shallow seepage or interflow mixed with subpermafrost groundwater. During this time active zone thaw depth would have been nearing maximum, so these inputs may have been greater during 2017 and 2018 with higher water tables. Winter sees a slight increase in the predominance of Ca and HCO_3, but overall levels of most ions increase besides SO_4, which decreases. This suggests a greater influence of Na-Cl and Ca-HCO_3 type waters compared to those in September. This could potentially represent a greater influence of groundwaters such as those emanating from around G-Lake which could include Cl-rich/SO_4-poor subpermafrost groundwaters and Ca-HCO_3 rich suprapermafrost groundwater. The timing of sampling appears to have a major influence on what the water chemistry will consist of, which is consistent with stream gauging evidence provided by Husky. This evidence suggests that spring freshet may continue well into the Mid-Summer, before the low water period in Late-Summer, then steadily increasing water levels well into Autumn.

In summary, the physical, geochemical and isotopic data suggest that suprapermafrost and to a lesser extent subpermafrost groundwaters are contributors to the streamflow of the middle and lower reaches of

Bogg Creek. Evidence for subpermafrost influence in the lower reaches between H030 and H001B is subtle but appeared over at least 2 years. This could be due to natural variability, but the evidence is still very promising when refining the conceptual model of the region.

6.1.4 Lakes

Lakes appear to be major purveyors of streamflow in the catchment, while also imparting a significant control on aqueous geochemistry. Lakes also seem to have significant inflows of groundwater. At H031 the effect of Ca-HCO_3 inputs is apparent and seems to suggest influence of suprapermafrost groundwater diluted by young, low concentration water. Springs and icings appear around the long linear string of lakes of which H040 is connected and seem to be imparting a Ca-SO_4 signature. This geochemical signature appeared to be a characteristic of groundwater or porewaters that were flowing mostly through organic soils, suggesting that peat and other organics may be acting as the primary aquifers in lakes such as H040.

W08 was sampled as a proxy for G-Lake and appeared to have a similar geochemical profile as the springs located nearby. This indicates that groundwater, whatever the source, may be a major influencer of lake geochemistry and could make up a significant portion of its water inputs. These then could feed downstream to the lower reaches of Bogg Creek. Unfortunately, this conclusion cannot be made indefinitely as the sample was used as a proxy for the lake.

Lakes outside the watershed also appear to be dominated by either Ca-HCO_3 type waters or Na-HCO_3/Cl type waters, or a mix of both. This suggests major influences on these additional lakes are suprapermafrost and subpermafrost groundwaters, such as that from the MHF. Some lakes demonstrated evidence of groundwater flow through presence of iron staining.

In general, lakes in and around the Bogg Creek Watershed are complex mixtures of different water sources, and the large surface areas may skew some of the estimates of groundwater influence through evaporation and concentration of solutes, although this effect is likely to be relatively minor. H040 was not completely frozen in February 2019, suggesting that the lake may not freeze completely and could support an open talik beneath it.

6.2 Conceptual Model of Groundwater Flow Conditions at Bogg Creek

The current site-specific conceptual model of groundwater flow in the Bogg Creek Watershed is shown below in Figure 58. This conceptual model incorporates a simplified permafrost distribution in the

watershed and interpretations of site geology as well as conceptualized flowlines. Beginning in the southwest (left of model) subpermafrost groundwater discharge from the LBF is hypothesized to be occurring where the confined aquifer subcrops. This is mainly along the edge or base of the ridge formed from the LBF. This is inferred from data suggesting W02 (furthest upstream sampling point from H044), could be influenced by subpermafrost groundwater, as well as from the thermal IR survey data that showed evidence for discharge occurring in these areas. Moving east at H046, a shallow talik is hypothesized to occur, preventing upward water migration from the subpermafrost zone, but allowing for shallow seepage and inputs of suprapermafrost groundwater. At H044, an open talik is conceptualized below the stream, with groundwater being supplied by the LBF or SRF. This branches off the original conceptual model, where only two subpermafrost aquifers were considered due to limitations in available data for other formations. The chain of lakes that includes H040 showed some evidence of potential subpermafrost groundwater discharge and so an open talik is also hypothesized to occur here, as well as under Bogg Creek in the lower reaches. Here, water from the MHF may be entering the stream, either directly or indirectly. The positions of taliks along this cross-section are conceptualized and so may not be actually occurring in the positions outlined in the profile. As discussed previously, open taliks may occur discreetly below the stream and may be more prominent under the lakes, which tend to be deeper. Groundwater inputs may be very localized and feed into the creek by more indirect means, such as through springs and into lakes, rather than direct seepage through the creek bed.

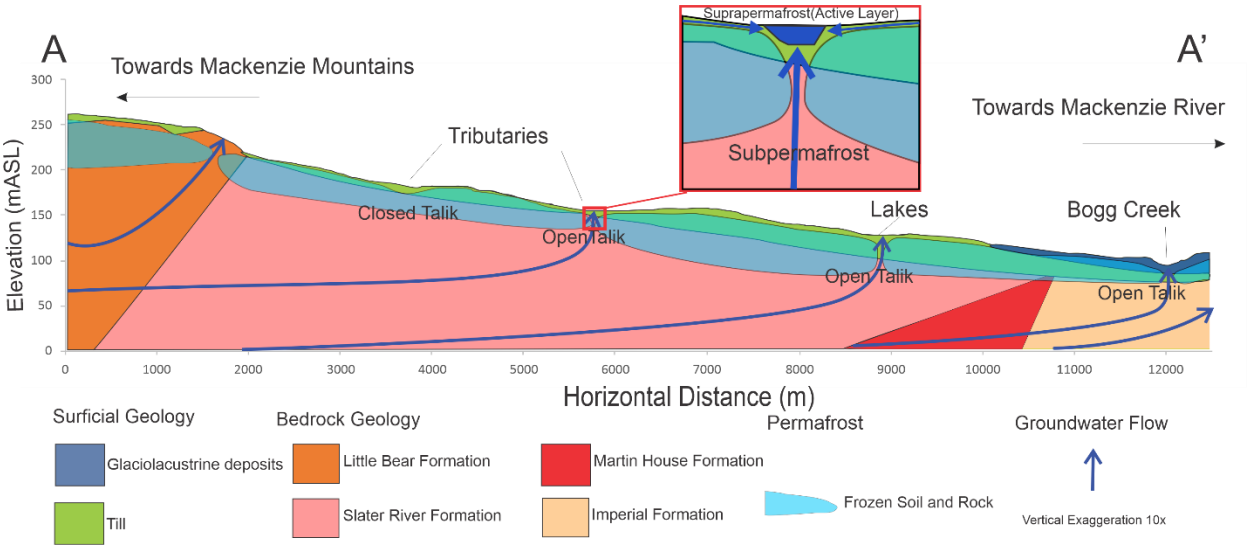

Figure 58: Conceptual model of groundwater flow in the Bogg Creek Watershed. Geology, permafrost distribution, groundwater flow lines and position of open taliks are inferred based on

geological and geochemical evidence. Permafrost is shown as semi-transparent to show stratigraphy.

6.3 Application of Methods

6.3.1 Priority Monitoring Site Selection

The remote sensing of icings laid the foundation for the initial priority site selection. These mapped features were usually found near water bodies, which could then be marked for further investigation. High-resolution satellite imagery also played an important part in site selection, as it allowed for clearings that would permit a helicopter to land to be discerned remotely. Both of these methods save considerable time and resources for the benefit they provide in strategizing fieldwork. The aerial IR survey was also critical in screening out some of these areas further, to those that are displaying active groundwater discharge at the surface. This removes even more guesswork that would be required to simply visit icing locations randomly, possibly missing the more important ones. One limitation of this method, however, is the need for large contrasts between groundwater and the surface water or ground surface. This limits when the technique could be used to either summer or winter. It also only works to determine temperature contrasts at the surface, discharging groundwater emerging from below surface water may not be discernible with this method.

6.3.2 Sample Collection and Groundwater Monitoring

Collection of shallow groundwater was successful with the portable PushPoint Samplers. These instruments are easy to push into water-logged sediments and require only a syringe or vacuum pump to draw water. A small diameter water level tape can easily be used to assess water level and obtain a quick estimate of vertical gradients. However, because of their diameter, sample volume is limited, and ample time must be given to collect detailed geochemistry and isotope samples. The sampling port is also easy to clog up especially in silty or clay rich sediments. Clogging can occur during sampling as fines are drawn into the screen or during installation as the sampler is advanced through fine layers. For this reason, mesh screens should be attached around the port in fine sediments to keep the screen from clogging. PushPoint samplers however would be preferred in locations where small sample volumes are required such as for $\delta^{18}O$ and $\delta^{2}H$ and methane analysis.

Although not as convenient as the PushPoint Sampler, mini-piezometers are also very useful in this environment. Requiring more equipment, mini-piezometers can be used in locations where water cannot

be obtained by the PushPoint due to clogging or where larger sample volumes are required. Because the mini-piezometers are not advanced through the sediment but instead installed in a pilot hole provided by a steel pipe, the screen is less likely to become clogged by muddy layers. The steel pipe may also be secured in place to act as a temporary casing if the hole is unlikely to collapse (such as when sampling shallow water tables).

A drive-point piezometer was attempted, however in the clay rich soils, it prevented any water from being obtained. It is also quite bulky and requires more tools to install and remove. In general, the PushPoint Samplers proved to be the most versatile sampling equipment, as well as the most portable as compared to the mini-piezometer. Despite the limitations, these are promising additions to any future baseline monitoring activities.

6.3.3 Geochemical and Isotopic Tracers

Much of this work relied on the existence of groundwater geochemistry and isotopic data that were known prior to sample collection. In total, four monitoring wells (and one exploration well) spanning three formations provided information on groundwater geochemistry and isotopic signatures that were used to infer groundwater interactions with surface water. This data was crucial in exploring groundwater quality, variability and identifying potential tracers. This work does not seek to minimize the usefulness of a subpermafrost monitoring well, however, careful characterization of the suprapermafrost zone may remove some of the need for extensive monitoring networks. Suprapermafrost groundwater and surface water is much easier to collect than subpermafrost groundwater and may be taken quite rapidly with portable instruments, if done strategically. Geochemical or isotopic patterns in water that deviate from a well-characterized suprapermafrost zone may indicate the presence of subpermafrost groundwater or another unidentified component. This assumption relies on distinct contrasts between the different types of water and may not apply in some areas, depending on local geology. One major limitation of this work is that even with the diverse range of isotopic and geochemical tracers, it was not always possible to identify the provenance of a sample. Overburden soil geochemistry had a similar high Cl, low SO4 composition as that of subpermafrost groundwater, and so it complicated the use of geochemistry as an indicator of subpermafrost water contributions to springs. Isotopes were also limited in their usefulness as critical endmember values were unknown.

Geochemistry was the most significant contributor to interpretations of groundwater presence and provenance, especially in surface water. Although highly variable, especially within the suprapermafrost

zone, geochemical patterns and ion ratios may be predictable based on aquifer lithology. For instance, suprapermafrost groundwater will take a shorter path than subpermafrost groundwater and consequently have a shorter residence time. It is therefore reasonable to conclude the chemistry will be dominated by carbonate weathering as these minerals are more soluble than silicates. Although this largely depends on local lithologies. Caution must be noted when carbonate rocks are within the area of interest, however. Actual ion concentrations rather than Piper plot position may be more useful in that regard. Subpermafrost groundwater flow is most likely to occur below glacial deposits and therefore should be more characteristic of bedrock aquifers. In this study where carbonate rocks were not the dominant aquifers, deep groundwater geochemistry was generally characteristic of silicate weathering reactions. This stark contrast allows for visual identification of groundwater endmembers and therefore potential mixing using a Piper plot. Usage of additional ion ratios may also prove useful in parsing out groundwater source contributions from a sample. Geochemical profile of permafrost also indicate that solutes generally increase with depth into the frozen ground. This could be used in future studies by tracking solute changes in shallow groundwater and surface water bodies and correlating them with thaw depths.

Longitudinal sampling along Bogg Creek was conducted by Husky as well as for this study in 2019. This method allows for changes along the length of the stream to be observed, and as demonstrated, may provide evidence of groundwater influences between certain sampling points. The lack of accessibility in this remote environment limited the amount of sampling points available, but even with just these few, subtle changes in the geochemistry or isotopes could be observed. This method is useful when large changes can be accounted for, such as the convergence of large tributaries, and more subtle changes are likely to be the result of groundwater inputs. Further information about where groundwater may be coming in between sampling points could be inferred from this type of sampling too.

BTEX was naturally occurring in deep, subpermafrost groundwater aquifers in this study and was therefore a natural tracer for deep groundwater discharge. Care must be given however if the study area is wetland rich, as toluene may also be naturally occurring in waterlogged soils. Further differentiation of biogenic and thermogenic toluene is possible through the presence of additional BTEX species, as thermogenic toluene will usually not be detected alone. This appeared to be the case in several areas of the watershed, where mostly toluene was detected alone. Further limitations are that it may be that in samples that are mixtures of subpermafrost and suprapermafrost, BTEX species may be diluted beyond detection limits. Biodegradation may also occur.

$\delta^{18}O$ and $\delta^{2}H$ are invaluable components of understanding water sources and interactions between surface water and groundwater. Evidence of isotopically light water was found in spring samples, suggesting subpermafrost groundwater may be a source component. As well, isotopic changes along Bogg Creek could also indicate minor inputs of isotopically lighter groundwater are occurring. Permafrost cores were also demonstrated as having an isotopically lighter signature, suggesting the frozen water was recharged during a colder climate and was not modern. However, these isotopes were limited in this environment as paleogroundwater, thawed permafrost, snowmelt, and water recharged at a high altitude could all potentially produce isotopically light $\delta^{18}O$ and $\delta^{2}H$. This does make interpretations limited without additional information, although altitudes do not change drastically within the region except further southwest towards the mountain ranges. If these sources can be identified, quantified and put into a regional context with a sample, this will reduce some uncertainty. Monitoring thaw depths could also indicate whether thawed permafrost could be a major contributor. Another limitation is that the sensitivity of $\delta^{18}O$ and $\delta^{2}H$ to mixing is also less than that for geochemistry, due mainly to the larger contrast inherent in geochemical species between old and young groundwater as compared to $\delta^{18}O$ and $\delta^{2}H$. Mixing relationships were generally easier to see when waters were not affected by evaporation (such as the spring groundwater). Despite these limitations future studies should strive to incorporate $\delta^{18}O$ and $\delta^{2}H$ into their toolbox as it is simple to collect and has a variety of uses.

^{3}H allows for a quick differentiation of modern and old (>50-60 years) water based on its presence or absence in the water sample. Care must be taken as it may also indicate water that is mixed if the ^{3}H values are greater than 0 TU but less than that of modern water. In this instance it was useful to gain a sense of groundwater residence times in certain locations of the watershed. Confusion, however, may arise where it is unclear if the sample has a certain TU value that is due to mixing or to natural ^{3}H decay. This limited the usefulness of this tracer in the spring samples. Future techniques may apply dating methods utilizing ^{3}H and ^{3}He to get a more accurate picture of residence times, but in general little useful information was gleaned just from ^{3}H alone.

$^{87}Sr/^{86}Sr$ and Sr concentration in groundwater is directly tied to the mineralogy and age of the aquifer. In this work, $^{87}Sr/^{86}Sr$ ratios were more variable in the suprapermafrost samples due to the suprapermafrost zone largely consisting of glacially transported sediments of various lithologies and widely varying residence times. While only comprising a small number of samples, subpermafrost groundwater was more consistent in its $^{87}Sr/^{86}Sr$. It provided further evidence of subpermafrost

groundwater influence on a tributary of Bogg Creek but was limited in interpretations of spring provenance. In general, $^{87}Sr/^{86}Sr$ was useful in confirming much of what the geochemical evidence was suggesting in regard to groundwater influences on the creek and would be an excellent complementary isotope to include in future baseline monitoring studies, as long as endmembers can be established reliably.

Lastly, ^{13}C in methane seemed to identify dissolved gases that could have some component of thermogenic methane. However, oxidation reactions of methane may push these values towards appearing thermogenic, limiting the usefulness of this technique in surface water. To account for this, when sampling groundwater for methane, taking measurements of DO could be used to verify whether there was likely oxidation that occurred or not. There is also uncertainty based on the large overlap between thermogenic and biogenic endmembers. Future studies may benefit from analyzing the ^{2}H in the methane and the ratios of the various other C_1, C_2 and C_3 species to remove some of this uncertainty.

Overall, these isotopes were effective but limited by lack of distinct endmembers for each conceptualized water source. Key questions could be answered with relatively little additional data (such as from monitoring wells), and the techniques may be employed in other regions as well. In future studies, additional isotopes could be included, or the suite of isotopes could be simplified around a few key analyses. Different isotopes such as ^{34}S in SO_4 or ^{13}C in DIC could provide some clue of physical subsurface conditions that can be used to differentiate a groundwater flow system from another. Further exploration of this would be useful.

6.3.4 Other Methods

Other methods utilized in this work included measurements of temperature profiles and hydraulic heads, stream gauging (Husky data), temperature monitoring of shallow permafrost (Husky data), direct permafrost probing and an EM survey. These methods all provided physical evidence for vertical groundwater flow directions, hydrologic conditions of the creek, or information on permafrost distribution and changes.

Temperature profiles and hydraulic heads were measured in select locations, their main purpose was to determine vertical groundwater flow directions. Temperature profiles act as a substitute for hydraulic measurements, but generally are used qualitatively to determine local flow conditions. They require a large contrast in groundwater and surface water temperatures and therefore are limited to certain times of

the year, such as in mid to late summer. However, they are slightly easier to measure as compared to hydraulic heads and require only one instrument. More detailed profiles can be used to estimate flux rates, but this was outside of the scope of this work. Hydraulic measurements in comparison are useful when actual flux rates are needed, or to confirm temperature profile data. Under artesian conditions these are much easier to determine, and no water level tape is needed. Due to clogging however, temperature profiles may be the more attractive option when a simple discharge condition is all that is needed.

Temperature monitoring provided insight into the changes that are occurring to permafrost over several years. The limitation with this data was that consistent intervals were not used in the installation of the thermistor cables, so direct comparisons between depth intervals across different thermistor wells were difficult. Additionally, many thermistors were installed below the active layer, and so monitoring actual active layer thaw depths was not always possible. Disturbances to the area surrounding the wells also made it challenging to determine what was causing changes in thaw depth.

Permafrost probing also provides a direct measurement of thaw depth at the time of data collection. These measurements are limited by the depth of the probe used but are easy to take. In this study the active layer thaw depth was not monitored over time, but this method could be used to confirm temperature measurements that record thaw changes in shallow thermistors.

Lastly, implementation of EM38 was an additional piece of evidence that can be used to scope out the presence of shallow taliks and the presence of higher conductivity water. In future work it may be useful to perform this survey prior to sampling, to further narrow down where high-conductivity water is emerging.

6.4 Recommendations for Baseline Monitoring in Similar Environments

Future baseline monitoring studies may benefit from incorporating methods outlined in this work. Some recommendations are outlined in Wicke & Rudolph (2020) in Appendix C, but they will be expanded in the following section. The approach taken in this project progressively narrowed the scale of investigation, starting with mapping of potential icings at the watershed scale (Glass et al., 2020) and inspection of geologic maps and high-resolution satellite photos. An aerial IR survey was then used to narrow down the list of potential sites to those that had evidence of groundwater discharge at the surface (Conant Jr., 2019). Site accessibility was assessed through the use of high-resolution satellite imagery. This strategy allowed for specific sites to be investigated that were most likely to be influenced by

subpermafrost groundwater and were also accessible from the road or by helicopter. This process is outlined below in Figures 59 and 60.

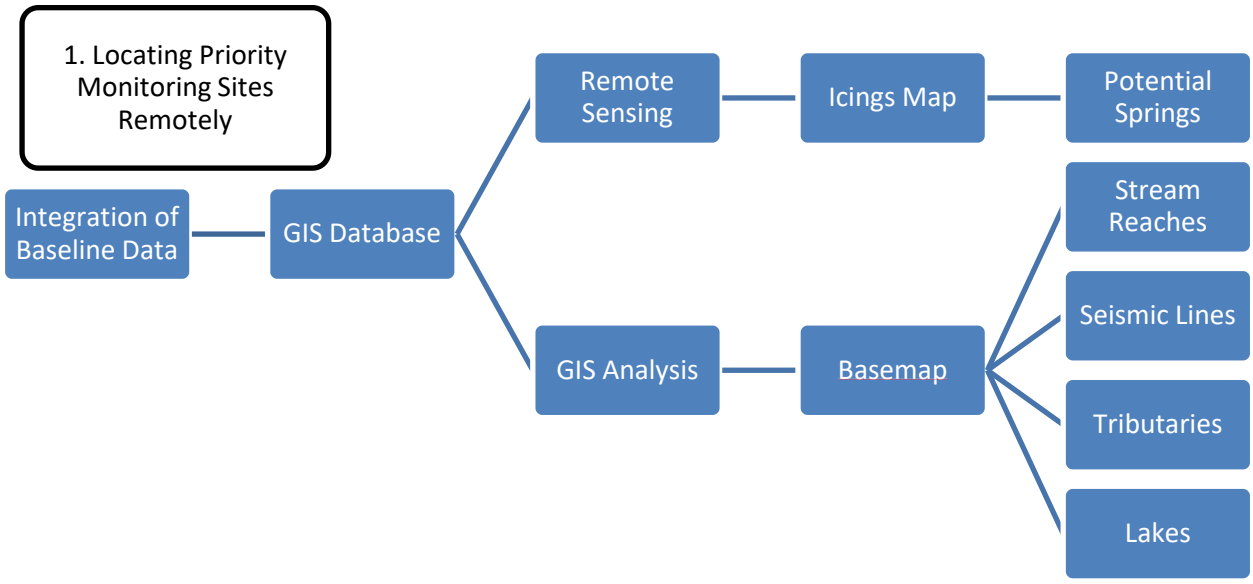

Figure 59: Initial framework for locating priority monitoring sites for the purpose of baseline monitoring within discontinuous permafrost environments. Taken from Wicke & Rudolph, (2020).

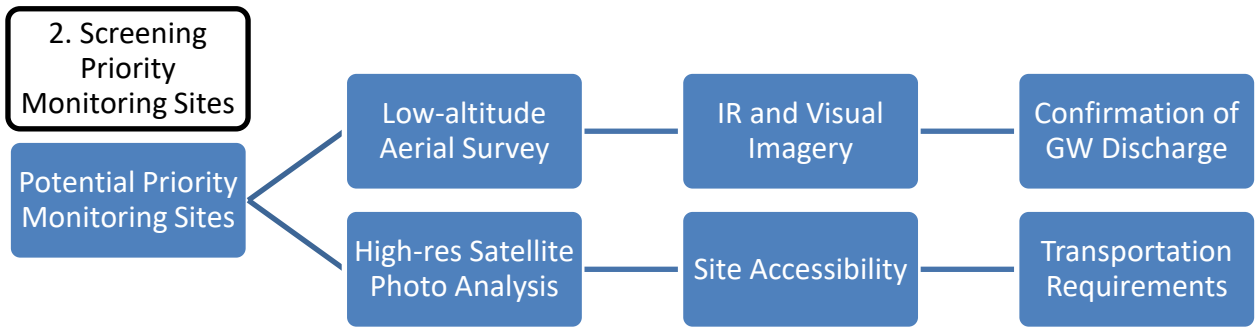

Figure 60: An overview of the priority monitoring site screening process, using an aerial IR survey and high-resolution satellite imagery. From Wicke & Rudolph, (2020)

With sites identified and screened, they can be separated into areas of potential groundwater discharge (springs and seeps) or that are suspected to be influenced by groundwater (nearby springs or icings), and

surface water bodies that could be chosen based on accessibility for the purposes of regular sampling to establish baseline water quality and to investigate potential groundwater influences. The field verification process can then be conducted, which is outlined below in Figure 61.

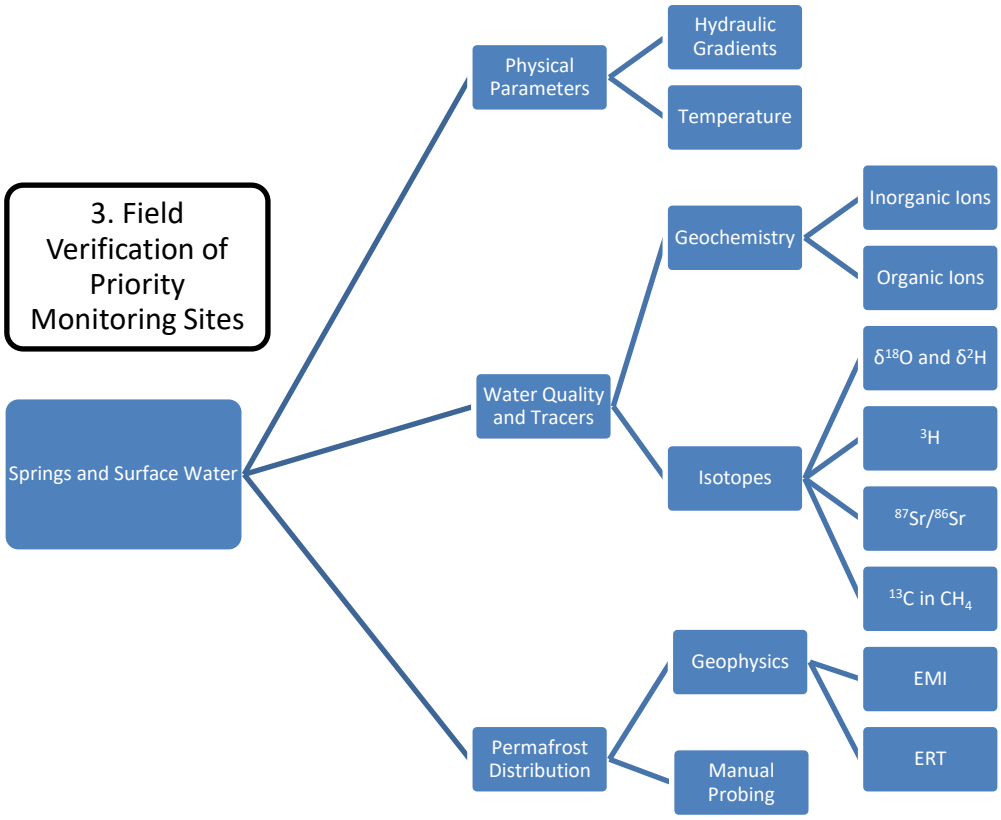

Figure 61: Field verification process outlining the techniques utilized in this study. Taken from Wicke & Rudolph (2020).

Baseline monitoring methods undertaken by Husky laid the foundation for much of this work to be successful. This included installation and sampling of three groundwater monitoring wells, one screened within the suprapermafrost zone and two in the subpermafrost zone (LBF). These samples, particularly the subpermafrost samples, were critical to the investigation of surface waters in Bogg Creek. Additional data for subpermafrost groundwater samples were acquired through additional reports and provided information on the MHF water quality. Without this evidence, straightforward conclusions about what sources were potentially impacting springs and surface water in the watershed would have been more difficult to make. Historical sampling of surface water also provided a long-term dataset that could be investigated for evidence of subpermafrost groundwater influence. As well, temperature measurements

within the overburden permafrost provided evidence of warming and permafrost thaw. However, these datasets were oftentimes treated as separate entities of the overall hydrologic system of the study area. Future baseline monitoring should interpret these datasets holistically.

In future baseline monitoring studies, for groundwater influence to be investigated properly, the various groundwater sources must be identified and attempted to be sampled. This could include at least one sample from the main bedrock aquifers underlying the study area (if applicable) and a well characterized suprapermafrost groundwater system. Shallow sampling from nearby and below water bodies can be conducted while surface water sampling with portable equipment, while more permanent suprapermafrost monitoring wells may be installed in other areas. Other samples could be collected randomly from the active layer with portable sampling. With enough contrast between the suprapermafrost and subpermafrost waters comparisons to the surface water can be made more easily. This contrast may be site specific however, and there may not be as much contrast in other study areas unless underlain by a similar geology and with similar water residence times. Large contrasts found in the springs or surface water that differ from the suprapermafrost endmembers could be indicative of subpermafrost groundwater influence, without the need for extensive subpermafrost sampling. In similar environments with a large regional flow system, contrasts in geochemistry would likely be expected. Depending on the age of the water, contrasts in $\delta^{18}O$ and $\delta^{2}H$ and the other isotopes such as $^{87}Sr/^{86}Sr$ could be expected too. If these samples are available, this will remove the uncertainty that would arise by making interpretations without complete data.

Changes in active layer thaw depths were documented in this study but were complicated by external factors that may have exacerbated thawing. However, changes to permafrost would likely occur over several years, and could be documented through thermistor profile temperature monitoring and physical probing for active layer thaw depths. Data from weather stations could be used to correlate changes to warming temperatures or changes in precipitations.

Changes to the shallow groundwater system are likely to be slower, as permafrost thaws and active layers deepen, there is increased aquifer volume available for flow, and flow paths will become deeper. As well, more fresh mineral grains will be available for weathering reactions, leading to changes in groundwater solute concentrations. Physical changes to permafrost distribution and aquifer volume may be documented with thermistor readings or through thaw depth probing. Changes to the subpermafrost groundwater system are likely to take many decades to occur, mainly as taliks widen and allow for

increased subpermafrost groundwater discharge. Changes in subpermafrost groundwater geochemistry are not likely to occur on these time scales but the discharging groundwater could change as it intercepts the shallow system, which may be observed in spring sampling. Shallow samplers used in the same monitoring locations and suprapermafrost groundwater monitoring wells should be able to capture these changes with consistent sampling at similar times every year, potentially several times a year. Combining this with nearby thermistor profile data and physical measurements of active layer thaw depth would lend evidence as to what would be causing changes in this shallow system. Consistent sampling and monitoring of hydraulic heads in springs would also help to document changes that may be occurring with permafrost loss, these can also be correlated with physical or geophysical measurements of permafrost distribution. Resampling of subpermafrost groundwater and measurements of hydraulic heads could occur every number of years, just to observe if there are any changes occurring to the endmembers.

Surface water quality is also likely to be impacted over time, as suprapermafrost groundwater flowpaths deepen, and there is increased baseflow during colder months due to widening of taliks. These changes are likely going to occur on similar time scales as the shallow groundwater. Surface water quality monitoring over time provides information on baseline conditions and any potential changes that may be occurring. However, as demonstrated in this work, substantial variability can occur between sampling periods when only done once a year, even when sampled in the same month. Water levels and geochemistry can change substantially over a short period of time due to seasonal changes. A general framework for surface water sampling should incorporate longitudinal sampling at the same points along the stream, both at bridge crossings or other easy access points, and at other points along the stream that are accessible, with regular sample timing. In this environment, consistent, scheduled monitoring is difficult, but it is critical to establishing the true baseline conditions as well as allowing natural variability to be differentiated between changes that are forced by external factors. More specifically, periodic sampling conducted throughout the year, with subsequent sampling taking place during the same weeks in the next year. This would hopefully capture enough seasonal variability and reduce uncertainty about natural fluctuations in the geochemistry and isotopes that may be caused by large precipitation events. These data can be correlated with nearby groundwater and permafrost data, to investigate the source of any changes. Baseline spatial geochemical variability along the length of the stream can be determined with one sampling event, which can then be assessed by comparing it to the other conceptualized water sources to determine groundwater influences that occur moving downstream. This longitudinal sampling should be conducted during low water periods, when the stream is most likely to be impacted mainly by

groundwater baseflow. In this study this was around mid to late August, however stream gauging could be used to confirm this in other regions.

In summary, a future baseline monitoring approach should attempt to synthesize data from a variety of different scales in order to gain a clearer picture of baseline conditions. With climate change and human activities, it is documented that environmental change is occurring in remote regions, but it is unclear how things will change. The preceding recommendations could hopefully be used to establish a baseline and document transitions more effectively.

Chapter 7
Conclusions

This work serves as an exploration of various methods for characterizing groundwater flow in a discontinuous permafrost environment using unconventional techniques. This work demonstrates that certain aspects of baseline groundwater flow conditions can be established and monitored through a strategic approach utilizing portable sensors and sampling equipment, especially when combined with remote sensing and aerial surveys.

Remote sensing of icings completed in previous work combined very well with GIS analysis of terrain and geology to locate priority monitoring sites. Further site exploration and screening was performed with an aerial survey utilizing visual and IR cameras, which led to identification of probable spring sites. Geochemical and isotopic tracers provided evidence of groundwater presence in surface water but were somewhat limited as to what questions could be answered due to lack of identified groundwater endmembers, which provided the basis to compare surficial and shallow sub-surficial samples.

Despite these limitations, these methods provided crucial evidence for complex groundwater flow and groundwater/surface water interactions in the Bogg Creek Watershed. Overall, groundwater geochemistry was the most important tool utilized to infer groundwater contributions in the Bogg Creek Watershed. Geochemical signatures and solute concentration contrasts in the geochemical endmembers allowed for mixing relationships to be interpreted rather quickly with the use of Piper plots. The isotope suite had varying levels of success. $\delta^{18}O$ and $\delta^{2}H$ showed some evidence of isotopically light water influencing the creek and springs but was less sensitive due to lower contrasts between subpermafrost and suprapermafrost sources. This data suggested that subpermafrost groundwater contributions were relatively minor in the creek and its tributaries, but more substantial in the springs. $^{87}Sr/^{86}Sr$ seemed to largely agree with the geochemical conclusions, most namely the influence of LBF water along one tributary. However, results were ambiguous when applied to the spring samples, as groundwater mixing, or geochemical evolution could both be interpreted from that data.

Application of these methods in other discontinuous permafrost regions should be possible. One conclusion from this work was that characterization of deeper subpermafrost groundwater endmembers is still important in directly inferring their influence on springs or in surface water. Subpermafrost groundwater wells should therefore be utilized to capture the geochemical and isotopic fingerprints of formation waters, but extensive networks may not be necessary. It is hypothesized that efforts could be

concentrated on first sampling the shallow suprapermafrost groundwater zone in detail, within organic and mineral soils, to capture variability in this zone and to characterize the water type. Should there be large contrasts between selected endmembers of suprapermafrost and subpermafrost waters, discerning mixing relationships should be fairly straightforward, even with relatively few subpermafrost samples. At least one subpermafrost groundwater well in each distinct formation in the study area should be necessary. These should also be sampled for all the same analytes as the surface water and springs. It should be expected that large contrasts should exist between shallow and deep samples where permafrost is thick, and it effectively partitions the subpermafrost groundwater into long flowpaths through deeper sections of sedimentary bedrock.

Other uncertainties are in the potential environmental impacts that may arise due to shale oil and gas activities and climate change, although these were only briefly explored in this thesis. Some data suggests changes are occurring in the region, but some are difficult to correlate with climate due to added circumstances (such as removal of vegetation possibly impacting permafrost). Additional work in this area might focus on improving spatial and temporal resolution of the sampling regime along Bogg Creek and its main tributaries and lakes. Thermal anomalies that were identified but not investigated could also be included in further investigations.

Bibliography

AMEC. (2013). Central Mackenzie Valley Subsurface Groundwater Baseline Study. *Indigenous and Northern Affairs Canada and the North, Northern Petroleum Resources*, (July). Retrieved from https://www.aadnc-aandc.gc.ca/eng/1100100036430/1100100036431

Anderson, M. P. (2005). Heat as a ground water tracer. *Ground Water*, *43*(6), 951–968. https://doi.org/10.1111/j.1745-6584.2005.00052.x

Aylsworth, J. M., & Kettles, I. M. (2001). Distribution of peatlands. *Bulletin of the Geological Survey of Canada*, (547), 49–55.

Babiy, R. (2013). Norman Wells Field – a long history of oil production in the Central Mackenzie Valley [Abstract]. In *geoConvention 2013* (pp. 1–2).

Barker, J.F., & Fritz, P. (1981). Carbon isotope fractionation during microbial methane oxidation. *Nature, 293,(24), 289-291 DOI: 10.1038/293289a0*

Bense, V. F., Ferguson, G., & Kooi, H. (2009). Evolution of shallow groundwater flow systems in areas of degrading permafrost. *Geophysical Research Letters*, *36*(22), 2–7. https://doi.org/10.1029/2009GL039225

Burgess, M. M., & Smith, S. L. (2001). Shallow ground temperatures. In *Bulletin 547 of the Geological Survey of Canada* (pp. 89–103).

Burt, T. P., & Williams, P. J. J. (1976). Hydraulic conductivity in frozen soils. *Earth Surface Processes and Landforms*, *1*(4), 349–360. https://doi.org/10.1002/esp.3290010404

Canadian Water Network. (2015). *Water and Hydraulic Fracturing Report*. https://cwn-rce.ca/report/2015-water-and-hydraulic-fracturing-report/

Chapman, E. C., Capo, R. C., Stewart, B. W., Kirby, C. S., Hammack, R. W., Schroeder, K. T., & Edenborn, H. M. (2012). Geochemical and Strontium Isotope Characterization of Produced Waters from Marcellus Shale Natural Gas Extraction. *Environmental Science and Technology* https://doi.org/10.1021/es204005g

Clark, I., & Fritz, P. (1997). *Environmental Isotopes in Hydrogeology*. Lewis, Boca Raton.

Clark, I., Lauriol, B., Harwood, L., & Marschner, M. (2001). Groundwater Contributions to Discharge in

a Permafrost Setting , Big Fish River, NWT, Canada. *Arctic, Antarctic, and Alpine Research*, *33*(1), 62–69.

Conant Jr, B. (2004). Delineating and Quantifying Ground Water Discharge Zones Using Streambed Temperatures. *Ground Water*, *42*(2), 243–257.

Conant Jr, B. (2009). *Infrared Thermography to Identify Groundwater Discharges for Fisheries Habitat Assessments in the Northwest Territories*. Prepared for the Arctic Sciences Division Central and Arctic Region, Fisheries and Oceans Canada. June 1, 2009

Conant Jr, B. (2019). *Low Altitude Aerial Thermal Infrared Survey to Detect Groundwater Discharges and Melting Permafrost*.

Conant Jr, B., Robinson, C. E., Hinton, M. J., & Russell, H. A. J. (2019). A framework for conceptualizing groundwater-surface water interactions and identifying potential impacts on water quality , water quantity , and ecosystems. *Journal of Hydrology*, *574*(April), 609–627. https://doi.org/10.1016/j.jhydrol.2019.04.050

Connon, R. F., Quinton, W. L., Craig, J. R., Hanisch, J., & Sonnentag, O. (2015). The hydrology of interconnected bog complexes in discontinuous permafrost terrains. *Hydrological Processes*, *29*(18), 3831–3847. https://doi.org/10.1002/hyp.10604

Connon, R. F., Quinton, W. L., Craig, J. R., & Hayashi, M. (2014). Changing hydrologic connectivity due to permafrost thaw in the lower Liard River valley, NWT, Canada. *Hydrological Processes*, *28*(14), 4163–4178. https://doi.org/10.1002/hyp.10206

Constantz, J. (2008). Heat as a tracer to determine streambed water exchanges. *Water Resources Research, 44*, W00D10, doi:10.1029/2008WR006996.

Cook, P. G. (2003). *A Guide to Regional Groundwater Flow in Fractured Rock Aquifers*. Glen Osmond, SA, Australia: CSIRO Land and Water. https://doi.org/10.18520/cs/v111/i3/524-534

Coplen, T. B., Herczeg, A. L., & Barnes, C. (2000). Isotope Engineering-Using Stable Isotopes of the Water Molecule to Solve Practical Problems. In P. Cook & A. L. Herczeg (Eds.), *Environmental Tracers in Subsurface Hydrology* (pp. 79–110). New York: Springer Science+Business Media.

Côté, M. M., Duchesne, C., Wright, J. F., & Ednie, M. (2013). Digital compilation of the surficial sediments of the Mackenzie Valley corridor, Yukon Coastal Plain, and the Tuktoyaktuk Peninsula.

Geological Survey of Canada Open File 7289 https://doi.org/10.4095/292494

Couch, A., & Eyles, N. (2008). Sedimentary record of glacial Lake Mackenzie, Northwest Territories, Canada: Implications for Arctic freshwater forcing. *Palaeogeography, Palaeoclimatology, Palaeoecology*, *268*(1–2), 26–38. https://doi.org/10.1016/j.palaeo.2008.06.011

Day, J. H., & Rice, H. M. (1964). The Characteristics of Some Permafrost Soils in the Mackenzie Valley, N.W.T. *Arctic*, *17*(4), 222–236.

Deitchman, R. S., Loheide, S. P., & Ii, S. P. L. (2009). Ground-based thermal imaging of groundwater flow processes at the seepage face. *Geophysical Research Letters*, *36*(14), 1–6. https://doi.org/10.1029/2009GL038103

Dingman, S. L. (1994). *Physical Hydrology*. Englewood Cliffs, New Jersey: Prentice-Hall Inc.

Dyke, A. S. (2004). An outline of the deglaciation of North America with emphasis on central and northern Canada. *Quaternary Glaciations-Extent and Chronology, Part II: North America*, *2b*, 373–424. https://doi.org/10.1016/S1571-0866(04)80209-4

Dyke, A. S., Andrews, J. T., Clark, P. U., England, J. H., Miller, G. H., Shaw, J., & Veillette, J. J. (2002). The Laurentide and Innuitian ice sheets during the Last Glacial Maximum. *Quaternary Science Reviews*, *21*(1–3), 9–31. https://doi.org/10.1016/S0277-3791(01)00095-6

Environment Canada. (2019). Historical Climate Data for Norman Wells, NWT. Retrieved from http://climate.weather.gc.ca/index_e.html

Fallas, K. M., & MacNaughton, R. B. (2013). Geology, Norman Wells (southeast), Northwest Territories. *Geological Survey of Canada, Canadian Geoscience Map* 100 . https://doi.org/10.4095/292292

Fallas, K. M., & MacNaughton, R. B. (2014). Geology, Carcajou Canyon (southeast), Northwest Territories. *Geological Survey of Canada, Canadian Geoscience Map* 96. https://doi.org/10.4095/292288

Fallas, K. M., MacNaughton, R. B., Maclean, B. C., & Hadlari, T. (2013). Geology, Norman Wells (southwest), Northwest Territories. *Geological Survey of Canada, Canadian Geoscience Map*, *101*, 292293. https://doi.org/10.4095/292293

Fetter, C. W. (2001). *Applied Hydrogeology* (4th ed.). Upper Saddle Hall, NJ: Prentice Hall.

French, H. M. (1996). *The Periglacial Environment* (2nd ed.). Essex, England: Addison Wesley Longmang Ltd.

Frost, C. D., Pearson, B. N., Ogle, K. M., Heffern, E. L., & Lyman, R. M. (2002). Sr isotope tracing of aquifer interactions in an area of accelerating coal-bed methane production , Powder River Basin , Wyoming. *Geology*, *30*(10), 923–926. https://doi.org/10.1130/0091-7613(2002)030<0923:SITOAI>2.0.CO;2

Frost, C. D., & Toner, R. N. (2004). Strontium Isotopic Identification of Water-Rock Interaction and Ground Water Mixing. *Ground Water*, *42*(3), 418–432.

Glass, B. (2019). *Examining Hydrogeological Processes in Freezing Soils using Remote Geophysical and Numerical Techniques.* MSc. Thesis, Department of Earth and Environmental Sciences, University of Waterloo, Waterloo, Ontario, Canada.

Glass, B., Rudolph, D., Duguay, C., & Wicke, A. (2020). Identifying Groundwater Discharge Zones in the Central Mackenzie Valley Using Remotely Sensed Optical and Thermal Imagery. *Canadian Journal of Earth Sciences, 58 (2), 105-121*.

Golder Associates. (2015). Central Mackenzie Surface Water and Groundwater Baseline Assessment. Prepared for the Government of Northwest Territories. May 21, 2015

Grasby, S., Ferguson, G., Brady, A., Sharp, C., Dun, P., & Mcmechan, M. (2016). Deep groundwater circulation and associated methane leakage in the northern Canadian Rocky Mountains. *Applied Geochemistry*, *68*, 10–18. https://doi.org/10.1016/j.apgeochem.2016.03.004

Hayes, B. R., & Dunn, J. (2012). *Deep Subsurface Saline Aquifer Characterization, Central Mackenzie Valley, Northwest Territories*. *NWT Open File 2012-07*.

Hem, J. D. (1985). *Study and Interpretation of the Chemical Characteristics of Natural Water*. *USGS Water-Supply Paper 2254*. United States Geological Survey.

Herczeg, A. L., & Edmunds, W. M. (2000). Inorganic Ions as Tracers. In P. Cook & A. L. Herczeg (Eds.), *Environmental Tracers in Subsurface Hydrology* (pp. 31–78). New York: Springer Science+Business Media.

Husky Oil Operations Ltd. (2016). *2016 Surface Water Quality Assessment*. Prepared for the Sahtu Land and Water Board, December 2016.

Husky Oil Operations Ltd. (2018). *2017 Surface Water Quality Assessment*. Prepared for the Sahtu Land and Water Board, May 2018.

Ireson, A. M., van der Kamp, G., Ferguson, G., Nachshon, U., & Wheater, H. S. (2013). Hydrogeological processes in seasonally frozen northern latitudes: understanding, gaps and challenges. *Hydrogeology Journal*, *21*(1), 53–66. https://doi.org/10.1007/s10040-012-0916-5

Jacques, J. M. S., & Sauchyn, D. J. (2009). Increasing winter baseflow and mean annual streamflow from possible permafrost thawing in the Northwest Territories, Canada. *Geophysical Research Letters*, *36*(1), 1–6. https://doi.org/10.1029/2008GL035822

Jessen, S., Holmslykke, H. D., Rasmussen, K., Richardt, N., & Holm, P. E. (2014). Hydrology and pore water chemistry in a permafrost weland, Ilulissat, Greenland. *Water Resources Research*, *50*, 1–15. https://doi.org/10.1002/2013WR014376.

Kalo Stantec Ltd. (2014). *Sahtu Land and Water Board LUP / WL Application and National Energy Board OA Application Environmental Effects Report*. Prepared for Husky Oil Operations Limited, March, 2014

Keller, K., Blum, J. D., & Kling, G. W. (2010). Stream geochemistry as an indicator of increasing permafrost thaw depth in an arctic watershed. *Chemical Geology*, *273*(1–2), 76–81. https://doi.org/10.1016/j.chemgeo.2010.02.013

Kokelj, S. V, & Burn, C. R. (2005). Geochemistry of the active layer and near-surface permafrost, Mackenzie delta region, Northwest Territories, Canada. *Canadian Journal of Earth Sciences*, *42*(1), 37–48. https://doi.org/10.1139/e04-089

Kresic, N., & Stevanovic, Z. (2010). *Groundwater Hydrology of Springs*. Burlington, MA, MA: Elsevier.

Lacelle, D., Fontaine, M., Forest, A. P., & Kokelj, S. (2014). High-resolution stable water isotopes as tracers of thaw unconformities in permafrost : A case study from western Arctic Canada. *Chemical Geology*, *368*, 85–96. https://doi.org/10.1016/j.chemgeo.2014.01.005

Lamoureux, S. F., & Lafrenière, M. J. (2018). More than just snowmelt : integrated watershed science for changing climate and permafrost at the Cape Bounty Arctic Watershed Observatory. *Wiley Interdisciplinary Reviews: Water*, *5*(February), 1–15. https://doi.org/10.1002/wat2.1255

Lee, D. R., & Cherry, J. A. (1979). A field exercise on groundwater flow using seepage meters and mini-

piezometers. *Journal of Geological Education*, *27*(1), 6–10.

Leibundgut, C., Maloszewski, P., & Külls, C. (2009). *Tracers in Hydrology*. Wiley-Blackwell.

Lemieux, J., Fortier, R., Talbot-Poulin, M.-C., Molson, J., Therrien, R., Ouellet, M., Banville, D., Cochard, M., & Murray, R. (2016). Groundwater occurrence in cold environments: examples from Nunavik, Canada. *Hydrogeology Journal*, *24*(6), 1497–1513. https://doi.org/10.1007/s10040-016-1411-1

Maclean, B. C. (2012). GIS-enabled structure maps of subsurface Phanerozoic strata, north-western Northwest Territories, Canada. *Geological Survey of Canada, Open File 7172*.

Maclean, B. C., Fallas, K. M., & Hadlari, T. (2015). The evolution of Keele Arch, a multiphase feature of the northern mainland, Northwest Territories. *Geological Survey of Canada, Bulletin 606.*

McKenzie, J. M., & Voss, C. I. (2013). Permafrost thaw in a nested groundwater-flow system. *Hydrogeology Journal*, *21*(1), 299–316. https://doi.org/10.1007/s10040-012-0942-3

McNutt, R. H. (2000). Strontium Isotopes. In Peter G Cook & A. L. Herczeg (Eds.), *Environmental Tracers in Subsurface Hydrology* (pp. 233–260). Boston, MA: Springer US. https://doi.org/10.1007/978-1-4615-4557-6_8

Michaud, Y., & Bégin, C. (2001). Past environmental change recorded in dune fields. *Bulletin of the Geological Survey of Canada*, (547), 79–87.

Michel, F. A. (1986). Hydrogeology of the central Mackenzie Valley. *Journal of Hydrology*, *85*(3–4), 379–405. https://doi.org/10.1016/0022-1694(86)90068-5

Michel, F. A., & Fritz, P. (1982). Significance of isotope variations in permafrost waters at Illisarvik, NWT. *Hydrology in Permafrost Regions*, *Proc. 4th*, 173–181. Retrieved from http://pubs.aina.ucalgary.ca/cpc/CPC4-173.pdf

Moncur, M. C., Blowes, D. W., & Ptacek, C. J. (2013). Pore-water extraction from the unsaturated and saturated zones. *Canadian Journal of Earth Sciences*, *1058*(July), 1051–1058.

Neumann, K., & Dreiss, S. (1995). Strontium 87 / strontium 86 ratios as tracers in groundwater and surface waters in Mono Basin, California. *Water Resources Research*, *31*(12), 3183–3193.

Northern EnviroSearch Ltd. (2015). 2014 Hydrological & Surface Water Evaluation Slater River Project,

EL494 Tulita District, Sahtu Region, Northwest Territrories. Prepared for Sahtu Land and Water Board. April, 2015. Retrieved from http://www.mvlwb.ca/Boards/slwb/Registry/2012/S12X-006 - Husky Oil Operations Limited/S12X-006 - 2014 EL494 Husky Slater River Hydrological Assessment - Report - Apr 30_15.pdf

Pandey, P., Gleeson, T., & Baraer, M. (2013). Toward quantifying discrete groundwater discharge from frozen seepage faces using thermal infrared images. *Geophysical Research Letters*, *40*(1), 123–127. https://doi.org/10.1029/2012GL054315

Philp, R. P., & Monaco, G. Lo. (2012). Applications of Stable Isotopes in Hydrocarbon Exploration and Environmental Forensics. In M. Baskaran (Ed.), *Handbook of Environmental Isotope Geochemistry: Vol I* (pp. 639–677). Berlin, Heidelberg: Springer Berlin Heidelberg. https://doi.org/10.1007/978-3-642-10637-8_31

Quinton, W. L., Chasmer, L. E., & Petrone, R. M. (2011a). Permafrost loss and a new approach to the study of subarctic ecosystems in transition. *Cold Region Hydrology in a Changing Climate (IAHS Publ.)*, *346*, 98–102.

Quinton, W. L., Hayashi, M., & Chasmer, L. E. (2009). Peatland Hydrology of Discontinuous Permafrost in the Northwest Territories: Overview and Synthesis. *Canadian Water Resources Journal*, *34*(4), 311–328. https://doi.org/10.4296/cwrj3404311

Quinton, W. L., Hayashi, M., & Chasmer, L. E. (2011b). Permafrost-thaw-induced land-cover change in the Canadian subarctic : implications for water resources. *Hydrological Processes*, *158*(November 2010), 152–158. https://doi.org/10.1002/hyp.7894

Quinton, W. L., Hayashi, M., & Pietroniro, A. (2003). Connectivity and storage functions of channel fens and flat bogs in northern basins. *Hydrological Processes*, *17*(18), 3665–3684. https://doi.org/10.1002/hyp.1369

Quinton, W. L., & Pomeroy, J. W. (2006). Transformations of runoff chemistry in the Arctic tundra, Northwest Territories, Canada. *Hydrological Processes*, *20*(14), 2901–2919. https://doi.org/10.1002/hyp.6083

Raska, N. (2017). *3D geologic subsurface modeling within the Mackenzie Plain , Northwest Territories , Canada.* Master's Thesis, Department of Geography and Ecosystem Science, Lund University, Lund,

Sweden.

Richards, P. I., & Sandau, C. D. (2018). Forensic Source Attribution for Toluene in Environmental Samples. *Environmental Toxicology and Chemistry*, *37*(3), 729–737. https://doi.org/10.1002/etc.4008

Rosenberry, D. O., & LaBaugh, J. W. (2008). *Field Techniques for Estimating Water Fluxes Between Surface Water and Ground Water*. *USGS Techniques and Methods 4–D2*.

Rudolph, D. (2019). *Regional hydrologic and ecologic characterization and baseline assessment of remote northern Canadian terrain in advance of shale oil and gas development Second Annual* Prepared for : NWT ESRF Management Board. Waterloo ON.

Rudolph, D., Baltzer, J. L., Marsh, P., Quinton, W. L., Kokelj, S., Grasby, S., & Wolfe, S. (2016a). *Regional hydrologic and ecologic characterization and baseline assessment of remote northern Canadian terrain in advance of shale oil and gas development [Proposal]*. Prepared for NWT ESRF Management Board, December, 2016.

Rudolph, D., Lotimer, A. R., & Barker, J. F. (2016b). Final Report Baseline Hydrogeological Evaluation of Central Mackenzie Valley Oil and Gas Exploration Areas Sahtu Region, Northwest Territories, (June), 1–35.

Ryan, M. C., Alessi, D., Mahani, A. B., Cahill, A., Cherry, J., Eaton, D., Evans, R., Farah, N., Fernandes, A., Forde, O., Humez, P., Kletke, S., Ladd, B., Lemieux, J.M., Mayer, B., Mayer, K.U., Molson J., Muehlenbachs L, Nowamooz, A., & Parker, B. (2015). *Subsurface Impacts of Hydraulic Fracturing : Contamination, Seismic Sensitivity, and Groundwater Use and Demand Management*. Prepared for the Canadian Water Network, October, 2015.

Schmidt, C., Schirmer, M., & Conant Jr, B. (2007). Evaluation and field-scale application of an analytical method to quantify groundwater discharge using mapped streambed temperatures, *Journal of Hydrology, 347* 292–307. https://doi.org/10.1016/j.jhydrol.2007.08.022

Shand, P., Darbyshire, D. P. F., Love, A. J., & Edmunds, W. M. (2009). Sr isotopes in natural waters: Applications to source characterisation and water-rock interaction in contrasting landscapes. *Applied Geochemistry*, *24*(4), 574–586. https://doi.org/10.1016/j.apgeochem.2008.12.011

Smith, D. G. (1992). Glacial Lake Mackenzie , Mackenzie Valley, Northwest Territories, Canada.

Canadian Journal of Earth Sciences, *29*, 1756–1766. https://doi.org/10.1139/e92-138

Smith, I. R. (2010). Seismic shothole drillers ' log records: A wealth of new permafrost-related geoscience information , Northwest Territories and northern Yukon , Canada. *63rd Canadian Geotechnical Conference & 6th Canadian Permafrost Conference*, 1450–1457.

Smith, I. R. (2015). Seismic shothole drillers' lithostratigraphic logs: Unearthing a wealth of regional geoscience information in northwestern Canada. *GeoResJ*, *6*, 21–29. https://doi.org/10.1016/j.grj.2015.01.005

Smith, S. L., Chartrand, J., Duchesne, C., & Ednie, M. (2017). Report on 2016 field activities and collection of ground thermal and active layer data in the Mackenzie corridor , Northwest Territories. *Geological Survey of Canada Open File 8303*.

Solomon, D. K., & Cook, P. G. (2000). 3H and 3He. In Peter G Cook & A. L. Herczeg (Eds.), *Environmental Tracers in Subsurface Hydrology* (pp. 397–424). Boston, MA: Springer US. https://doi.org/10.1007/978-1-4615-4557-6_13

Spence, C., Kokelj, S., & Ehsanzadeh, E. (2011). Precipitation trends contribute to streamflow regime shifts in northern Canada. *Cold Region Hydrology in a Changing Climate (IAHS Publ.)*, *346*, 3–8. Retrieved from http://cat.inist.fr/?aModele=afficheN&cpsidt=24546588

Sutphin, J. D., Atkinson, L. C., Mahoney, J. J., & Hydrologic Consultants. (2006). Monitoring and Sampling of of Groundwater Beneath Deep Permafrost. Conference Paper: Sea to Sky Geotechnique, 59th Canadian Geotechnical Conference and 7th Joint CGS/IAH-CNC Groundwater Specialty Conference, 1613–1618.

Taylor, A. E., Burgess, M. M., Judge, A. S., & Allen, V. S. (2001). Deep ground temperatures. *Bulletin of the Geological Survey of Canada*, (547), 105–109.

Twidale, C. R. (2004). River patterns and their meaning. *Earth-Science Reviews*, *67*(3–4), 159–218. https://doi.org/10.1016/j.earscirev.2004.03.001

Utting, N. (2012). *Geochemistry and Noble Gases of Permafrost Groundwater and Ground Ice in Yukon and the Northwest Territories*. Ph.D. Thesis, Ottawa-Carleton Geoscience Center, University of Ottawa, Ottawa, Ontario, Canada.

Utting, N., Lauriol, B., Mochnacz, N., Aeschbach-Hertig, W., & Clark, I. (2013). Noble gas and isotope

geochemistry in western Canadian Arctic watersheds: tracing groundwater recharge in permafrost terrain. *Hydrogeology Journal*, *21*(1), 79–91. https://doi.org/10.1007/s10040-012-0913-8

van Everdingen, R. O. (1982). Frost Blisters of the Bear Rock Spring Area Near Fort Norman, N.W.T. *Arctic*, *35*(2), 243–265.

Veizer, J. (1989). Strontium Isotopes in Seawater Through Time. *Annual Review of Earth and Planetary Science*, (3).

Walter, J., Chesnaux, R., Cloutier, V., & Gaboury, D. (2017). The influence of water / rock − water / clay interactions and mixing in the salinization processes of groundwater. *Journal of Hydrology: Regional Studies*, *13*(July), 168–188. https://doi.org/10.1016/j.ejrh.2017.07.004

Walvoord, M. A., & Kurylyk, B. L. (2016). Hydrologic Impacts of Thawing Permafrost — A Review. *Vadose Zone Journal*. https://doi.org/10.2136/vzj2016.01.0010

Walvoord, M. A., & Striegl, R. G. (2007). Increased groundwater to stream discharge from permafrost thawing in the Yukon River basin: Potential impacts on lateral export of carbon and nitrogen. *Geophysical Research Letters*, *34*(12). https://doi.org/10.1029/2007GL030216

Walvoord, M. A., Voss, C. I., & Wellman, T. P. (2012). Influence of permafrost distribution on groundwater flow in the context of climate-driven permafrost thaw: Example from Yukon Flats Basin, Alaska, United States. *Water Resources Research*, *48*(7), 1–17. https://doi.org/10.1029/2011WR011595

Waterline Resources Inc. (2013a). 2013 Shallow Environmental Investigation Slater River Project Near Norman Wells, Northwest Territories. *Prepared for Husky Oil Operations Limited, June 3, 2013.*

Waterline Resources Inc. (2013b). Slater River Project Groundwater Investigation Program 2013 Winter Mud-Rotary Drilling Summary Report. *Prepared for Husky Oil Operations Limited, September 19, 2013.*

Waterline Resources Inc. (2013c). Slater River Project Groundwater Investigation Program Waters Act License Application Support Document. *Prepared for Husky Oil Operations Limited, June 13, 2013.*

Wicke, A. & Rudolph, D. (2020). Hydrogeological Site Characterization Methods for Discontinuous Permafrost Terrain. *Prepared for Environment and Natural Resources and Government of Northwest Territories, April, 2020.*

Woo, M. K. (2012). *Permafrost Hydrology*. Verlag Berlin Heidelberg: Springer.

Wright, J. F., Smith, M. W., & Taylor, A. E. (2001). Potential changes in permafrost distribution in the Fort Simpson and Norman Wells regions. *Bulletin of the Geological Survey of Canada*, (547), 197–207.

Yager, R. M., & Ratcliffe, N. M. (2010). *Hydrogeology and Simulation of Groundwater Flow in Fractured Rock in the Newark Basin , Rockland County , New York*. New York.

Yoshikawa, K., Hinzman, L. D., & Kane, D. L. (2007). Spring and aufeis (icing) hydrology in Brooks Range, Alaska. *Journal of Geophysical Research: Biogeosciences*, *112*(4), 1–14. https://doi.org/10.1029/2006JG000294

Zoltai, S. C., Tarnocai, C., Mills, G. F., & Veldhuis, H. (1988). Wetlands of Subarctic Canada. *Wetlands of Canada*, 57–96.

Appendices

Appendix A

Additional Charts and Figures

Table A-1: Descriptions and sources for all obtained data.

Data	Source	Reference	Resolution / Scale	Description
Satellite Photos	ESRI	N/A	30 cm	High-resolution satellite imagery provided as an ESRI basemap.
DEM	(GCODC)[1]	Government of Canada, 2018	20 m	Raster, Digital Elevation Model of NT
Surficial Geology-Central Mackenzie Valley, NT	(GCGS)[2]	Côté et al., 2013	1:125000	Shapefile, surficial geology of map area, includes bedrock outcrops.
Bedrock Geology-Carcajou Canyon (southeast), NT	GCGS[2]	Fallas & MacNaughton, 2014	1:100000	Shapefile, bedrock geology of map area, including major structural features, faults, contacts etc.
Hydrology of Central Mackenzie Valley	GCODC[1]	Government of Canada	1:40000	Shapefiles, Streams, rivers lakes and wetlands of the CMV.
S12X-006 Husky EL 463 Access/Points/Areas	(SLWB)[3]	N/A	N/A	Shapefiles, Husky Energy Inc. access roads, monitoring wells, water sources, drill pads and other point features.
Seismic Shothole Drillers Logs	GCGS[2]	I. R. Smith, 2010, 2015	N/A	Shapefile, points representing seismic driller logs that contain stratigraphic information.
S12X-006 Husky Thermistor, Monitoring well data	SLWB[3]	Waterline Resources Inc., 2013b, 2013c, 2013a	N/A	Shapefiles, Excel Database, created from reported data. Contains well dimensions, stratigraphy and ice presence.
S12X-006 Groundwater and Surface Water Chemistry	SLWB[3]	Hayes & Dunn, 2012; Husky Oil Operations Ltd., 2016; Rudolph, Lotimer, et al., 2016; Waterline Resources Inc., 2013a, 2013b, 2013c	N/A	Major and minor ions, trace hydrocarbon compounds and isotopes taken throughout EL490 and surrounding area.
Climate Data for Norman Wells (1944-2011)	Historical Climate Data[4]	Environment Canada	N/A	Temperature, precipitation and windspeed data from 1944 to 2011 Norman Wells, NT

Icing Shapefiles and Coordinates	B. Glass Thesis Work	Glass, 2018	N/A	Icing extent and center coordinates determined by remote sensing.
Gas Isotopes	OROGO	N/A	N/A	^{13}C Isotope values for methane and other gases from the Canol Formation

[1] Government of Canada Open Data Catalogue GEOGRATIS http://geogratis.cgdi.gc.ca/
[2] Government of Canada GEOSCAN https://geoscan.nrcan.gc.ca/starweb/geoscan/servlet.starweb?path=geoscan/geoscan_e.web
[3] Sahtu Land and Water Board https://slwb.com/registry/S12X-006
[4] http://climate.weather.gc.ca/
[5] Office of the Regulator of Oil and Gas Operations (OROGO)-personal communication

Table A-2: Each surface water and groundwater sampling point that was sampled by Waterloo or by Waterline Resources on behalf of Waterloo. Includes Easting and Northing coordinates. See legend at bottom for explanation. Coordinates are in NAD83 coordinate system, UTM Zone 9

Site	Easting	Northing	Date	Present	Major Ions	Organic Analytes	^{18}O & ^{2}H	^{3}H	^{87}Sr	^{13}C in CH_4
H003	645799	7193837	08-28-2018	H & W	**SW**	**SW**	**SW**			
H016	629154	7194810	08-28-2018	H & W	**SW**	**SW**	**S+G**			
H043	635452	7197627	08-28-2018	H & W	**SW**	**SW**				
H023	631388	7204193	08-28-2018	H & W	**SW**	**SW**	**SW**			
H002	630032	7205644	08-28-2018	H & W	**SW**	**SW**	**S+G**		**GW**	
H042	617688	7204388	08-29-2018	H & W	**SW**	**SW**	**SW**			
H041	615844	7206650	08-29-2018	H & W	**SW**	**SW**				
H031	617878	7211864	08-29-2018	H & W	**SW**	**SW**	**S+G**			
H006	611329	7222272	08-29-2018	H & W	**SW**	**SW**				
H026	621169	7224635	08-29-2018	H & W	**SW**	**SW**	**S+G**			
H045	629280	7220871	08-29-2018	H & W	**SW**	**SW**				
H046a	619298	7210973	08-29-2018	H & W	**S+G**				**SW**	
H046b	619334	7211007	08-29-2018	H & W	**SW**	**SW**			**SW**	
H027	622346	7221298	08-29-2018	H & W	**SW**	**SW**	**SW**			
H030	623147	7217943	08-29-2018	H & W	**SW**	**SW**	**SW**		**SW**	
H028	625969	7220048	08-29-2018	H & W	**SW**	**SW**				
H001	631241	7214872	08-29-2018	H & W	**S+G**	**SW**	**S+G**		**SW**	
H044a	620862	7212376	08-30-2018	H & W	**S+G**		**S+G**			
H044b	620882	7212394	08-30-2018	H & W	**SW**	**SW**	**SW**			

Site	Easting	Northing	Date	Present	Major Ions	Organic Analytes	^{18}O & ^{2}H	^{3}H	^{87}Sr	^{13}C in CH_4
H040	623338	7214538	08-30-2018	H & W	**SW**	**SW**	**S+G**			
AWR5	626208	7217095	08-30-2018	H & W	**SW**	**SW**				
AWR4	626976	7217650	08-30-2018	H & W	**SW**	**SW**				**GW**
AWR3	627936	7218741	08-30-2018	H & W	**SW**	**SW**				
AWR2	628973	7219685	08-30-2018	H & W	**SW**	**SW**				
H001B	625708	7216727	08-30-2018	H & W	**S+G**		**S+G**		**SW**	
GL1	619752	7220722	09-01-2018	Waterloo	**S+G**	**S+G**	**S+G**	**GW**	**S+G**	**GW**
GL2	619566	7220872	09-01-2018	Waterloo	**S+G**	**S+G**	**S+G**	**GW**	**GW**	**GW**
GPH1	622986	7214593	09-01-2018	Waterloo	**S+G**	**S+G**	**S+G**	**GW**	**GW**	**S+G**
SL Seep	616730	7207723	09-01-2018	Waterloo	**SW**	**SW**	**SW**		**SW**	**SW**
SL SW	616771	7207695	09-01-2018	Waterloo	**SW**	**SW**	**SW**		**SW**	**SW**
H001B	625708	7216727	09-01-2018	Waterloo			**GW**			
MW4	625505	7216597	09-02-2018	Waterloo	**GW**		**GW**	**GW**	**GW**	
MW4 Pad	625506	7216555	09-02-2018	Waterloo			**SW**			
MW4 Forest	625475	7216523	09-02-2018	Waterloo			**SW**			
MW4 Culvert	625513	7216529	09-02-2018	Waterloo			**SW**			
H001B	625708	7216727	02-10-2019	Husky/Waterline	**SW**	**SW**	**SW**	**SW**	**SW**	**SW**
H040	623338	7214538	02-10-2019	Husky/Waterline	**SW**	**SW**	**SW**	**SW**	**SW**	**SW**
H046	619334	7211007	02-10-2019	Husky/Waterline	**SW**	**SW**	**SW**	**SW**	**SW**	**SW**
MW09A	617224	7209124	02-08-2019	Husky/Waterline	**DGW**	**DGW**	**DGW**	**DGW**	**DGW**	**DGW**
MW09B	617206	7209104	02-08-2019	Husky/Waterline	**DGW**	**DGW**	**DGW**	**DGW**	**DGW**	**DGW**
H043	635452	7197627	08-20-2019	H & W	**SW**	**SW**	**SW**			
H016	629154	7194810	08-20-2019	H & W	**SW**	**SW**	**SW**			
H002	630032	7205644	08-20-2019	H & W	**SW**	**SW**	**SW**			
H023	631388	7204193	08-20-2019	H & W	**SW**	**SW**	**SW**			
H001	631241	7214872	08-20-2019	H & W	**SW**	**SW**	**SW**		**SW**	
H028	625969	7220048	08-20-2019	H & W	**SW**	**SW**	**SW**			
H030	623147	7217943	08-20-2019	H & W	**SW**	**SW**	**SW**			
H031	617878	7211864	08-20-2019	H & W	**SW**	**SW**	**SW**			
H042	617688	7204388	08-20-2019	H & W	**SW**	**SW**	**SW**			

Site	Easting	Northing	Date	Present	Major Ions	Organic Analytes	^{18}O & ^{2}H	^{3}H	^{87}Sr	^{13}C in CH_4
H040	623338	7214538	08-21-2019	H & W	**SW**	**SW**	**SW**		**SW**	
H044	620882	7212394	08-21-2019	H & W	**S+G**	**S+G**	**SW**	**GW**	**S+G**	
H046	619334	7211007	08-21-2019	H & W	**S+G**	**S+G**	**SW**		**S+G**	
W08	619730	7219592	08-22-2019	Waterloo	**S+G**	**S+G**	**S+G**		**SW**	
W06	618733	7216278	08-22-2019	Waterloo	**SW**	**SW**	**SW**		**SW**	
W05	620185	7213825	08-22-2019	Waterloo	**SW**	**SW**	**SW**		**SW**	
W04	620619	7212734	08-22-2019	Waterloo	**SW**	**SW**	**SW**		**SW**	
W02	622141	7210637	08-22-2019	Waterloo	**SW**	**SW**	**SW**		**SW**	
W02A	622141	7210637	08-22-2019	Waterloo	**SW**	**SW**	**SW**	**SW**	**SW**	
GL3GW	619707	7220754	08-23-2019	Waterloo	**GW**	**GW**	**GW**	**GW**	**SW**	**GW**
GPH2	622986	7214593	08-23-2019	Waterloo	**GW**	**GW**	**GW**	**GW**	**SW**	**GW**

H & W	**Both Husky and Waterloo present during sampling**
SW	**Samples obtained from Surface water only (by Husky or Waterloo)**
GW	**Samples obtained from shallow groundwater only (by Waterloo)**
DGW	**Samples taken from deep groundwater (by Husky/Waterline)**
SG	**Samples obtained from both SW and GW (by Husky or Waterloo)**
Blank	**Not obtained**

Table A- 3 Sampling protocol summary.* denotes bottle pre-preserved by laboratory, ** is preservative not necessary if holding time not exceeded.

	Sample	Bottle Size	Bottle Type	Holding Time (days)	Filtered?	Preservative?	Zero Headspace?
Concentrations	Metals	60mL	PE	180	Yes	1 mL 1:4 Nitric Acid	No
	Routine Water Quality (anions)	500mL	PE	3 (Variable)	No	None	No
	Phenol/DOC/NH4	100mL	Amber Glass	28	No	Sulphuric Acid*	No
	VOCS (BTEX, CH4)	2x40mL	Glass	14	No	Sodium Bisulfite*	Yes
	DIC	60mL	PE	3	Yes	None	Yes
Isotopes	D&O	30mL	PE	Indefinite	No	No	Yes
	3H	250mL	PE	Indefinite	No	No	Yes
	87Sr	125mL	PE	Indefinite	Yes	1 mL 1:4 Nitric Acid	No
	DIC	40mL	Amber Glass	3	No	None	Yes
	Methane	60mL	Glass	14	No	Sodium Bisulfite**	Yes

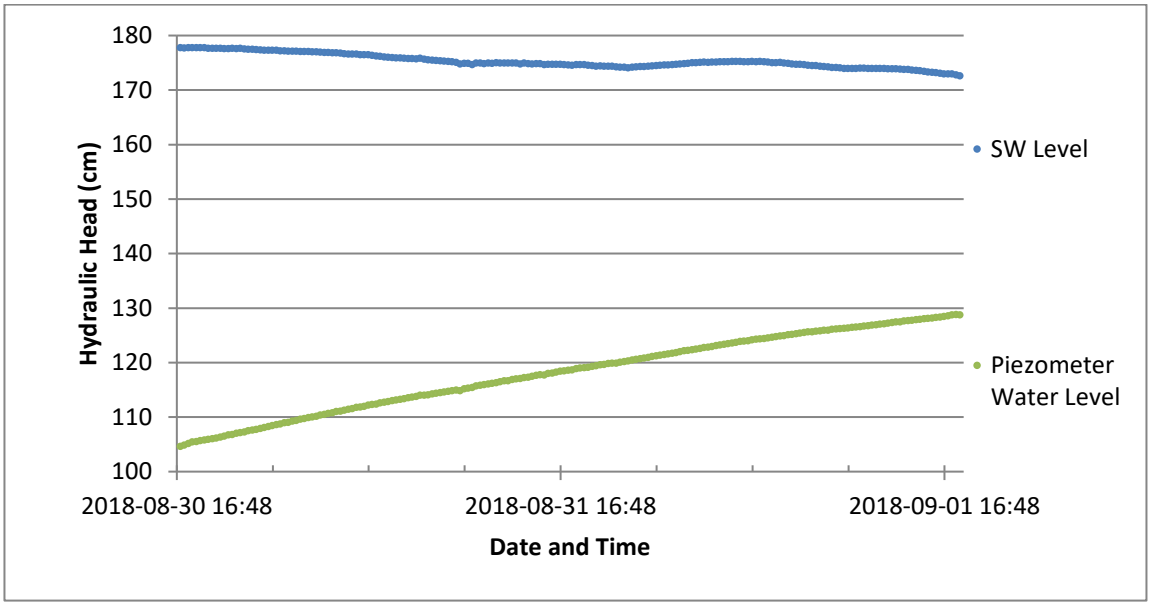

Figure A-1: Hydraulic head data for the piezometer and stilling well installed in H001B. WL in the piezometer did not reach static after 2 days. Head calculated in reference to bottom of piezometer.

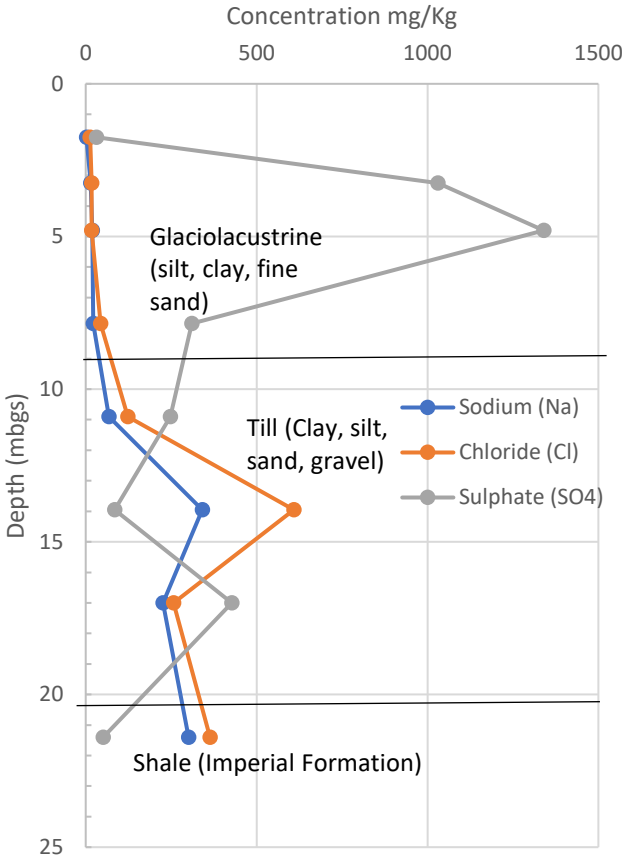

Figure A-2 Soil profile for MW04T showing sodium, chloride and sulphate concentrations with depth along with interpreted geology. Raw data obtained from Waterline Resources Inc., (2013a).

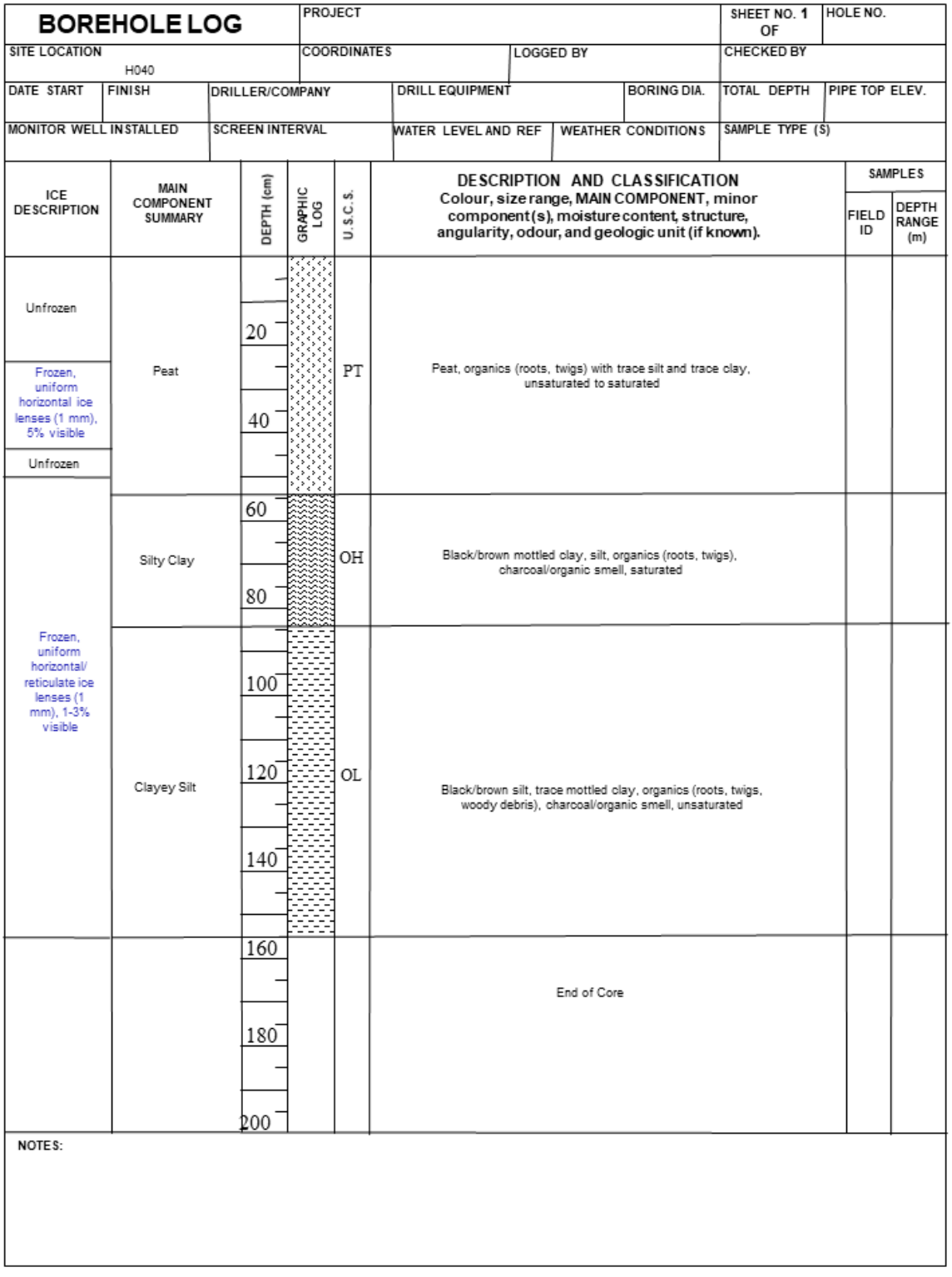

Figure A-3: Borehole and permafrost log for Core 1 at H040.

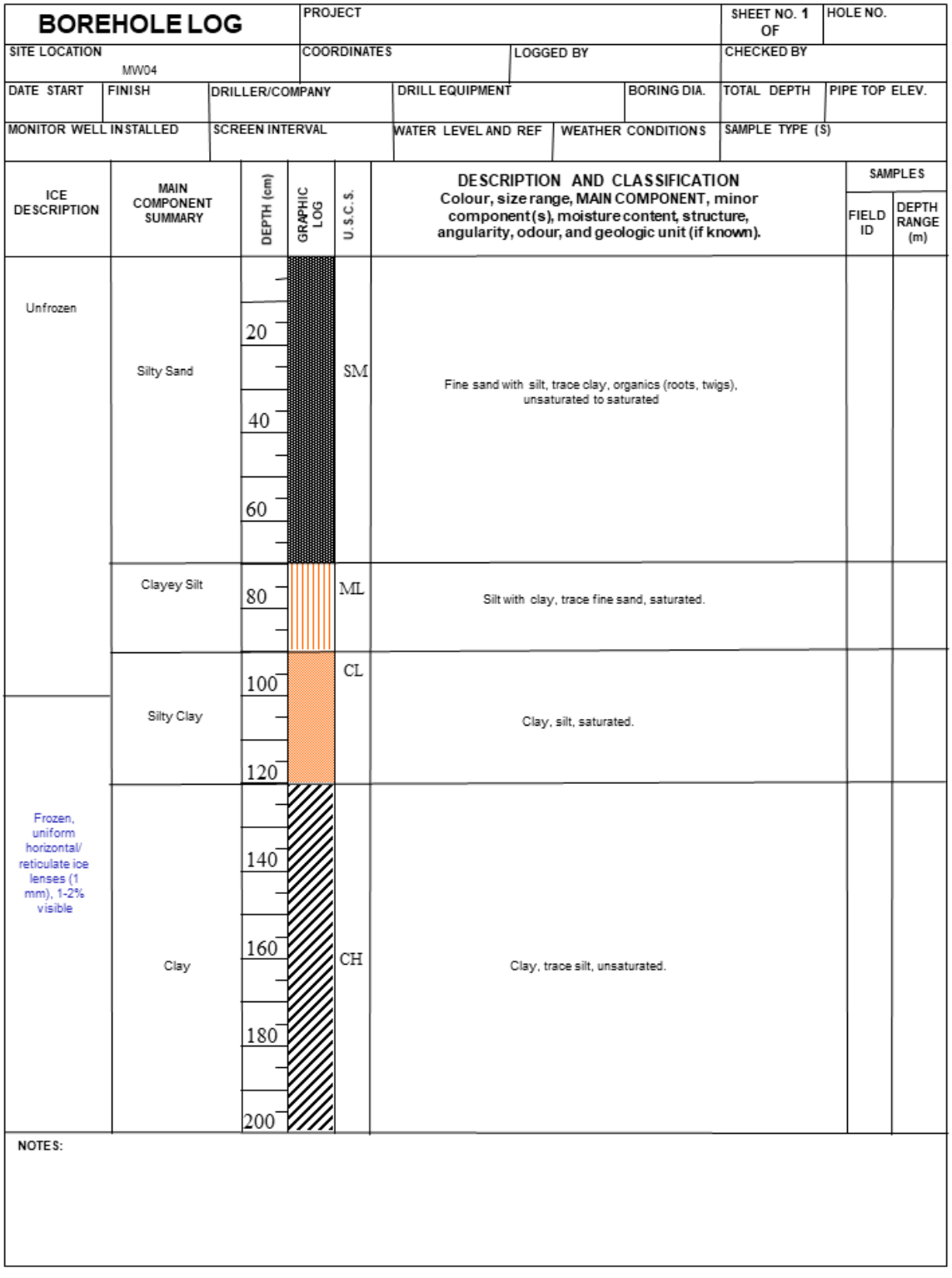

Figure A-4: Borehole and permafrost log for core taken from near MW04T.

Appendix B

Raw Data

Table B- 1: Raw temperature profile data for creek and spring sites.

Site	Temperature (°C)	Depth (mbgs)
H046	10.4	0.0
	7.8	0.2
	6.8	0.4
	5.4	0.6
	3.6	0.8
	1.4	1.0
H044	9.7	0.0
	8.6	0.1
	8.0	0.2
	7.6	0.3
	7.2	0.5
	6.9	0.6
	6.5	0.7
W05	9.6	0.0
	9.3	0.2
	9.4	0.3
	9.6	0.4
	9.8	0.5
	9.9	0.7
	9.6	0.9
W06	8.8	0.0
	8.9	0.1
	9.1	0.2
	9.5	0.4
	9.6	0.5
GL1	0.0	5.8
	6.1	0.3
	5.3	0.5
	3.9	0.7
	3.4	0.9
	2.8	1.4
GL3	7.6	0.0
	5.6	0.2
	3.6	0.4

Site	Temperature (°C)	Depth (mbgs)
	1.9	0.6
	1.3	0.8
	1.0	1.0

Table B-2: Historical groundwater geochemistry, with major ions taken from various wells both inside and outside the Bogg Creek Watershed. Data obtained from Husky, AMEC, (2014), Waterline Resources Inc., (2013a, 2013b) and Hayes & Dunn, (2012).

Site ID	Sample Date	Ca (mg/L)	Mg (mg/L)	Na (mg/L)	K (mg/L)	HCO_3 (mg/L)	CO_3 (mg/L)	Cl (mg/L)	SO_4 (mg/L)	F (mg/L)
WW04A	02-08-2013	5.1	3.0	1140.0	26.7	1530.0	<DL	1230.0	6.0	<DL
MW19B	02-10-2013	159.0	57.7	29.6	10.0	753.0	<DL	2.5	125.0	0.089
MW09A	02-03-2013	23.0	8.6	184.0	5.3	295.0	<DL	43.0	196.0	0.470
MW09B	02-21-2013	28.0	10.4	188.0	7.3	285.0	<DL	39.0	198.0	0.049
MW09A	02-06-2019	23.0	8.7	190.0	4.6	290.0	<DL	44.0	180.0	N/A
MW09B	02-08-2019	26.0	9.1	170.0	6.3	290.0	<DL	38.0	170.0	N/A
MW09B D	02-08-2019	26.0	9.2	170.0	6.4	290.0	<DL	40.0	170.0	N/A
I-78	N/A	14.0	8.0	1824.0	<DL	1176.0	<DL	2175.0	6.0	N/A

Table B-3: Historical major ion chemistry for creek and lake waters within Bogg Creek Watershed dating back to 2012, data provided by Husky.

Site ID	Sample Date	Ca (mg/L)	Mg (mg/L)	Na (mg/L)	K (mg/L)	HCO_3 (mg/L)	CO_3 (mg/L)	Cl (mg/L)	SO_4 (mg/L)	F (mg/L)
H001	07-27-2012	46.5	15.6	73.3	1.2	206.0	<DL	93.0	28.7	0.072
H001	06-18-2013	29.3	9.1	26.5	0.6	99.7	<DL	31.3	35.5	0.071
H001	09-14-2013	38.5	13.6	50.1	0.7	133.0	<DL	54.0	66.8	0.059
H001	08-29-2015	35.9	12.2	51.8	0.8	135.0	<DL	59.0	58.0	<DL
H001	08-20-2016	53.8	17.5	74.3	0.9	188.0	<DL	104.0	50.0	0.060
H001	08-29-2017	37.3	13.0	45.2	0.8	132.0	<DL	44.8	67.4	0.055
H001	08-29-2018	31.4	11.4	35.9	<DL	110.0	<DL	29.0	71.1	0.058
H001	08-20-2019	42.8	16.3	81.7	0.7	196.0	<DL	90.0	65.9	0.073
H001B	06-15-2014	25.6	8.7	30.3	0.7	90.0	<DL	28.0	27.0	<DL
H001B	09-20-2014	42.5	15.8	110.0	0.9	193.0	<DL	76.0	103.0	0.080
H001B	08-30-2015	32.6	11.4	52.5	<DL	133.0	<DL	52.0	41.4	<DL
H001B	08-21-2016	47.7	15.8	85.4	0.7	182.0	<DL	115.0	54.0	0.073
H001B	08-29-2017	32.5	11.7	48.7	0.8	131.0	<DL	44.3	74.2	0.075
H001B	08-30-2018	29.3	9.9	29.2	<DL	95.9	<DL	21.2	63.6	0.067
H001B	08-20-2019	40.0	15.7	108.0	0.7	211.0	<DL	91.5	74.8	0.086
H001B	06-15-2014	25.6	8.8	28.0	0.7	90.0	<DL	28.0	27.0	<DL
H001B	09-20-2014	49.3	18.3	115.0	0.9	191.0	<DL	86.0	117.0	0.140
H001B	08-30-2015	33.0	11.4	51.4	<DL	134.0	<DL	51.0	55.0	<DL

Site ID	Sample Date	Ca (mg/L)	Mg (mg/L)	Na (mg/L)	K (mg/L)	HCO_3 (mg/L)	CO_3 (mg/L)	Cl (mg/L)	SO_4 (mg/L)	F (mg/L)
H001B	08-21-2016	47.2	16.1	86.7	0.7	196.0	<DL	115.0	41.1	0.069
H001B	08-29-2017	33.7	12.3	51.8	0.8	131.0	<DL	44.3	75.0	0.069
H001B	08-30-2018	22.8	10.3	30.3	<DL	96.7	<DL	21.3	63.9	0.062
H001B	08-21-2019	35.2	15.0	91.7	0.7	205.0	<DL	84.9	72.0	0.085
H030	07-29-2012	43.4	14.8	78.7	1.4	196.0	<DL	91.6	35.8	0.100
H030	06-19-2013	25.4	7.4	23.7	<DL	83.1	<DL	20.2	32.7	0.053
H030	09-14-2013	34.8	13.0	51.1	0.6	120.0	<DL	42.5	86.3	0.069
H030	06-14-2014	27.3	9.2	30.0	0.9	86.0	<DL	24.0	27.0	0.050
H030	09-20-2014	46.1	16.9	91.0	0.8	170.0	<DL	65.0	90.0	0.110
H030	08-29-2015	33.4	11.7	68.0	1.3	133.0	<DL	89.0	78.0	0.050
H030	08-20-2016	49.6	17.7	105.0	1.0	214.0	<DL	112.0	78.5	0.083
H030	08-29-2017	35.2	12.6	58.7	0.9	122.0	<DL	43.1	103.0	0.062
H030	08-29-2018	27.1	10.0	30.9	<DL	93.6	<DL	20.8	67.0	0.056
H030	08-20-2019	34.4	14.4	92.8	0.6	199.0	<DL	73.0	81.2	0.083
H031	08-21-2016	15.8	6.4	4.0	<DL	65.2	<DL	0.3	11.7	0.043
H031	08-29-2017	16.5	6.3	5.7	<DL	67.3	<DL	0.3	13.7	0.048
H031	08-29-2018	14.3	6.1	4.4	<DL	65.8	<DL	0.3	11.7	0.055
H031	08-20-2019	14.5	6.4	5.2	0.7	66.2	<DL	0.5	13.3	0.035
H044	08-21-2016	53.7	17.4	43.7	0.8	118.0	<DL	38.2	134.0	0.061
H044	08-29-2017	55.5	17.6	43.4	0.9	108.0	<DL	39.8	157.0	0.081
H044	08-30-2018	47.1	15.2	39.6	0.7	104.0	<DL	36.4	125.0	0.060
H044	08-21-2019	45.4	17.0	41.7	0.9	122.0	<DL	37.1	124.0	0.064
H044	06-15-2014	38.6	15.4	140.0	0.8	257.0	<DL	57.0	99.0	<DL
H044	08-30-2015	42.9	19.2	190.0	0.8	367.0	<DL	92.0	177.0	<DL
H044	08-21-2016	65.1	31.6	442.0	1.5	709.0	<DL	168.0	366.0	0.263
H044	08-29-2017	52.4	19.4	72.4	0.8	114.0	<DL	28.2	225.0	0.093
H044	08-30-2019	35.1	13.9	59.5	<DL	160.0	<DL	19.4	113.0	0.096
H044	08-20-2019	43.7	25.8	370.0	1.1	604.0	12.1	129.0	417.0	0.291
H044	08-30-2015	45.6	20.2	180.0	0.9	342.0	<DL	53.0	200.0	<DL
H044	08-21-2016	62.7	30.9	452.0	1.5	734.0	<DL	168.0	370.0	0.250
H044	08-29-2017	41.5	16.7	104.0	0.9	183.0	<DL	44.0	186.0	0.115
H044	08-30-2019	34.6	13.2	64.2	<DL	175.0	<DL	21.8	100.0	0.101
H044	08-20-2019	52.7	25.8	425.0	1.1	637.0	19.3	135.0	335.0	0.306
H046	09-20-2014	24.7	11.2	5.4	0.8	64.0	<DL	0.5	56.0	<DL
H046	08-30-2015	24.0	7.2	4.3	0.7	86.0	<DL	0.5	26.0	<DL
H046	08-21-2016	16.9	7.4	3.4	<DL	61.2	<DL	0.3	13.6	0.049
H046	08-29-2017	16.3	7.3	3.5	<DL	54.2	<DL	0.3	16.7	0.034
H046	08-29-2018	15.0	6.4	3.1	<DL	57.6	<DL	0.3	10.2	0.030
H046	08-21-2019	17.2	7.0	3.7	<DL	70.6	<DL	0.3	7.9	0.049
H046	08-30-2015	14.1	5.9	3.5	0.7	51.0	<DL	2.0	12.0	<DL
H046	08-21-2016	14.4	6.7	3.4	<DL	62.2	<DL	0.3	7.8	0.050
H046	08-29-2017	17.0	7.6	3.6	<DL	58.9	<DL	0.3	18.2	0.033

Site ID	Sample Date	Ca (mg/L)	Mg (mg/L)	Na (mg/L)	K (mg/L)	HCO_3 (mg/L)	CO_3 (mg/L)	Cl (mg/L)	SO_4 (mg/L)	F (mg/L)
H046	08-30-2018	13.7	6.2	3.1	<DL	55.4	<DL	0.3	8.9	0.037
H046	08-21-2019	15.4	6.6	3.3	<DL	72.6	<DL	0.3	3.6	0.044

Table B-4: Major ion chemistry in lake waters outside of Bogg Creek watershed, dating back to 2016, data provided by Husky.

Site ID	Sample Date	Ca (mg/L)	Mg (mg/L)	Na (mg/L)	K (mg/L)	HCO_3 (mg/L)	CO_3 (mg/L)	Cl (mg/L)	SO_4 (mg/L)	F (mg/L)
H006	08-20-2016	37.8	10.8	13.0	1.8	155.0	<DL	10.0	15.1	N/A
H006	08-29-2017	20.8	6.7	5.6	0.6	72.3	<DL	3.8	13.3	N/A
H006	08-29-2018	21.7	8.5	10.9	1.1	116.0	<DL	9.3	14.0	N/A
H006	08-21-2019	17.3	9.0	11.3	0.3	92.1	<DL	8.6	12.6	N/A
H016	08-19-2016	6.7	2.5	0.5	0.3	27.8	<DL	<DL	1.5	N/A
H016	08-29-2017	6.5	2.5	0.5	0.5	23.9	<DL	<DL	1.5	N/A
H016	08-28-2018	6.0	2.6	0.5	0.3	24.4	<DL	<DL	1.2	N/A
H016	08-20-2019	6.6	2.8	0.5	0.3	27.6	<DL	<DL	2.1	N/A
H023	08-19-2016	22.5	7.7	6.8	0.8	82.5	<DL	2.7	23.5	N/A
H023	08-29-2017	25.6	8.3	7.8	1.0	90.5	<DL	3.3	31.5	N/A
H023	08-28-2018	26.1	9.3	7.5	0.6	89.3	<DL	3.1	33.4	N/A
H023	08-20-2019	23.0	9.1	8.1	0.6	97.7	<DL	3.0	28.7	N/A
H026	08-20-2016	42.4	13.8	52.7	<DL	132.0	6.3	103.0	0.7	N/A
H026	08-29-2017	41.2	14.0	73.9	<DL	131.0	<DL	146.0	0.7	N/A
H026	08-29-2018	43.7	13.9	83.3	0.7	162.0	<DL	163.0	0.5	N/A
H026	08-21-2019	42.7	14.7	73.4	0.7	164.0	<DL	142.0	1.3	N/A
H027	08-20-2016	32.7	11.0	21.2	0.9	139.0	<DL	27.8	0.7	N/A
H027	08-29-2017	33.0	9.8	21.1	1.1	148.0	<DL	28.4	0.9	N/A
H027	08-29-2018	26.8	9.3	20.2	0.6	128.0	<DL	29.1	0.6	N/A
H027	08-20-2019	27.5	10.9	22.2	1.0	149.0	<DL	31.6	1.7	N/A
H028	08-20-2016	39.9	12.7	50.7	1.4	157.0	<DL	84.2	1.7	N/A
H028	08-29-2017	39.7	13.4	60.3	1.3	161.0	<DL	99.1	1.2	N/A
H028	08-29-2018	31.9	11.0	50.8	0.8	143.0	<DL	88.5	1.0	N/A
H028	08-20-2019	33.6	13.2	52.8	0.3	159.0	<DL	82.6	1.0	N/A
H041	08-20-2016	6.5	2.9	<DL	<DL	26.5	<DL	<DL	2.4	N/A
H041	08-29-2017	7.1	3.2	<DL	<DL	29.6	<DL	<DL	3.0	N/A
H041	08-29-2018	6.1	2.8	<DL	<DL	27.8	<DL	<DL	2.1	N/A
H041	08-20-2019	6.7	3.2	<DL	<DL	30.4	<DL	<DL	2.9	N/A
H042	08-20-2016	7.7	3.1	<DL	0.6	32.2	<DL	<DL	2.1	N/A
H042	08-29-2017	7.5	2.9	<DL	0.6	29.6	<DL	<DL	2.3	N/A
H042	08-29-2018	6.4	2.6	<DL	0.3	28.7	<DL	7.9	1.8	N/A
H042	08-20-2019	6.3	3.2	1.6	0.5	35.5	<DL	<DL	2.7	N/A
H043	08-19-2016	11.0	4.6	3.0	0.7	50.3	<DL	<DL	2.7	N/A

Site ID	Sample Date	Ca (mg/L)	Mg (mg/L)	Na (mg/L)	K (mg/L)	HCO_3 (mg/L)	CO_3 (mg/L)	Cl (mg/L)	SO_4 (mg/L)	F (mg/L)
H043	08-29-2017	11.2	4.4	3.2	0.7	54.4	<DL	<DL	3.1	N/A
H043	08-28-2018	12.4	5.3	3.1	0.6	56.7	<DL	<DL	2.9	N/A
H043	08-20-2019	12.0	5.7	3.7	0.65	63.2	<DL	<DL	4.2	N/A

Table B-5: Major ion chemistry for water samples taken in the Bogg Creek watershed during the 2018 (summer) and 2019 (winter and summer) sampling campaigns. Note that sites sampled by Husky (ex. H044) are not shown here, with the exception of the winter samples.

Site ID	Sample Date	Ca (mg/L)	Mg (mg/L)	Na (mg/L)	K (mg/L)	HCO_3 (mg/L)	CO_3 (mg/L)	Cl (mg/L)	SO_4 (mg/L)	F (mg/L)
H002 GW	08-28-2018	41.5	8.7	11.6	1.8	57.1	<DL	3.0	64.2	0.123
H046	08-29-2018	14.5	5.9	2.5	<DL	30.5	<DL	0.3	22.6	0.035
MW04	09-01-2018	102.0	25.4	3.7	2.0	414.0	<DL	0.6	31.8	0.159
GL1 SW	09-01-2018	17.8	6.0	7.9	<DL	44.8	<DL	3.5	0.8	<DL
GL1 GW	09-01-2018	193.0	58.3	220.0	0.7	792.0	<DL	415.0	0.3	<DL
GL2 SW	09-01-2018	20.9	7.5	16.7	1.2	45.6	<DL	36.1	2.8	0.027
GL2 GW	09-01-2018	178.0	57.5	187.0	<DL	839.0	<DL	267.0	0.2	<DL
GPH SW	09-01-2018	27.1	8.2	13.8	<DL	37.0	<DL	18.3	99.5	<DL
SL Seep	09-01-2018	6.9	2.3	0.5	<DL	2.5	<DL	0.3	5.4	<DL
SL SW	09-01-2018	12.5	4.3	0.5	<DL	49.3	<DL	0.3	0.5	<DL
H001B	02-10-2019	84.0	30.0	130.0	1.7	360.0	<DL	150.0	58.0	N/A
H040	02-10-2019	160.0	49.0	120.0	2.3	410.0	<DL	110.0	320.0	N/A
H046	02-10-2019	56.0	23.0	11.0	0.9	220.0	<DL	3.7	36.0	N/A
H046D	02-10-2019	57.0	23.0	11.0	0.9	220.0	<DL	3.6	35.0	N/A
W08-SW	08-22-2019	30.6	11.4	20.8	0.3	80.2	<DL	66.2	1.1	<DL
W08-GW	08-22-2019	39.0	16.2	32.9	0.7	216.0	<DL	72.8	0.2	<DL
W06-SW	08-22-2019	42.9	19.6	212.0	0.9	403.0	<DL	91.8	204.0	0.175
W05-SW	08-22-2019	39.2	19.2	227.0	0.7	416.0	17.5	94.2	217.0	0.183
W04-SW	08-22-2019	41.3	18.8	207.0	0.8	384.0	9.7	85.6	198.0	0.172
W02-SW	08-22-2019	26.6	11.8	51.4	0.3	236.0	<DL	3.3	20.6	0.087
W02A-SW	08-22-2019	133.0	33.5	105.0	1.0	<DL	<DL	20.5	755.0	0.171
H046-GW	08-22-2019	156.0	22.8	3.9	0.3	64.8	<DL	0.3	400.0	0.023
H044-GW	08-22-2019	652.0	302.0	681.0	1.6	935.0	<DL	1010.0	2280.0	<DL
GL3GW	08-23-2019	229.0	74.2	137.0	0.6	1050.0	<DL	207.0	0.2	<DL
GPH2-GW	08-23-2019	50.1	12.2	14.2	0.3	200.0	<DL	8.2	2.8	<DL

Table B-6: Stable water isotope data for groundwater samples taken by Husky and Waterline Resources.

Sample	Date	$\delta^{18}O$ (VSMOW ‰)	$\delta^{2}H$ (VSMOW ‰)
MW19B	02-10-2013	-20.8	-161.6
MW09A	02-03-2013	-25.2	-193.7
MW09B	02-21-2013	-25.2	-195.1
MW09A	02-06-2019	-22.8	-191.0
MW09B	02-08-2019	-17.8	-184.5
MW09BD	02-08-2019	-17.7	-183.8

Table B-7: Stable water isotope data taken during the 2018 summer field campaign, within and around the Bogg Creek Watershed.

Sample	Date	$\delta^{18}O$ (VSMOW ‰)	$\delta^{2}H$ (VSMOW ‰)
H016 SW	08-28-2018	-18.7	-152.5
H016 GW	08-28-2018	-20.3	-161.2
H023	08-28-2018	-16.1	-138.2
H002 SW	08-28-2018	-18.8	-150.6
H002 GW	08-28-2018	-19.2	-151.9
H042	08-29-2018	-20.7	-159.1
H031 SW	08-29-2018	-19.1	-154.1
H031 GW	08-29-2018	-22.5	-171.3
H026 SW	08-29-2018	-16.7	-143.1
H026 GW	08-29-2018	-20.7	-161.0
H027	08-29-2018	-14.4	-134.3
H030	08-29-2018	-19.1	-153.3
H001 SW	08-30-2018	-19.4	-153.9
H001 GW	08-30-2018	-19.3	-153.7
H044 US SW	08-30-2018	-21.1	-161.1
H044 US GW	08-30-2018	-21.7	-168.1
H044 DS SW	08-30-2018	-21.1	-160.6
H040 SW	08-30-2018	-16.2	-140.1
H040 GW	08-30-2018	-21.7	-167.9
H001B SW	08-30-2018	-19.5	-153.3
H001B GW	08-30-2018	-21.8	-171.8
GL1 SW	09-01-2018	-21.5	-161.6
GL1 GW	09-01-2018	-22.8	-179.5
GL2 SW	09-01-2018	-21.1	-161.5

Sample	Date	$\delta^{18}O$ (VSMOW ‰)	$\delta^{2}H$ (VSMOW ‰)
GL2 GW	09-01-2018	-22.6	-176.2
GPH SW	09-01-2018	-20.9	-161.2
GPH GW#1	09-01-2018	-23.3	-180.0
GPH GW#2	09-01-2018	-23.9	-184.4
SL Seep	09-01-2018	-20.8	-159.4
SL SW	09-01-2018	-15.4	-138.6

Table B-8: Stable water isotope data taken during the 2019 winter field campaign by Waterline Resources and Husky, within the Bogg Creek Watershed.

Sample	Date	$\delta^{18}O$ (VSMOW ‰)	$\delta^{2}H$ (VSMOW ‰)
H001B	02-10-2019	-19.6	-158.5
H040	02-10-2019	-19.2	-158.4
H046	02-10-2019	-22.0	-169.8
H046	02-10-2019	-22.0	-169.9

Table B-9: Stable water isotope data taken during the 2019 summer field campaign, within and around the Bogg Creek Watershed.

Sample	Date	$\delta^{18}O$ (VSMOW ‰)	$\delta^{2}H$ (VSMOW ‰)
H043	08-20-2019	-16.2	-142.0
H016	08-20-2019	-20.5	-161.8
H002	08-20-2019	-18.5	-151.7
H023	08-20-2019	-14.7	-133.0
H001	08-20-2019	-17.8	-148.1
H028	08-20-2019	-18.1	-146.9
H030	08-20-2019	-17.5	-146.3
H031	08-20-2019	-17.4	-145.5
H042	08-20-2019	-15.9	-138.2
H040	08-21-2019	-14.5	-131.7
H044GW1	08-21-2019	-21.1	-169.3
H046GW2	08-21-2019	-20.5	-162.5
H046	08-21-2019	-17.8	-148.2
W08	08-22-2019	-18.5	-146.1
W08GW	08-22-2019	-20.2	-160.7
W06	08-22-2019	-18.2	-150.8
W05	08-22-2019	-18.8	-153.1
W04	08-22-2019	-18.7	-153.2
W02	08-22-2019	-20.6	-162.0
W02A	08-22-2019	-18.0	-149.4

Sample	Date	$\delta^{18}O$ (VSMOW ‰)	$\delta^{2}H$ (VSMOW ‰)
H046GW2	08-22-2019	-20.5	-163.4
GL3GW	08-23-2019	-21.9	-174.5
GPH2	08-23-2019	-22.2	-172.6

Table B-10: Tritium values for samples taken within the Bogg Creek Watershed during the 2018 and 2019 field campaigns. Some data provided by Husky and Waterline Resources.

Sample	Date	^{3}H (TU)
MW09A	02-03-2013	<0.8
MW19B	02-10-2013	5.2
MW09B	02-21-2013	<0.8
GL1 GW	09-01-2018	7.86
GL2 GW	09-01-2018	5.32
GPH GW	09-01-2018	8.08
MW4 GW	09-02-2018	10.13
MW09A	02-06-2019	<0.8
MW09B	02-08-2019	<0.8
MW09BD	02-08-2019	<0.8
H001B	02-10-2019	9.3
H040	02-10-2019	10.3
H046	02-10-2019	9.4
H046	02-10-2019	9.3
H044GW	08-22-2019	3.9
W02A	08-22-2019	10.6
GL3	08-23-2019	4.9

Table B-11: Strontium concentrations and $^{87}Sr/^{86}Sr$ for surface water and groundwater samples taken during the 2018 and 2019 field campaigns, some data provided by Waterline Resources.

Sample	Date	Sr (mg/L)	$^{87}Sr/^{86}Sr$
H002 GW	08-28-2018	0.099	0.710918
H001	08-29-2018	0.068	0.712383
H030	08-29-2018	0.061	0.712396
H046 LB	08-29-2018	0.036	0.713275
H046 RB	08-29-2018	0.037	0.713508
H001B	08-30-2018	0.064	0.712413
GL 1 GW	08-30-2018	0.773	0.712012
GL 1 SW	08-31-2018	0.044	0.713033
GPH1	09-01-2018	0.455	0.712407
GL 2 GW	09-01-2018	0.633	0.712100

Sample	Date	Sr (mg/L)	$^{87}Sr/^{86}Sr$
SL LAKE	09-01-2018	0.020	0.714462
SL SEEP	09-01-2018	0.011	0.714056
MW4	09-01-2018	0.329	0.712535
MW-09A	02-06-2019	0.460	0.710840
MW09B	02-06-2019	0.470	0.710926
MW-09BD	02-08-2019	0.470	0.710930
MW09A	02-08-2019	0.460	0.710881
MW09BD	02-08-2019	0.470	0.710946
H001B	02-10-2019	0.240	0.711893
H046	02-10-2019	0.130	0.713218
H046D	02-10-2019	0.130	0.713212
H040	02-10-2019	0.300	0.711869
H001	08-20-2019	0.121	0.712042
H030	08-20-2019	0.099	0.711804
H044	08-20-2019	0.146	0.711381
H040-1 (Core)	08-20-2019	0.070	0.713131
H001B	08-21-2019	0.117	0.711778
H046	08-21-2019	0.046	0.712955
W02	08-22-2019	0.074	0.712634
W04	08-22-2019	0.113	0.711665
W05	08-22-2019	0.102	0.711693
W06	08-22-2019	0.119	0.711727
W08	08-22-2019	0.071	0.712671
W02A	08-22-2019	0.294	0.712095
H044GW	08-22-2019	1.340	0.712265
H046GW	08-22-2019	0.326	0.711664
W08GW	08-22-2019	0.093	0.712425
GPH2	08-23-2019	0.112	0.712273
GL3GW	08-23-2019	0.768	0.712117

Table B-12: August 23, 2019 EM38 survey results, from GL3-A to A'.

Position (x) [m]	Conductivity Vertical Dipole [mS]	Conductivity Horizontal Dipole [mS]
0	7.6	5.4
1	7.3	4.9
2	7.3	4.6
3	7.4	4.7
4	7.3	4.4

Position (x) [m]	Conductivity Vertical Dipole [mS]	Conductivity Horizontal Dipole [mS]
5	7.1	4.5
6	7.5	4.4
7	7.6	4.6
8	7.7	4.5
9	7.7	4.7
10	8.7	5.3
11	9.8	5.9
12	10.7	6.2
13	14.1	8.4
14	15.5	10.4
15	23.0	16.1
16	26.5	17.2
17	28.5	17.3
18	28.6	16.5
19	30.5	18.5
20	29.7	17.7
21	29.8	17.2
22	29.2	16.9
23	30.6	17.7
24	30.5	17.3
25	29.7	16.3
26	31.9	17.8
27	33.0	19.3
28	34.4	19.4
29	35.0	20.6
30	35.7	21.2
31	36.0	22.0
32	34.6	20.4
33	34.1	20.5
34	32.6	19.6
35	34.4	20.2
36	34.4	20.6
37	34.1	19.6
38	33.7	20.5
39	34.2	20.6
40	33.2	19.4
41	33.0	19.1
42	32.9	19.3
43	31.7	18.5

Position (x) [m]	Conductivity Vertical Dipole [mS]	Conductivity Horizontal Dipole [mS]
44	31.5	18.1
45	31.5	18.1
46	30.4	18.0
47	30.5	17.6
48	29.4	17.1
49	29.4	17.4
50	29.6	17.3
51	28.9	16.8
52	29.6	16.6
53	32.1	18.4
54	32.6	19.3
55	32.8	19.4
56	32.6	19.1
57	32.0	17.9
58	32.0	18.2
59	34.8	19.8
60	34.2	19.8
61	37.0	22.4
62	35.9	21.7
63	36.0	22.2
64	36.8	22.8
65	34.1	20.8
66	34.9	21.2
67	35.8	21.2
68	35.3	21.6
69	36.0	21.8
70	33.7	19.6
71	34.6	20.0
72	36.7	22.4
73	36.4	22.3
74	37.1	23.4
75	36.1	21.4
76	37.3	21.8
77	37.3	22.4
78	37.6	22.4
79	38.8	23.9
80	37.1	22.1
81	37.3	22.4
82	39.9	24.3

Position (x) [m]	Conductivity Vertical Dipole [mS]	Conductivity Horizontal Dipole [mS]
83	41.3	26.0
84	44.6	28.2
85	44.9	28.1
86	45.6	28.3
87	47.2	29.1
88	47.5	28.0
89	47.8	28.5
90	48.3	28.9
91	49.1	29.2
92	51.5	30.2
93	50.1	30.4
94	52.6	31.7
95	53.1	31.5
96	51.4	30.5
97	52.9	31.8
98	53.8	32.2
99	55.5	32.9
100	54.4	34.0
101	56.3	33.8
102	57.1	34.7
103	57.1	34.6
104	59.3	36.5
105	63.3	42.6
106	63.8	42.7
107	63.4	41.9
108	64.6	42.9
109	63.3	41.9
110	62.5	42.7
111	61.4	40.7
112	58.9	40.6
113	52.0	33.3
114	51.1	31.7
115	49.1	31.0
116	41.7	25.9
117	38.7	25.0
118	34.0	21.1
119	28.4	17.0
120	24.0	13.4
121	21.8	12.6

Position (x) [m]	Conductivity Vertical Dipole [mS]	Conductivity Horizontal Dipole [mS]
122	20.7	11.7
123	20.7	11.8
124	21.5	12.2
125	21.4	12.3
126	22.9	13.1
127	23.5	13.8
128	25.9	15.5
129	28.7	18.1
130	27.8	17.2
131	26.2	16.2
132	22.7	13.4
133	19.3	11.2
134	17.8	10.4
135	16.1	10.2

Appendix C
Groundwater Methods Report

The following report, titled **Hydrogeological Site Characterization Methods for Discontinuous Permafrost Terrain,** was drafted in April, 2020 as a culmination of the field and lab work outlined in this thesis. It was drafted for the Canadian Department of Environment and Natural Resources and for the Government of Northwest Territories. It is included here as an additional appendix with permission, in its entirety, with original formatting and page numbers.

Hydrogeological Site Characterization Methods for Discontinuous Permafrost Terrain

Prepared for:

Environment and Natural Resources

Government of the Northwest Territories

By:

Andrew Wicke and David Rudolph

Department of Earth and Environmental Sciences

University of Waterloo

April, 2020

Executive Summary

A compilation of various hydrogeologic site characterization techniques for application in remote, discontinuous permafrost regions is presented. Methods prioritize a strategic approach to selecting field monitoring targets, primarily at areas of active groundwater flow such as springs or groundwater fed water bodies. It is understood that springs and surface water may represent areas of interaction between the suprapermafrost and subpermafrost groundwaters, potentially making these features of interest for detailed terrestrial monitoring. Initial identification of these priority monitoring sites can be aided through the use of Geographic Information Systems (GIS). The GIS tools can be applied to the mapping areas of potential groundwater discharge features identified through remote sensing methods and through analysis of regional geologic and hydrologic patterns based on available information from a specific site of interest. Airborne thermal infrared imagery surveys complement these methods by the determination of precise locations of potential groundwater discharge, guided by previous desktop site assessment. This is achieved by the combined usage of thermal infrared and visible light cameras to capture imagery of cold thermal anomalies, which in summertime indicate potential groundwater fed springs and other discharge features. After selection of priority monitoring sites, a number of terrestrial geophysical instruments can be utilized to map the permafrost table and active layer thickness in locations of interest, which can be complemented by physical depth sounding of permafrost using probes. Groundwater sampling and hydraulic parameter estimates at priority monitoring sites can be conducted using lightweight, inexpensive and portable instruments. Vertical gradients can be determined by hydraulic head and temperature measurements, while sampling for particular geochemical and isotopic species provides insight into groundwater sources, contributions, flowpaths, and residence times. These tracer methods are limited in that different conclusions can be drawn from the same lines of evidence, but they provide a first step in understanding behavior of both the shallow and deep groundwater flow systems. Future monitoring decisions can be guided by these approaches, which may evolve moving forward.

Table of Contents

List of Figures and Tables

1.0 Introduction

The principle objective of this methods review document is to present and briefly discuss a suite of hydrogeologic field tools and strategies that can be used within remote terrain characterized by discontinuous permafrost to document groundwater flow phenomena. Permafrost development and maintenance requires an energy balance where more heat energy is lost in the winter than is gained in the summer (Woo, 2012). With climate warming trends, this balance may reverse and result in the degradation of the permafrost. Due to the heat capacity of water, this energy balance may be significantly disrupted below surface water bodies such that there could be an exaggerated influence on permafrost occurrence and continuity. Permafrost may therefore be thinner or absent entirely below a surface water body such as a river or lake, which may become exacerbated from climate warming (Woo, 2012). As such, the investigation of groundwater flow in the vicinity of surface water bodies may be of significant importance in these types of environments, which will influence the type of monitoring approach employed in these areas.

Upon freezing, unconsolidated sediment with high soil water content may lose much of its ability to transmit water. Hydraulic conductivity may decrease by 4-5 orders of magnitude as temperature decreases from 0°C to -0.5°C (Burt & Williams, 1976). If pores or fractures in rock and soil are saturated upon freezing, the ability to conduct water may cease, effectively causing the aquifer to behave as an aquitard. This means that in continuous and discontinuous permafrost regions, groundwater is partitioned within unfrozen geologic materials above (in the seasonal active zone) or below the permafrost. These groundwater systems are termed *suprapermafrost* if positioned above the permafrost table, and *subpermafrost* if below the permafrost. Suprapermafrost groundwater is typically younger, takes a shorter flowpath from infiltration to discharge, and can be more dilute than subpermafrost groundwater (Woo, 2012). Due to the longer residence time of the deeper subpermafrost groundwater, it tends to be much older and can be more solute-rich as a result of extensive interaction with subsurface materials. The nature of the groundwater geochemistry and isotopic composition can be used to interpret its source and age. Areas within permafrost terrain that remain devoid of permafrost year-round are known as *taliks* (Woo, 2012). Taliks that penetrate completely through permafrost can connect surface water with groundwater in the suprapermafrost zone and the subpermafrost zone; they create “hydraulic windows” through permafrost, allowing exchange between the different groundwater systems (Woo, 2012). As conventional groundwater monitoring wells require unfrozen conditions to function properly, the occurrence and persistence of the permafrost within the subsurface significantly influences their utility.

In developing this methods document, it was anticipated that through the use of novel groundwater monitoring and sampling techniques, some aspects of the groundwater flow systems within remote, discontinuous permafrost environments could be characterized without the need for conventional methods that require road site access and are prohibitively expensive. This includes approaches such as standard drilling and monitoring well installation. The suprapermafrost zone can be characterized through direct measurements while the subpermafrost zone behavior can be characterized indirectly from data collected in the vicinity of areas of groundwater discharge such as surface water and springs. Essentially, by finding evidence for subpermafrost groundwater in springs or surface water, it is possible to infer that the deeper groundwater flow systems are active and contributing to the shallow, suprapermafrost groundwater and surface water bodies. It is also anticipated that these combined groundwater characterization methods may provide insight into the interaction of deeper aquifers with the near surface environment and potentially assist in understanding how the overall hydrologic system is changing over time.

A variety of physical, geochemical and isotopic-based methods were explored in developing this report and it is anticipated this this will be a living document that will be updated as experience is derived from additional field testing. The methods include:

- Geographical Information Systems (GIS)
- Remote sensing
- Terrestrial and Air borne Geophysics
- Thermal infrared imagery
- Measurement of physical hydrogeological parameters
- Analysis of water geochemistry and isotopes

Geochemical species and isotopes are used primarily as "environmental tracers" which reflect information about the groundwater flowpaths, age, and source. For demonstration purposes, this document outlines the different methods as they were utilized to characterize hydrologic baseline conditions within a small watershed in the Central Mackenzie Valley, near Norman Wells, NWT. The field area is referred to as the Bogg Creek watershed (Figure 1). Emphasis is placed on how a strategic approach can be taken to determine how and where monitoring and sampling should occur a priori by initial identification of priority monitoring sites. We define priority monitoring sites as locations of potential groundwater discharging conditions or those under influence of groundwater that may provide insight into local and regional groundwater flow phenomena.

This document is intended as a guideline for characterizing groundwater flow phenomena in this specific environment and is not intended to be an exhaustive list of all methods and techniques that may be viable. Future updates to this document will be made as new information becomes available.

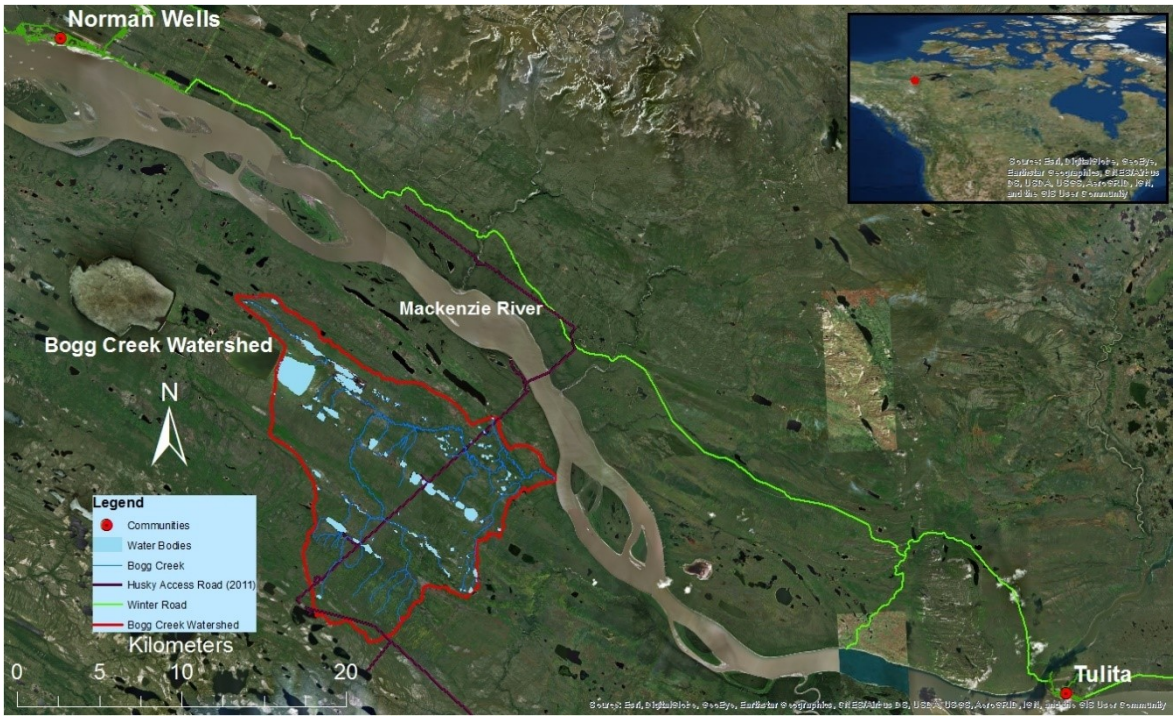

Figure 1: Map of study area and regional context. The Bogg Creek watershed is shown as a red outline and nearby communities as red dots. Winter and all-weather roads in the watershed provide access to several monitoring sites (Wicke, 2020).

2.0 Methods

2.1 Selection and Screening of Priority Monitoring Sites

Prior to consideration of a field site visit and specific terrestrial monitoring activities, it may be possible to make use of existing information, data and remote sensing tools to design the field sampling campaign. Using a combination of the different techniques there may be the potential to identify priority sampling and monitoring sites in advance of arriving at the field area of interest. Based on the nature of the identified field sites, specific monitoring plans can then be developed consistent with the anticipated site conditions.

The various techniques and strategies will be presented in order of data collection scale ranging from orbit-based remote sensing tools to detailed terrestrial measurement approaches. The technical aspects of each method will be briefly discussed with the emphasis being placed on the practical utility of the different methods and the information/data that could be expected to be obtained. It is clearly acknowledged that the objectives of individual projects may be highly variable and as such the methods are presented for general application in discontinuous permafrost terrain, utilizing the application within the Bogg Creek Watershed (Figure 1) as an illustrative example.

2.1.1 Remote Methods

Selection of priority monitoring sites begins with the use of desktop tools. Geographic Information Systems (GIS) programs such as ArcGIS are essential tools to display, modify and analyze geographic information that may be available at a specific site. Examples of useful information that can be informative for a desktop survey using GIS tools include surficial and bedrock geologic maps, Digital Elevation Maps (DEMs), climate data, road maps, stream and lake networks, and airborne geophysical surveys (e.g., Electromagnetic, Gravity). More detailed subsurface information can be obtained through the interpretation of terrestrial geophysics including seismic survey lines, point information from seismic shothole logs (I. R. Smith, 2015), and exploratory boreholes related to geological and geotechnical drilling. Combining the information from these different data sources can be useful in developing base maps of the area of interest and developing initial conceptual models of the geologic and hydrogeologic conditions at the site. This initial information can be used to evaluate access limitations, surface and subsurface geological materials that are likely to be encountered, and the nature of the surface water hydrology, all of which is valuable information in planning subsequent field investigations.

A specific example of the use of remote sensing data to inform hydrogeologic field investigations in this type of terrain involves the interpretation of precision optical and thermal imagery collected from satellites to map the locations of icing features on the land surface. In permafrost terrain, a common feature in the winter landscape is an “icing” or “aufeis”, which is a large sheet of ice formed by expelled groundwater or river water (Woo, 2012). Three primary types of icings have been documented: the spring icing, river icing, and ground icing. Land-fast icings in the form of spring and ground type icings are important to consider as these are typically sourced from groundwater (Glass, 2019). The spring icing is formed from a perennially flowing spring, often sourced from subpermafrost groundwater. The ground icing is formed as a result of an encroaching freezing front during winter that forces groundwater to the surface. The identification of these icing features may be of use in locating the position of groundwater discharge points, which could be of interest as priority monitoring sites for detailed field investigation with many of the techniques outlined in subsequent sections.

A remote sensing method used within the Bogg Creek Watershed to locate icings using optical and thermal satellite imagery is explained in detail in Glass (2019) following the methods developed by

Morse and Wolfe (2015). The identification of icings is performed with the use of Landsat 4-5 Thematic Mapper (TM) and Landsat-8 Operational Land Imager (OLI) optical imagery, RapidEye-3 optical imagery, and Landsat 4-5/8 120 m thermal imagery for various years with available data that would be appropriate for assessment. Following the algorithm process developed by Morse and Wolfe (2015), late spring imagery from each of these years is used to identify areal icing coverage. Although the details on the interpretation process is beyond the scope of this current document, they can be found in Morse and Wolfe (2015), Glass (2019), and Glass et al. (2020). The icing coverage from multiple years can be compared to locate areas where they consistently occur, which is indicative of a perennial spring area. These locations may be of priority interest to visit during field investigations as they may represent locations of deeper groundwater discharge. An example of icing maps generated in this fashion within the Bogg Creek Watershed is shown in Figure 2 (Glass, 2019; Rudolph, 2019).

Figure 2: Location of an icing cluster within the Bogg Creek Watershed between 2004-2017 (icings shown in pink) (from Glass, 2019) modified from Rudolph (2019).

The icings map can then be integrated with other relevant data sources to further develop maps of priority field investigation sites. For example, in combination with the icings map, analysis of terrain and geologic structures may further inform priority monitoring sites. Groundwater springs are often associated with a break in topographic slope, faulting or jointing, or between the contacts of a high hydraulic conductivity and low hydraulic conductivity formation (such as sandstone transitioning to shale) (Kresic & Stevanovic, 2010). Where these features coincide with surface water and icings there is potential for active groundwater flow, and these can be included as priority monitoring sites. High resolution satellite imagery can also be utilized to assess vegetation conditions that may limit site accessibility. Again, GIS tools can be employed to automate the construction of maps that can be continually updated as new information is obtained. Collectively this is used to update the initial conceptual geologic and hydrogeologic models. A summary of this process is presented in Figure 3 as a flow chart.

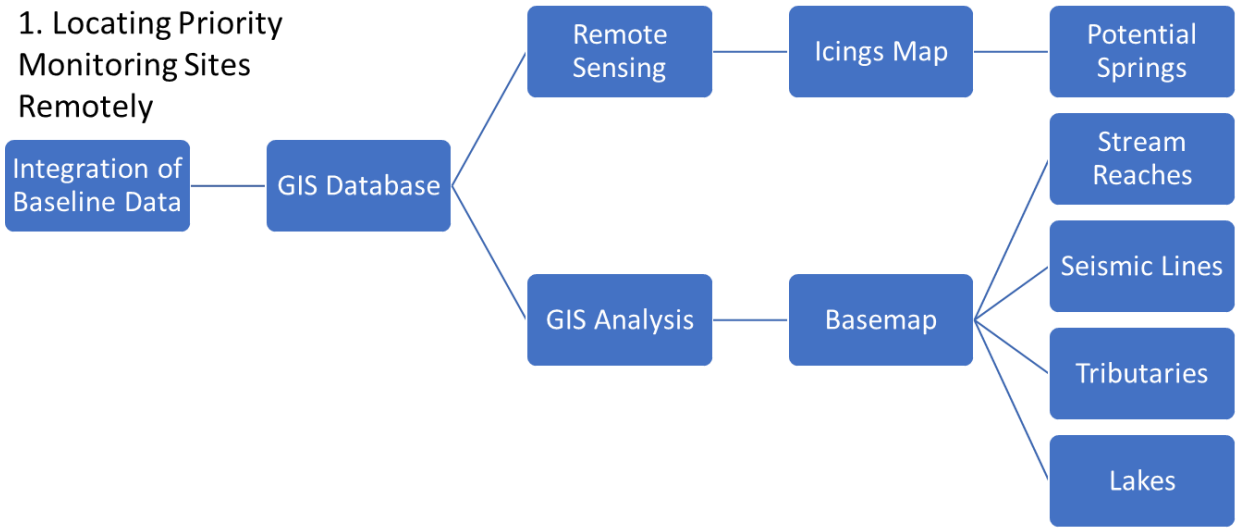

Figure 3: Process for remotely siting priority monitoring sites beginning with integration of any available site information.

2.1.2 Airborne Methods

Further screening of priority monitoring sites can be achieved through the implementation of a low-altitude thermal infrared (IR) survey, to verify if groundwater discharge is potentially occurring in priority sites. Flowing groundwater transfers heat energy by convection and conduction, and temperature variations are dampened with increased depth into the subsurface. This leads to less temperature fluctuations in groundwater compared to surface water or air temperature (Anderson, 2005). Because of this stability, temperature acts as a useful tracer for locating and characterizing groundwater and surface water interactions through temperature contrasts. In the summertime, groundwater temperatures are typically cooler than surface water and ambient temperatures, while in winter they are typically warmer (Conant Jr, 2004; Rudolph, 2019).

Groundwater emerging through seeps and springs with enough temperature difference from the surrounding surface water or nearby vegetation can be detected with IR cameras (Rudolph, 2019). The greater the temperature difference, the easier detection is. In summertime at midday when surface water temperatures are much warmer than groundwater, discharge can be highly visible by use of an IR camera. The opposite occurs in mid-winter when surface waters are colder compared to groundwater (Rudolph, 2019). This technology is most useful when paired with a helicopter flying at low elevation, allowing rapid characterization of groundwater discharge locations over a large area. A coupling of IR and visual cameras allows for imagery of ground and water temperatures to be recorded. With enough contrast, springs will appear as thermal anomalies against their surroundings. In the summer, these anomalies will appear cold and in winter they will appear relatively warm (Rudolph, 2019). Aerial traverses should be pre-planned and attempt to cover potential priority sites. Continuous footage combined with a GPS system allows for sites to be selected as ground targets for further groundwork. Other opportunistic survey targets can include creek banks, seismic cut lines, and lake shores. This footage can be used to make decisions on what targets are high priority and which will be less important to visit, depending on strength of the anomaly and its accessibility and position relative to icings or other features determined through geologic analysis. Some specific examples of cold anomalies and potential springs from the Bogg Creek watershed are illustrated in Figure 4. The summary of the screening process is presented in Figure 5.

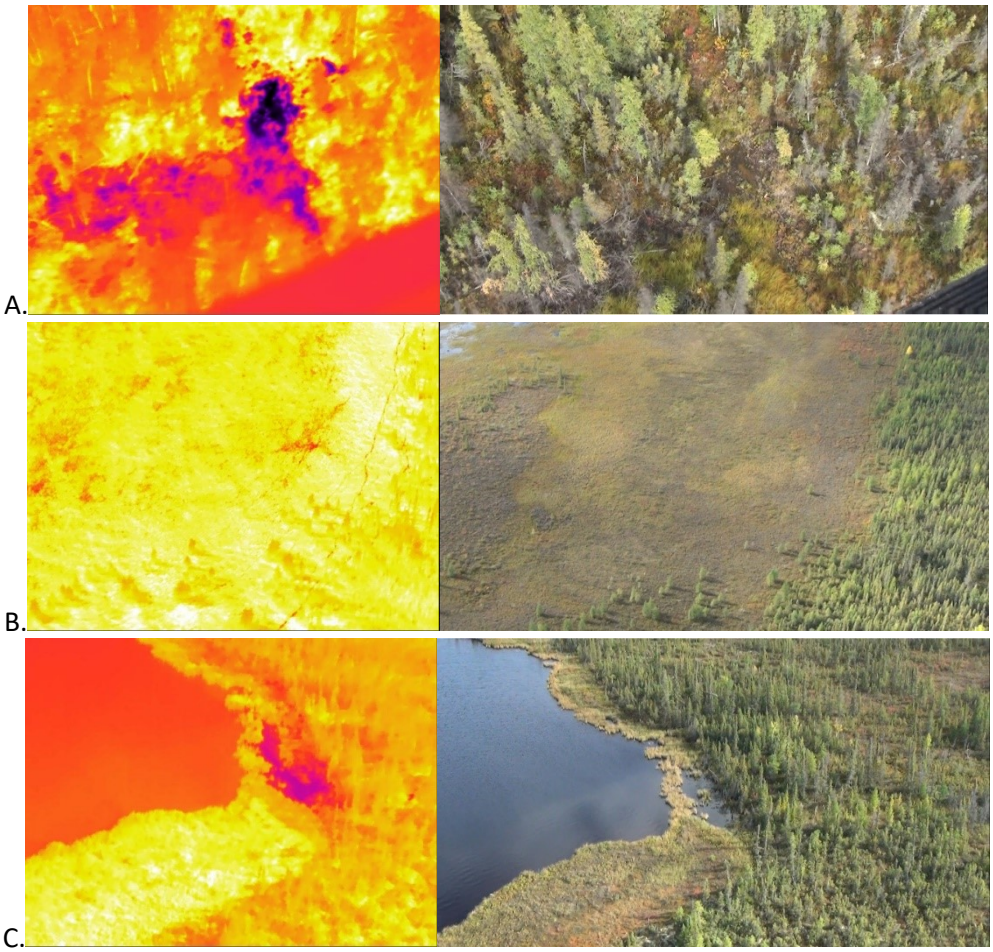

Figure 4: A): A large cold anomaly within a seismic cutline. B): Two thermal anomalies in a wetland adjacent to a lake. C): Thermal anomaly from spring-fed water pooling on the sides of a lake. Photos by B. Conant Jr.

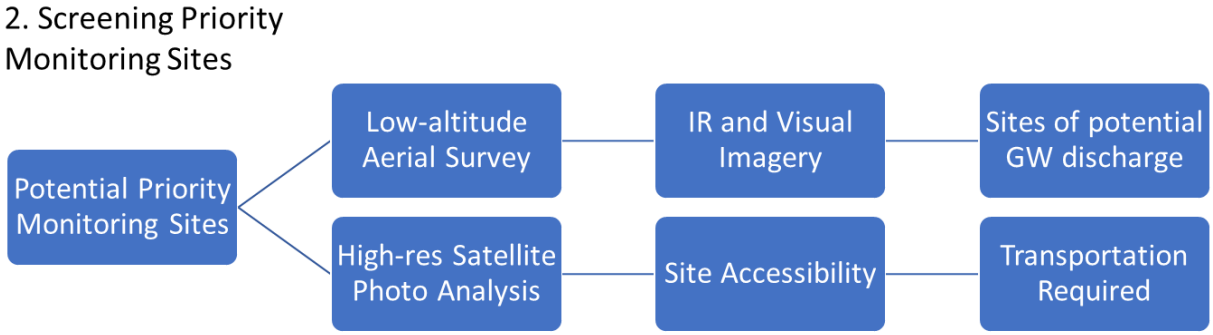

Figure 5: Screening process of priority monitoring sites using both satellite photo analysis and a thermal infrared image aerial survey. The aerial survey can be used to verify if there is potential groundwater discharge occurring at a particular site especially those identified through icing mapping. Both the aerial survey and photo analysis can be used to determine if a site will be accessible and is therefore worth visiting. This effectively removes many sites identified but that may not be accessible and prioritizes those with actual IR evidence of groundwater discharge and are more accessible.

2.2 Terrestrial Geophysical Methods

Terrestrial geophysical methods that have proven effective at mapping the presence of permafrost in the shallow environment include electromagnetic geophysics and specifically, electrical resistivity tomography (ERT). This system is relatively portable and can be managed by a small field crew although it requires the installation of electrode arrays into the ground surface. Another similar method is electromagnetic induction (EMI), which is also based on the electrical properties of the subsurface. This system does not require the installation of a terrestrial array and can be hand carried along a survey line making it a faster and less labor-intensive option (Walvoord et al., 2012).

The ERT method is designed to measure the vertical resistivity of the subsurface materials through a variety of different electrode arrays that can be selected to measure to different depth profiles. The EMI systems, on the other hand, consist of a transmitter and receiver coil, whereby the transmitter generates a primary electromagnetic field that interacts with the subsurface constituents. Conductive materials in the ground will contribute and generate a secondary electromagnetic field. Both the primary and secondary electromagnetic fields are measured by the receiver coil. The EMI instruments are manually moved from site to site and can be run along transects to collect laterally continuous information. Because there is a major contrast between the electrical conductivity and resistivity of sediments containing frozen water as compared to sediments with liquid water, these methods have proven useful in tracking the depth and continuity of the permafrost table (Walvoord et al., 2012; Rudolph, 2019).

In order to briefly demonstrate the utility of these two geophysical methods at mapping permafrost continuity in this type of terrain, data collected along the shoreline of a lake within the Bogg Creek watershed where the permafrost table was observed to plunge deeply and close to the shoreline (based on manual measurements with a permafrost probe, explained in subsequent sections) is used as an example. For the ERT mapping, a 25 m survey line was established perpendicular to the shoreline at the study site and 75 cm electrode spacing was selected in order to collect resistivity information along the survey line to an average depth of approximately 5 m. The resistivity data are presented in Figure 6. The geophysical profiles closely match the trend of the manual measurements of permafrost depth made along the survey line with the permafrost table dropping significantly towards the edge of the lake at the right side of the profile in Figure 6. `

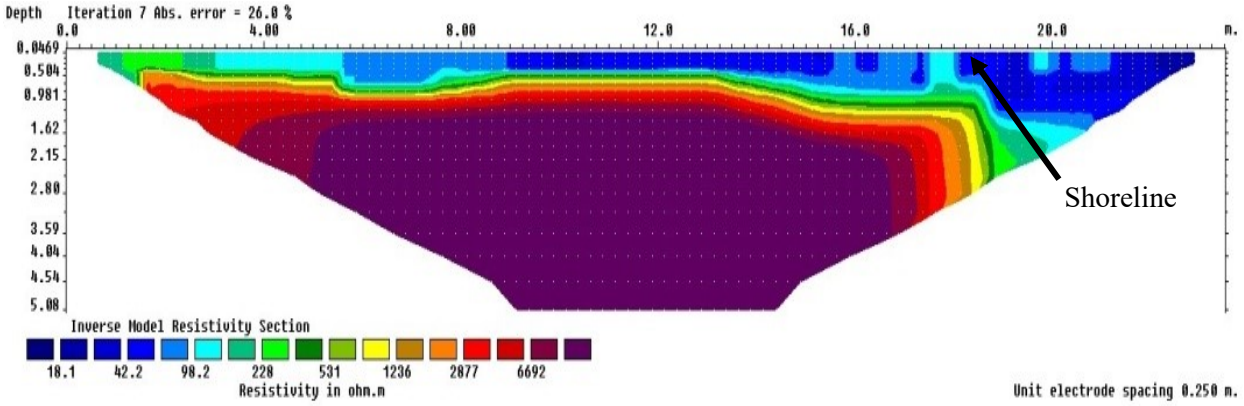

Figure 6: ERT survey data collected along a survey line oriented perpendicular to a large lake (right side of the profile) illustrating a significant increase in depth to the permafrost table near the lake (zone of lower resistivity in blue shades) (Rudolph, 2019).

The same survey line was used for the electromagnetic induction (EMI) method based on the frequency domain electromagnetic (FDEM) method (Geonics Limited EM-34-3™ and EM-31™). Coil spacings of

between 10 m and 20 m were selected for the EM-34 surveys, and the fixed 3.4 m is the built in spacing for the EM-31. The coils can be arranged either perpendicular to the ground surface (horizontal dipole) or parallel to it (vertical dipole). With each measurement, one depth-averaged data point is obtained along the survey line as opposed to several data points being collected for different depths with the ERT method. Both geophysical instruments were manually carried along the survey line.

The results of the EMI surveys using both the horizontal and vertical dipole configuration are presented in Figure 7. As with the ERT method, the EMI approach also clearly detects the change in depth of the permafrost table approaching the shoreline. Considering the portable and less labor-intensive nature of the EMI systems, this geophysical method may be of value in remote terrain as a rapid mapping tool for the continuity of shallow permafrost as opposed to the more intrusive and less portable ERT methods. Both methods, however, provide useful approaches for rapidly estimating the depth and continuity of the permafrost table where the table is relatively shallow (upper 5 m). Where the table is deeper, stronger ERT systems with wider electrode spacings can be employed (Walvoord et al. 2012).

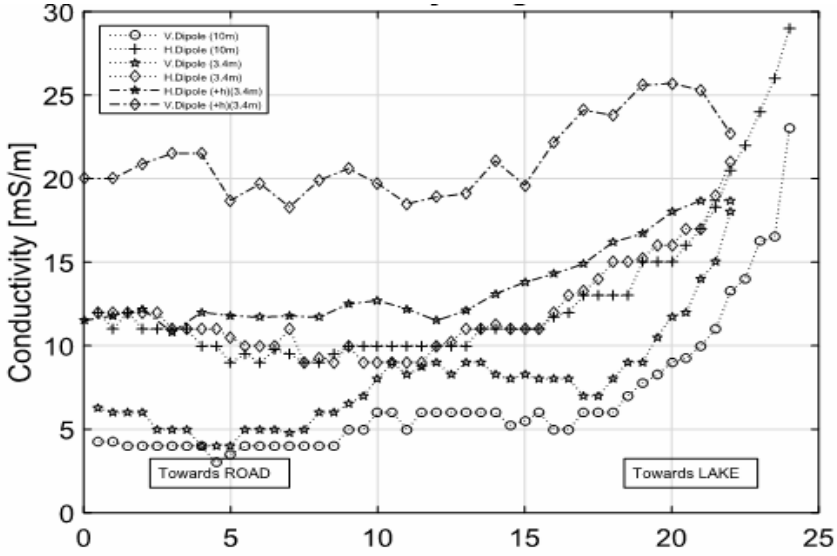

Figure 7: EMI survey data collected using several coil spacings and orientations along a survey line oriented perpendicular to a large lake (right side of the profile) illustrating a significant increase in depth to the permafrost table near the lake (zone of higher electrical conductivity) (Rudolph, 2019).

2.3 Groundwater Monitoring

2.3.1 Groundwater Samples and Physical Parameters

Taking samples of suprapermafrost groundwater, stream porewater, or spring water can be facilitated effectively through the use of lightweight, transportable sampling equipment. Portable sampling instruments such as the PushPoint “Henry” Sampler (MHE Products Ltd.) and pre-constructed mini-piezometers can be used to take groundwater head measurements and samples quickly and easily in remote areas. The PushPoint Sampler is a small drivepoint piezometer designed for taking porewater samples from the shallow subsurface or below surface water bodies. It consists of stainless-steel tubing, with a narrow drive-point tip and slotted screen at one end, and a small welded handle and sampling port on the other. An inner rod remains inside the sampler during insertion to minimize formation material from entering the screen and is removed prior to sample collection. The sampler is available in

three lengths (62 cm, 124 cm and 184 cm) and is selected depending on how soft the subsurface materials are anticipated to be on site, a characteristic that controls how deep the thin probe can be manually installed. Use of the available mesh screens installed around the slotted tip is recommended with any length of sampler as smearing of clays and blockage of the slotted screen is possible.

The Henry sampler can be simply installed into soft sediment by hand without the need for a hammer and removed just as easily by pulling it out by hand. For collection of a groundwater sample, only narrow gauge plastic tubing and a syringe or vacuum pump are required. Once the inner rod is removed, groundwater level measurements can be taken easily with these samplers using a slim water level tape. This simple manual sampling tool works in water-logged wetlands, near or below surface water bodies, or on dry land areas where the water table is close to surface.

The pre-constructed mini-piezometer tips consist of small mesh screens wrapped around tubing (3/8”) that has been notched to allow for water entry. The tips average 10 cm in length and are connected to a smaller diameter tubing cut to the desired depth of installation (Lee & Cherry, 1979). The mini-piezometer is installed in sediments by manually driving a ½” steel pipe with an expendable tip to the desired depth. The pipe functions as a temporary access tube to permit the installation of the mini-piezometer and is subsequently removed from the ground, exposing the mini-piezometer tip. Installation depths are commonly between 1 m and 1.5 m and can be placed at multiple depths at the same location to monitor vertical hydraulic gradients in the shallow subsurface and collect groundwater samples from various depths. Groundwater samples can be collected from the mini-piezometer by connecting a syringe, vacuum pump, or peristaltic pump to the small diameter plastic tube and groundwater levels can be measured using a small diameter water level tape.

Both mini-piezometers and the PushPoint sampler are highly portable and easy to install and remove. Sample volumes are limited however, especially in the PushPoint sampler, so careful consideration should be given to what kind of samples will be required. Time needed to collect samples will depend heavily on the hydraulic conductivity of the subsurface materials. Physical parameters such as the hydraulic head at the sampling interval are also relatively quick to obtain with a water level tape, and several samplers can be installed at different depths to obtain a vertical (minimum 2) and horizontal gradient (minimum 3). Hydraulic conductivity can also be determined for the formation materials by performing constant, falling, or rising head single well response tests (Fetter, 2001). The measurements from these instruments can provide crucial baseline data that can be used later to determine if more long-term monitoring solutions are appropriate at a specific location. Photos of these instruments in use are shown in Figure 8.

Figure 8: The mini-piezometer and PushPoint "Henry" Sampler used to take groundwater levels and samples on dry land (left). The PushPoint sampler showing upward gradient at a spring site (right). Photo on right taken by B. Conant Jr.

Vertical hydraulic gradients can also be determined through use of simple temperature measurements below springs or in stream or lake beds. A thin steel probe with an electronic thermistor installed at the tip (temperature probe) can be manually driven into shallow sediments to obtain a profile of groundwater temperatures to compare to the temperature of surface water. Stream and lakebed temperatures are a function both of a heat transport balance between the surface water and groundwater. Under groundwater discharge conditions, the subsurface temperature is influenced by the downward conduction of heat from overlying surface water, and upwelling groundwater convection. Under recharge conditions, both convection and conduction of heat will be downwards from infiltrating surface water (Conant Jr, 2004). Simple temperature measurements of both stream water and streambed temperatures to depths of around 0.5 m below bed surface may allow for reasonable determinations of groundwater flow directions, and in some cases the rate of flux (Conant Jr, 2004). If desired, a measurement can be taken every 10 or 20 cm to obtain a full profile of subsurface temperatures. This eliminates some of the possibility of measuring natural diurnal fluctuations that may be mistaken for background temperatures. An example of this as well as a profile of groundwater recharge and discharge is shown below in Figure 9. If the flux of water upwards is high, the convective transport of heat will exceed the conduction from surface water, forming a steeper slope in the profile.

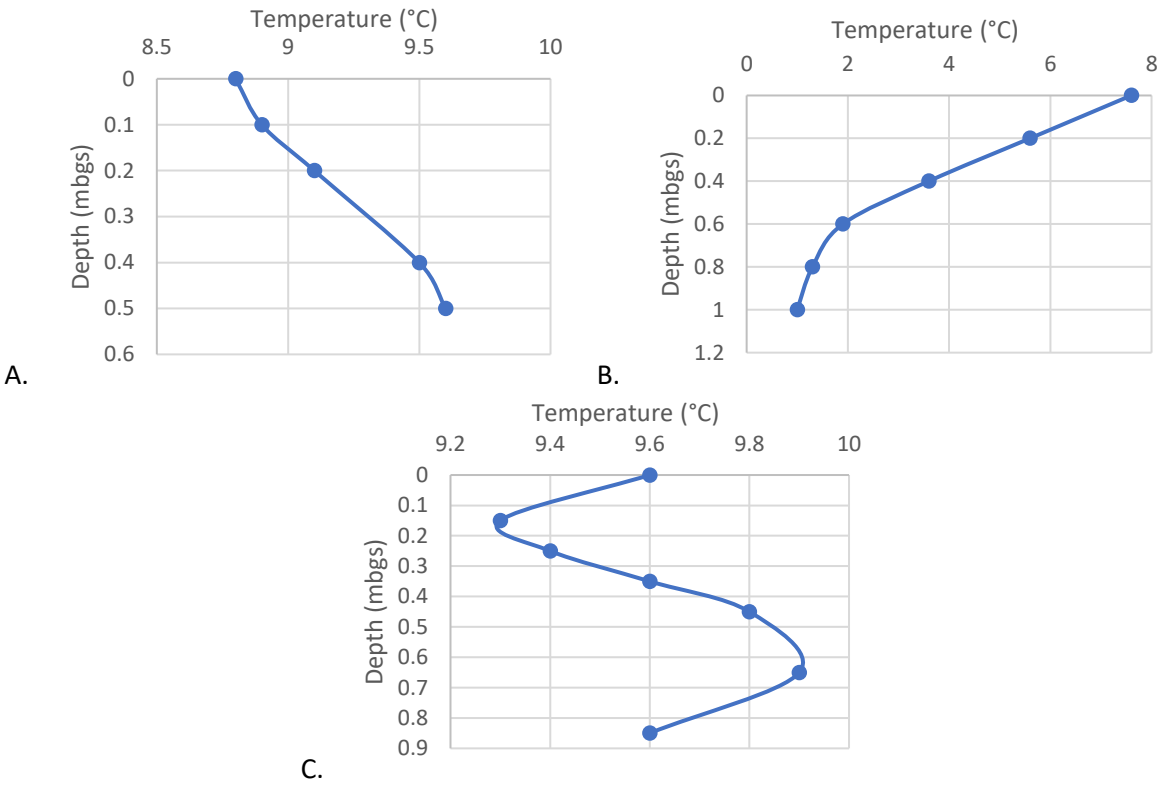

Figure 9: Temperature profiles showing A. Recharge conditions at a particular stream reach B. Dishcarge conditions measured at a groundwater spring and C. Diurnal fluctuations that penetrate below 20-30 cm. Note that these conditions are only possible in summer when groundwater temperature is less than surface water temperature. (Wicke, 2020).

2.3.2 Shallow Permafrost Conditions

The active layer or current summer thaw depth and permafrost continuity is useful information in informing the depth of the suprapermafrost zone and the presence of shallow taliks. A permafrost probe consisting of a graduated aluminum or steel rod with a handle can be used to measure the depth of the permafrost table and extent of thaw during a site visit, randomly or along a transect. Note that the true thickness of the annual active layer may not be possible to measure until just before winter freeze up, so measurements should be taken later in the year if that is required. Usage of portable sampling and measurement devices are shown below in Figure 10. Permafrost geochemistry, isotopes, ice content, and stratigraphy can also be useful parameters in determining potential for future changes and for characterizing a site. Small cores collected via specialized auger from the active layer and below the permafrost table can be logged for ice content, morphology, and sediment texture in the field and then kept frozen until further analysis can be performed in a laboratory setting. A squeezing apparatus will allow for extraction of porewaters after cores are allowed to thaw, following methods outlined in Moncur et al. (2013) and adapted in Wicke (2020). Geochemistry or isotopic composition can be analyzed in these extracted porewater samples depending on volumes produced and species of interest. The analysis of progressively deeper samples from the core can permit a determination of changes in these chemical and isotopic trends in the shallow subsurface.

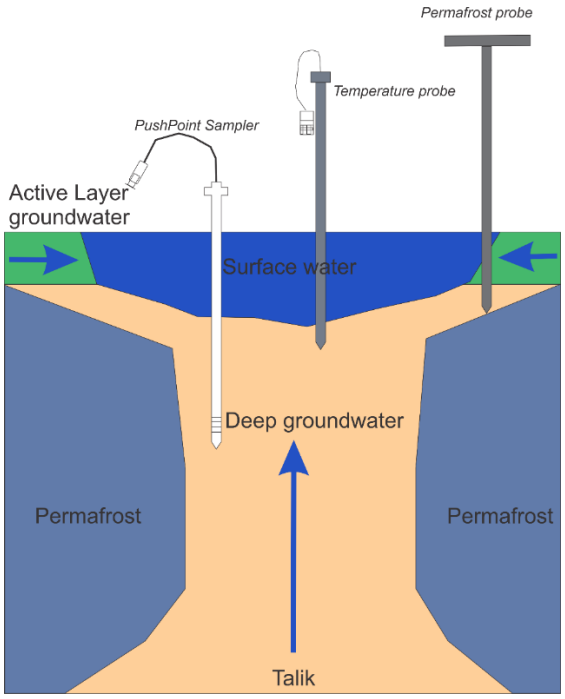

Figure 10: Conceptual diagram of equipment usage. PushPoint Sampler is used to collect samples below surface water, ideally to capture evidence of discharging subpermafrost groundwater before complete mixing. Temperature probes are used to measure temperature differences that may indicate discharge conditions, while the permafrost probe is used to map the permafrost table in the vicinity of the water body (Wicke, 2020).

2.4 Environmental Isotopes and Geochemistry

2.4.1 Geochemistry

Inorganic ions in water can often be used as groundwater tracers. Solute concentrations in groundwater evolve as water flows and encounters different rock types or lithologies (Hem, 1985). In most natural waters, the majority of the salinity is composed of 8 specie: calcium, magnesium, sodium, potassium, bicarbonate or carbonate, chloride, sulphate, and nitrate (Ca, Mg, Na, K, HCO_3 and/or CO_3 Cl, SO_4 and NO_3). Concentrations and proportions of these ions are largely controlled by lithology, water-rock interactions, flowpaths, and residence time. Water can be classified into a "type" based on the proportions of these elements (positively charged cations and negatively charged anions) relative to one another.

Initially, solute evolution within a groundwater flow system begins with rain or snowfall, which contains atmospherically derived solutes (Herczeg & Edmunds, 2000). Interacting with geologic materials, groundwater then begins to reflect the dominant rock and soil types of an area as a result of weathering reactions and mineral dissolution (Hem, 1985; Herczeg & Edmunds, 2000). Depending on the residence time and the flowpath the groundwater takes, geochemical evolution will occur, altering the water chemistry over time. Suprapermafrost groundwater flow usually takes place in shallow soils and is typically dominated by carbonate with some minor silicate dissolution. Subpermafrost groundwater flow may occur well below any unconsolidated overburden, within bedrock. Weathering reactions will then depend on the mineral make-up of the rock, with primary mineral types being carbonates (such as in limestones or dolostones) or silicates (such as in sandstones or granites) but with ion concentrations potentially being greater than in the suprapermafrost zone (Herczeg & Edmunds, 2000).

Hydraulic connections between shallow and deep aquifers allow for mixing of different groundwater flow systems to occur. Overall ion compositions are often plotted on piper diagrams, which allow basic geochemical “endmembers” to be established and provide visual indication of potential mixing (Hem, 1985). An endmember is a representative water sample from an aquifer or other water source, usually the most extreme samples that are available (such as very dilute or solute rich). In the study of regional groundwater flow systems, some subpermafrost groundwater monitoring may be required to establish important endmembers in the deep systems. Otherwise, if major rock types and minerals are known, water chemistry can be somewhat predicted. Furthermore, characterizing the suprapermafrost groundwater zone and its variability should reduce some uncertainty about a spring or surface water sample, as a significant deviation is likely indicative of another source. Mixing of different endmembers will produce a new geochemical make-up, which can often be distinguished through diagrams and calculations.

Some examples of groundwater endmembers and some surface water from Bogg Creek is shown in Figure 11. Endmembers include runoff and organic active layer porewater (Ca-SO_4 type water, top of diamond), suprapermafrost groundwater in the unconsolidated overburden (Ca-HCO_3 type water, left of diamond), and subpermafrost groundwater from two sources (Na-HCO_3 to Na-Cl type waters, right of diamond). Surface water from Bogg Creek for multiple years is also shown (Data provided directly by Husky Energy and some obtained from Husky Oil Operations, (2016)). Two tributaries overlap endmembers of the suprapermafrost and one of the subpermafrost endmembers separately, reflecting large influences (water inputs) from those sources. Water from lower reaches of Bogg Creek are shown plotting mostly in the center of the diamond, reflecting mixing of several unique water sources. Variability in the data is likely due to the different proportions of waters making up the bulk chemistry in a sample. For instance, stream water from early summer tends to plot closer to the runoff endmember, reflecting enhanced runoff as much of the ground is still frozen. As active layers thaw in late summer and rains decrease, waters then plot closer to the suprapermafrost and subpermafrost endmembers. This reflects the increased shallow groundwater flow coupled with increasing influence of all groundwater due to decreased runoff.

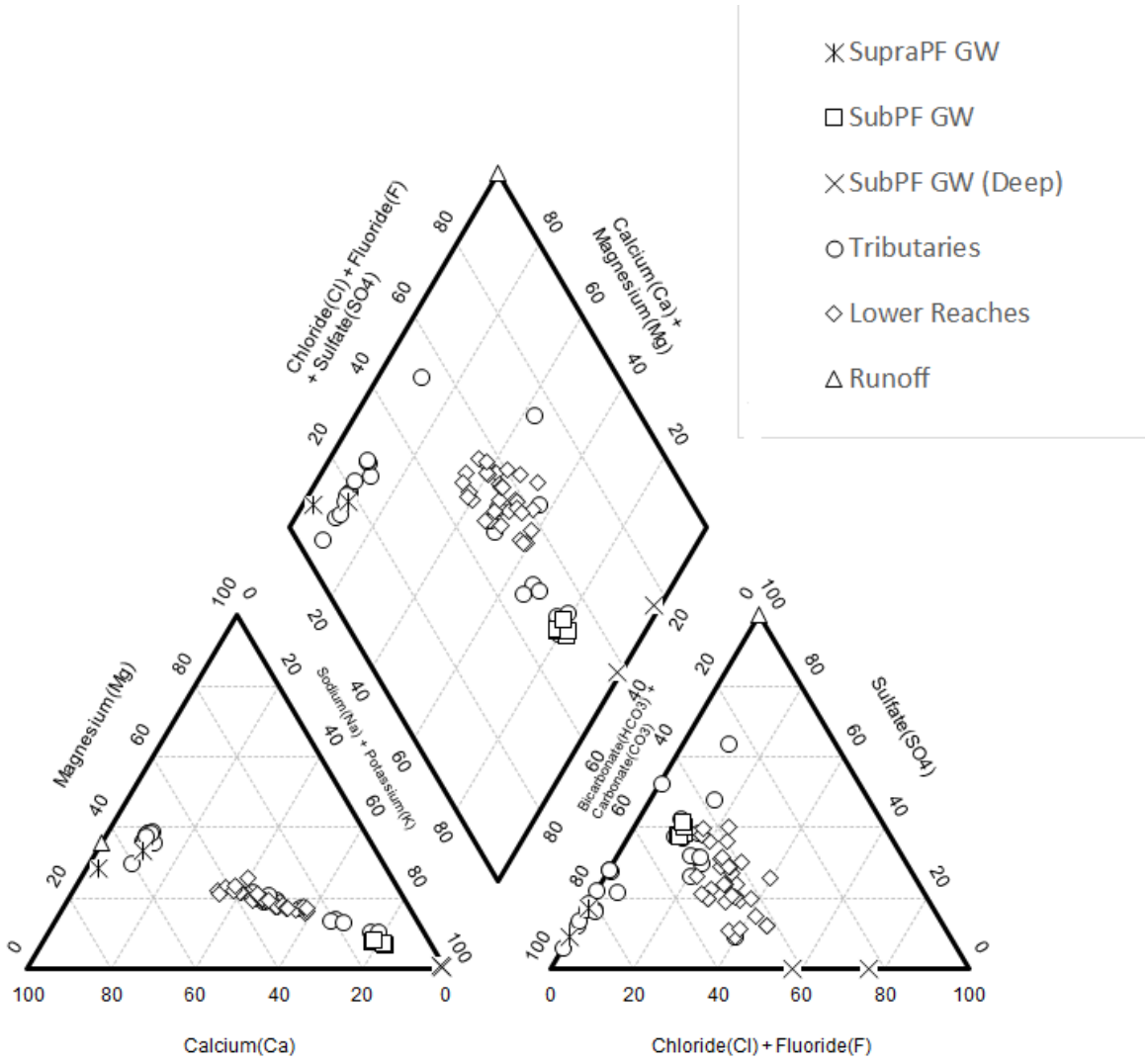

Figure 11: Piper plot of site wide groundwater and stream water. Tributaries show distinct overlap with certain endmembers and some variability due to different contributions of runoff and groundwater. Lower reaches appear to be mixtures of several endmembers and so do not overlap but vary due to different proportions of runoff and groundwater Some data provided directly from Husky Energy or obtained from Husky Oil Operations Ltd (2016) and Waterline Resources Inc., (2013a, 2013b).

Site specific chemical species may work as potential tracers as well. For example, hydrocarbon compounds are hypothesized to also act as tracers of deep groundwater flow in a bedrock environment where hydrocarbon-bearing strata are present. For example, natural seeps of petroleum exist along the Mackenzie River (Babiy, 2013) and may act as tracers for deeper subpermafrost flow (Rudolph, Lotimer, et al., 2016). BTEX (Benzene, Toluene, Ethylbenzene and Xylenes) is hypothesized to act as a natural tracer in this environment. In the Bogg Creek example, toluene appeared in several waters but was unaccompanied by the other species. This has been reported to indicate toluene that is produced biogenically, or by microbes within a water-logged, anaerobic environment, rather than thermogenically, from temperature and pressure in oil reservoirs (Richards & Sandau, 2018).

2.4.2 Stable Isotopes of Oxygen and Hydrogen

Oxygen is known to have three stable isotopes and numerous radioactive isotopes, while hydrogen has two stable isotopes and one radioactive isotope. In isotope hydrology the oxygen isotopes ^{18}O and ^{16}O and hydrogen isotopes ^{2}H and ^{1}H are commonly used to study the sources and dynamics of groundwater or surface waters (Clark & Fritz, 1997). These isotopes are typically expressed in delta (δ) notation, in units of per mille (‰). This notation expresses the proportion of heavier (^{18}O and ^{2}H) isotopes to lighter isotopes (^{16}O and ^{1}H) that there are in a sample, in reference to a standard. Globally, $\delta^{18}O$ and $\delta^{2}H$ in precipitation is controlled by moisture sources, inland or oceanic topography, and latitude and longitude; typically, they are higher in warmer regions and lower in colder regions. Measuring $\delta^{18}O$ and $\delta^{2}H$ in precipitation throughout a given year in a particular area forms a straight line when graphed, called the Local Meteoric Water Line (LMWL) which is unique to a region (Figure 12). Precipitation $\delta^{18}O$ and $\delta^{2}H$ will vary seasonally and as such the precipitation source of groundwater within shallow groundwater flow systems may be recognizable by its $\delta^{18}O$ and $\delta^{2}H$ compared to a LMWL. Typically, snow will be more isotopically "light" (lower values) and summer rains will be more isotopically "heavy" (higher values). In many regions, LMWLs have been established through prior studies and data may be included in the Global Network of Isotopes in Precipitation (GNIP) database for a region near the study area.

A water sample that falls higher up the slope of the LMWL or is more isotopically heavy is generally composed mostly of summer precipitation that is also heavier. In contrast, water that is lower on the LMWL is more isotopically light and is comprised of lighter sources such as snow. Other sources of isotopically light water can be contributors, however, which can make interpretations difficult without other lines of evidence. Old groundwater recharged during the past in a colder climate such as during the last glaciation or water recharged at a higher elevation can both be light isotopically. Some of this old water can be flowing through deep, subpermafrost aquifers or locked up as permafrost ice. Modern groundwater in shallow aquifers is often comprised of a mixture of light and heavy isotopic waters corresponding to the amounts of snow and rainwater that recharges the aquifer. Reflecting this mixture, the $\delta^{18}O$ and $\delta^{2}H$ of modern groundwater is often around the same value as that of the weighted mean precipitation for a region (isotope values normalized to amount of precipitation) (Clark & Fritz, 1997).

In surface water, evaporation of water from an open body of water causes selective enrichment of $\delta^{18}O$ and $\delta^{2}H$ values, and a deviation off the LMWL onto a Local Evaporative Line (LEL). Groundwater with an evaporated signature suggests that the water has undergone evaporation from a shallow aquifer or was recharged by an evaporating water body (Clark & Fritz, 1997; Coplen et al., 2000).

Some example data are shown in Figure 12. $\delta^{18}O$ and $\delta^{2}H$ was used in Bogg Creek to determine the sources of surface water and groundwater. Surface water generally plots off the LMWL and along the LEL showing variability in the amount of evaporation, but some can be observed falling on or close to the LMWL. This indicates that this surface water is generally replenished with unevaporated sources such as groundwater or precipitation. Groundwater plots along the LMWL and reflects the dominant source of recharge, with most plotting around the average ($\delta^{18}O$ of -21.9‰). The lightest samples ($\delta^{18}O$ of -25.2‰) were subpermafrost groundwater taken from a series of deeper groundwater monitoring wells installed by Husky Energy within the Bogg Creek watershed as part of a baseline monitoring program (Waterline, 2012). This water was carbon dated to around 20,000 years old, placing its recharge age during the last glaciation (Waterline Resources, 2013b). Seeps and springs in the area also plotted around the average but with similar spread reflecting the complexity of water sources. Some springs plotted well below the average, indicating some component of isotopically light water may have derived from thawed permafrost, snowmelt, or subpermafrost groundwater.

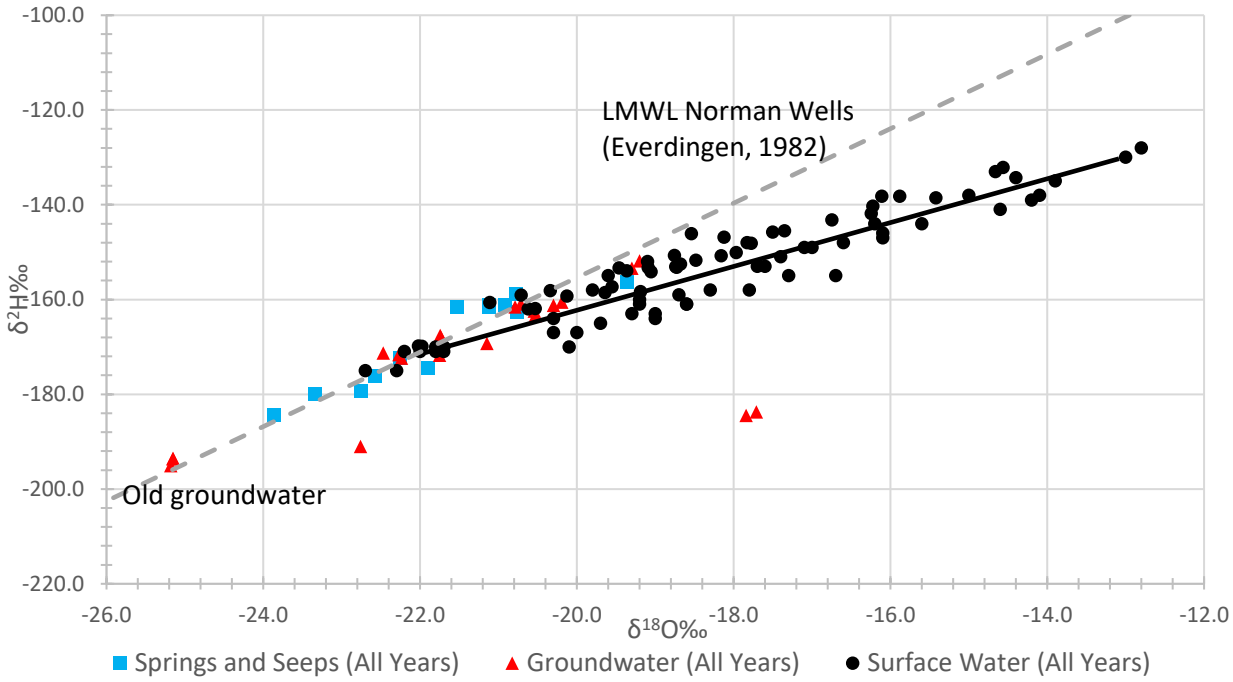

Figure 12: $\delta^{18}O$ and $\delta^{2}H$ data from 2012, 2018, and 2019 from around Bogg Creek and its surrounding area. Typically, groundwater (red) plot closer to the weighted average for precipitation, but some fall above or below. This case is also true for seeps and springs (blue). Surface water (black) generally shows an evaporated signal and falls on the LEL Some data retrieved from AMEC, (2013) and Husky Oil Operations Ltd., (2016)

2.4.3 Tritium

The radioactive isotope of hydrogen, ^{3}H, commonly referred to as tritium, is another routinely used tracer of the water molecule. With a half-life of 12.43 years, ^{3}H allows a relative or even absolute age constraint for young groundwater to be determined (Solomon & Cook, 2000). Tritium is often reported in Tritium Units (TU), in which 1 TU is equal to 1 tritium atom per 10^{18} Hydrogen (^{1}H) atoms.

Tritium is often used to determine the residence time of groundwater up to 60 years, as during the 1950-1960's, large amounts of it were produced by atomic bomb testing. Levels of tritium have since decreased steadily since the bomb peak, but due to the prevalence of nuclear power generation and natural generation levels, atmospheric TU values are usually around an average of 10 TU. Due to its short half-life, presence of a measurable amount of tritium in water provides an excellent indication of groundwater that has been recharged within the last 50 to 60 years (Clark & Fritz, 1997; Solomon & Cook, 2000).

Some example of tritium data from spring water collected within the Bogg Creek watershed are shown in Table 1. Geochemistry of these samples indicated the possibility of mixed type waters, and TU values were below that of modern water. Age calculations would place this water as being 4-13 years but this may in fact be water of different ages that have mixed to develop this tritium signature. Both lines of evidence here suggest a mix of different groundwaters. Other lines of evidence may assist in isolating the different sources and their contributions including physical hydrogeological measurements as outlined earlier.

Table 14: Samples from a large spring near a lake within the Bogg Creek watershed with TU values that suggest a component of modern water 4-13 years old.

Site	Date	^{3}H (TU)	Age
GL1	01-09-2018	7.9	4.5
GL2	01-09-2018	5.3	11.5
GL3	23-08-2019	4.9	13.0

2.4.4 Strontium

Strontium is a metal with two useful stable isotopes for groundwater tracing from a specific aquifer unit or rock type. In water samples, the ratio of $^{87}Sr/^{86}Sr$ is often determined in the dissolved strontium. Geologic materials will often contain a specific $^{87}Sr/^{86}Sr$ made up as a weighted average of the $^{87}Sr/^{86}Sr$ of all the minerals in that material (Clark & Fritz 1997). Groundwater that flows through an aquifer will dissolve strontium from minerals within the rock, resulting in a specific $^{87}Sr/^{86}Sr$ of the dissolved strontium similar to the aquifer host material. The length of time the water is in contact is important, however, as minerals have varying solubilities and $^{87}Sr/^{86}Sr$ values. Eventually the water will come to equilibrium and share a similar $^{87}Sr/^{86}Sr$ as that of the whole rock, while continued dissolution will increase the concentration of strontium. Typically, carbonates will have low $^{87}Sr/^{86}Sr$ but high strontium concentrations, sandstones will have intermediate $^{87}Sr/^{86}Sr$ and strontium concentrations and shales often high $^{87}Sr/^{86}Sr$ but intermediate strontium concentrations (McNutt, 2000).

In unconsolidated sediments and soil, the use of $^{87}Sr/^{86}Sr$ ratios is more complex due to the higher variability in water flow paths and soil mineralogy; typically it will contain higher $^{87}Sr/^{86}Sr$ and lower strontium concentrations compared to many rocks (McNutt, 2000; Shand et al., 2009). In surface waters, $^{87}Sr/^{86}Sr$ will depend on water sources as well as inputs from atmospheric and dust deposition and sediment weathering (McNutt, 2000). Runoff signatures are typically higher in $^{87}Sr/^{86}Sr$ but with low strontium concentrations, and groundwaters have lower ratios but higher strontium concentration in general (McNutt, 2000). For these reasons, $^{87}Sr/^{86}Sr$ makes a unique tracer of groundwater sourced from a particular formation, if the ratio can be determined (McNutt, 2000). This makes it difficult to interpret strontium data without appropriate endmembers. Whole rock $^{87}Sr/^{86}Sr$ values can be determined for different aquifers and used to constrain endmembers. There is some evidence that rock ratios do not always match ratios of their groundwater exactly, but these can be used to assess potential upper and lower bounds of dissolved $^{87}Sr/^{86}Sr$ endmembers when water endmembers are unavailable (Frost & Toner, 2004)

An example of this type of data used in groundwater mixing analysis is seen in data from Bogg Creek and several springs within that watershed (Figure 13). Several springs can be seen roughly plotting along a line originating from suprapermafrost groundwater. Two interpretations can be derived from this data. The first is that this demonstrates geochemical evolution of suprapermafrost groundwater taking a longer flowpath and dissolving less soluble minerals with a lower $^{87}Sr/^{86}Sr$. The second interpretation is that this is the result of mixing of two endmembers, one from the shallow suprapermafrost zone, and one from a deeper groundwater source.

These data also show the relationship between three predetermined endmembers: tributary baseflow, surface runoff, and subpermafrost groundwater within several creek samples. Samples that plot closer to a certain endmember are likely to have a greater contribution of that water. Tributary 1 plots closer to the baseflow and runoff endmembers suggesting a greater influence of those waters. Tributary 2 plots quite close to the subpermafrost endmember which lends further evidence of the deeper groundwater influence on this tributary.

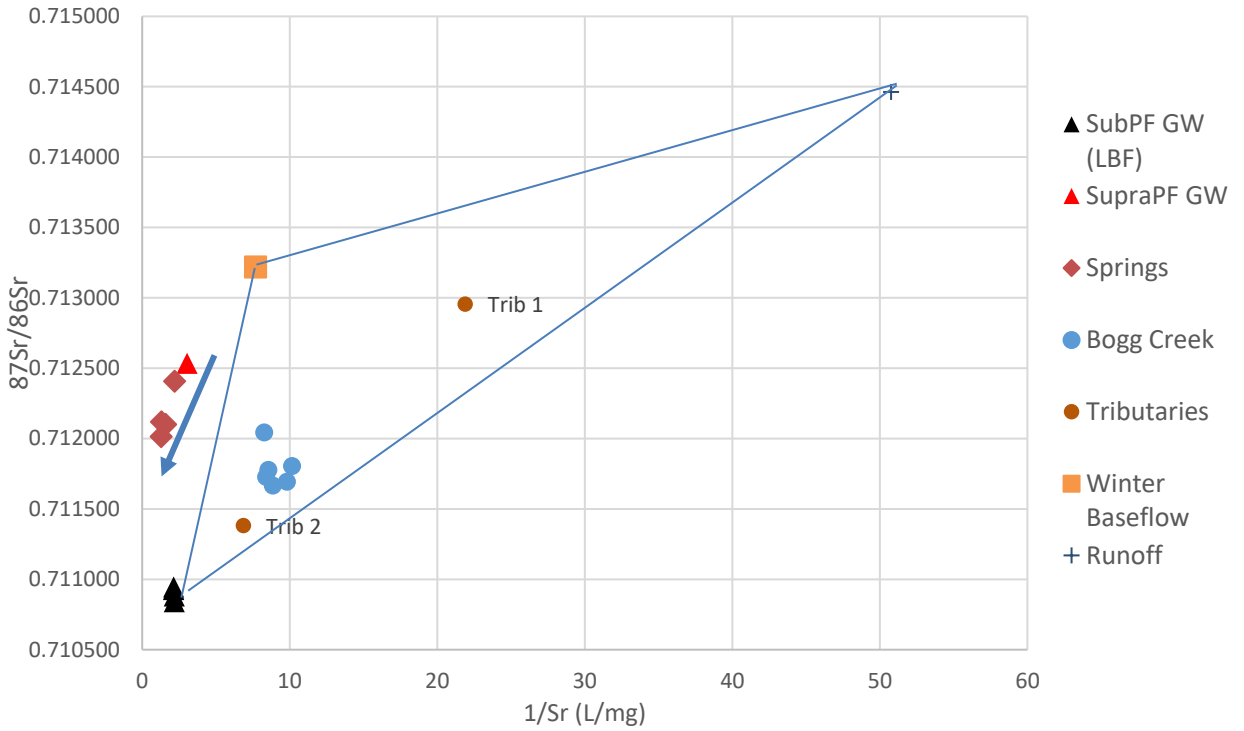

Figure 13: $^{87}Sr/^{86}Sr$ vs 1/Sr for some spring and creek samples collected within the Bogg Creek watershed and various endmembers (Wicke 2020).

2.4.5 Carbon

Two stable isotopes of carbon, ^{12}C and ^{13}C can be analyzed in DIC to determine certain conditions under which water was flowing. Another, more novel use, is tracing the origin of methane gas, CH_4. Carbon is expressed in similar notation as the stable isotopes of water, using the ratio of $^{13}C/^{12}C$ of a sample to the $^{13}C/^{12}C$ of a reference standard as $\delta^{13}C$ reported in ‰. Carbon in methane is fractionated according to its source. Methane can be produced in several ways naturally, but most commonly it is produced by thermal maturation of hydrocarbons (thermogenic) or through the breakdown of organic matter by microbes in the near-surface environments such as wetlands or bogs (biogenic) (Philp & Monaco, 2012). This methane may migrate upwards as a gas or be dissolved in groundwater, and has been used as a tracer of deeper groundwater flow (Philp & Monaco, 2012; Grasby et al., 2016). Biogenic $\delta^{13}C$ is often very isotopically light, between -80 to -42‰, while thermogenic methane is often higher at between -30 to -50‰ (Philp & Monaco, 2012).

Examples of thermogenic and biogenic gas from the study area are shown in Figure 14. Gas was taken from a subpermafrost aquifer, springs, a lake, and the creek (tributary and lower reach). The spring samples were taken in the summer season while all other samples were taken in winter. Spring and lake $\delta^{13}C$ fall within the biogenic range, while the subpermafrost groundwater falls within the range of thermogenic methane. The creek samples appear to fall close to the end of the biogenic range and quite close to the thermogenic range. There is a possibility that this gas is a mixture from biogenic and thermogenic sources, producing a value on the higher end of biogenic. This would imply a connection to the subpermafrost zone, allowing gaseous or dissolved methane to accumulate in the creek during winter.

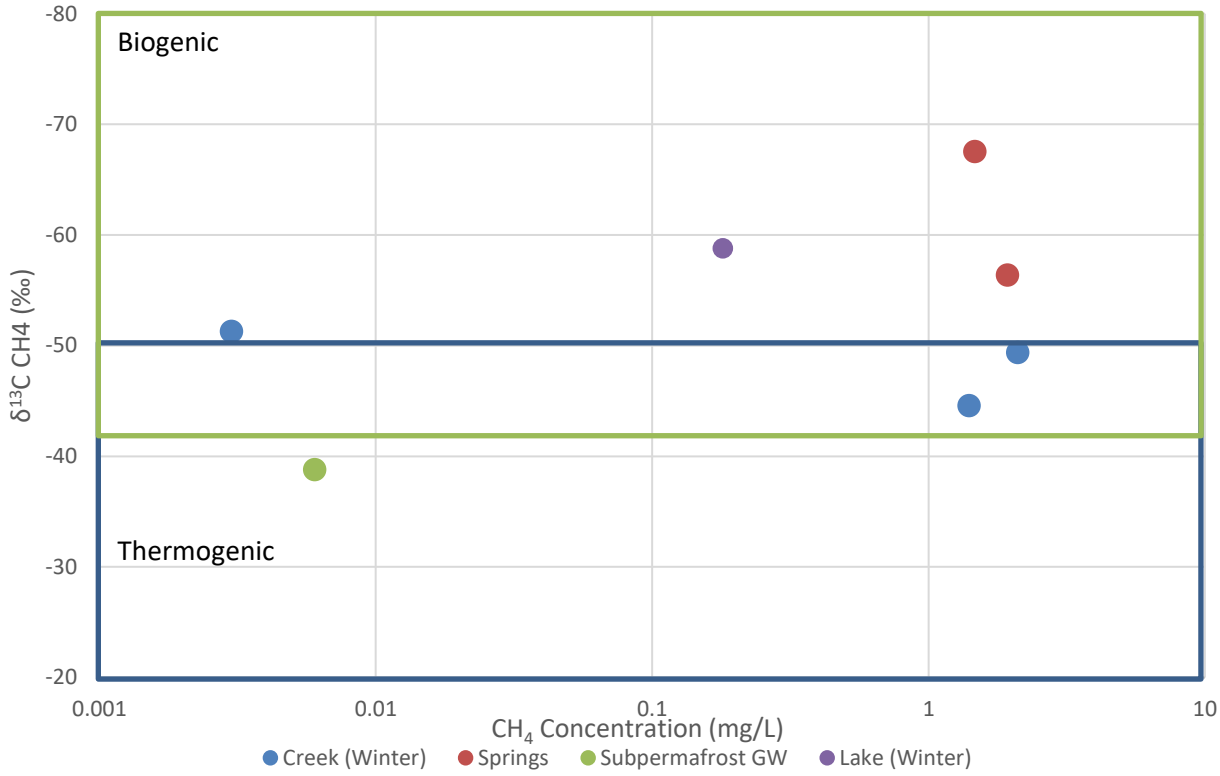

Figure 14: Methane samples given as an example in Bogg Creek. Note that concentrations are expressed on a log scale (Wicke, 2020).

3.0 Conclusions

The methods outlined above may be used to characterize baseline hydrogeological conditions in remote, discontinuous permafrost environments. These included the use of GIS and remote sensing, application of IR, geophysical and groundwater sampling technology and various geochemical and isotopic tracers in order to locate sites and characterize permafrost and groundwater flow conditions strategically. Each method complements the others, offering additional insights and perspective when fully integrated, as was demonstrated in the example of the Bogg Creek field site. Limitations do arise however, especially in regards to using these geochemical and isotopic tracers as different conclusions can be interpreted from the same data. This list is also not exhaustive and only includes methods that were tested and implemented at the Bogg Creek field site. Other techniques or tracers may be applicable in this environment. Moving forward, this document could be updated as new methods are identified and tested in the field, but those outlined provide a crucial launching point to guide future monitoring decisions at field sites underlain by discontinuous permafrost. A summary of the different data collection methods is presented as a flow chart in Figure 15 while the interpretations and utility of the various methods are presented in Figure 16.

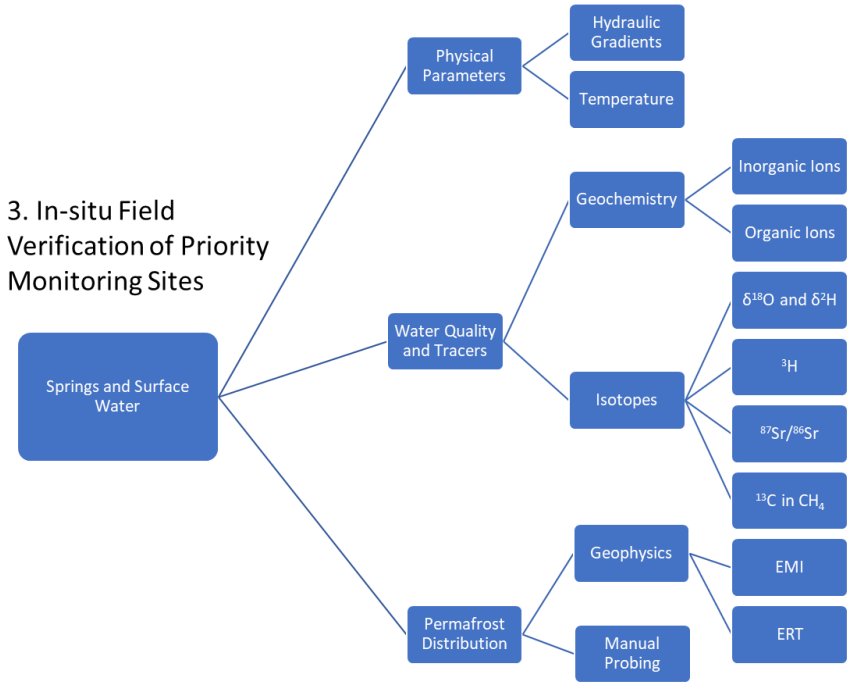

Figure 15: Summary of the in-situ field verification of the priority monitoring sites, including the various methods outlined above in previous sections.

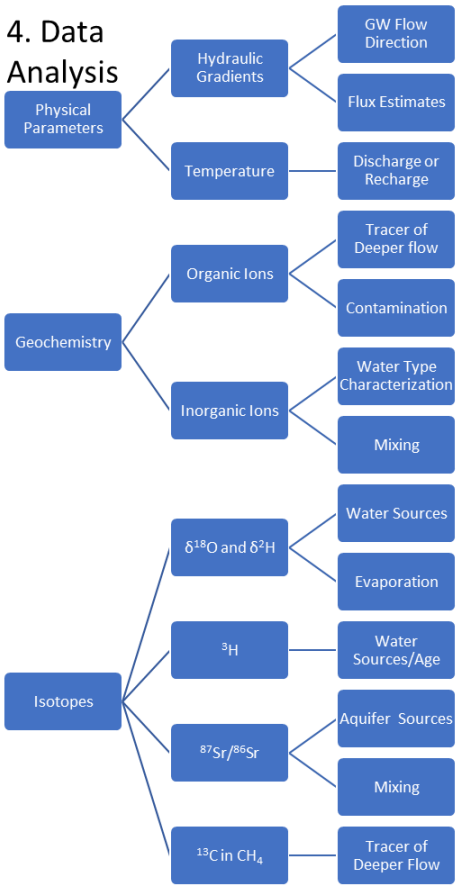

Figure 16:: Summary of the various data types and their utility in understanding baseline conditions in a field site.

4.0 References

AMEC. (2013). Central Mackenzie Valley Subsurface Groundwater Baseline Study. Indigenous and Northern Affairs Canada and the North, Northern Petroleum Resources, (July). Retrieved from https://www.aadnc-aandc.gc.ca/eng/1100100036430/1100100036431

Anderson, M. P. (2005). Heat as a ground water tracer. Ground Water, 43(6), 951–968. https://doi.org/10.1111/j.1745-6584.2005.00052.x

Babiy, R. (2013). Norman Wells Field – a long history of oil production in the Central Mackenzie Valley [Abstract]. In geoConvention 2013 (pp. 1–2).

Burt, T. P., & Williams, P. J. J. (1976). Hydraulic conductivity in frozen soils. Earth Surface Processes and Landforms, 1(4), 349–360. https://doi.org/10.1002/esp.3290010404

Clark, I., & Fritz, P. (1997). Environmental Isotopes in Hydrogeology. Lewis, Boca Raton.

Conant Jr, B. (2004). Delineating and Quantifying Ground Water Discharge Zones Using Streambed Temperatures. Ground Water, 42(2), 243–257.

Coplen, T. B., Herczeg, A. L., & Barnes, C. (2000). Isotope Engineering-Using Stable Isotopes of the Water Molecule to Solve Practical Problems. In P. Cook & A. L. Herczeg (Eds.), Environmental Tracers in Subsurface Hydrology (pp. 79–110). New York: Springer Science+Business Media.

Fetter, C. W. (2001). Applied Hydrogeology (4th ed.). Upper Saddle Hall, NJ: Prentice Hall.

Glass, B. (2019). Examining Hydrogeological Processes in Freezing Soils using Remote Geophysical and Numerical Techniques [Thesis]. University of Waterloo

Glass, B., Rudolph, D., Duguay, C., and Wicke, A. (2020). Identifying Groundwater Discharge Zones in the Central Mackenzie Valley Using Remotely Sensed Optical and Thermal Imagery. Canadian Journal of Earth Sciences. Under review (submission number: cjes-2019-0169

Grasby, S., Ferguson, G., Brady, A., Sharp, C., Dun, P., & Mcmechan, M. (2016). Deep groundwater circulation and associated methane leakage in the northern Canadian Rocky Mountains. Applied Geochemistry, 68, 10–18. https://doi.org/10.1016/j.apgeochem.2016.03.004

Hem, J. D. (1985). Study and Interpretation of the Chemical Characteristics of Natural Water. USGS Water-Supply Paper 2254. United States Geological Survey.

Herczeg, A. L., & Edmunds, W. M. (2000). Inorganic Ions as Tracers. In P. Cook & A. L. Herczeg (Eds.), Environmental Tracers in Subsurface Hydrology (pp. 31–78). New York: Springer Science+Business Media.

Husky Oil Operations Ltd. (2016). 2016 Surface Water Quality Assessment. Tulita District, NT.

Kresic, N., & Stevanovic, Z. (2010). Groundwater Hydrology of Springs. Burlington, MA, MA: Elsevier.

Lee, D. R., & Cherry, J. A. (1979). A field exercise on groundwater flow using seepage meters and mini-piezometers. Journal of Geological Education, 27(1), 6-10.

McNutt, R. H. (2000). Strontium Isotopes. In P. G. Cook & A. L. Herczeg (Eds.), Environmental Tracers in Subsurface Hydrology (pp. 233–260). Boston, MA: Springer US. https://doi.org/10.1007/978-1-4615-4557-6_8

Moncur, M. C., Blowes, D. W., & Ptacek, C. J. (2013). Pore-water extraction from the unsaturated and

saturated zones. Canadian Journal of Earth Sciences, 1058(July), 1051–1058.

Morse, P. D., & Wolfe, S. A. (2015). Geological and meteorological controls on icing (aufeis) dynamics (1985 to 2014) in subarctic Canada. Journal of Geophysical Research F: Earth Surface, 120(9), 1670–1686. https://doi.org/10.1002/2015JF003534

Philp, R. P., & Monaco, G. Lo. (2012). Applications of Stable Isotopes in Hydrocarbon Exploration and Environmental Forensics. In M. Baskaran (Ed.), Handbook of Environmental Isotope Geochemistry: Vol I (pp. 639–677). Berlin, Heidelberg: Springer Berlin Heidelberg. https://doi.org/10.1007/978-3-642-10637-8_31

Richards, P. I., & Sandau, C. D. (2018). Forensic Source Attribution for Toluene in Environmental Samples. Environmental Toxicology and Chemistry, 37(3), 729–737. https://doi.org/10.1002/etc.4008

Rudolph, D. (2019). Regional hydrologic and ecologic characterization and baseline assessment of remote northern Canadian terrain in advance of shale oil and gas development Second Annual Report to: NWT ESRF Management Board. Waterloo ON.

Rudolph, D., Lotimer, A. R., & Barker, J. F. (2016). Final Report Baseline Hydrogeological Evaluation of Central Mackenzie Valley Oil and Gas Exploration Areas Sahtu Region , Northwest Territories, (June), 1–35.

Shand, P., Darbyshire, D. P. F., Love, A. J., & Edmunds, W. M. (2009). Sr isotopes in natural waters: Applications to source characterisation and water-rock interaction in contrasting landscapes. Applied Geochemistry, 24(4), 574–586. https://doi.org/10.1016/j.apgeochem.2008.12.011

Smith, I. R. (2015). Seismic shothole drillers' lithostratigraphic logs: Unearthing a wealth of regional geoscience information in northwestern Canada. GeoResJ, 6, 21–29. https://doi.org/10.1016/j.grj.2015.01.005

Solomon, D. K., & Cook, P. G. (2000). 3H and 3He. In P. G. Cook & A. L. Herczeg (Eds.), Environmental Tracers in Subsurface Hydrology (pp. 397–424). Boston, MA: Springer US. https://doi.org/10.1007/978-1-4615-4557-6_13

Walvoord, M. A., Voss, C. I., & Wellman, T. P. (2012). Influence of permafrost distribution on groundwater flow in the context of climate-driven permafrost thaw: Example from Yukon Flats Basin, Alaska, United States. *Water Resources Research*, *48*(7), 1–17. https://doi.org/10.1029/2011WR011595

Waterline Resources Inc. (2013a). 2013 Shallow Environmental Investigation Slater River Project Near Norman Wells, Northwest Territories.

Waterline Resources Inc. (2013b). Slater River Project Groundwater Investigation Program 2013 Winter Mud-Rotary Drilling Summary Report.

Wicke, A. (2020). Characterizing Aspects of Groundwater Flow in a Discontinuous Permafrost Region, Sahtu Settlement Area, NT [Thesis]. University of Waterloo.

Woo, M. K. (2012). Permafrost Hydrology. Verlag Berlin Heidelberg: Springer.